ROLES OF SEMINOLIPID AND ITS ASSOCIATED MEMBRANE DOMAIN IN MALE FERTILITY

Kessiri Kongmanas

Thesis submitted to

the Faculty of Graduate and Postdoctoral Studies

in partial fulfillment of the requirements

for the Doctorate in Philosophy degree in Biochemistry

Department of Biochemistry, Microbiology and Immunology

Faculty of Medicine

University of Ottawa

ABSTRACT

Our research aims at understanding the roles of seminolipid (sulfogalactosylglycerolipid or SGG) and its associated membrane domains in male reproduction. SGG is a sulfoglycolipid present selectively and abundantly in mammalian male germ cells. Therefore, information on its properties would be relevant towards the development of male fertility biomarkers and spermicide-based contraceptives. We have shown that SGG has direct affinity for zona pellucida (ZP, egg extracellular matrix) and plays a role in the formation of sperm lipid rafts, the ZP-binding platforms on the sperm anterior head plasma membrane (APM), the initial ZP binding site. For a better understanding of mechanisms underlying sperm-ZP interaction, I performed proteomic characterization of APM vesicles (SGG-associated membrane domains with ZP affinity) isolated from sperm before and after capacitation, a process through which sperm gain maximal ZP affinity. Proteomic results revealed that capacitated APM vesicles contained high-molecular-weight protein complexes, with higher ZP affinity and levels of ZP-binding proteins as compared with those of the non-capacitated samples. ZP-binding proteins known to exist in the acrosome (i.e., zonadhesin, proacrosin/acrosin) were found in these APM protein complexes. Immunofluorescence suggested that a fraction of these proteins trafficked from the acrosome to APM during capacitation. These findings provided a new mechanism on how sperm gain full ZP-binding ability during capacitation. Since SGG is a major component of APM, proper SGG levels at this site would be important for male fertility. Levels of sperm SGG are regulated through the synthesis and degradation. In fact, lack of SGG-synthesis enzymes causes a spermatogenesis disruption, resulting in male infertility. However, significance of SGG degradation remains unknown. SGG can be desulfated *in vitro* by arylsulfatase A (ARSA), an enzyme existing in the acrosomes of sperm/spermatids and lysosomes of Sertoli cells, testicular somatic cells that nurture developing germ cells. Sertoli cells also phagocytose ~50% of germ cells that become apoptotic during spermatogenesis. To understand physiological importance of SGG degradation, the fertility status and SGG levels of *Arsa*$^{-/-}$ male mice were determined. We found that *Arsa*$^{-/-}$ males became subfertile when they were older than 5 months, and when they were 8-month-old (~40-year-old men) they produced sperm at 50% wild type rate. *Arsa*$^{-/-}$ sperm had minimal *in vitro* fertilizing ability and a number of them showed abnormal

morphology. Quantitative mass spectrometry revealed that SGG levels in Sertoli cells of 8-month-old *Arsa*$^{-/-}$ mice were increased to ~250% of the wild type level; this SGG accumulation may lead to a decrease in Sertoli cell ability to support spermatogenesis. However, SGG levels in sperm of 8-month-old *Arsa*$^{-/-}$ mice were ~50% of the wild type value, a result that partly explained the decreased fertilizing ability of these sperm. The reduced SGG level of *Arsa*$^{-/-}$ sperm was likely due to a lack of SGG's building-block lipid (palmitylpalmitoylglycerol) putatively generated in *Arsa*$^{-/-}$ Sertoli cells and recycled to the next generation of primary spermatocytes for SGG synthesis. Hence, levels of sperm SGG are a promising bioindex for male fertility. Since Sertoli cells also regulate SGG homeostasis, their functionality should be now included in male fertility/subfertility diagnosis.

ACKNOWLEDGMENTS

First of all, I would like to express my deep gratitude towards my supervisor, Dr. Nongnuj Tanphaichitr, for her excellent supervision. She has taught me many skills that will be beneficial to my future scientific career, and provided me great opportunities to visit other laboratories so that I can acquire new skills and knowledge from experts in the field.

I would also like to express my appreciation to all my thesis advisory committee members (Drs. Daniel Figeys, Xiaohui Zha, and Mike Wade) for their valuable guidance, as well as our collaborators (Drs. Kym Faull, Julian Whitelegge, Mark Baker, John Aitken, Trish Berger, and Louis Hermo) for their continued support and contributions to my Ph.D. research project. In addition, this work would not have been possible without paramount help and moral support I received from past and present members of our laboratory. My special thanks are given to Drs. Arpornrad Sae-wu, Hongbin Xu, Suraj Kadunganattil and Hathairat Kruevaisayawan, who provided technical assistance in some of my experiments. I would also like to thank Ms. Terri van Gulik, our administrative assistant, and Ms. Phyllis Gunther, my English tutor, for their help during my thesis preparation.

I gratefully acknowledge the Development and Promotion of Science and Technology Talented Project (DPST), Thailand and CIHR Strategic Training Initiative in Health Research (STIHR) in Reproduction, Early Development, and the Impact on Health (REDIH), Canada for providing scholarships to support my graduate studies.

Last but not least, I would like to thank my family including my parents, brother and sister, whose love and understanding have enabled me to complete this work.

TABLE OF CONTENTS

LIST OF FIGURES

LIST OF FIGURES

APPENDIX FIGURES

LIST OF TABLES

APPENDIX TABLES

LIST OF ABBREVIATIONS

ABBREVIATION	DESCRIPTION
ACRBP	Acrosin-binding protein
APM	Anterior head plasma membrane of sperm
ARSA	Arylsulfatase A (protein)
Arsa	Arylsulfatase A (gene)
Cap	Capacitated
CE	Cholesteryl ester
Chol	Cholesterol
CGT	UDP-galactose:ceramide galactosyltransferase (protein)
Cgt	UDP-galactose:ceramide galactosyltransferase (gene)
COC(s)	Cumulus oocyte complex(es)
CST	Cerebroside sulfotransferase (protein)
Cst	Cerebroside sulfotransferase (gene)
ESI	Electrospray ionization
FSH	Follicle stimulating hormone
GC	Galactosylceramide
GG	Galactosylglycerolipid
GnRH	Gonadotropin releasing hormone
HMW	High molecular weight
KO	Knockout
LC	Liquid chromatography
LH	Luteinizing hormone
MLD	Metachromic leukodystrophy
MFGM	Milk fat globule-EGF factor 8
MRM	Multiple reaction monitoring
MS	Mass spectrometry
MS/MS	Tandem mass spectrometry
NCS	*p*-nitrocatechol sulfate
Non-cap	Non-capacitated
OG	Octylglucoside
PAPS	3'-phosphoadenosine-5'-phosphosulfate
PC	Phosphatidylcholine
PE	Phosphatidylethanolamine
PGC	Percoll gradient centrifugation
PUFA	Polyunsaturated fatty acid
SGC	Sulfogalactosylceramide
SGG	Sulfogalactosylglycerolipid
SM	Sphingomyelin
TAG	Triacylglycerol
WT	Wild type
ZAN	Zonadhesin
ZP	Zona pellucida

CHAPTER ONE

INTRODUCTION

1.1 Preamble to my research studies

The world population presently totals 7.2 billion and is predicted to reach 9.6 billion in 2050 (Gerland et al., 2014). This rapid population growth can create a range of global challenges, such as the spread of poverty, disease and environmental degradation. Widespread contraceptive usage may be one of key solutions to the problem of overpopulation. Although a number of contraceptive methods, including hormonal and non-hormonal-based types, are currently available, none of them provides all of the desirable properties:100%-efficiency, reversibility, minimal side effects (especially to the overall physiological system), low cost, and ease of administration and minimal interference with sensuality during intercourse. For example, the most commonly used are female hormonal contraceptives (e.g., pills, patches), which are reliable in preventing pregnancy but can have adverse side effects and cannot prevent sexually transmitted diseases (STDs). Common barrier contraceptives, i.e., condoms, are safer because they can prevent pregnancy as well as STDs. However, they are not always 100% effective in preventing sperm from entering the female genital tract (Zhao et al., 2014). Also, they are less popular than the female contraceptives because they reduce sensation for both partners. Therefore, new types of contraceptives, especially with the above-mentioned desirable properties would promote their use worldwide and provide individuals with both choice and suitablity.

While the greatest population growth is occurring in developing countries, infertility is being experienced in developed nations (de Kretser, 1997; Smeeding, 2014). Infertility is

a common clinical problem defined as a couple's failure to conceive after a year of regular and unprotected sexual intercourse. It is estimated that approximately 72.4 million couples worldwide experience fertility problems (Boivin et al., 2007), with approximately 50% of the infertility cases being attributed to male factors (De Kretser and Baker, 1999). Known factors causing male infertility include varicocele, endocrine disturbances, and genetic abnormalities (e.g., a deletion of azoospermia factor region (*AZF*) of the Y chromosome and mutations in the cystic fibrosis transmembrane conductance regulator (*CFTR*) gene) (Dohle et al., 2002; Hackstein et al., 2000; Tahmasbpour et al., 2014). The hormonal and genetic factors associated with male infertility often result in azoospermia or severe oligospermia (Tahmasbpour et al., 2014). However, there is unexplained infertility in about 10 to 15% of infertile couples (Quaas and Dokras, 2008), where men show normal semen parameters, commonly used in fertility clinics to assess the male fertility status. According to the WHO 2010 guidelines, fertile men should have sperm counts > 15 million/ml, sperm motility >40% and normal sperm morphology >4% (WHO, 2010). However, normal semen analysis results do not always assure fecundity. For example, men with semen parameters lower than the WHO threshold values can still impregnate their partners in due time, whereas men with semen parameters above these threshold values remain infertile. This is not a surprising fact because all of these semen parameters do not directly reflect sperm functions, especially the sperm ability to fertilize the egg. The direct way to test sperm fertilizing ability is to co-incubate sperm and eggs and then determine whether the sperm are capable of fertilizing the eggs. Obviously this test cannot be set up due to ethical issues in obtaining human eggs. Because of the unavailability of reliable semen analyses, the roots of male infertility are not being corrected and assisted reproductive technology (ART) appears to be the preferred channel for treating male infertility/subfertility. However, ART, especially invasive

procedures such as intracytoplasmic sperm injection (ICSI), may have possible long-term effects on the conceived children (aberrant growth and behaviour, early aging, and affliction of genetic rare diseases). In addition, ICSI of genetically defective sperm that creates embryos for implantation definitely propagates the "bad genes" to the next generation. Thus, it is critical to develop practical and accurate analyses of sperm functionality for proper treatment of male infertility.

Understanding the molecular mechanisms underlying key physiological processes in male reproduction (e.g., spermatogenesis, capacitation and sperm-egg interaction) is the first important step leading to proper development of contraceptives and biomarkers for male fertility, and to proper treatment of infertility/subfertility. Logically, this understanding will be reached much rapidly by focusing on molecules selectively present in male germ cells or somatic cells in the male reproductive system. For this reason, our lab has been investigating the roles of sulfogalactosylglycerolipid (SGG), which is present selectively and abundantly in mammalian germ cells. To date, we have shown that SGG has dual functions as: 1) an adhesion molecule, involved in sperm-zona pelludica (ZP) binding and sperm-egg plasma membrane binding *in vitro* (Ahnonkitpanit et al., 1999; Weerachatyanukul et al., 2001; White et al., 2000), and 2) a structural lipid, important for the formation of capacitated sperm lipid rafts, the ZP-binding platforms on the sperm surface (Bou Khalil et al., 2006; Tanphaichitr et al., 2007a; Tanphaichitr et al., 2007b). Moreover, mice which are genetically null in genes encoding for enzymes responsible for SGG synthesis are infertile due to spermatogenesis disruption, implicating that SGG plays a physiological role in this process (Fujimoto et al., 2000; Honke et al., 2002). Due to its unique properties and significant roles in male fertility, SGG may serve as a reliable biomarker of sperm function as well as a

potential target for contraceptive development. However, prior to any clinical and translational applications, a comprehensive understanding of the roles of SGG and its associated molecules/membrane domains in male fertility is required. My thesis research is aimed at providing a better understanding of: 1) the molecular components of the sperm anterior head plasma membrane, the SGG associated membrane that possesses ZP affinity, and 2) the significance of SGG homeostasis on male fertility.

1.2 Overview of the male reproductive system

Under androgenic support, sperm are produced in the seminiferous tubules within the testis through a process called “spermatogenesis”. This process involves cell division and differentiation of diploid round male germ cells to form haploid sperm with a polarized anatomical structure. Throughout spermatogenesis, developing male germ cells are in close contact with Sertoli cells, somatic cells which span the whole epithelium of the seminiferous tubules. Sertoli cells provide structural and nutritional support for developing germ cells and are also responsible for phagocytic elimination of apoptotic germ cells (approximately 50% of the total germ cells). After spermatogenesis, testicular sperm do not yet have motility and fertilizing abilities, including the ability to bind to the zona pellucida (ZP), an extracellular glycoprotein matrix surrounding the egg. To gain these abilities, testicular sperm have to undergo two maturation processes. The first process occurs when sperm transit through the epididymis where a number of new molecules, including the ZP-binding molecules, are adsorbed onto the sperm surface. The second maturation process, called “capacitation”, occurs when ejaculated sperm travel through the female reproductive tract. During

capacitation, the sperm plasma membrane undergoes changes in its molecular components. Most importantly, cholesterol efflux takes place, resulting in increased global membrane fluidity on capacitated sperm, concurrent with increased levels of lipid raft microdomains, the platforms for ZP-binding. Capacitated sperm also gain the hyperactivated motility needed for penetration through the ZP layer. The anterior sperm head plasma membrane (APM) overlying the acrosome is the site where sperm initially interact with ZP. Capacitated sperm must undergo acrosomal exocytosis, which can occur before or during the sperm binding to the ZP, and which involves fusion at many sites on the plasma membrane overlying the acrosome and outer acrosomal membrane. This fusion leads to the formation of vesiculated structures on the sperm head surface and allows a gradual release to the surroundings of hydrolytic enzymes, molecular constituents of the acrosome that facilitate sperm penetration through the ZP layer. Finally, when the acrosomal content is substantially released, the sperm anterior head surface is covered with the inner acrosomal membrane, with only some insoluble acrosomal matrix; the whole acrosomal exocytosis is referred to as the “acrosome reaction”. Acrosome-reacting/reacted sperm continue to bind to and further penetrate the ZP. However, only acrosome-reacted sperm are found in the perivitelline space and will then bind to the egg plasma membrane. Only one acrosome-reacted sperm will fuse with the egg plasma membrane, followed by its incorporation into the egg proper, signifying that fertilization has occurred (Figure 1.1). More details and important features of the key physiological processes in male reproduction (i.e., spermatogenesis, epididymal maturation, capacitation and sperm-egg interactions) are described below.

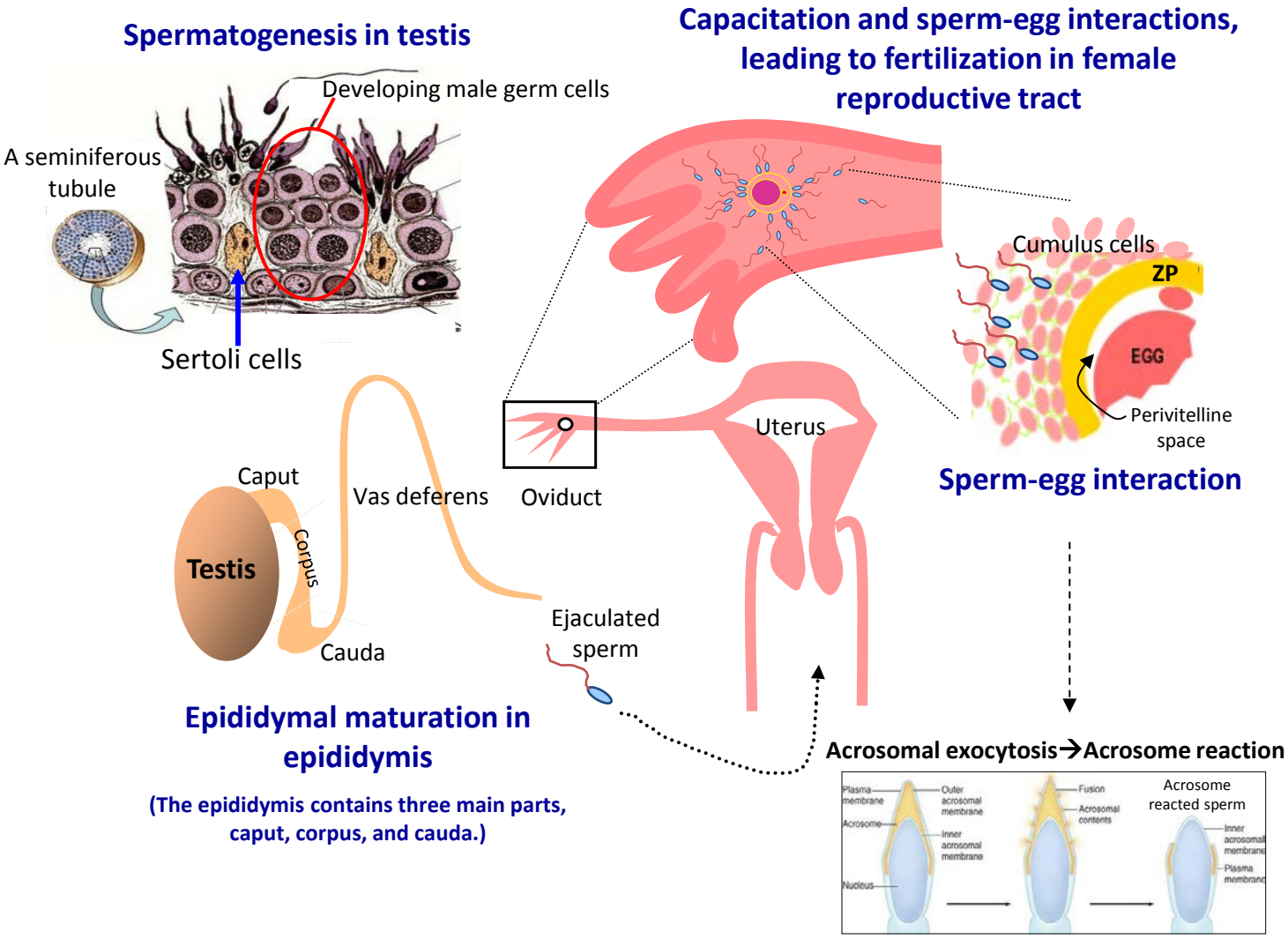

Figure 1.1: Overview of male reproduction. Sperm (or spermatozoa) are produced in the testis under hormonal control through the process called "spermatogenesis", which transforms round germ cells into polarized sperm cells with heads and tails. Throughout spermatogenesis, developing germ cells are structurally and nutritionally supported by Sertoli cells, somatic cells which span the whole epithelium of the seminiferous tubules. Although testicular sperm, the final product of spermatogenesis, are anatomically mature, they do not yet have the ability to move or fertilize the egg. The testicular sperm must undergo two modification processes, which allow sperm to gain their motility and full fertilizing ability: the first process, called "epididymal maturation", occurs when sperm transit through the epididymis and the second process, called "capacitation", occurs when ejaculated sperm travel through the female reproductive tract. The sperm anterior head plasma membrane is the site where sperm initially interact with the ovulated egg, surrounded by layers of cumulus cells and the zona pellucida (ZP), an extracellular glycoprotein matrix. During the movement of sperm through the cumulus cell layers and then the ZP, acrosomal exocytosis occurs. The acrosome, a cap-like structure localized at the sperm head anterior, is a secretory granule, which contains a number of hydrolytic enzymes. These released enzymes facilitate the digestion of the cumulus cell layer network materials and the ZP, thus creating paths for the sperm to move through. Sperm become fully acrosome reacted (i.e., with all acrosomal contents released) when they reach the perivitelline space and subsequently bind to the egg plasma membrane. However, only one acrosome-reacted sperm fuses with the egg plasma membrane and gets into the egg proper, signifying that fertilization has occurred.

1.2.1 Spermatogenesis

Spermatogenesis is a process taking place in the seminiferous tubules of the testis, whereby haploid cells with a polarized structure, i.e., spermatozoa, are produced from diploid spermatogonia through a series of mitotic and meiotic divisions. Each seminiferous tubule consists of the epithelium and the lumen in the center, into which mature spermatozoa are released. The seminiferous epithelium contains two distinct cell populations: 1) Sertoli cells, somatic columnar cells which extend from the basement membrane to the lumen, and 2) spermatogenic cells, including spermatogonia, primary and secondary spermatocytes, and round and elongated spermatids (Figure 1.2A). The two adjacent Sertoli cells form specific junctions near the basement membrane (known as the blood-testis-barrier (see more below)), dividing the seminiferous epithelium into two compartments: 1) the basal compartment below the junctions, where spermatogonia and early stages of primary spermatocytes are located and 2) the adluminal compartment above the junctions, where more advanced germ cell stages of primary spermatocytes, secondary spermatocytes and spermatids reside (Figure 1.2B). The seminiferous epithelium is surrounded by a basement membrane and a thick tubular wall, consisting of peritubular myoid cells, collagenous fibers, and fibroblasts. The space in between the seminiferous tubules (referred to as testicular interstitium) is filled with blood vessels, lymphatic sinusoids, macrophages, and clusters of androgen-producing Leydig cells (aka interstitial cells of Leydig) (Kierszenbaum, 2002).

Spermatogenesis, which begins at puberty, is under hormonal control through the hypothalamic-pituitary-testicular axis (Figure 1.3). Gonadotropin-releasing hormone (GnRH) produced by the hypothalamus triggers the pituitary to produce and release

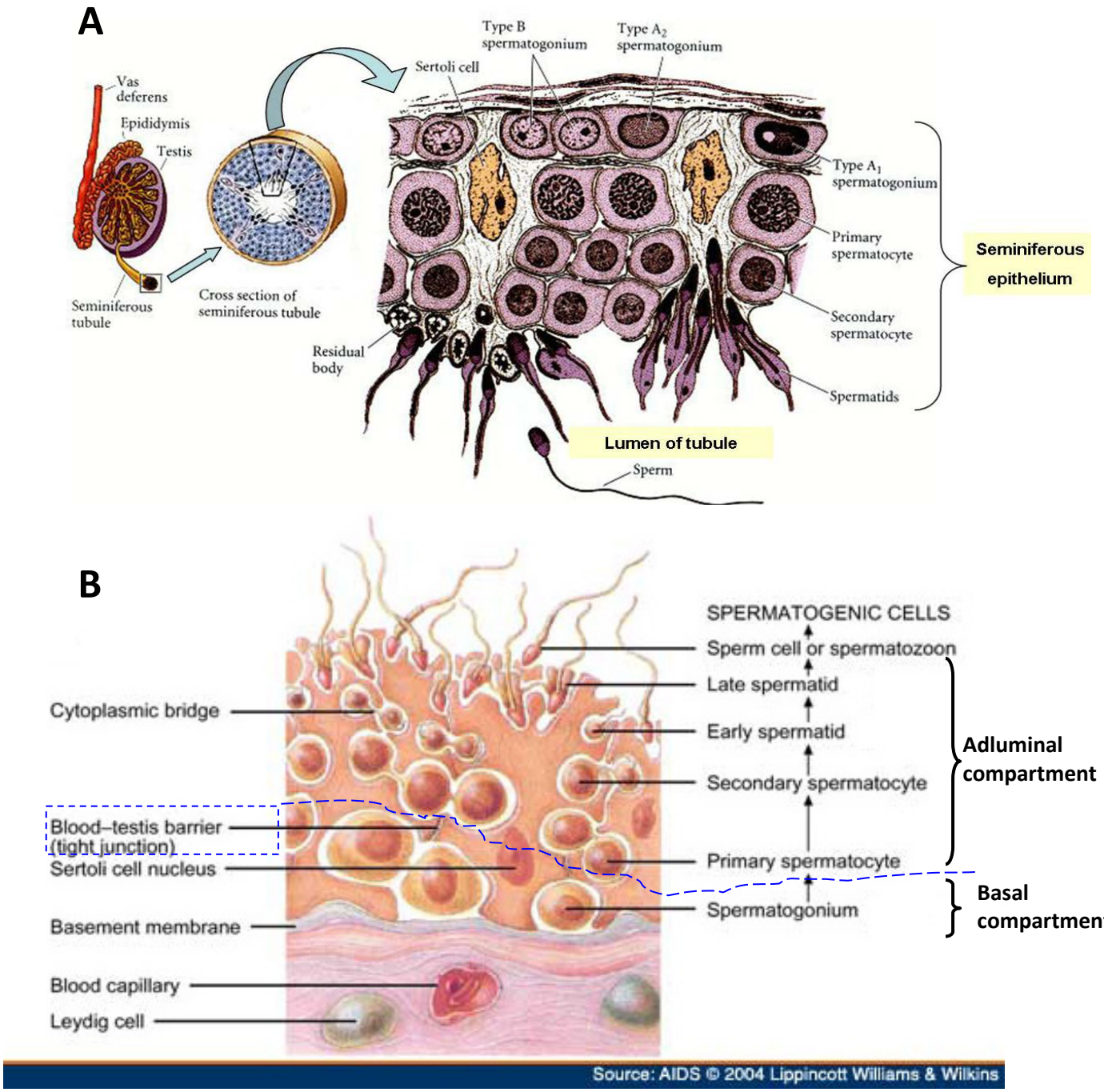

Figure 1.2: A) Spermatogenesis occurs in the seminiferous tubules of the testis. Each seminiferous tubule is composed of a lumen lined by a specialized epithelium, which contains two cell populations: Sertoli cells and spermatogenic cells (spermatogonia, spermatocytes, and spermatids) **B)** Blood-testis barrier is formed by junctions between adjacent Sertoli cells. It prevents proteins including antibodies, from reaching developing spermatogenic cells and divides seminiferous epithelium into two compartments: the basal compartment, below the junctions and the adluminal compartment, above the junctions.

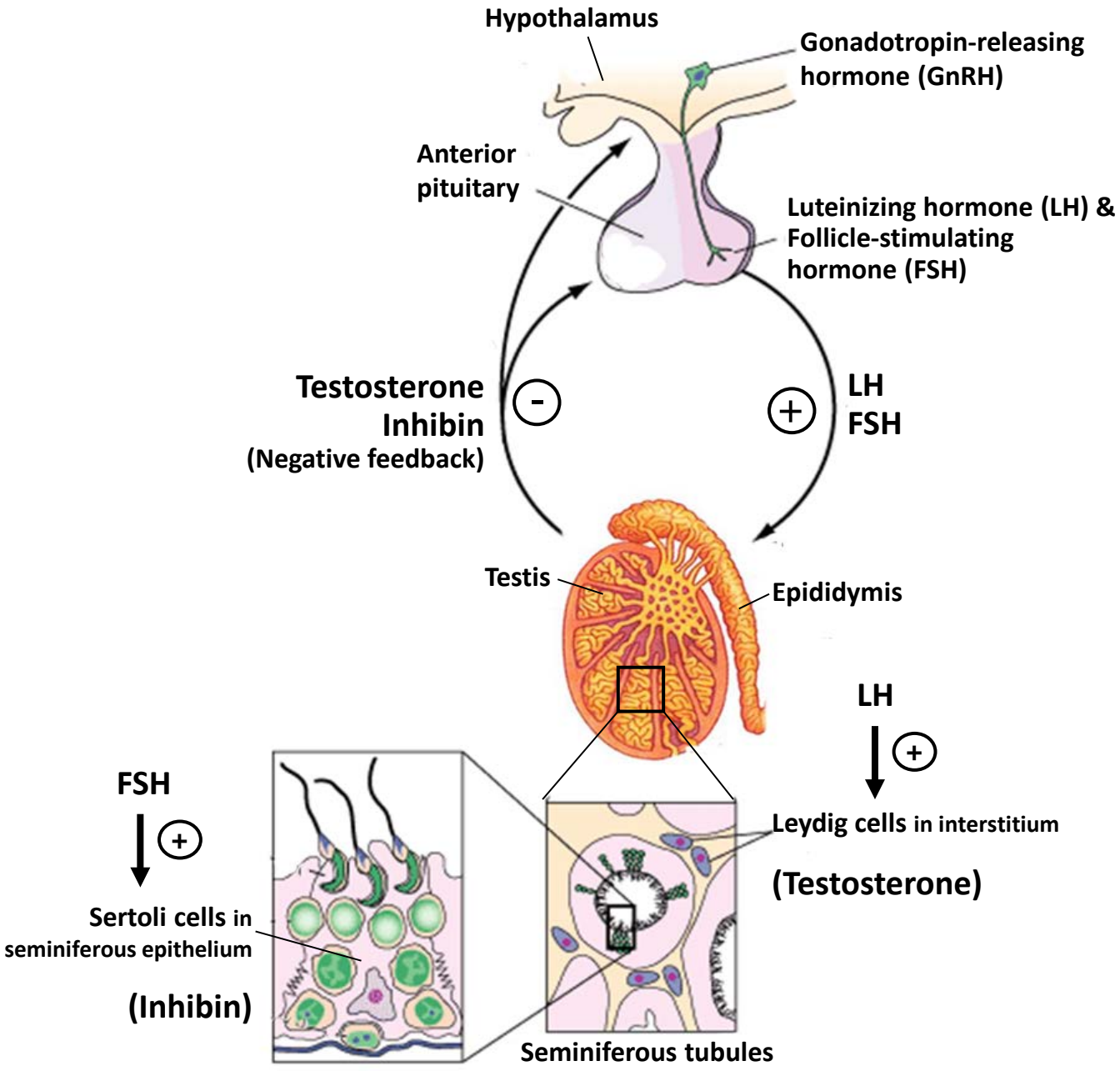

Figure 1.3: Hormonal regulation of spermatogenesis via Sertoli cells (modified from *Harrison's Principles of Internal Medicine*, 16th Edition: http://www.accessmedicine.com)

follicle-stimulating hormone (FSH) and luteinizing hormone (LH). FSH regulates the Sertoli cell functions in supporting the proliferation and development of spermatogenic cells throughout spermatogenesis. LH stimulates Leydig cells in steroidogenesis with the main production of testosterone, which regulates spermatogenesis. As well, dihydrotestosterone is important for sperm maturation in the epididymis (Alves et al., 2013; Cheng and Mruk, 2010). In some rodent species, FSH seems to play a role in spermatogenesis only in the prepubertal animal; in the adult, FSH actions are replaced by testosterone (Griswold, 1995). Negative feedback to the pituitary also occurs via testosterone secreted from Leydig cells and inhibin secreted from Sertoli cells (Cheng and Mruk, 2010) (Figure 1.3).

In mammals, spermatogenesis is composed of three phases (Figure 1.4): 1) the proliferative phase, during which diploid spermatogonial type A stem cells undergo several mitotic divisions to reproduce themselves for a constant supply of germ stem cells for spermatogenesis, and to produce differentiating spermatogonia (intermediate (In) and type B spermatogonia). The differentiating spermatogonial cells then divide and give rise to more specialized cells, called primary spermatocytes, which will enter a lengthy meiotic phase; 2) the meiotic phase, during which the diploid primary spermatocytes continue to mature as they go through a long prophase (leptotene, zygotene, pachytene, diplotene and diakinesis) where they are actively engaged in DNA synthesis and have a total DNA content twice (4C) that of diploid somatic cells (2C). After the first meiotic division, one primary spermatocyte gives rise to two secondary spermatocytes, which contain half the number of chromosomes (haploid) and half the DNA content (2C) of primary spermatocytes. The second meiotic division occurs shortly after the first one. During this process, the two sister chromatids of each chromosome of the secondary spermatocytes separate into two daughter cells, termed

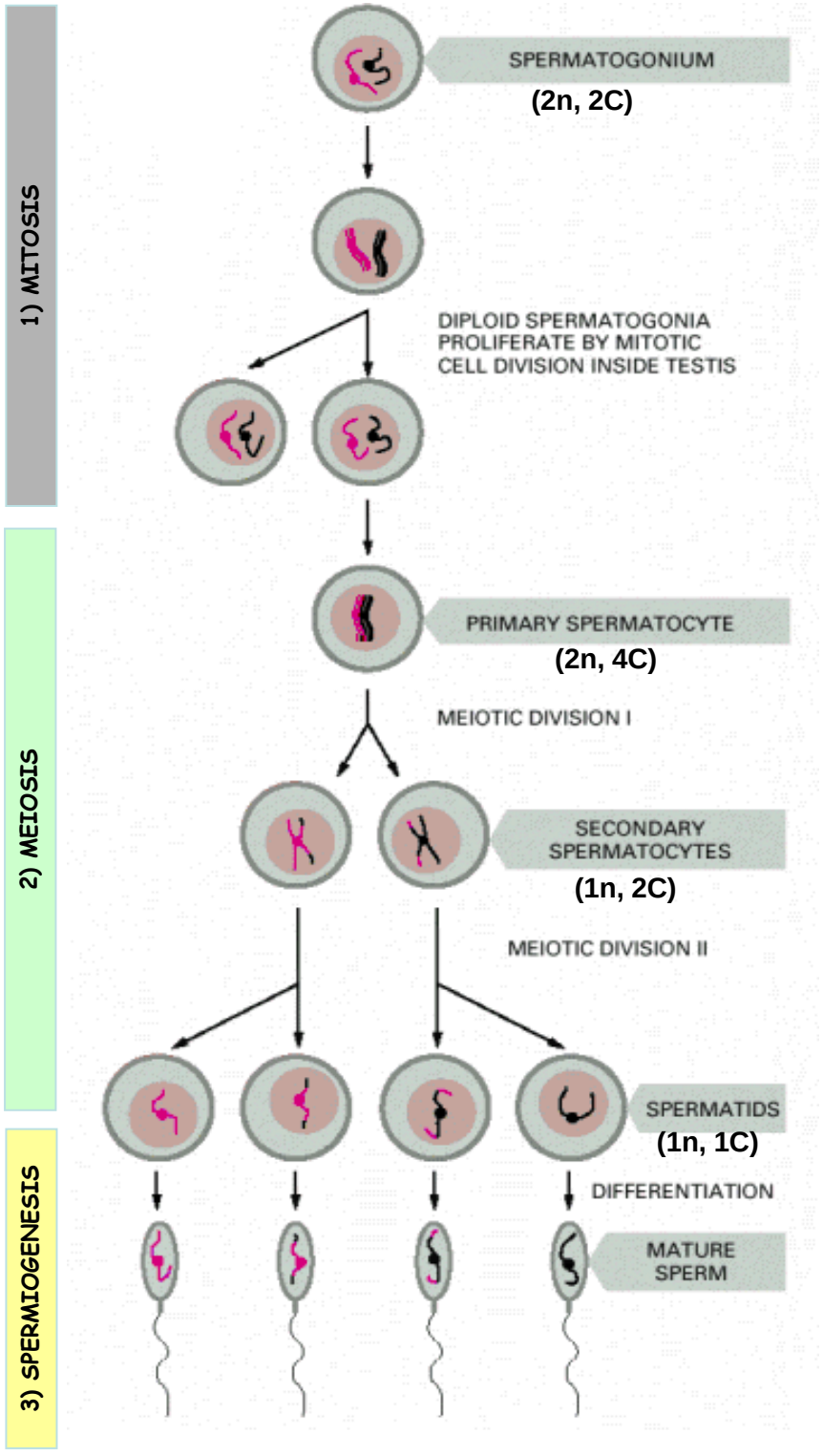

Figure 1.4: Three phases of mammalian spermatogenesis: 1) proliferative phase (mitosis of spermatogonia), 2) meiotic phase, and 3) spermiogenesis (differentiation of spermatids into spermatozoa) (modified from Alberts et al., 2002). The chromosome number (n) and DNA amount (C) of each stage of spermatogenic cells are indicated

spermatids. Thus, through meiosis, each primary spermatocyte should yield four spermatids, with a haploid number of chromosomes and half the DNA content of the secondary spermatocyte (1C). Since the first meiotic division is a long process (days) and the second meiotic division is very short (minutes), primary spermatocytes (~20%) and round spermatids (~80%) are often seen in the seminiferous epithelium at a much higher number than the secondary spermatocytes (Kierszenbaum, 2002); 3) the final phase, called spermiogenesis, which corresponds to the differentiation of round spermatids into spermatozoa (sperm) with a unique structure and fully compacted chromatin (Figure 1.5A). Round spermatids (step 1) differentiate into elongated spermatids via 16 steps in mice, and 12 steps in humans, until spermiation, the last step of spermiogenesis, at which time the mature testicular sperm are ejected from the seminiferous epithelium into the lumen. The major features of spermiogenesis involve: (i) formation of the acrosome from the Golgi apparatus of round spermatids. The acrosome, a membrane-enclosed organelle sitting as a cap over the anterior part of the sperm nucleus, consists of a number of egg-binding proteins and hydrolytic enzymes necessary for sperm-egg interactions and sperm penetration through the egg vestments (including the cumulus layers and zona pellucida (ZP) (Eddy, 2006); (ii) condensation and elongation of the nucleus. Chromatins of elongated spermatids become condensed as a result of the replacement of histones by protamines, very basic nuclear proteins enriched in cysteine residues, which can form disulfide bonds for further condensation of the chromatin. This tightly packed chromatin structure leads inactivation of transcriptional and translational activities in sperm (Eddy, 2006; Florman and Ducibella, 2006); (iii) the formation of a motility apparatus, the flagellum, with a microtubular axoneme structure as its core structure (Eddy, 2006) (see more details about sperm structure in the section below); (iv) shedding of the cytoplasm (Figure 1.5B). Prior to spermiation,

elongating/elongated spermatids (of later steps) embed their heads into the Sertoli cell cytoplasm at the apical membrane region, with their tails extruding into the seminiferous lumen. The overall polarized structure of these elongating/elongated spermatids is perpendicular to the basement membrane. During the final development steps of these spermatids, most of their cytoplasm is diverted to one side of their necks. This cytoplasmic material, the so called residual body, which lies next to the Sertoli cell apical membrane, is then engulfed by the Sertoli cell. Almost simultaneously, the anatomically mature spermatozoon is ejected into the lumen. Matrix metalloproteases and serine proteases (e.g., plasmin, which is activated by the plasminogen activator) are important for this spermiation (release of the spermatozoa). The engulfed residual bodies then fuse with the Sertoli cell lysosomes to form late residual bodies, and their contents are then degraded by the lysosomal hydrolytic enzymes (Clermont, 1972; Dym, 1977). The entire spermatogenesis process takes about 75 days in humans and about 35 days in mice (Cooke and Saunders, 2002).

1.2.1.1 Spermatogenic stage and cycle

During mammalian spermatogenesis, the organization of spermatogenic cells in seminiferous tubules is not random but organized into well-defined cellular associations. For example, spermatids at a given step of spermiogenesis are always associated with the same types of spermatocytes and spermatogonia. This specific cellular organization occurs due to the following reasons: 1) the spermatogenic cells arrange themselves in layers (i.e., the more developed spermatogenic cells are closer to the lumen of the seminiferous tubule); 2) the time period that spermatogenic cells being in each stage is constant; 3) more than one spermatogonium enters the spermatogenesis process along the length of the seminiferous tubule. The typical associations of spermatogenic cells are referred to as “spermatogenic

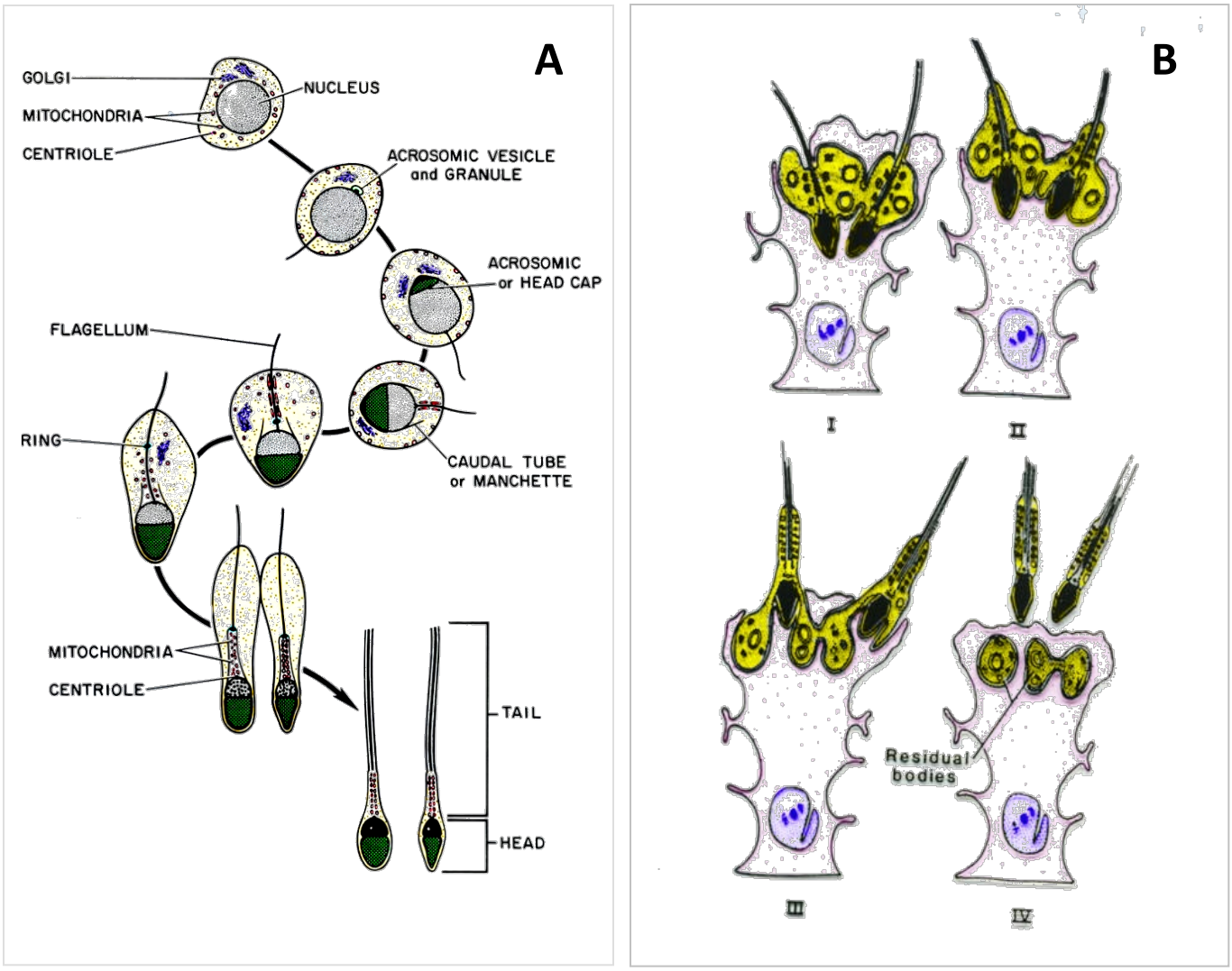

Figure 1.5: Spermiogenesis, the final phase of spermatogenesis. **A)** A graphic illustration showing transformation of a round spermatid into a polarized spermatozoon during spermiogenesis (modified from Dym, 1977), **B)** A schematic drawing showing the Sertoli cell-germ cell interaction during the final stages of spermiogenesis. At these stages, the processes of Sertoli cell cytoplasm essentially "pull off" the residual cytoplasm (residual body) from the elogated spermatids and retain it within their cytoplasm (occurring in the order from image I to IV) (modified from Kerr et al., 2006).

stages" and a number of criteria are used for assigning the various stages. The most useful criterion is based on the acrosomal development of the spermatids as seen in periodic acid-Schiff-hematoxylin stained sections (Clermont, 1972). With this method, 14 stages have been defined in the rat (Figure 1.6A), 12 stages in the mouse (Figure 1.6B) and 6 stages in the human (Franca et al., 1998; Kierszenbaum, 2002). The spermatogenic stages succeed one another and the sequence repeats itself indefinitely. The time it takes for the same spermatogenic stage within a given area of the seminiferous tubule to reappear is defined as "a spermatogenic cycle or a cycle of seminiferous tubule".

1.2.1.2 Sertoli cell functions

The seminiferous epithelium consists of polarized Sertoli cells, irregularly shaped columnar cells which can be characterized by their unique features, including tripartite nucleoli and numerous veil-like cytoplasmic processes (Russell, 1993). Sertoli cells play crucial roles in testicular functions at different stages in life (i.e., fetal, prepubertal and pubertal stages) (Tarulli et al., 2012). In the fetus, during the differentiation of the primordial gonad to a testicular phenotype, Sertoli cells are the first testicular cell types formed.They then act as the organizing center that coordinates the migration and differentiation of all other cell types, such as primordial germ cells, and somatic Leydig and peritubular myoid cells. During the fetal and prepubertal stages, Sertoli cells can proliferate in response to FSH, which promotes the proliferative activity of these cells. At puberty (i.e., ~2 weeks old in rodents, 10-14 years old in humans), Sertoli cells become nonresponsive to the mitogenic effects of FSH (Crepieux et al., 2001; Orth, 1984), and their roles in male reproduction switch to the support of male germ cell development. Therefore, the number of

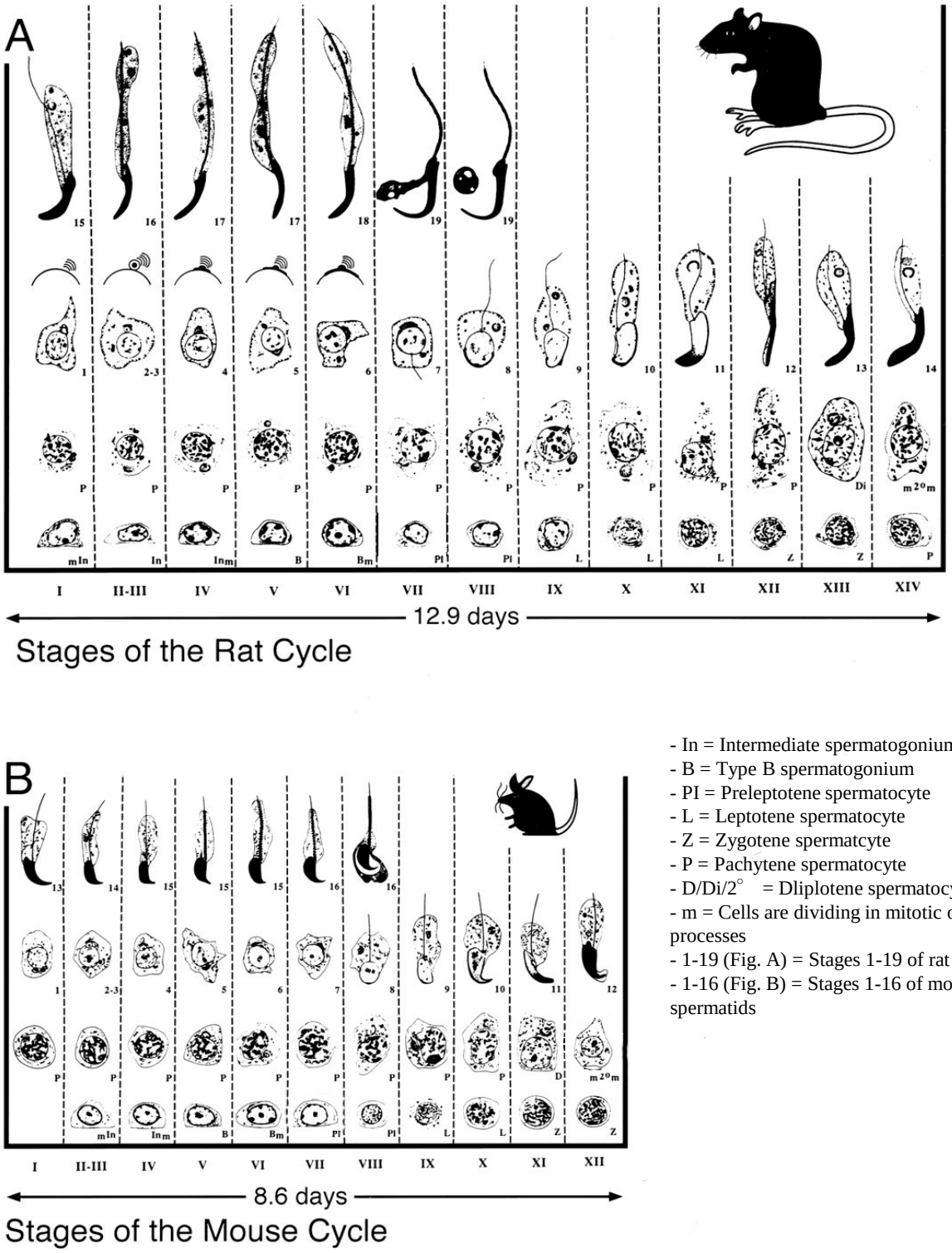

- In = Intermediate spermatogonium
- B = Type B spermatogonium
- PI = Preleptotene spermatocyte
- L = Leptotene spermatocyte
- Z = Zygotene spermatcyte
- P = Pachytene spermatocyte
- D/Di/2° = Dliplotene spermatocyte
- m = Cells are dividing in mitotic or meiotic processes
- 1-19 (Fig. A) = Stages 1-19 of rat spermatids
- 1-16 (Fig. B) = Stages 1-16 of mouse spermatids

Figure 1.6: Spermatogenic cycles of rat and mouse. The diagrams show the histological relationship of spermatogenic cells in the rat (**A**) and mouse (**B**) seminiferous tubules of the testis during spermatogenesis. In each diagram, the lower row of cells is generally closer to the basement membrane and the upper row of cells is generally closer to the lumen of the seminiferous tubule. In the rat, there are 14 stages (indicated by the Roman numerals) that repeat at the same location of the tubule at a 12.9-day interval. In the mouse, there are 12 stages (indicated by the Roman numerals) that repeat at an 8.6-day interval. (Modified from Franca et al., 1998)

Sertoli cells remains relatively constant in the testis throughout adulthood and this number varies depending on the species (i.e., numbers of Sertoli cells per testis are ~18-40 million in rats, ~4 million in mice, and ~130-1800 million in humans) (Auharek et al., 2011; Russell, 1993). While Sertoli cells stop dividing at puberty, germ cells are produced throughout life. However, each Sertoli cell has the ability to support only ~30-50 different germ cells at each stage of the spermatogenic cycle (Weber et al., 1983). The ability of Sertoli cell to sufficiently support limited germ cell numbers would be one of the main reasons why more than 50% of testicular germ cells are destined to undergo apoptosis during spermatogenesis (Cheng and Mruk, 2010). Throughout germ cell development, Sertoli cells play multiple important roles, including structural support, nutritional supply, and phagocytosis of apoptotic germ cells and residual bodies for degradation and recycling of energy/metabolites (see below).

Structural support and immunoprotection: A key feature of Sertoli cell structural support is the blood-testis barrier (BTB), which is made up of tight junctions (TJs) and basal ectoplasmic specialization (ES), a testis specific adherens junction. BTB creates a microenvironment for developing germ cells (beyond the preleptotene primary spermatocytes), and restricts the entry of biomolecules into the adluminal compartment, as well as provides stability for the organization of germ cells in the seminiferous epithelium (Mruk and Cheng, 2004). Since spermatogenic cells beyond the spermatogonial stage first appear at puberty, these cells are not recognized as self, but rather as foreign cells. Therefore, the BTB junctions act as a barrier against the humoral system by isolating the more advanced germ cell types from the immune system so that their antigens do not stimulate autoimmunity (Cheng and Mruk, 2012). Another important structural feature of

Sertoli cells is the apical ES junction in the adluminal compartment. During the last steps of spermatogenesis, elongated spermatids impregnate their heads into the actin basket in the apical ES junction within the Sertoli cell cytoplasm. During these steps, Sertoli cells play important roles in the reconstruction/differentiation of spermatids for normal formation of the sperm head morphology and the final ejection of structurally mature testicular sperm into the seminiferous lumen.

The interactions between Sertoli cells and germ cells are established and maintained via development of direct cellular contact, as well as indirect paracrine mechanisms by their secreting factors (Mruk and Cheng, 2004). Various cell adhesion molecules have been implicated in mediating Sertoli cell-germ cell interactions; for example, *N*-cadherins existing on both the Sertoli cell and germ cell surface, β-1,4-galactosyltransferase on the germ cell surface that binds a carbohydrate receptor on Sertoli cells (Jegou, 1993; Newton et al., 1993). Sertoli cells also secrete several regulatory factors that are important for maintaining a normal spermatogenesis process (Mruk and Cheng, 2004; Russell, 1993); these include growth factors and paracrine/endocrine factors (i.e., transforming growth factor-β, insulin-like growth factor I, epidermal growth factor, stem cell factor, inhibin, activin), transport and bioprotective proteins (i.e., androgen binding protein, transferrin, prosaposin), and proteases and protease inhibitors (i.e., cathepsin L, plasminogen, plasminogen inhibitor).

Nutritional support and energy recycling from phagocytosed/endocytosed substances: Germ cells have specific metabolic needs, which change during their development into spermatozoa. Sertoli cells utilize a variety of substrates, including glucose and fatty acids, and pathways to fulfill their own metabolic requirements and those of developing germ cells. The developing germ cells, especially those that are shielded behind

BTB, are metabolically inactive and depend mainly on Sertoli cells for nutritional support. For example, glucose, which is unable to pass through BTB, is taken up and converted to lactate by Sertoli cells, and lactate is then transported to and used by germ cells (mainly spermatids) to synthesize ATP (Rato et al., 2012). In addition, under normal physiological conditions, a large number of apoptotic germ cells (>50% of all germ cells produced) are phagocytosed and degraded by Sertoli cells. These materials provide an enormous amount of precursors that can be converted to metabolites for the energy resources of Sertoli cells as well as of developing germ cells. Recent studies have demonstrated that Sertoli cells cultured *in vitro* can use engulfed apoptotic spermatogenic cells to form lipid droplets (Wang et al., 2006), which can then produce energy through the β-oxidation pathway (Xiong et al., 2009). Specifically, in the complete absence of glucose, cultured Sertoli cells can still maintain their viability and produce ATP and lactate via the metabolism of lipids (Xiong et al., 2009). In mice, inactivation of the genes involved in lipid metabolism (i.e., hormone-sensitive lipase) causes defects in spermatogenesis and results in infertility. The hormone-sensitive lipase (HSL) is an enzyme that catalyzes the hydrolysis of triacylglycerols and cholesteryl esters and is expressed in adipose and non-adipose tissues. However, HSL has long been thought to play a major role in lipolysis, principally in the adipose tissues. Surprisingly, HSL-deficient mice have a modest adipose phenotype with unexpectedly reduced fat mass and body weight, but show major defects in spermatogenesis (i.e., multinucleation of spermatids, abnormal shapes and reduced numbers of elongating spermatids, vacuolization of seminiferous epithelium) (Chung et al., 2001). Although the exact mechanisms of how HSL regulates the shaping of spermatids are not known, the phenotypes of HSL-deficient mice provide compelling evidence that proper lipid metabolism is needed for normal germ cell development (Chung et al., 2001; Hermo et al., 2008). It is

possible that the arrest/defects in spermatogenesis in HSL-deficient mice come from the lack of fatty acids normally generated HSL from triacylglycerols and cholesteryl esters. This pool of fatty acids may be essential for the continuation of spermatogenesis.

1.2.1.3 Sperm structure

Highly differentiated and polarized spermatozoa are the final product of the spermatogenesis process. Each spermatozoon consists of two major parts: the head and the tail (Figure 1.7A). The sperm head consists of a highly compact nucleus containing the male haploid genome, very little cytoplasm, and the acrosome. The acrosome, located on the anterior portion of the sperm head, is a large secretory vesicle enclosed with a continuous membrane, which is generally recognized as having two zones (i.e., the outer acrosomal and the inner acrosomal membrane). The outer acrosomal membrane is beneath the anterior sperm head plasma membrane, and the inner acrosomal membrane lies over the nuclear membrane (Figure 1.7A). The acrosome houses a number of molecules, including hydrolytic enzymes and egg binding proteins, which are believed to aid sperm to penetrate the ZP. In this thesis, however, I will present evidence that certain acrosomal proteins are involved in the initial sperm-ZP interaction.

The sperm head plasma membrane also exhibits further lateral surface heterogeneity, which can be identified based on differences in its biophysical and biochemical properties as shown by freeze fracture methods and staining patterns with specific lectins and antibodies (Eddy, 2006). The major regions of the sperm head plasma membrane are the acrosomal region (or anterior sperm head) and the postacrosomal region (posterior head); the size and shape of these sperm plasma membrane regions vary between species (Figure 1.7B).

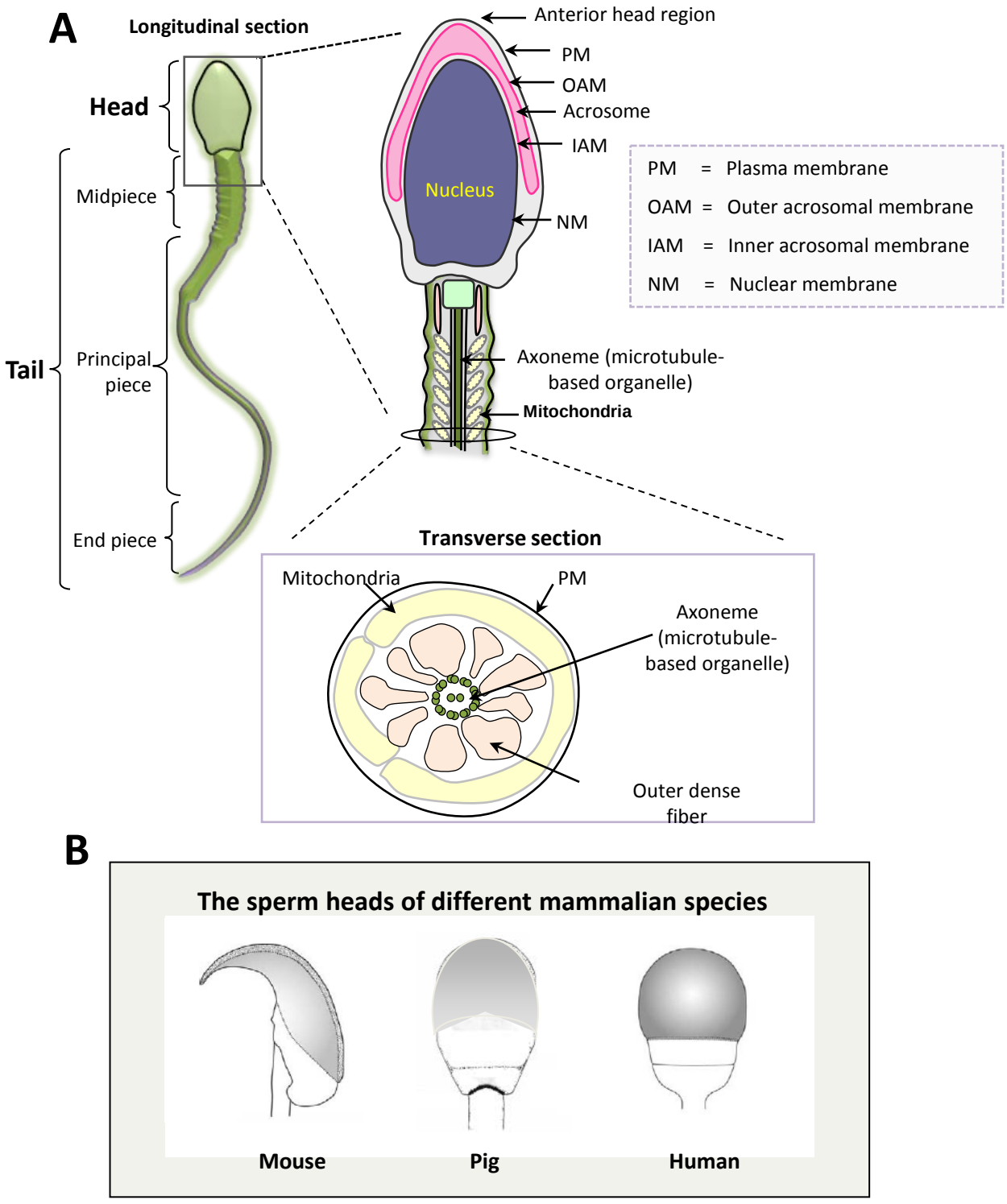

Figure 1.7: Sperm structure. A) Diagram showing anatomical structure of spermatozoon. A mammalian spermatozoon consists of a head and a tail. The head contains a nucleus with a highly condensed chromatin structure, and an acrosome, a secretory granule located at the anterior portion of the sperm head. A tail consists of midpiece, principal piece and endpiece. The midpiece contains the helically arranged mitochondrial sheath surrounding the axoneme core. These mitochondria play a role in energy production for sperm motility. **B)** Surface view of mouse, pig and human sperm heads. The sperm head surface can be divided into two major regions, the acrosomal region (gray color) and the post acrosomal region (white color). The acromal region or the anterior sperm head plasma membrane (APM) that overlies the acrosome is the site for initial sperm-egg binding and acrosome reaction.

The acrosomal region or anterior sperm head plasma membrane (APM) is the site responsible for the initial sperm-egg interactions and the acrosome reaction, which involves fusion of the APM and the outer acrosomal membrane (Boerke et al., 2008; Eddy, 2006).

The sperm tail consists of the connecting piece, the midpiece, the principal piece, and the end piece (Figure 1.7A). The connecting piece of the tail is a narrow segment containing the paired centrioles. The midpiece of the tail consists of the helically arranged mitochondrial sheath, the axoneme and the outer dense fibers of the flagellum. The mitochondria are important for energy production for sperm motility. The lower limit of the midpiece is marked by the termination of the mitochondrial helix at the annulus. The principal piece, the longest segment of the tail, is composed of a central axoneme surrounded by the outer dense fibers and the fibrous sheath. The end piece is a very short segment of the tail in which only the axoneme is present (Eddy, 2006; Kierszenbaum, 2002).

1.2.2 Epididymal sperm maturation

The epididymis is a highly convoluted tubule connected to the testis and comprised of three major segments: caput (head), corpus (body), and cauda (tail) (Figure 1.1). Early discovery revealed that testicular sperm were unable to either move forward progressively or to interact with the ZP of the oocyte; however, sperm retrieved from the caudal epididymis into an appropriate medium (containing energy metabolites and a buffering substance) possessed both forward motility and ZP-binding ability (Cooper and Orgebin-Crist, 1975, 1977). These studies provided the first evidence that sperm undergo changes during their transit in the epididymis that allow them to acquire motility and fertilization capacity. Since

sperm that enter the epididymis are already in a transcriptionally inactive state with limited biosynthesis capacity, the modification process occurring on epididymal sperm is not under genomic control (Eddy, 2002). The molecular changes during this process are therefore driven by dynamic interactions between the surface of the epididymal sperm and their surrounding microenvironment. Proteomic studies in several mammalian species reveal dramatic changes in the composition of epididymal fluid collected from different regions of the epididymis, reflecting dynamic protein secretion and absorption throughout the epididymal duct (Dacheux et al., 2006; Dacheux et al., 2009). Within the caput epididymis, testicular fluid/proteins (e.g., transferrin, albumin) are known to be removed from the entering testicular sperm. As the caput epididymal sperm descend through the corpus epididymis, they begin to acquire their motility and fertilizing ability; these attributes carry on as the sperm move through the corpus, and reach an optimum level as they enter the cauda region, where they are stored in a quiescent state prior to ejaculation (Cornwall, 2009; Gatti et al., 2004).

The mechanisms underlying the acquisition of forward motility by caudal epididymal sperm have not yet been completely understood. However, a number of potential contributing factors have been identified, including the forward motility protein (FMP), which enhances the forward motility of bovine caput epididymal sperm (Acott et al., 1983). Proteins involved in glycolysis (i.e., phosphoglycerate kinase 2, glyceraldehyde 3-phosphate dehydrogenase) have also been suggested to play roles in providing energy for the forward progressive movement of sperm (Danshina et al., 2010; Miki et al., 2004). In addition, post-translational modifications of sperm proteins, such as proteolysis and phosphorylation, have been suggested to promote the motility status of epididymal sperm (Baker et al., 2005).

The acquisition of ZP-binding ability by caudal epididymal sperm is likely dependent on adsorption of new components secreted from the epididymal epithelium onto the sperm surface, as well as on modification of the existing sperm surface molecules (Dacheux et al., 2003). A number of proteins with ZP affinity, additional to those already synthesized during spermatogenesis, are deposited onto the sperm surface during the epididymal transit; these include milk fat globule-EGF factor 8/MFGM (aka SED1, P47, or lactadherin) (Ensslin and Shur, 2003), arylsulfatase A (ARSA) (Weerachatyanukul et al., 2003), and sperm adhesion molecule 1 (SPAM1) (Zhang and Martin-Deleon, 2003). Chaperones with relevance in sperm-egg interaction, including those in the heat shock protein family (i.e., Hsp10, Hsp60, and Grp78), are also acquired from epididymal fluid onto the sperm surface (Lachance et al., 2010; Walsh et al., 2008). Moreover, some of the pre-existing proteins on the epididymal sperm plasma membrane, such as fertilin alpha and beta (aka ADAM1 and ADAM2, respectively), cyritestin (aka ADAM3) and alpha-D-mannosidase, are cleaved by proteolytic enzymes or redistributed into different sperm plasma membrane domains. The processed forms of these proteins are presumably those required for their later actions in sperm-egg interactions (Gatti et al., 2000; Kim et al., 2006; Stein et al., 2005; Tulsiani et al., 1995). Moreover, there are other proteins found in substantial amounts in the epididymal fluid of many mammalian species, such as lactoferrin, clusterin, cholesterol transfer protein, glutathione-peroxidase, albuminoidal proteins, prostaglandin, prostaglandin D2 synthase, hexosaminidase and procathepsin D (Dacheux et al., 2009; Fouchecourt et al., 2000). These proteins, which exhibit either transport and binding functions or enzymatic activity, likely contribute to sperm fertilizing capacity by facilitating the exchange of proteins or lipids between the spermatozoa and the surrounding fluid during epididymal maturation (Dacheux et al., 2005).

In addition to changes in the sperm proteome, modification of the lipid components on the epididymal sperm plasma membrane has been suggested to contribute to the forward motility and fertilizing ability of sperm (Yanagimachi, 1994). For example, in mice, phospholipids containing polyunsaturated fatty acid (PUFA) (i.e., 20:4 *n*-6; 22:6 *n*-3) were found in significantly increased levels in the caudal epididymal sperm plasma membrane (Rejraji et al., 2006). Since a high level of these PUFA-containing phospholipids was detected in mouse epididymosomes (small membranous vesicles present in epididymal fluid), the epididymosomes have been suggested to facilitate the transfer of these lipids onto the sperm surface (Rejraji et al., 2006). The enrichment of PUFA-containing phospholipids on the sperm plasma membrane would contribute to higher sperm membrane fluidity, which is important for sperm movement as well as for subsequent membrane fusion related events, such as the acrosome reaction and sperm-egg plasma membrane fusion (see below).

1.2.3 Capacitation

Although sperm acquire the potential to fertilize an egg within the epididymis, their fertilizing ability is suppressed until they undergo additional physiological and biochemical changes in the female reproductive tract. These additional changes were first recognized by MC Chang (Chang, 1951) and CR Austin (Austin, 1951), who observed that freshly ejaculated mammalian sperm were unable to fertilize eggs *in vivo* until they had resided within the female reproductive tract for a certain period of time. The term “capacitation” is then used to collectively describe these changes, and sperm that have completed the capacitation process are referred to as “capacitated” (Austin, 1952; Chang, 1959). As a

consequence of capacitation, sperm acquire hyperactivated motility, characterized by a vigorous whiplash-like beating pattern of flagellum (Yanagimachi, 1994; Yanagimachi and Chang, 1963), which is required for sperm navigation through the oviduct and for penetration of the ZP (see more in sperm-egg interaction section below). The capacitated sperm also gain full fertilizing ability mainly through sperm surface remodelling, which allows the ZP-binding molecules on the sperm head to become exposed and reorganized in such a way that they are together and ready for further ZP interaction, leading to acrosome reaction and fertilization (see more in sperm-egg interaction section below).

Capacitation can be induced *in vitro* by simply incubating sperm in a chemically defined medium containing albumin, bicarbonate (HCO_3^-) and calcium (Ca^{2+}) ions, all of which are known to be enriched in the female reproductive tract environment (Bavister, 1973; Edwards et al., 1968; Yanagimachi, 1994). This simplified *in vitro* capacitation system has allowed researchers to study the molecular mechanisms underlying capacitation. So far, although the precise mechanisms remain to be unambiguously established, some biochemical and biophysical alterations pertinent to capacitation have been identified, including modification of the sperm surface and the initiation of specific signal transduction pathways (Aitken and Nixon, 2013; Florman and Ducibella, 2006).

1.2.3.1 Sperm surface modifications during capacitation

Several lines of evidence indicate that during capacitation sperm undergo changes on their surface, especially at the anterior head region where sperm interact with ZP, so that they can gain full ability to bind to ZP and fertilize the egg (Florman and Ducibella, 2006). During capacitation, one of the early changes on the sperm surface is the loss of

decapacitation factors that inhibit the fertilizing ability of sperm (Fraser, 1984; Fraser et al., 1990; Reddy et al., 1979; Redgrove et al., 2012). The decapacitation factors can be of either epididymal fluid or seminal plasma origin and they are believed to prevent sperm from undergoing premature capacitation and acrosome reaction (Lasserre et al., 2001; Redgrove et al., 2012). In fertility clinics or laboratories, sperm are prepared by the "swim up" method and/or by Percoll density gradient centrifugation to ensure that seminal plasma or epididymal fluid containing these decapacitation factors is removed prior to the induction of capacitation. Several protein candidates with potential decapacitation activity have been identified, including a high molecular weight antifertility factor (AF-1) (Reddy et al., 1982), decapacitation factor (DF) glycoprotein (Fraser, 1998), phosphatidylethanolamine binding protein 1 (Gibbons et al., 2005), and beta-defensin 126 (DEFB126) (Tollner et al., 2008).

Cholesterol efflux from the sperm plasma membrane is known to be a major change during capacitation. This efflux occurs when sperm are exposed to an environment rich in appropriate cholesterol sinks, such as albumin and high-density lipoproteins (HDL) and apoliporoteins (e.g. apo A-I), present in the female reproductive tract (Argraves and Morales, 2004; Davis et al., 1980; Davis et al., 1979; Jaspard et al., 1997; Langlais et al., 1988; Therien et al., 1997). In human sperm, a fraction of cholesterol (~6%) is stabilized in the sperm plasma membrane as cholesterol sulfate (Langlais et al., 1981; Sion et al., 2001). It has been proposed that while sperm ascend the female reproductive tract, cholesterol sulfate (or desmosterol sulfate in some rodent species) is converted to cholesterol via steroid sulfatase activity (Roberts, 1987), and the free cholesterol can then be removed from the sperm surface by sterol acceptor molecules. The efflux of cholesterol from the sperm plasma membrane decreases the cholesterol/phospholipid ratio (Davis, 1981) and accounts for a

striking increase in the membrane fluidity (Wolf et al., 1986) as well as for redistribution of sperm surface components, detected by fluorescently labeled lectins or specific antibodies (Cross and Overstreet, 1987; Rochwerger and Cuasnicu, 1992; Shalgi et al., 1990). Moreover, a recent real time tracking study using fluorescently conjugated sperm antigens demonstrated that cholesterol efflux initiates the diffusion of clusters of ZP-binding molecules over the acrosomal region of live boar sperm (Jones et al., 2010). The observed redistribution of sperm surface components is in line with results from our lab and other groups showing increased levels of the liquid-ordered membrane domains, also called lipid rafts, on the sperm surface following capacitation (Bou Khalil et al., 2006; Nixon et al., 2007; Shadan et al., 2004; Thaler et al., 2006; Van Gestel et al., 2005).

Lipid rafts are defined as liquid-ordered membrane microdomains containing high amounts of cholesterol, glycosphingolipids, and saturated phospholipids (Brown and London, 2000; Simons and Toomre, 2000). Lipid rafts have been isolated from somatic cells as detergent resistant membranes (DRMs) with a low buoyant density (1.1 g/ml); cells are treated with a low concentration of a non-ionic detergent (e.g., Triton X-100) in the cold, followed by sucrose density ultracentrigation, which allows the extracted DRMs to float as a light scattering band towards the top of the gradient (Schuck et al., 2003). In somatic cells, numerous proteins involved in cell adhesion and signaling are found in the isolated DRMs/lipid rafts. These membrane domains are therefore implicated as platforms of cell adhesion and cell signaling molecules (Foster et al., 2003; Simons and Ehehalt, 2002). Significantly, a number of ZP-binding and cell-signaling molecules have been identified in the capacitated sperm lipid rafts isolated as DRMs; therefore, these sperm membrane domains are believed to serve as platforms of key molecules important for sperm-ZP

interaction (Nixon and Aitken, 2009; Redgrove et al., 2012; Tanphaichitr et al., 2007a; Van Gestel et al., 2005). In fact, our lab has demonstrated that capacitated sperm have increased levels of lipid rafts/DRMs that possess direct ZP affinity, with a lower K_d value than that of non-capacitated sperm DRMs (Bou Khalil et al., 2006). The increased capacity and affinity of capacitated sperm lipid rafts for the ZP interaction may result from the increase in sperm plasma membrane fluidity. This increased membrane fluidity promotes the lateral movement of ZP-binding molecules to an appropriate proximity (complex formation) for further ZP interaction (see more about sperm lipid rafts and their roles in sperm-egg interaction below). The increase in plasma membrane fluidity may also facilitate docking of the outer acrosomal membrane to the overlying sperm anterior head plasma membrane; hybrid membrane vesicles are in fact isolated from pig sperm subjected to nitrogen cavitation (see below for the APM (sperm anterior head plasma membrane) vesicle section) (Tsai et al., 2010). This observed membrane apposition implicates that the sperm anterior head plasma membrane may become porous, thus initiating the trafficking of molecules in an intracellular compartment (i.e., acrosome) to the sperm head surface (as shown here in my thesis).

1.2.3.2 Signaling events related to (or leading to) sperm capacitation

The influx of HCO_3^- and Ca^{2+} into the sperm cytosol is important for sperm capacitation because it activates a signalling cascade involving cross-talk between several pathways, which ultimately lead to the enhanced fertilizing ability and hyperactivated motility of capacitated sperm (Breitbart, 2002; Redgrove et al., 2012). The most recognized pathway known as a hallmark of capacitation is the cAMP-dependent tyrosine

phosphorylation. The HCO_3^-/Ca^{2+} influx into the sperm cell activates a unique form of soluble adenylyl cyclase (SACY), which synthesizes cAMP from ATP, and results in an increase of intracellular cAMP concentration (Buffone et al., 2014; Esposito et al., 2004; Wertheimer et al., 2013). cAMP then activates protein kinase A (PKA), leading to the induction of tyrosine phosphorylation across a number of protein substrates. Since PKA can only phosphorylate proteins on serine/threonine residues, tyrosine phosphorylation through PKA is likely mediated by activation of an intermediary protein tyrosine kinase (PTK) and/or inhibition of protein tyrosine phosphatase (PTP), or both (Battistone et al., 2014; Redgrove et al., 2012; Visconti et al., 2002). A number of proteins localized in the sperm tail are known to be tyrosine phosphorylated during capacitation, such as A-kinase anchor proteins (AKAPs) (Ficarro et al., 2003), voltage-dependent anion channels (VDACs) (Arcelay et al., 2008). Significantly, the tyrosine phosphorylation of sperm tail proteins has been causally related to the induction of hyperactivated motility of capacitated sperm (Mahony and Gwathmey, 1999; Nassar et al., 1999). In addition to the increased phosphorylation, hyperactivated motility requires the alkanization of the sperm tail by calcium influx through calcium ion channel proteins, such as proteins in the Catsper family (Qi et al., 2007; Singh and Rajender, 2014). Moreover, proteins localized to the sperm head, including acrosin-binding protein (sp32 or ACRBP), heat shock protein 60 (Hsp60 or HSPD1) and endoplasmin (HSP90B1), have also been shown to become tyrosine phosphorylated in capacitated sperm (Arcelay et al., 2008; Asquith et al., 2004). The tyrosine phosphorylation of sperm head proteins during capacitation has been suggested to facilitate the protein translocation from an intracellular site onto the sperm surface at the ZP-binding site (Asquith et al., 2004; Dube et al., 2005).

Furthermore, in response to the HCO_3^- influx, the cAMP-dependent tyrosine phosphorylation pathway has been shown to activate a sperm-specific phospholipid scramblase activity, which causes disruption of the asymmetric distribution of plasma membrane phospholipids (de Vries et al., 2003; Gadella and Harrison, 2000, 2002). The redistribution of phospholipids between outer and inner leaflets of the capacitated sperm plasma membrane is suggested to prime the cholesterol efflux and contribute to the global membrane fluidity increase (Harrison and Gadella, 2005). In addition, changes in intracellular concentrations of ions (e.g., HCO_3^-) may be responsible for the increase in intracellular pH of sperm, which is known as an important regulator of capacitation (Vredenburgh-Wilberg and Parrish, 1995; Zeng et al., 1996).

Besides HCO_3^- and Ca^{2+}, reactive oxygen species (ROS) (e.g., superoxide, hydrogen peroxide, and nitric oxide) is also recognized as an upstream inducer of the tyrosine phosphorylation events associated with capacitation in several mammalian species (Aitken, 1995; O'Flaherty et al., 2006; Rivlin et al., 2004; Roy and Atreja, 2008). Moreover, ROS scavengers (i.e., superoxide dismutase) have been shown to robustly suppress human sperm capacitation (de Lamirande and Gagnon, 1993). During capacitation, ROS likely regulates tyrosine phosphorylation of sperm tail proteins via downstream events, including the cAMP/PKA pathway, which results in an increase in cAMP. The cAMP increase leadsto activation of PKA and phosphorylation of PKA substrates, as well as the phosphorylation of mitogen-activated protein kinase kinase (MEK)-like proteins and that of Thr-Glu-Tyr motif-containing proteins (de Lamirande and O'Flaherty, 2008).

1.2.4 Sperm-egg interactions

1.2.4.1 Sperm-egg interaction steps that result in fertilization

Sperm-egg interactions take place in the oviduct, which consists of three major parts: the uterotubal junction, the isthmus, and the ampulla (Figure 1.8). In the ampulla of the oviduct, capacitated sperm meet an ovulated egg(s) (or oocyte), which is encased within a thick layer (7-20 μm) of the extracellular matrix, zona pellucida (ZP). ZP glycoproteins interacting with each other in the form of fibrils are the main constituents of the ZP. Hyaluronic acid is also part of the ZP (Talbot, 1984). Surrounding the ZP are layers of cumulus cells interlinked with long chained glycosaminoglycans (GAGs), namely hyaluronic acids and chondroitin sulfate proteoglycans. Both of these GAGs endow viscosity to the cumulus oocyte complexes (COCs) (Figure 1.8), allowing their safe capture by the oviductal infundibulum during ovulation (Florman and Ducibella, 2006; Gadella, 2012). Capacitated sperm must penetrate through the cumulus cell layers and the ZP prior to entering the egg. The original concept, based on studies in the mouse system, is that the capacitated sperm that have traversed the cumulus cell layers are still acrosome intact, and that acrosome-intact sperm have maximum ability to bind to the ZP. The ZP glycoprotein (mZP3 in the mouse system-see below) then induces the acrosomal exocytosis on the ZP-bound sperm. The completion of acrosomal exocytosis occurring on the ZP is known as the acrosome reaction, which involves fusion of the sperm plasma membrane overlying the acrosome and the outer acrosomal membrane. This fusion results in the release of the whole acrosomal content from the surface and leaves only the inner acrosomal membrane on the anterior head surface of the acrosome-reacted sperm.

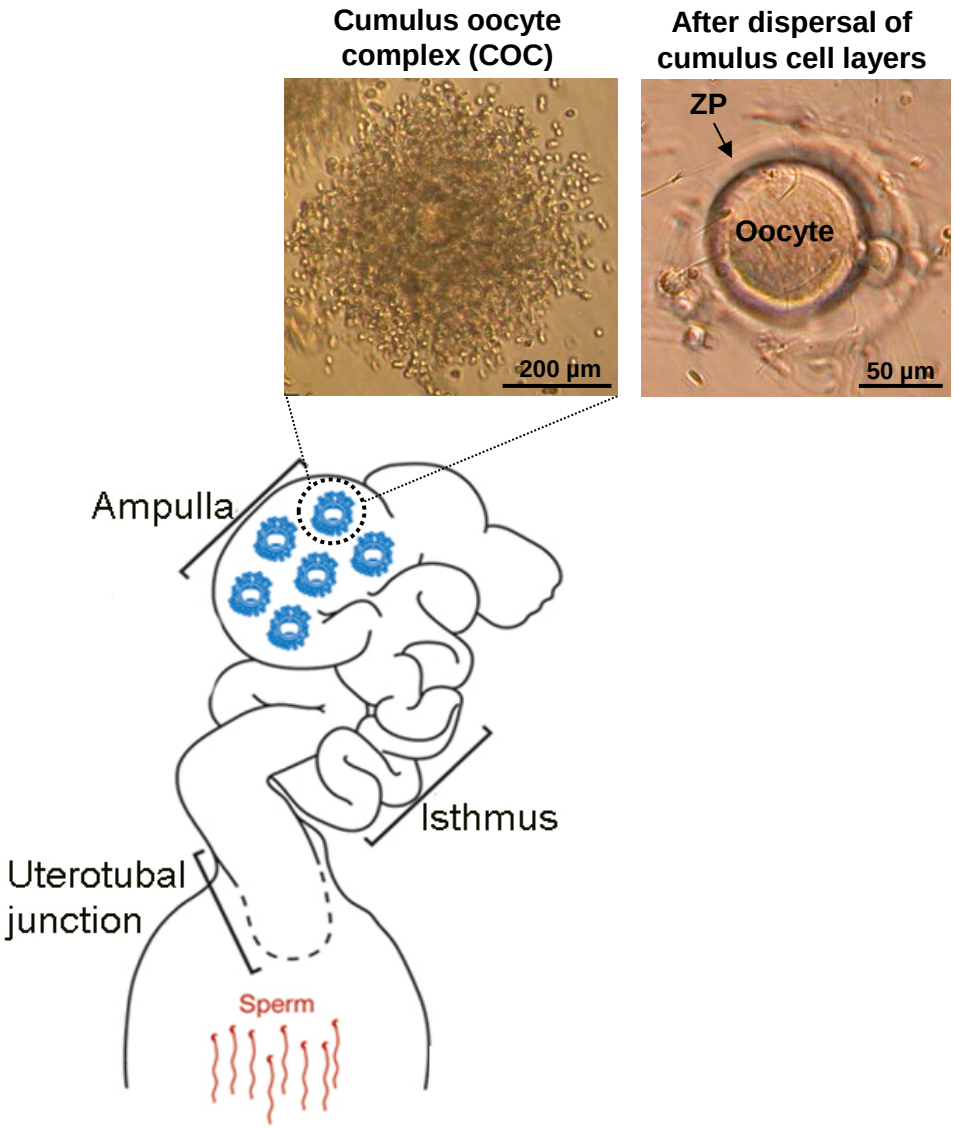

Figure 1.8: Oviduct with ovulated cumulus oocyte complexes (COCs). A diagram showing three main parts of the mouse oviduct: uterotubul junction, isthmus, and ampulla (modified from Ikawa et al., 2010). Sperm must swim through the oviduct until they locate the ovulated COCs in the ampulla of the oviduct. Each ovulated COC consists of the oocyte covered by ZP that is surrounded by multilayers of cumulus cells interlinked with long chained glycosaminoglycans. Light microscopic images showing intact COC (left) and the COC after the cumulus cell dispersion (right).

Following the acrosome reaction, the acrosome-reacted sperm still continue to bind to the ZP (Florman and Ducibella, 2006; Yanagimachi, 1994). However, the concept that acrosomal exocytosis is initiated by the ZP has been recently challenged by new observations via high-powered videomicroscopy of capacitated mouse sperm incubated with COCs. This finding indicates that acrosomal exocytosis has already been initiated during penetration of the sperm through the cumulus cell layers, even before they come in contact with the ZP (Jin et al., 2011). This result also agrees with the finding that cumulus cell-derived progesterone can induce acrosomal exocytosis (Guidobaldi et al., 2008). Nonetheless, the acrosome matrix is still relatively intact and sperm still have to complete the acrosome reaction on the ZP (as described above). Hydrolases (e.g., proteases, hyaluronidase) released from the acrosome during the acrosome reaction, together with the thrusting force of hyperactivated motility attained during capacitation, would allow acrosome-reacting/reacted sperm to penetrate through the ZP layer (Florman and Ducibella, 2006; Yanagimachi, 1994). Acrosome-reacted sperm with the inner acrosomal membrane exposed on their head surface then enter the perivitelline space, and bind to the egg plasma membrane. One acrosome-reacted sperm then fuses with the egg plasma membrane; these binding and fusion processes likely rely on interactions between the sperm surface molecules (i.e, ADAMs, Izumo) and the egg plasma membrane molecules (i.e., integrin, CD9, Juno) (Bianchi et al., 2014; Florman and Ducibella, 2006). Finally, the spermatozoon that has fused with the egg plasma membrane becomes incorporated into the egg proper, signifying that fertilization has occurred.

1.2.4.2 Zona pellucida (ZP)

The mammalian ZP consists of 3-4 highly glycosylated proteins, each of which shows peptide sequence homology across species (Florman and Ducibella, 2006; Harris et al., 1994; Tanphaichitr et al., 2007a). The ZP glycoproteins of different mammalian species are known to be differentially glycosylated and the differences in their carbohydrate moieties are considered as the main factor underlying the species-specific binding to the sperm (Tulsiani and Abou-Haila, 2012). Among all mammalian species, the biochemical properties of mouse ZP glycoproteins have been most studied, mainly through the pioneering work of Paul Wassarman. Wassarman et al showed that mouse ZP is composed of three ZP glycoproteins, mZP1 (~200 kDa-dimeric form), mZP2 (120 kDa), and mZP3 (83 kDa); the mZP2/mZP3 heterodimers form long filaments that are cross-linked by mZP1 (Greve and Wassarman, 1985; Litscher et al., 2009; Wassarman and Litscher, 2008). Wassarman's group also demonstrated that mZP3 is the sperm "primary receptor" responsible for the interaction with acrosome-intact sperm and for the subsequent induction of the acrosome reaction, whereas mZP2 is the "secondary receptor" for acrosome-reacted sperm (Bleil and Wassarman, 1980; Wassarman and Litscher, 2008). The terms "primary and secondary receptors" came from the original concept that sperm binding to ZP occurs in a two-step manner: the acrosome-intact sperm first bind to the primary receptor (mZP3), which results in the acrosome reaction (believed to be an all-or-none event); the acrosome-reacted sperm then stay bound to the ZP via interaction with the secondary receptor (mZP2) (Florman and Ducibella, 2006; Yanagimachi, 1994). However, more recent studies from Gerton et al reveal that the acrosome reaction occurs in a gradual, continuous manner and that both mZP3 and mZP2 are involved in the binding of sperm undergoing exocytosis (Buffone et al., 2008;

Kim and Gerton, 2003). Dean et al. later revealed that mZP2 also plays a role in the binding of acrosome-intact sperm (Avella et al., 2014; Gahlay et al., 2010). Regardless of this confusion, the studies from knockout mice reveal that female mice lacking either mZP2 or mZP3 are infertile (Rankin et al., 1996; Rankin et al., 2001). Although the female mice without ZP1 can sire offspring, they have eggs with structurally defective ZP and reduced fecundity (Rankin et al., 1999). All of these results indicate the significance of mouse ZP glycoproteins, especially mZP2 and mZP3, in female fertility.

The porcine ZP is the second most characterized mammalian ZP and it has been shown to contain four glycoproteins (ZP1, ZP2, ZP3, ZP4 with molecular masses of ~90, ~65, ~55, ~25 kDa, respectively) following separation under a reducing condition on a 2D-gel electrophoresis (Hedrick and Wardrip, 1987; Tulsiani et al., 1997). Among these four pig ZP glycoproteins, pig ZP3 exists at the highest level and constitutes ~75% by weight of the total ZP glycoproteins. The pig ZP3 is a heterooligomer of pig ZP3α (aka ZPB) and ZP3β (aka ZPC). Based on peptide sequence homology, pig ZP3β and pig ZP3α are orthologues of mZP3 (~66% homology) and mZP1 (~50% homology), respectively (Tanphaichitr et al., 2007a). However, it is a known fact that pig ZP3 is the sperm receptor, with ZP3α being the major player in sperm binding (Sacco et al., 1989; Yurewicz et al., 1993; Yurewicz et al., 1998). Since pig ZP3 is the major glycoprotein component of pig ZP and possesses sperm binding ability, it can be used in place of the whole pig ZP particulate for the binding study with intact sperm (Yonezawa et al., 1995) or sperm protein extracts (as shown in my thesis study).

1.2.4.3 Sperm proteins with ZP affinity: lessons learned from studies of knockout mice

While only a few ZP glycoproteins are involved in the sperm-ZP interaction, a number of sperm head proteins have been individually shown to possess ZP affinity (Ikawa et al., 2010; Stein et al., 2006) (see Table 1.1 for the list of ZP-binding proteins). These proteins have different origins and their locations on the sperm head vary, depending on the stage of sperm development/maturation. Some of the ZP-binding proteins are synthesized in testicular germ cells, and targeted to the acrosome or to the sperm head surface during spermiogenesis or subsequent stages of sperm development/maturation (including capacitation, as shown in my thesis). These proteins include UDP-galactose:beta-N-acetylglucosamine beta-1,4 galactosyltransferase I (GALT) (Scully et al., 1987), zonadhesin (ZAN) (Bi et al., 2003; Hickox et al., 2001), and proacrosin/acrosin (ACRO) (Anakwe et al., 1991). Alternatively, some ZP-binding proteins existing on the plasma membrane of mature sperm heads are originated from epididymal fluid, including MFGM (aka SED1/P47) (Ensslin et al., 1998) and ARSA (Weerachatyanukul et al., 2003), or from seminal plasma, such as spermadhesins (AQN-1, AQN-3, AWN) (Calvete et al., 1996; Dostalova et al., 1995; Jonakova et al., 2007). Interestingly, a number of ZP-binding proteins, particularly those synthesized during spermatogenesis, are known for their presence in the acrosome of non-capacitated sperm; these include ZAN (Hickox et al., 2001; Tardif et al., 2010), proacrosin/acrosin (Howes et al., 2001), sperm acrosomal protein SP-10 (ASPX) (Coonrod et al., 1996), sperm protein 56/sp56 (aka ZP3R) (Cheng et al., 1994), and zona pellucida binding protein 1 (ZPBP1, aka IAM38, and sp38) (Mori et al., 1993; Yu et al., 2006). The roles of these acrosomal ZP-binding proteins in the initial sperm-ZP interaction have been overlooked because they are thought to become exposed on the sperm head surface only

when sperm are undergoing or have undergone acrosomal exocytosis on the ZP. In other words, these acrosomal proteins have been considered to play roles in adhering acrosome-reacting/reacted sperm to the ZP (Buffone et al., 2008; Tanphaichitr et al., 2007a). However, recent findings suggest that acrosomal proteins with ZP affinity may be exposed on and/or trafficked to the capacitated sperm surface prior to sperm-ZP interaction (Avella and Dean, 2011; Jin et al., 2011). New evidence supporting the roles of the acrosomal proteins on the initial binding of sperm to ZP is presented here (see RESULTS).

The existence of so many ZP-binding proteins on the sperm head leads to the question of which proteins are truly essential for the sperm-ZP interaction, and thus male fertility. To verify the physiological significance of each ZP-binding molecule, knockout mice genetically null in a ZP-binding molecule have been generated and assessed for various parameters that indicate their male fertility status (i.e., ability to sire offspring, sperm number, motility, morphology, and *in vitro* fertilizing ability). Unexpectedly, the results show that males in a number of these knockout mouse colonies, including *Galt*$^{-/-}$, *Zan*$^{-/-}$, *SED1*$^{-/-,}$ *Acr*$^{-/-}$, *Arsa*$^{-/-}$, can still sire offspring, although they are usually subfertile (Baba et al., 1994a; Ensslin and Shur, 2003; Hess et al., 1996; Lu et al., 1997; Tardif et al., 2010; Xu et al., 2011). These findings indicate that a single ZP-binding molecule can be dispensable for the ZP binding, leading to the concept that a number of ZP-binding molecules may act together as a complex or as backups for one another (Tanphaichitr et al., 2007a). However, why there is such redundancy in the ZP-binding molecules on the sperm head requires an explanation. One logical explanation is that fertilization is the fundamental process to sustain the continuation of a species; therefore, the functional redundancy of several ZP-binding molecules may be needed to secure this process.

Table 1.1: Sperm proteins that have been described for their ZP affinity

#	Full names	Alternative names	*In vitro* studies showing ZP affinity	Localization on protein in non-capacitated sperm [species]	Knockout mice and their fertility
1	Milk fat globule EGF-factor 8	MFGM, MFG-E8, P47, SED1	Yes (Ensslin et al., 1998)	APM [mouse, pig] (Ensslin and Shur, 2003; Petrunkina et al., 2003)	YES, Fertile (Ensslin and Shur, 2003)
2	N-acetylglucosamine beta-galactosyltransferase	GalT, GalTase	Yes (Miller et al., 1992)	APM [mouse] (Lopez et al., 1985)	YES, Fertile (Lu et al., 1997)
3	Hyaluronidase PH-20	SPAM1	Yes (Hunnicutt et al., 1996; Primakoff et al., 1985)	APM [mouse, guinea pig, human] (Lin et al., 1994; Overstreet et al., 1995; Primakoff et al., 1985)	YES, Fertile (Baba et al., 2002)
4	Carbohydrate-binding protein AQN1	AQN1, spermadhesin	Yes (Veselsky et al., 1999)	APM [pig] (Jonakova et al., 1998)	n/a
5	Carbohydrate-binding protein AQN3	AQN3, spermadhesin	Yes (Veselsky et al., 1999)	APM [pig] (Jonakova et al., 1998)	n/a
6	Carbohydrate-binding protein AWN	AWN, spermadhesin	Yes (Calvete et al., 1994)	Whole plasma membrane [pig] (Petrunkina et al., 2000)	n/a
7	Glutathione S-transferase	GST	Yes (Hemachand et al., 2002)	APM and post acrosomal region [goat] (Gopalakrishnan et al., 1998)	n/a
8	Arylsulfatase A	ARSA	Yes (Carmona et al., 2002; Tantibhedhyangkul et al., 2002; Xu et al., 2012)	APM [mouse, pig] (Carmona et al., 2002; Weerachatyanukul et al., 2003)	YES, Subfertile (Hess et al., 1996; Xu et al., 2011)
9	Proacrosin-binding protein	ACRBP/sp32	n/a	Acrosome [mouse, pig] (Tardif et al., 2012; Dube et al., 2005)	n/a
10	Zonadhesin	ZAN	Yes (Hardy and Garbers, 1995)	Outer acrosomal membrane [pig] (Bi et al., 2003)	YES, Fertile (Tardif et al., 2010)
11	Zona pellucida binding protein 1	ZPBP1, Sp38, IAM38	Yes (Mori et al., 1995)	Acrosome [rat, pig, mouse] (Lin et al., 2007; Yu et al., 2006)	YES, Infertile (Lin et al., 2007)
12	Zona pellucida binding protein 2	ZPBP2	Yes (Redgrove et al., 2011)	Acrosome [mouse] (Lin et al., 2007)	YES, Subfertile (Lin et al., 2007)
13	Proacrosin/acrosin	ACRO	Yes (Howes et al., 2001)	Acrosome [mouse, bovine, guinea pig, human] (Barros et al., 1992; De los and Barros, 2000; Tardif et al., 2012)	YES, Fertile (Baba et al., 1994)
14	Zona pellucida sperm-binding protein 3 receptor	ZP3R, sp56, AM67	Yes (Bleil and Wassarman, 1990; Cheng et al., 1994)	Acrosome [mouse, guinea pig] Foster et al., 1997; Kim et al., 2001)	Yes, Fertile (Muro et al., 2012)
15	Sperm acrosomal protein SP-10	MSA-63, ASPX	Yes (Coonrod et al., 1996)	Acrosome [mouse] (Foster and Herr, 1992)	n/a
16	Angiotensin-converting enzyme	ACE	Yes (Deguchi et al., 2007)	Plasma membrane overlying acrosomal and post-acrosomal regions and midpiece [human] (Kohn et al., 1998)	Yes, Infertile (Hagaman et al., 1998)

1.2.4.4 Roles of sperm lipid rafts and high molecular weight complexes containing ZP-binding proteins/molecules in sperm-egg interaction

The concept that several proteins/molecules act together (or in a coordinated manner) in the ZP binding process is in line with emerging evidence demonstrating the existence of sperm lipid raft microdomains with ZP affinity (Bou Khalil et al., 2006; Nixon et al., 2009; Tanphaichitr et al., 2007a). Since lipid rafts in somatic cells are known as platforms of cell adhesion and signaling molecules (Simons and Ehehalt, 2002), sperm lipid rafts would likely play a similar role in sperm-egg interaction processes, i.e., adhesion to the ZP with subsequent signalling in sperm. For a better understanding of the functions of sperm lipid rafts, a number of investigators in the gamete field, including us, have characterized the molecular components of sperm lipid rafts, isolated as DRMs. Through lipidomic analysis, our lab has shown that SGG, a major sulfoglycolipid of sperm, is an integral component of sperm DRMs (Bou Khalil et al., 2006; Tanphaichitr et al., 2007b; Weerachatyanukul et al., 2007). SGG plays a significant role not only in the formation of sperm lipid rafts but also in the ZP binding of these membrane domains (Bou Khalil et al., 2006). Proteomic analyses from Atiken's group (in collaboration with us) and Gadella's group further reveal that sperm DRMs contain a number of proteins with known ZP affinity (i.e., MFGM, GALT, ARSA, AQN-1, AWN, proacrosin, SP-10) as well as their binding partners (e.g., proacrosin-binding protein, aka sp32 (ACRBP)) (Nixon et al., 2009; Sleight et al., 2005; Van Gestel et al., 2005). The proteomic studies have also demonstrated the presence of a number of molecular chaperones in sperm DRMs, including Hsp60, Hspa5 (or Grp78), Hsp90, Hsp90b1, and calnexin (Nixon et al., 2009). These molecular chaperones have been proposed to play a role in facilitating the assembly of the multimeric complex of ZP receptors on the capacitated

sperm surface (Asquith et al., 2004; Nixon et al., 2007; Nixon et al., 2005). Indeed, Han et al. have recently shown that Hspa5 and calnexin associate with a number of client proteins (i.e., ADAM7) to form a stable complex on the surface of mouse sperm (Han et al., 2011). These findings strongly suggest that the ZP-binding proteins and chaperone proteins in isolated sperm lipid rafts may be associated with one another to form high molecular weight protein (HMW) complexes for further ZP interaction. This idea is further supported by the recent findings from Aitken's group showing that HMW protein complexes with ZP affinity exist in the mouse and human sperm plasma membrane detergent extracts, and that ZP-binding proteins and chaperone proteins are components of these complexes (Dun et al., 2011; Redgrove et al., 2011). While these findings are intriguing, they can be challenged in two aspects: 1) only a few ZP-binding proteins (ZPBP1, ZPBP2, and ARSA) have been described in the sperm surface HMW complexes with ZP affinity, and 2) the plasma membrane extracts used for the characterization of the HMW ZP-binding complexes were prepared from both sperm head and tail parts. On the second aspect, the co-isolated sperm tail proteins, which are likely not pertinent to ZP binding, might adversely affect the intactness of these complexes. As well, they may create ion suppression of the relevant proteins in the sperm head HMW complexes, disallowing them to be detected by mass spectrometry. Since ZP interactions take place over the anterior portion of the sperm head, molecules specifically isolated from this area would be more appropriate material for characterizing the protein components relevant to ZP binding.

In fact, nitrogen cavitation at 650 psi has long been used in the sperm field to specifically prepare vesicles from the pig sperm anterior head plasma membrane (APM), the site of ZP binding (Flesch et al., 1998; Gillis et al., 1978; Peterson et al., 1980). Isolated

APM vesicles from capacitated pig sperm have been shown to have direct ability to bind to the homologous ZP glycoproteins, in particular pig ZP3, which are sperm receptor ZP glycoproteins (see above) (Bou Khalil et al., 2006; Yurewicz et al., 1998). Importantly, our lab has demonstrated that the ZP-binding ability of capacitated sperm APM vesicles is very similar to that of capacitated sperm DRMs (the K_d values are 0.058 and 0.056 μM, respectively) (Bou Khalil et al., 2006); this result indicates that the functional properties of APM vesicles are similar to the sperm head lipid rafts isolated as DRMs. However, APM vesicles would be a better biological source for proteomic characterization than isolated sperm DRMs or whole sperm plasma membrane extracts for a few important reasons. First, APM vesicles are confined only to the sperm head anterior plasma membrane, the site of ZP binding. Second, isolation of APM vesicles does not involve any use of a detergent, which could have caused protein aggregation and redistribution. In fact, towards the end of the year 2000, concerns were strongly voiced among researchers in the lipid raft field that isolated DRMs might not represent in situ microdomains in live cells. Suggestions have since been made to isolate lipid rafts via physical force (Pike, 2009; Sprenger and Horrevoets, 2007; Tanphaichitr et al., 2007b). Nitrogen cavitation has been used for decades to prepare sperm APM vesicles (Gillis et al., 1978; Peterson et al., 1980). I therefore have taken advantage of this serendipity by performing the proteomic characterization of APM vesicles isolated from non-capacitated and capacitated pig sperm. Ianticipate that information about the protein identities in the whole APM vesicles and their HMW complexes will provide a better understanding of the molecular mechanisms of how sperm attain their full fertilizing ability during capacitation.

1.3 Sulfogalactosylglycerolipid (SGG)

1.3.1 General properties of SGG and its structural analog

Sulfogalactosylglycerolipid (SGG, aka seminolipid or SM4g), 1-*O*-alkyl-2-*O*-acyl[β-D-(3'-sulfatoxy)galactopyranosyl(1'-3)]*sn*-glycerol, is an evolutionarily conserved sulfoglycolipid present substantially (10 mol% of the total lipids) and selectively on the surface of mammalian male germ cells (Ishizuka et al., 1973; Tanphaichitr et al., 2003). SGG consists of a glycerol backbone with 3-*O*-sulfated galactose at the *sn*-3 position and alkyl and acyl chains at the *sn*-1 and *sn*-2 positions, respectively (Figure 1.9A) (Ishizuka et al., 1973). SGG with hexadecyl and hexadecanoyl chains (C16:0/C16:0 SGG with M.W. of 796) is the major SGG molecular species in the male germ cells of all mammalian species characterized so far, including rats (Kornblatt et al., 1972), pigs (Ishizuka et al., 1973), bulls (Alvarez et al., 1990), humans (Ueno et al., 1977) and mice (Kongmanas et al., 2010). Although other SGG molecular species with different alkyl and acyl chains (i.e., C16:0/C14:0, C16:0/C18:0, C16:0/C18:1, and C17:0/C16:0) have also been identified in mouse testes, their levels are less than 10% of the main molecular species (Goto-Inoue et al., 2009).

SGG is a structural analog of sulfogalactosylceramide (SGC, aka sulfatide or SM4s), [β-D-(3'-sulfatoxy)galactopyranosyl]-(1'-1)]-*N*-tetracosanoylsphingosine. SGC has the same head group (galactose sulfate moiety) as SGG, but it has ceramide (instead of alkylacylglycerol) as its lipid backbone (Figure 1.9B). Since the head group of SGG and SGC is the same, and the 3-D conformations of the two lipids are similar, the antibodies made against one sulfoglycolipid can recognize the other one. In mammals, SGC is found

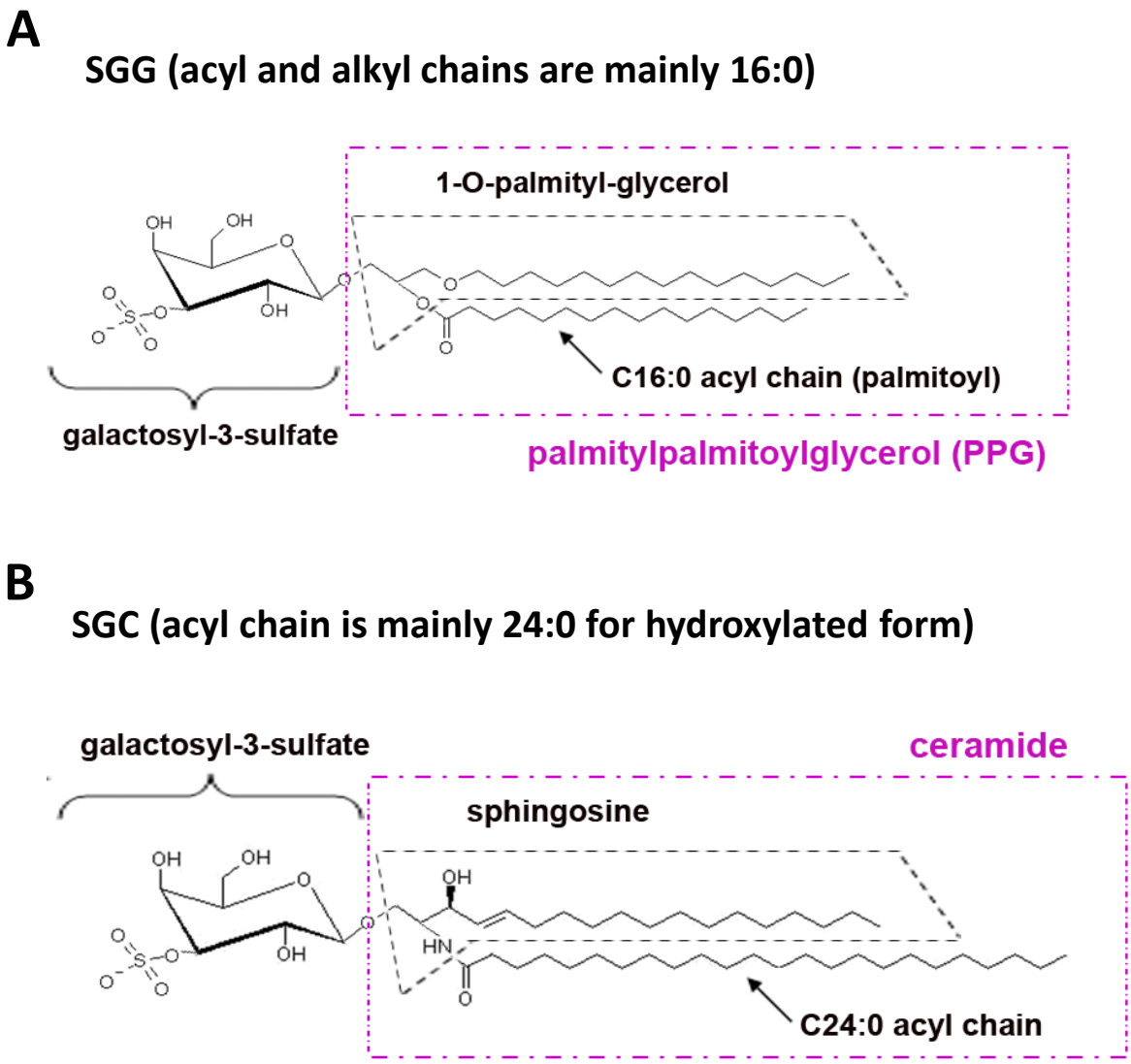

Figure 1.9: Structures of sulfogalactosylglycerolipid (SGG, aka seminolipid) and its analog, sulfogalactosylceramide (SGC). A) SGG consists of a glycerol backbone with 3-*O*-sulfated galactose at the *sn*-3 position and an akyl and acyl chain (both mainly 16:0) at the *sn*-1 and *sn*-2 position, respectively. **B)** SGC, a structural analog of SGG, has the same sulfogalactosyl head group as SGG but it has a ceramide (instead of an alkylacylglycerol) as the lipid precursor. The ceramide moiety of SGC can exist in either hydroxylated or non-hydroxylated form with different acyl chain lengths, i.e., C24:0 or C24:1, C18:0 or C18:1 (only the 24:0 species of the hydroxylated form is shown here).

mainly in myelinating cells (i.e., oligodendrocytes and Schwann cells) of the nervous system (4% of total myelin lipids), and in epithelial cells of the kidney, digestive tract, cervix and vagina (Ishizuka, 1997), as well as in β cells in the islet of Langerhans (Fredman et al., 2000). In addition, SGC is expressed in a very low amount in human sperm (Levine et al., 1976) but in a high amount in male germ cells of lower vertebrates and invertebrates (Ishizuka, 1997). Depending on the tissue types where SGC is expressed, SGC exhibits various molecular species with different lengths of the acyl chain and ceramide moiety, which can be either hydroxylated or non-hydroxylated (Takahashi and Suzuki, 2012).

1.3.2 Biosynthesis of SGG and SGC

SGG and SGC are known to share the same two enzymes in their biosynthesis pathway (Fujimoto et al., 2000; Honke et al., 2002) (Figure 1.10). The first enzyme is UDP-galactose:ceramide galactosyltransferase (CGT; EC 2.4.1.62), which transfers the galactosyl group from UDP-galactose onto the lipid precursors (i.e., alkylacylglycerol and ceramide for SGG and SGC, respectively). This glycosylation step occurs in the endoplasmic reticulum where CGT is localized and results in the formation of galactosylglycerolipid (GG) and galactosylceramide (GC) (Eckhardt, 2008; Sprong et al., 1998). The glycolipids are then transported to the Golgi apparatus for the subsequent sulfation by the second enzyme, cerebroside sulfotransferase (CST; EC 2.8.2.11), which transfers a sulfate group from 3'-phosphoadenosine-5'-phosphosulfate (PAPS) to form an ester at the 3' position of the galactose residue of the glycolipids (Knapp et al., 1973; Sakac et al., 1992). The common

biosynthesis pathway of SGG and SGC is derived from the findings that mice genetically null of *Cgt* and *Cst* have neither SGC in their brains nor SGG in their male germ cells (Fujimoto et al., 2000; Honke et al., 2002). SGC depletion in the brains of *Cgt* and *Cst* knockout mice leads to abnormalities in the myelin functions, which manifest as tremors, ataxia and hindlimb movement disability, whereas the lack of SGG in their male germ cells resultsin infertility due to the spermatogenesis disruption (Fujimoto et al., 2000; Honke et al., 2002).

Several lines of evidence indicate that SGG is actively synthesized in the early stages of primary spermatocytes during spermatogenesis (Kornblatt et al., 1974; Letts et al., 1978). Once synthesized, SGG is presumably targeted via vesicular transport to the outer leaflet of the germ cell plasma membrane and remains at this site throughout the subsequent stages of germ cell development (Ishizuka, 1997; Tanphaichitr et al., 2003; Vos et al., 1994).

1.3.3 Degradation of SGG and SGC

SGG and SGC are suggested to share similarity not only for their synthesis pathway, but also for their degradation pathway. However, only the SGC degradation pathway has been confirmed *in vivo*. SGC degradation in the lysosome starts with sulfate hydrolysis by arylsulfatase A (ARSA; EC 3.1.6.8), followed by deglycosylation of GC through the action of galactosylceramidase (aka galactosylceramide β-galactosidase) (GALC; EC 3.2.1.46) (Figure 1.11). The *in vivo* degradation of SGC and GC by these lysosomal enzymes is derived from the findings that individuals having natural mutations of *Arsa* and *Galc* suffer lysosomal storage disorders, the so called metachromatic leukodystrophy (MLD) and globoid

cell leukodystrophy (aka Krabbe's disease), with accumulation of SGC and GC (also lysoGC from GC hydrolysis), respectively in their brains (Matsuda and Suzuki, 2007; von Figura et al., 2001). Storage of these glycoshingolipids in the brains of these patients causes progressive demyelination, leading to a variety of neurological symptoms and eventually lethality (Matsuda and Suzuki, 2007; von Figura et al., 2001). Mice genetically null of *Arsa* and mice mutant in *Galc* (aka twitcher mice) were also available and have been used as models for the study of these human lysosomal storage disorders (Duchen et al., 1980; Gieselmann et al., 1998; Hess et al., 1996; Igisu et al., 1983). As expected, SGC and lysoGC are accumulated in the brains of *Arsa*-deficient and *Galc*-mutant mice, respectively (Molander-Melin et al., 2004; Whitfield et al., 2001). However, the *Arsa* null mice live past 1.5 years of age with mild MLD phenotypes, whereas *Galc*-mutant mice die at 45 days of age. It is possible that the accumulation of lysoGC is more cytotoxic than SGC.

The enzymatic actions of ARSA and GALC on lipid degradation require help from cofactors, the so called specific sphingolipid activator proteins (aka saposins). Saposin B is required for ARSA activity, whereas saposin A participates in GALC reaction (Figure 1.11). These saposins facilitate the substrate-enzyme interactions by extracting the target lipids from the membrane and delivering them, one by one, to the active site pocket of the enzymes (Ahn et al., 2003; Kolter and Sandhoff, 2005; von Figura et al., 2001). These saposins are derived from the same precursor protein, called "prosaposin", which is processed by the proteolytic activity of cathepsin D (Hiraiwa et al., 1997; O'Brien and Kishimoto, 1991). Individuals with genetic mutations in saposin A and saposin B also suffer the neurological disorders of Krabbe's disease and MLD, respectively (Deconinck et al., 2008; Spiegel et al., 2005).

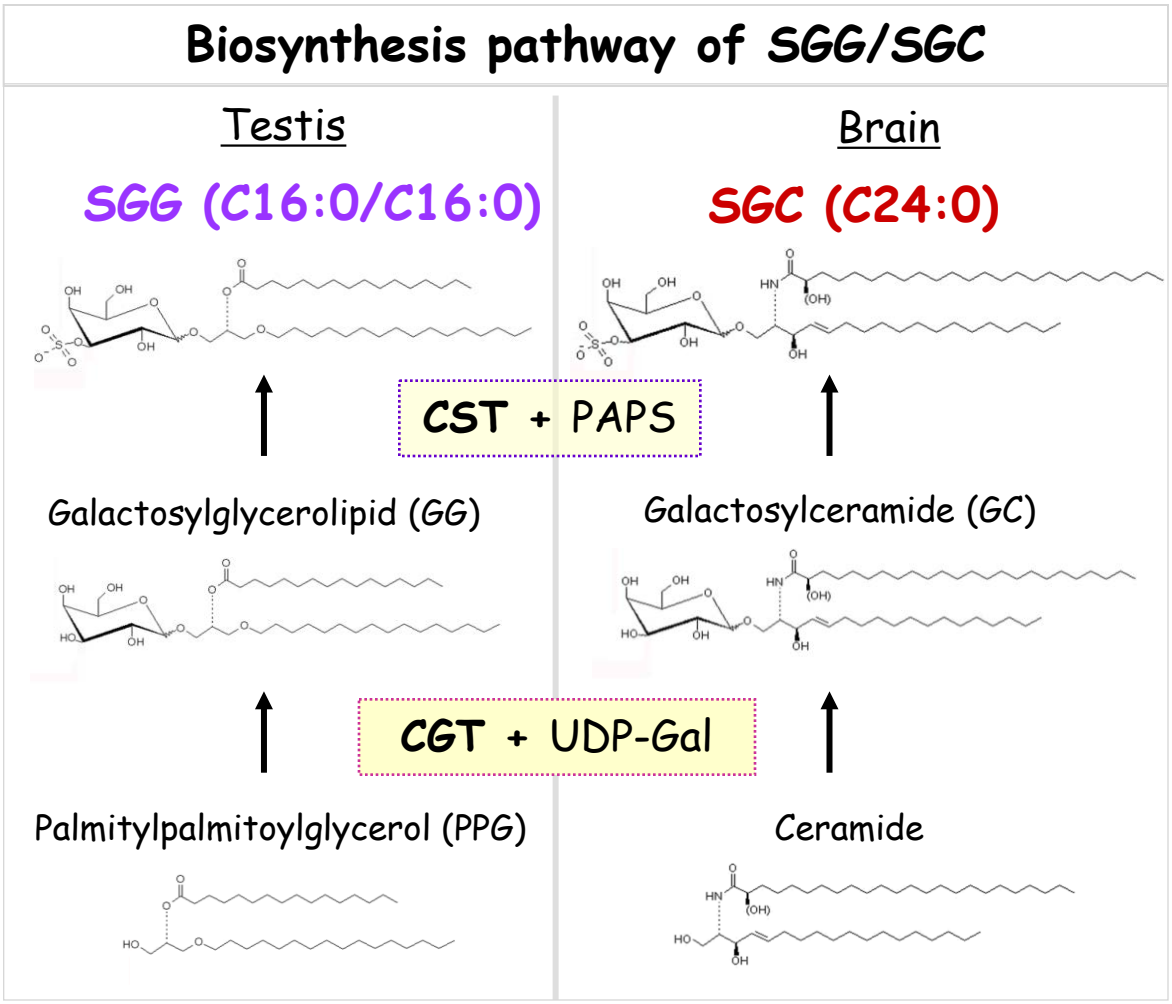

Figure 1.10: Biosynthesis pathway of SGG and SGC. SGG synthesis occurs during spermatogenesis at the stage of primary spermatocytes by the actions of two enzymes: ceramide galactosyltransferase (CGT) and cerebroside sulfotransferase (CST). SGC synthesis occurs mainly in the brain. These two sulfoglycolipids utilize the same enzymes for their biosynthesis.

Abbreviations: PAPS-3'-phosphoadenosine-5'-phosphosulfate; UDP-Gal-uridine diphos-phate galactose.

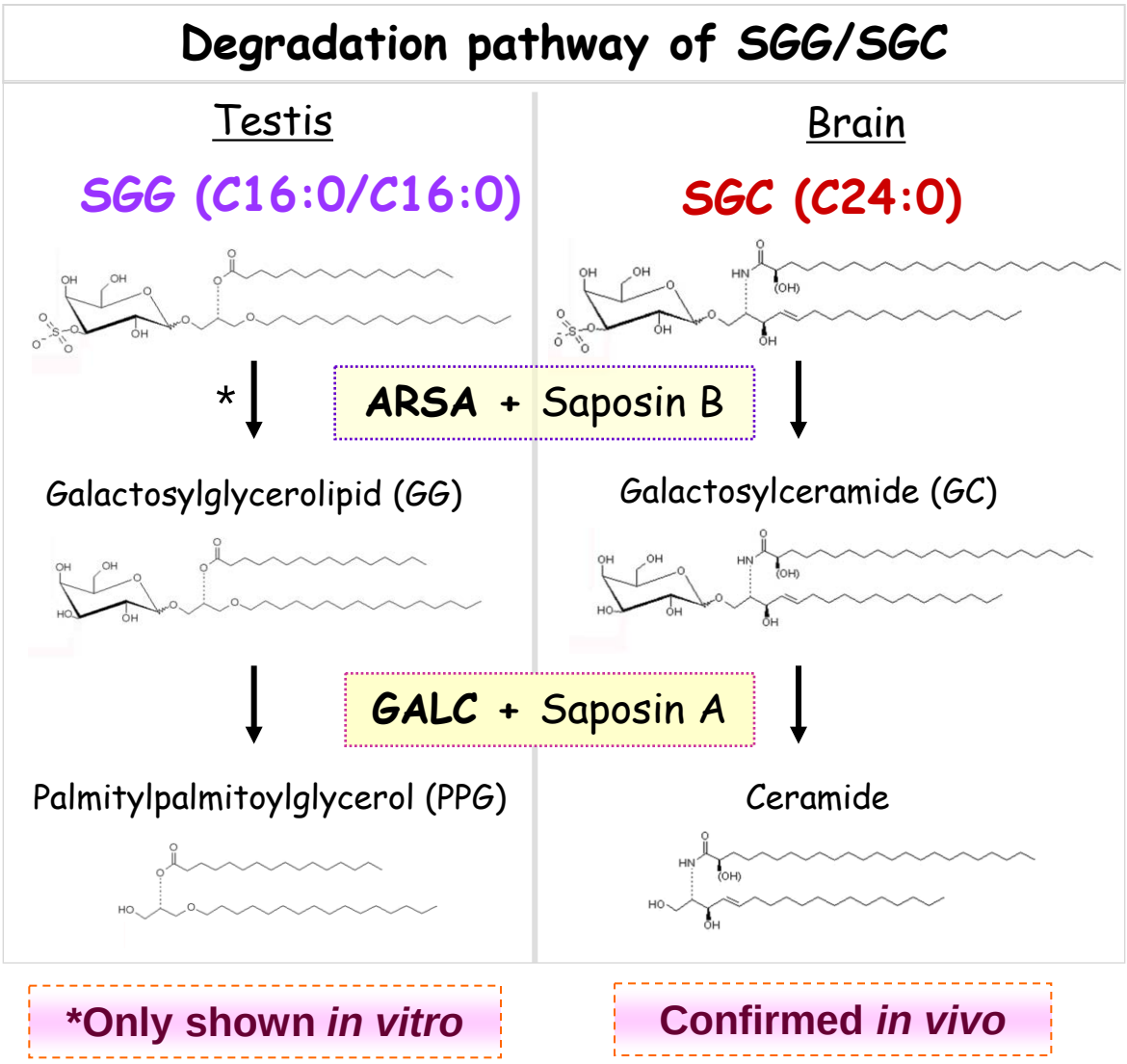

Figure 1.11: Degradation pathway of SGG and SGC. Desulfation of SGC by arylsulfatase A (ARSA) results in GC that is further degraded by galactosylceramidase (GALC), yielding ceramide as a final product; this pathway is confirmed *in vivo* (Gieselmann et al., 1998; Sakai et al., 1995; Molander-Melin et al., 2004; Whitfield et al., 2001). The catalytic actions of ARSA and GALC require saposin B and saposin A as their co-factors, respectively. The saposins facilitate the enzyme actions by extracting a lipid substrate from biomembranes and bringing the lipid molecule (one by one) into the active site pocket of the enzymes. The significance of saposin B and saposin A in SGC and GC degradation, respectively has also been shown *in vivo* (Spiegel et al., 2005; Deconinck et al., 2008). Unlike in the case of SGC, role of ARSA in desulfation of SGG, presolubilized with saposin B or detergent, has only been demonstrated *in vitro* (Fluharty et al., 1974; Yamato et al., 1974). GG accumulation is detected in testes of the mice with mutation in *Galc* gene, suggesting that GG is a physiological substrate of testicular GALC (Luddi et al., 2005).

However, unlike the case of SGC, the *in vivo* degradation of SGG by ARSA and GALC has not yet been verified in humans. Male individuals with true MLD and Krabbe's disease are severely ill and most die young (their disease status is referred to as an infantile form). Consequently, their fertility status as well as the SGG and GG levels in their reproductive system cannot be investigated (Kohlschutter, 2013; von Figura et al., 2001). Although there are patients with late-onset (juvenile and adult) forms of Krabbe's disease and MLD who manifest mild neurological symptoms and can live until puberty (Kohlschutter, 2013), their male fertility status has not been well documented. For the mouse system, the levels of SGG in the male reproductive system of *Arsa* knockout (KO) mice have never been characterized. Therefore, one of the main objectives in my Ph.D. thesis study is to determine the SGG levels in the male reproductive system (i.e., whole testes extracts, Sertoli cells, testicular germ cells, and sperm) as well as the male fertility status of *Arsa* knockout mice, in comparison to those of age-matched wild type animals (see more details of *Arsa* KO mice in the ARSA section). Our study using this animal model will provide a better understanding of the roles of SGG and its homeostasis in male fertility, with the anticipation that the information obtained will provide a background for future studies in humans.

While SGC is synthesized and degraded (to generate the lipid backbone for the new round of its synthesis) in the same cells (i.e., oligodendrocytes, kidney epithelial cells) (Eckhardt, 2008; Takahashi and Suzuki, 2012), SGG synthesized in the male germ cells is postulated to be degraded by Sertoli cells, the somatic reproductive cells present in the seminiferous epithelium (see more details about Sertoli cell and spermatogenic cell organization in the spermatogenesis section). This postulation is derived from the following

three findings: First, both ARSA and GALC are expressed in Sertoli cells and their enzymatic activities are much higher in Sertoli cells as compared to those in the germ cells (our unpublished data; see more about ARSA in the section below). Second, prosaposin (precursor of saposins A and B) is expressed by Sertoli cells and not by germ cells (Morales et al., 1998). Finally, prosaposin and ARSA are both localized to the lysosomes of Sertoli cells (Igdoura et al., 1996; Weerachatyanukul et al., 2003).

1.3.4 Common molecular properties of SGG and SGC and their possible molecular mechanisms

SGG and SGC have been demonstrated for their common biophysical and biochemical properties. Our biophysical studies reveal that both SGG and SGC are ordered lipids with T_m of ~45°C, and that they have preferential interaction with saturated phospholipids and cholesterol (Attar et al., 2000; Attar et al., 1998; Bou Khalil et al., 2006; Weerachatyanukul et al., 2007). In fact, SGC and SGG have been demonstrated to co-exist with cholesterol and saturated phospholipids in the liquid-ordered membrane domains (lipid rafts), isolated as detergent resistant membranes from myelin and sperm, respectively (Arvanitis et al., 2005; Bou Khalil et al., 2006). These findings suggest that both sulfoglycolipids serve as structural lipid components endowing orderedness to lipid rafts or the equivalent membranes thereof (such as sperm anterior head plasma membrane (APM) vesicles-see below).

Lipid rafts are known to contain not only ordered lipids but also a number of proteins which have been implicated in cell adhesion and cell signalling processes (Brown and

London, 1998; Simons and Toomre, 2000; Sonnino and Prinetti, 2013). SGG and SGC have been shown *in vitro* to possess affinity for a number of proteins, including cell adhesion proteins, extracellular matrix glycoproteins, and growth factors (Table 1.2); therefore, it is possible that these sulfoglycoilipids may also act as an adhesion molecule that recruits key proteins into the lipid rafts. This role of SGC in oligodendrocyte lipid rafts has actually been supported by a recent study showing that Fyn and Lyn, two Src family tyrosine kinases existing in lipid rafts, are co-immunoprecipitated with SGC, using anti-SGC (O4) antibody (Miki et al., 2013). However, whether SGG in sperm lipid rafts plays a similar role to that of SGC has yet to be determined (see more below).

Due to its ubiquitous expression in several mammalian cell/tissue types, SGC has been more extensively studied than SGG. The roles of SGC have been implicated in various biological systems, including the nervous and immune systems. Particularly, in the nervous system, abnormal metabolism of SGC has been correlated with various neurological diseases, such as MLD, Alzheimer's disease, and Parkinson's disease, implicating that homeostasis of SGC is important for the neurological system (Takahashi and Suzuki, 2012). Owing to the fact that SGG is uniquely present int substantial amounts in the male germ cells, the roles of SGG in male reproduction cannot be underestimated. For this reason, our lab has spent many years investigating the roles of SGG in male reproduction (see below) with anticipation to eventually use SGG as a male fertility biomarker and/or a target for the development of non-hormonal male contraceptives. However, prior to any translational applications, the molecular mechanisms of SGG involvement in the key physiological processes in male reproduction (i.e., spermatogenesis, epididymal maturation, capacitation, sperm-egg interaction) must be clearly understood.

Table 1.2: List of proteins with SGG/SGC affinity

Type	SGG/SGC-binding molecules	Description	References	Theoretical pI[1]	# TM domains (SOSUI)[2]
Microorganisms, viruses and their surface proteins	*Escherichia coli* Enterotoxin b	A protein in a specific *E. coli* strain that causes diarrhea in animals and humans	Rousset et al., 1998	8.67	1
	Mycoplasmas	A human pathogen that is transmitted sexually and causes infertility	Olson and Gilbert, 1993; Lingwood et al., 1990	-	-
	Circumsporozoite proteins	A coat protein of malaria (plasmodia) sporozoites	Pancake et al., 1992	5.38	2
	gp120	A surface glycoprotein of the human immunodeficiency virus (HIV-1)	Brogi et al., 1996; Brogi et al., 1995	5.11	0
Adhesive proteins	Antistatin/Antistatin	A saliva protein from the leech that inhibits blood coagulation	Holt et al., 1989	8.65	1
	Thrombospondin	A major component of platelet α granules	Roberts, 1988	9.41	0
	Von Willebrand factor	A large plasma glycoprotein which binds to platelet and promotes platelet adhesion	Roberts et al., 1986	5.89	0
	L-selectin	A protein in the selectin family found on leukocytes	Needham and Schnaar, 1993; Suzuki et al., 1993	6.64	2
	Amphoterin (p30)	A 30 kDa protein found in the rat cerebellum	Mohan et al., 1992	5.62	0
	Galectin-4 and -8	A β-galactoside-binding lectin involved in mediating cell-cell adhesion	Ideo et al., 2002; Ideo et al., 2003	9.2, 9.11	0
	Annexin V	A calcium-dependent phospholipid-binding protein	Ida et al., 2004	4.94	0
Extracellular matrix (ECM) glycoprotein	Laminin	A major noncollagenous glycoprotein of the basement membranes	Roberts et al., 1985	5.94	1
	Perlecan (C-terminal domain V)	An abundant proteoglycan component of the basement membranes	Friedrich et al., 1999	6.06	1
	Zona Pellucida (ZP); mZP2 and mZP3	An extracellular glycoprotein matrix surrounding the egg	Tantibhedhyangkul et al., 2002	5.57	-
Components of myelin lipid rafts	Myelin and lymphocyte protein (MAL)	A myelin membrane protein expressed in central and peripheral nerve, and found in rafts of the myelin; A T-cell differentiation protein	Frank, 2000	5.55	4
	GC and SGC	Major glycolipids of the myelin	Boggs et al., 2000	-	-
Chaperone	Heat shock protein 70 (Hsp70)	Molecular chaperones found on the surface of bacteria, male germ cells, and carcinoma cell lines	Mamelak and Lingwood, 2001	5.77	0
Growth factor	Midkine	A basic heparin-binding growth factor in the nervous system	Kurosawa et al., 2000	9.84	1
Enzyme	Arylsulfatase A	An acrosomal/lysosomal enzyme and a sperm surface protein	Carmona et al., 2002b	5.37	0

[1]The pI of a protein is calculated from a protein sequence by ExPAsy.

[2]The presence of transmembrane helices in a protein is predicted by SOSUI software.

1.3.5 Localization and functions of SGG in male reproduction

SGG has been localized on the cell surface of live spermatogenic cells (primary spermatocytes, round and elongated spermatids) by immunofluorescence, using our affinity purified rabbit polyclonal anti-SGG IgG antibody (Tanphaichitr et al., 2003). SGG expression in testicular germ cells is known to be important for ongoing spermatogenesis process. As mentioned above, *Cgt* and *Cst* knockout male mice whose germ cells are depleted of SGG are infertile due to a spermatogenesis arrest at the meiotic division of primary spermacytes (Fujimoto et al., 2000; Honke et al., 2002). Later study has shown that the spermatogenesis process of *Cst* null mice could be completed after transplanting spermatogonia from wild type animals into the seminiferous tubules of these mice (Zhang et al., 2005). This finding indicates that the absence of testicular SGG specifically causes defects to germ cell function but not to that of Sertoli cells. However, the molecular mechanisms through which SGG regulates/impacts/ influences spermatogenesis are still unknown. The completion of spermatogenesis is heavily dependent on proper cyto-organization between testicular germ cells, as well as between Sertoli cells and germ cells (Cheng and Mruk, 2002) (see above in spermatogenesis section). Since SGG is known as an adhesion molecule, it is possible that SGG on the germ cell surface is responsible for these intercellular interactions. Like SGC, SGG molecules on adjacent germ cells may interact with each other (Boggs et al., 1988). Also, there may exist SGG binding proteins on the surface of germ cells and Sertoli cells, which promote such intercellular associations.

On the mature sperm, SGG is shown to localize on the sperm head plasma membrane at the site where sperm binds to the ZP (i.e., convex ridge in the mouse sperm; APM in the pig sperm; APM and equatorial segment in human sperm) (White et al., 2000; Bou Khalil et

al., 2006; Weerachatyanukul et al., 2001). For decades, our lab has been focusing on the roles of SGG on the sperm head surface in the post-testicular biological processes of male reproduction. So far, we have demonstrated that SGG plays dual functions as a cell adhesion molecule and a structural lipid. During sperm transit in the epididymis, SGG serves as a ligand for the adsorption of ARSA, also a ZP-binding molecule (see more in ARSA section below), onto the sperm surface (Weerachatyanukul et al., 2003). With its direct affinity for ZP, SGG is involved in *in vitro* fertilization as a ZP-binding molecule on the mouse and human sperm head surface (White et al., 2000; Weerachatyanukul et al., 2001).

In addition to the adhesion property, SGG on the sperm surface serves as a structural lipid for the formation of capacitated sperm lipid rafts, the platforms for ZP binding. We have shown that the majority of SGG (70% of its total sperm amount) exists along with cholesterol and saturated phospholipids in the lipid rafts of capacitated pig sperm (Bou Khalil et al., 2006). The SGG-associated lipid rafts, isolated from capacitated pig sperm DRMs or APM vesicles, have been shown for their direct ZP-binding ability (Bou Khalil et al., 2006). Since SGG possesses affinity for ZP, it likely contributes to the ZP-binding ability of the sperm lipid rafts. Moreover, as stated above, a number of proteins with known SGG affinity (i.e., Hsp70, ARSA) are known for their existence in mouse and human sperm lipid rafts, isolated as DRMs (Nixon et al., 2009; Nixon et al., 2011). Several proteins existing in sperm lipid rafts (i.e., Hsp70, ARSA) have been shown for SGG/SGC affinity (Carmona et al., 2002b; Mamelak and Lingwood, 2001; Nixon et al., 2009). Therefore, it is possible that SGG plays a role in recruiting these proteins to the sperm lipid rafts during capacitation; however, this possibility awaits further verification.

1.4 Arylsulfatase A

1.4.1 General properties of sulfatases

Sulfatases (EC 3.1.5.6) are enzymes of the esterase class that catalyze the hydrolysis of sulfate ester bonds of a wide variety of substrates, including sulfated proteoglycans, sulfoglycolipids, and steroid sulfates. To date, seventeen human sulfatase proteins and their genes have been identified, and several of them have been implicated in the onset of various pathophysiological conditions (Ghosh, 2007). The members of the sulfatase family share significant similarities, including: 1) 20-60% sequence homology over the entire protein length (~500-800 amino acids); 2) a highly conserved N-terminal region containing the consensus sulfatase motifs; and 3) a unique active-site cysteine residue, which is post-translationally converted into formylglycine by the action of formylglycine-generating enzyme, encoded by the *SUMF1* gene (Ghosh, 2007; Hanson et al., 2004). The conversion of cysteine to formylglycine is known to be crucial for the catalytic activity of all human sulfatases because mutations in the *SUMF1* gene result in severely decreased activity in all sulfatases, characteristic of a rare fetal autosomal recessive disorder known as multiple sulfatase deficiency (Dierks et al., 2003). So far, the crystal structures of three human sulfatases, arylsulfatases A, B and C (ARSA, ARSB and ARSC) have been determined (Bond et al., 1997; Hernandez-Guzman et al., 2003; Lukatela et al., 1998). Strikingly, the overall three-dimensional structures of all three sulfatases exhibit a high degree of homology. Moreover, the spatial arrangement of amino acids responsible for sulfate ester hydrolysis is virtually identical in all of these enzymes, demonstrating their conserved catalytic mechanism. Namely, the active site of these sulfatases is comprised of 10 highly interconnected polar residues (i.e., Fgly, AspA, AspB, AspC, ArgA, HisA, HisB, LysA, LysB, and AsnA, which is conservatively replaced by a glutamine residue in ARSC) and a

divalent metal ion (i.e., Mg^{2+} for ARSA, and Ca^{2+} for ARSB and ARSC) (Hanson et al., 2004). Although these sulfatases share considerable similarity in their amino acid sequences and tertiary structures, they prefer differential natural substrates (i.e., sulfoglycolipids for ARSA; dermatan sulfate and chondroitin sulfate for ARSB; and steroid sulfates for ARSC) and exhibit maximal activity at different pH, suggesting that the residues and/or structural architectures responsible for their substrate interactions are different. Since the C-terminal sequence of sulfatases bears the highest structural diversity, it likely serves as a substrate-discerning region. However, the crystal structures of sulfatases in complex with their specific natural substrates are not yet available; thus the amino acid residues that play a role in the substrate specificity of sulfatases remain largely unknown.

1.4.2 Biochemical properties of ARSA

Lysosomal ARSA has been the most extensively studied of all sulfatases because of its physiological significance in keeping a proper balance of SGC (sulfatide), an integral component of myelin. As mentioned above, individuals with a genetic deficiency of ARSA have an intralysosomal accumulation of SGC in their brains and suffer the neurological disorder of metachromatic leukodystrophy (Gieselman et al., 1998). ARSA was initially purified from the human liver and urine for characterization of its biochemical properties (Baum et al., 1959; Fluharty and Edmond, 1978). On SDS gel electrophoresis, the human liver ARSA shows two components (~49 and ~59 kDa) while the urine enzyme gives a single band of ~55 kDa (Fluharty and Edmond, 1978). In an acidic environment at pH~5, ARSA shows optimal catalytic activity and exists as a highly stable homo-octomer, whereas

in the neutral and alkaline pH, it is present mainly as a homo-dimer (Nichol and Roy, 1965). *In vitro,* ARSA activity is conveniently assayed using a small artificial substrate, *p*-nitrocatecholsulfate (NCS) or *p*- methylumbelliferone sulfate (MUS), which can directly enter its active site pocket (Fluharty and Edmond, 1978). Desulfation of natural substrates, such as SGC, SGG, psychosine sulfate, ascorbic acid sulfate, and tyrosine sulfate by ARSA can also be assayed *in vitro*, provided that their liposomal forms are pre-solubilized into micelles with saposin B or a chemical detergent (i.e., taurodeoxycholate), thus allowing their accessibility into the active site pocket (Baum et al., 1959; Fluharty et al., 1974; Fluharty et al., 1976; Mehl and Jatzkewitz, 1968; Waheed and Van Etten, 1980). The limited accessibility of lipids to the ARSA active site pocket may explain why the rates of ARSA in the desulfation of sulfoglycolipids are lower than those of the water-soluble artificial substrate, NCS (i.e., V_{max} for SGC/SGG is ~6-23 and V_{max} for NCS is ~1700 µmol/h/mg) (Carmona et al., 2002a; Hanson et al., 2004). However, the K_m values of ARSA for the natural lipids are lower than that of NCS (i.e., ~100 µM for SGC/SGG and ~6900 µM for NCS), indicating the stronger binding of the lipid substrates to the ARSA active site pocket (Carmona et al., 2002a; Hanson et al., 2004).

For a better understanding of the ARSA mechanisms in the desulfation process, X-ray crystallography has been performed on human recombinant ARSA, both wild type and mutant forms, as well as on the native form of ARSA (Chruszcz et al., 2003; Lukatela et al., 1998; Von Bulow et al., 2001). The crystal structure of recombinant ARSA complexed with the artificial substrate NCS was achieved by using a mutant ARSA with the active site residue Cys69 replaced with alanine (called C69A). This result revealed that NCS can still bind to the active site of C69A but it cannot be desulfated, indicating that the Cys69 residue

of ARSA is important for the sulfate ester hydrolysis (Von Bulow et al., 2001). Besides the C69A-ARSA mutant, alanine-mutants of nine other putative active site amino acids (i.e., Asp29, Asp30, Asp281, Asn282, His125, His229, Lys123, Lys302, and Ser150) have been made for analysis of their function in binding and cleaving sulfate esters (Waldow et al., 1999). In all mutants, the V_{max} for NCS desulfation was decreased to 1-26% of the wild type ARSA activity; the K_m was 10-fold increased in the two lysine residue mutants and up to 5-fold higher in the other mutants, as compared to that of the wild type. These results indicate that each of the nine residues is critical for the catalytic activity; while Lys 123 and Lys302 are important for substrate (NCS) binding, the other residues are likely involved directly or indirectly in catalysis (Waldow et al., 1999). The coordination of a magnesium ion in the center of the active site is also important for ARSA catalytic activity (Waldow et al., 1999). Although these findings have provided a better understanding of the ARSA mechanisms in NCS binding and desulfation, the details of interactions between ARSA and its natural sulfoglycolipid substrates should also be obtained. We therefore performed computational docking of sulfoglycolipids to the ARSA crystal structure to gain insights into the specificity in substrate recognition of this enzyme (Schenk et al., 2009). Our results revealed that Cys69 was the active site residue and Lys123 and Lys302 were the residues for anchoring the sulfate group of sulfoglycolipids to the ARSA active site pocket, a mechanism similar to that previously described for the artificial NCS substrate (Von Bulow et al., 2001; Waldow et al., 1999). However, additional intermolecular hydrogen bonding and hydrophobic interactions between ARSA and the lipid substrates were suggested to contribute to the specificity of substrate binding (Schenk et al., 2009).

1.4.3 Synthesis and subcellular localization of ARSA

ARSA has been characterized as a lysosomal enzyme in the somatic cells of different tissue types, including brain, liver, kidney and testis (Freysz et al., 1979; Lullmann-Rauch et al., 2001; Schott et al., 2001; Stein et al., 1989; Weerachatyanukul et al., 2003), and an acrosomal enzyme in male germ cells (Dudkiewicz, 1984; Weerachatyanukul et al., 2003; Xu et al., 2012). In somatic cells (kidney cell line), ARSA is synthesized as a 507 amino acid preprotein, then translocated into the endoplasmic reticulum (ER) where its 18 amino acid signal peptide at the N-terminal region is cleaved, yielding a 489 amino acid mature enzyme. ARSA is also N-glycosylated at three amino acid sites (Asn158, Asn184, and Asn350) with core fucosylated high-mannose type oligosaccharides (Sommerlade et al., 1994). The ARSA from the ER is subsequently transported to the Golgi apparatus to receive the mannose-6-phosphate recognition markers and finally delivered to the lysosomes (Sommerlade et al., 1994), where the enzyme octomerizes in a pH-dependent manner (Vagedes et al., 2002). Acrosomal ARSA is likely derived from *de novo* synthesis in primary spermatocytes (Kreysing et al., 1994b); once synthesized, ARSA is probably trafficked to the developing acrosomal granules during the spermatid stage and remains at this location for the subsequent stages of germ cell development (Weerachatyanukul et al., 2003).

1.4.4 Enzymatic roles of ARSA in male reproduction

Studies on the enzymatic roles of ARSA in male reproduction were initiated around the 1970 when ARSA was partially purified from the testes and acrosomes of sperm from

several mammalian species (Dudkiewicz et al., 1979; Yamato et al., 1974; Yang and Srivastava, 1976; Yang et al., 1974). Although a few studies were conducted later on to show the possible enzymatic functions of ARSA during sperm-egg interaction, no conclusive roles of ARSA could be drawn from these studies. For example, Dudkiewicz (1984) demonstrated that ARSA purified from boar sperm acrosome could disperse cumulus masses prepared from the ovarian follicles of hamsters, rabbits and pigs; however, this result has never been confirmed at the sperm level. Ahuja and Gilburt (1985) also showed that NCS, a general substrate of arylsulfatases, could inhibit hamster *in vitro* fertilization in a dose-dependent manner, suggesting that arylsulfatases might play a role in sperm-egg binding; however, they did not further identify which arylsulfatases existed on sperm. It was not until the year 2002 that the work from our lab conclusively revealed that sperm contain ARSA (see below).

While the enzymatic roles of sperm ARSA were a subject of investigation in the 1970s and 1980s, parallel functional studies of testicular ARSA were not performed, despite the fact that ARSA is expressed at the highest level in the testis as compared to other tissues, such as liver and kidney (Kreysing et al., 1994a; Kreysing et al., 1994b) and information on its biochemical properties is also available. ARSA purified from boar testis has desulfation activity on detergent solubilized SGG *in vitro* (Yamato et al., 1974), suggesting that SGG may be a physiological substrate of ARSA. Our previous study reveals that ARSA exists mainly in two locations in the mouse testis: the lysosomes of Sertoli cells and the acrosomal granules of spermatids (Weerachatyahukul et al., 2003). The presence of *Arsa* transcript in isolated spermatogenic cells (Kreysing et al., 1994b) and Sertoli cells (our unpublished data) suggested that both cell types can synthesize ARSA. However, our *in vitro* assay using NCS

as ARSA's substrate revealed that the enzymatic activity of ARSA in testicular germ cells was much lower than that in Sertoli cells (our unpublished data); this result suggests that ARSA in Sertoli cells likely plays a major role in degradation of SGG. Considering that Sertoli cells are highly responsible for degrading all apoptotic germ cells and residual bodies, both of which likely contain SGG, the degradation of SGG by ARSA would be an important task for Sertoli cells. Moreover, prosaposin (precursor of saposin B) has been localized in the lysosomes of Sertoli cells (Morales et al., 1998; Moviglia et al., 1982), suggesting that saposin B may facilitate the desulfation of SGG by ARSA in these cells. All of these accumulated findings strongly suggest that the testicular ARSA in Sertoli cells may be important for keeping a balance of SGG during germ cell development. In this thesis, I have validated this postulate for the first time.

1.4.5 Roles of ARSA as an adhesion molecule during sperm-egg interaction

We have shown through a series of experiments that sperm surface ARSA is involved in sperm-ZP interaction. The discovery that ARSA at this entity is involved in the gamete adhesion process was serendipitous. In the 1990s, we characterized the functional roles of "sulfolipid immobilizing protein 1 (SLIP1)", first described by our colleague, Cliff Lingwood (Hospital for Sick Children) as a conglomerate of proteins of an apparent molecular weight of ~68,000, extracted from a rat testicular homogenate and captured on a SGG affinity column (Lingwood, 1985). Through immunoblotting using a polyclonal antibody raised against SLIP1, Law et al. have shown that the 68 kDa protein(s) was evolutionarily conserved in the testis of all vertebrates tested (e.g., rat, mouse, pig, ram,

rooster) (Law et al., 1988). Using the anti-SLIP1 antibody, our lab immunolocalized SLIP1 to the mouse sperm head surface at the same position as SGG, and further demonstrated that SLIP1 is involved in *in vivo* mouse fertilization (Tanphaichitr et al., 1992) and *in vitro* sperm-ZP binding in both mice and humans (Rattanachaiyanont et al., 2001; Tanphaichitr et al., 1993). Interestingly, SLIP1 isolated by the original method of Dr. Lingwood's group (Lingwood, 1985; Lingwood and Nutikka, 1991) consists of a few proteins, including a ZP-binding protein, a testicular Hsp70 and an albumin. However, neither Hsp70 nor albumin has affinity for ZP, suggesting that they are unlikely to be the ZP-binding protein component of SLIP1 (Tanphaichitr et al., 1998a). Consequently, we purified this ZP-binding component of SLIP1 from an extract of the pig sperm surface (where the protein is supposed to be most functionally active) by isoelectrofocusing, using anti-SLIP1 antibody to track its separation from other proteins. The protein purified as a single band on SDS-PAGE, renamed P68, was verified for its ability to bind to SGG/SGC and the intact zona pellucida from various mammals (Tanphaichitr et al., 1998a). Peptide mass fingerprinting of three tryptic peptides of the purified band of P68 revealed 100% identity to those of human and mouse ARSA (Kreysing et al., 1994a; Stein et al., 1989; Tanphaichitr et al., 1998b; Tanphaichitr et al., 1999), and they are present with a 100% match in the pig testis ARSA sequence obtained by molecular cloning (Carmona et al., 2002a). This finding confirms that P68, a ZP-binding component of SLIP, is actually ARSA.

Using an antibody specific to ARSA produced by us, we have localized ARSA to the sperm head plasma membrane at the site known for sperm-ZP binding (convex ridge of mouse sperm and the anterior head plasma membrane overlying the acrosome of pig sperm) (Carmona et al., 2002a; Tantibhedhyangkul et al., 2002). We have also shown in both mice

and pigs that ARSA on the sperm plasma membrane is involved in *in vitro* fertilization via its interaction with the ZP (Carmona et al., 2002a; Tantibhedhyangkul et al., 2002). In mice, the ZP is composed of three glycoproteins (mZP1, mZP2, and mZP3), and the mZP2 and mZP3 glycoproteins are known as the sperm receptors (Wassarman, 2008; Wassarman and Litscher, 2008). For a better understanding of the ARSA-ZP binding mechanisms, we have isolated individual mouse ZP glycoproteins and performed the binding of these proteins with purified sperm ARSA and recombinant ARSA proteins having mutations in the active site pocket amino acids (i.e., with no ARSA enzymatic activity). Our results revealed that purified sperm ARSA indeed has direct affinity for mZP2 and mZP3. However, the binding of ARSA to mZP2/mZP3 occurs in a non-enzymatic manner; recombinant ARSA with the active site amino acids mutated still binds to both mZP2 and mZP3 (Xu et al., 2012).

In addition to the sperm head plasma membrane location, ARSA has long been known to be in the acrosome of mammalian sperm (Dudkiewicz et al., 1979; Dudkiewicz, 1984). Our lab has recently shown that ARSA is specifically localized to the inner acrosomal membrane and within the acrosome (Xu et al., 2012). Based on the affinity of ARSA to mZP2/mZP3, ARSA at this acrosomal location may contribute to the ongoing ZP interaction of acrosome-reacting/reacted sperm (Buffone et al., 2008; Xu et al., 2012). Besides its ZP adhesion property, sperm ARSA has been shown to bind non-enzymatically to chondroitin sulfate B, a component of the cumulus matrix proteoglycans network surrounding the egg, and to facilitate cumulus matrix dispersion during sperm-egg interaction (Wu et al., 2007). Since we have demonstrated that ARSA with mutations in active site pocket amino acids (Cys69, Lys132 and Lys322) and denatured ARSA can still bind to mZP2/mZP3 and chondroitin sulfate B, respectively (Wu et al., 2007; Xu et al.,

2012). Our findings have argued against previous studies suggesting that sperm ARSA played enzymatic roles in cumulus matrix dispersion and ZP digestion (Dudkiewicz, 1984; Ahuja and Gilburt, 1985).

Unlike acrosomal ARSA, which is *de novo* synthesized in testicular germ cells, sperm surface ARSA is originated from the epididymis. We have shown that ARSA, synthesized and secreted by epididymal epithelial cells, is deposited onto the surface of the transit sperm via its specific interaction with SGG (Weerachatyanukul et al., 2003). We have shown that purified sperm surface ARSA binds specifically to SGG monolayers immobilized in the microtiter wells with a high affinity (K_d = 8.9 nM) (Carmona et al., 2002b). This interaction of ARSA with SGG is non-enzymatic, resulting in no production of GG; thus, it indicates that SGG does not access the ARSA's active site pocket. Our computational docking suggests that this non-enzymatic binding of SGG occurs on a positively charged cleft around Arg496 and Ile487 on the ARSA surface (Figure 1.12) (Xu et al., 2012). SGG, which remains intact on the sperm surface, may therefore bind to ARSA at this alternative site. The co-existence of ARSA and SGG has also been demonstrated on the capacitated sperm plasma membrane (specifically in the lipid rafts) (Nixon et al., 2009) as well as on the inner acrosomal membrane of acrosome-reacted sperm (Xu et al., 2012), suggesting that ARSA and SGG may act together during the initial and later steps of sperm-ZP interactions. The findings on the *in vitro* roles of ARSA in sperm-egg interaction have prompted us to further verify the physiological importance of ARSA in fertilization (see below).

1.4.6 *Arsa* knockout mice: a tool for our study on the physiological roles of ARSA in male reproduction

Arsa knockout (KO) mice were produced by Dr. Volkmar Gieselmann, University of Bonn, Germany with the intention of using them as experimental models of MLD. However, these mice have mild MLD phenotypes despite the accumulation of SGC in their brain, a result suggesting that the mouse brain is more tolerant of this sulfoglycolipid accumulation (Hess et al., 1996; Gieselman et al., 1998; my unpublished data in Appendix Figure 1). Dr. Tony Rupar, University of Western Ontario, Canada obtained a breeding pair of these KO mice and back-crossed them to the B6 congenic background. It is obvious that both the male and female *Arsa* KO mice are fertile and the sustaining of the colony is through the breeding of the KO pairs. However, both Drs. Gieselmann and Rupar mentioned to us through our phone conversations that the litter sizes obtained from the KO mouse breeding were smaller than those expected from WT mouse breeding, although a systematic natural breeding study to find out whether the male or female KO mice were subfertile was never performed. Part of my Ph.D. thesis addresses this question. Since results show that *Arsa* KO mice are subfertile with increasing age, I used them as tools in studying the roles of ARSA in male reproduction. These include the role of sperm surface ARSA in sperm-ZP binding and the significance of ARSA enzymatic activity in Sertoli cells in keeping SGG homeostasis in the testis. Since the ARSA KO mice show very mild MLD phenotypes with no obvious changes in their neurological/behavioral characteristics; the reproduction results obtained are likely not a consequence of the severe brain/neurological disorder.

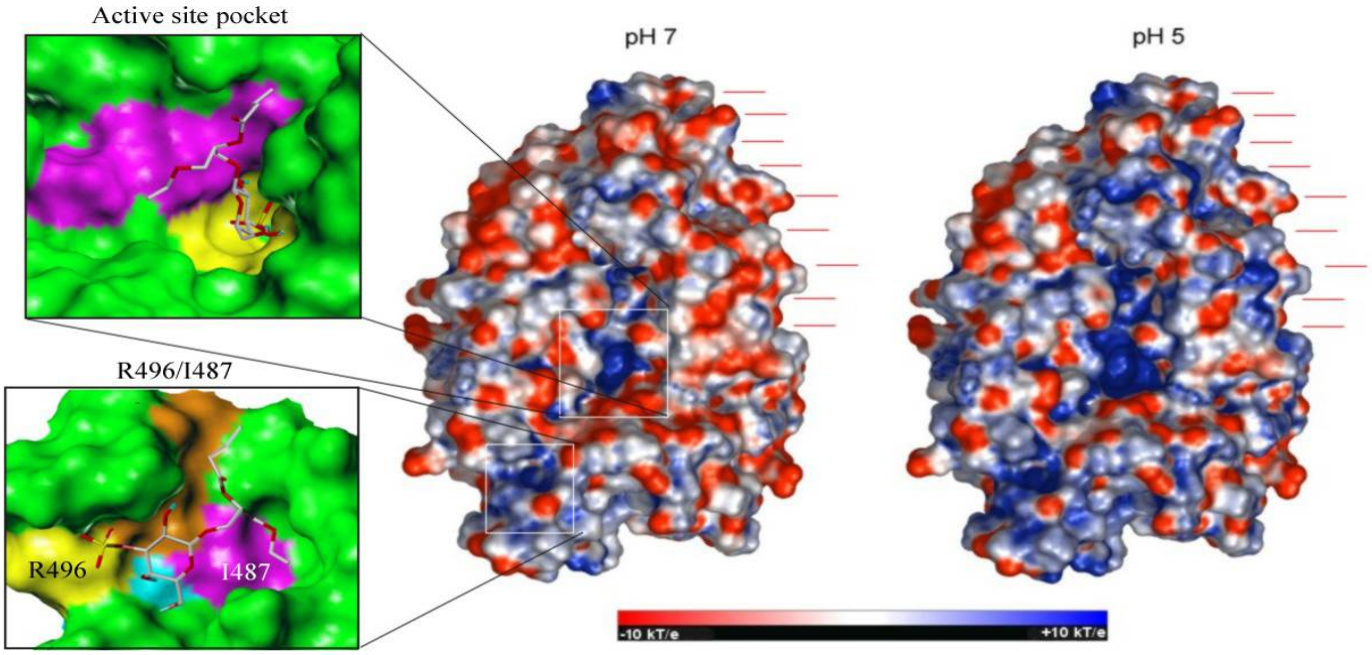

Figure 1.12: Electrostatic surface of ARSA at pH 7 and pH 5 and computational docking of SGG to the active site and the alternative site on the molecular surface of ARSA. The electrostatic potential of ARSA was calculated at pH 7 and 5 based on the p*K*a values of individual amino acids in the area. The surfaces are displayed with negative and positive potential values in red (negative) and blue (positive), respectively (in energy units of kT/e). The active site pocket (indicated by a big white box) of ARSA has the highest positive charges at both pH7 and pH 5. At both pH values, there exists a cleft on ARSA molecular surface consisting of R496 and I487 (indicated by a small white box) with the second highest positive charges. SGG docked well into both sites of ARSA active site (Schenk et al., 2009; Xu et al., 2012).

1.5 Proteomic and lipidomic analyses by mass spectrometry

Mass spectrometry (MS) is a powerful analytical tool on which the emerging "omics" technologies are based because it allows sensitive and accurate measurement of many components simultaneously in a complex sample mixture (Di Girolamo et al., 2013; Griffiths and Wang, 2009). A mass spectrometer measures the mass-to-charge ratios (m/z) of gas-phase ions of atoms or molecules in the sample, which can then be identified by correlating known masses to the measured masses or through a characteristic fragmentation pattern. A mass spectrometer consists of three basic components: an ion source, a mass analyzer (or combination of analyzers), and a detector (Figure 1.13). In a usual "omics" experiment, a sample is commonly delivered to the mass spectrometer via a chromatographic device (e.g., liquid chromatography column), and ionized and vaporized in the ion source. The two most commonly used ionization techniques are electrospray ionization (ESI) and matrix-assisted laser desorption ionization (MALDI). The gas-phase ions are then separated on the basis of their m/z in the mass analyzer. The separated ions are finally detected as an electric charge obtaining signals proportional to the abundance of each ion species, and the results are displayed as a plot of the relative abundance of the ions against their m/z, so called a "mass spectrum" (Di Girolamo et al., 2013; Griffiths and Wang, 2009).

Most proteomics and lipidomics experiments are conducted using tandem mass spectrometry (MS/MS), which is required for the identification of proteins and lipids in a sample. A tandem mass spectrometer consists of a series of mass analyzers; the first and the final mass analyzers are used for ion isolation, whereas the second analyzer is a collision cell for ion fragmentation. Different methods of ion fragmentation can be used, for example, collision-induced dissociation (CID), electron capture dissociation (ECD), and electron

transfer dissociation (ETD). There are 4 major MS/MS modes (Figure 1.14), including i) product ion scan, ii) precursor ion scan, iii) neutral loss scan, and iv) selected or multiple reaction monitoring (Di Girolamo et al., 2013; Griffiths and Wang, 2009). These MS/MS scan modes, usually operated by a triple quadrupole (mass analyzer) system, have been the most commonly used approach for lipidomic research (Griffiths and Wang, 2009; Wenk, 2005). For protein identification by MS, there are two commonly used strategies: top-down and bottom-up proteomics. In top-down proteomics, intact proteins are introduced into a mass spectrometer and subjected to gas-phase fragmentation by ECD or ETD. In contrast, in bottom-up proteomics, the proteins are first separated by gel electrophoresis or chromatography and subsequently digested by trypsin prior to introduction into the mass spectrometer. The bottom-up approach has higher sensitivity but limited protein sequence coverage as compared with the top-down method. The peptide/protein identification relies on the comparison of masses of the proteolytic peptides or their tandem mass spectra with those predicted from a sequence database (such as Uniprot). The protein is identified from the best overlap between the experimental and theoretical spectra (Di Girolamo et al., 2013).

The availability of databases with genome and amino acid sequence information of several species as well as advances in bioinformatics technologies has made MS a powerful technique for the large-scale analysis of proteins in a wide range of biological samples, including sperm. Sperm are inactive in regard to gene transcription or protein translation due to their highly condensed chromatin structure. Changes during the sperm maturation processes (i.e., epididymal maturation, capacitation), where sperm acquire their fertilizing capability, mainly occur through surface component modifications, such as post-translational modification of proteins, acquisition of new molecules and/or removal of existing

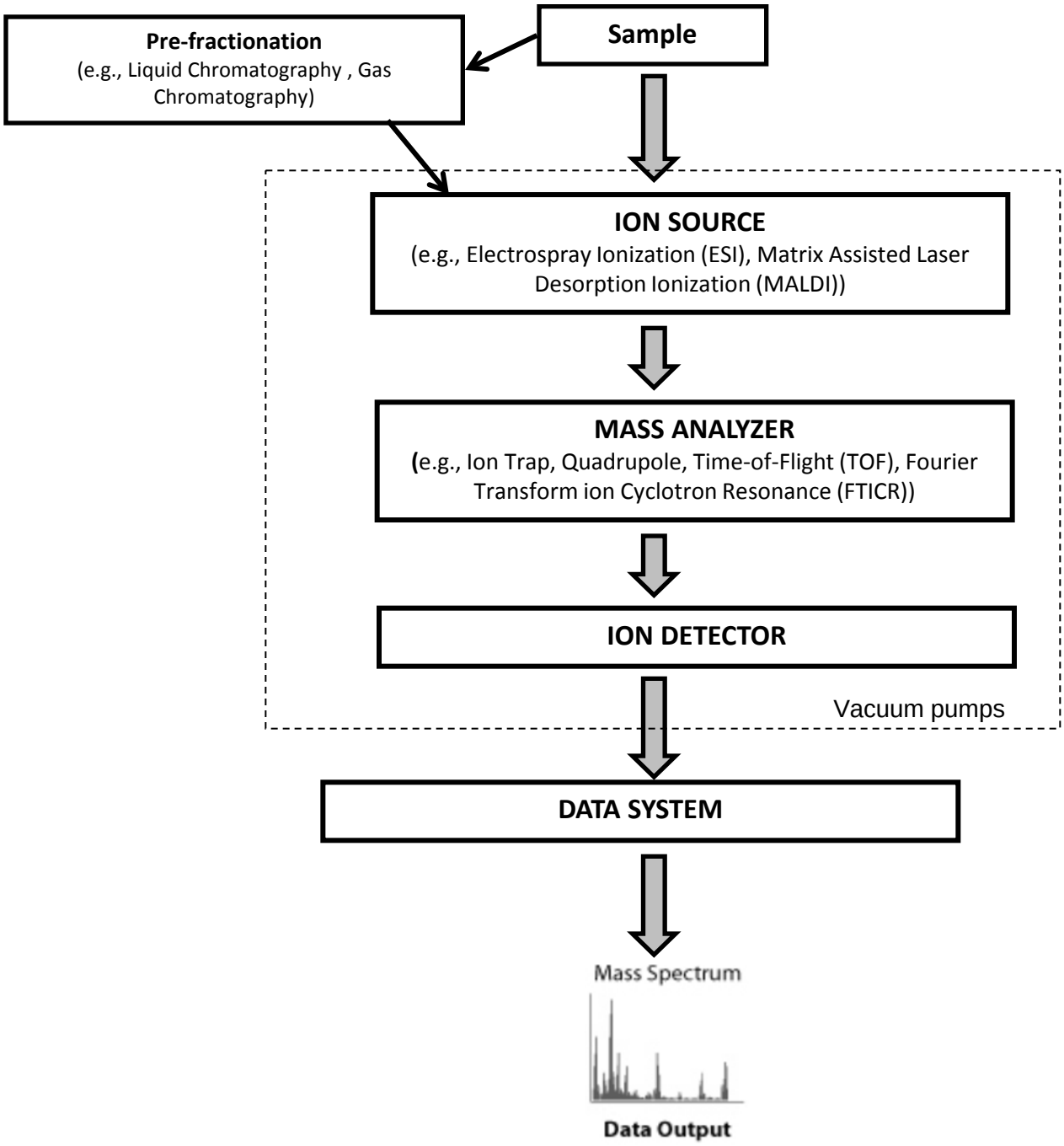

Figure 1.13: Basic components of a mass spectrometer. A pre-fractionation module, such as liquid or gas chromatography, is usually used to introduce sample into a mass spectrometer. Three fundamental elements of a mass spectrometer are an ion source, a mass analyzer (or combinations of analyzers), and an ion detector; all of which are maintained under high vacuum to allow ions to travel from one end to the other end of the instrument without any hindrance from air molecules. The signals from the ion detector are then further processed to generate a mass spectrum.

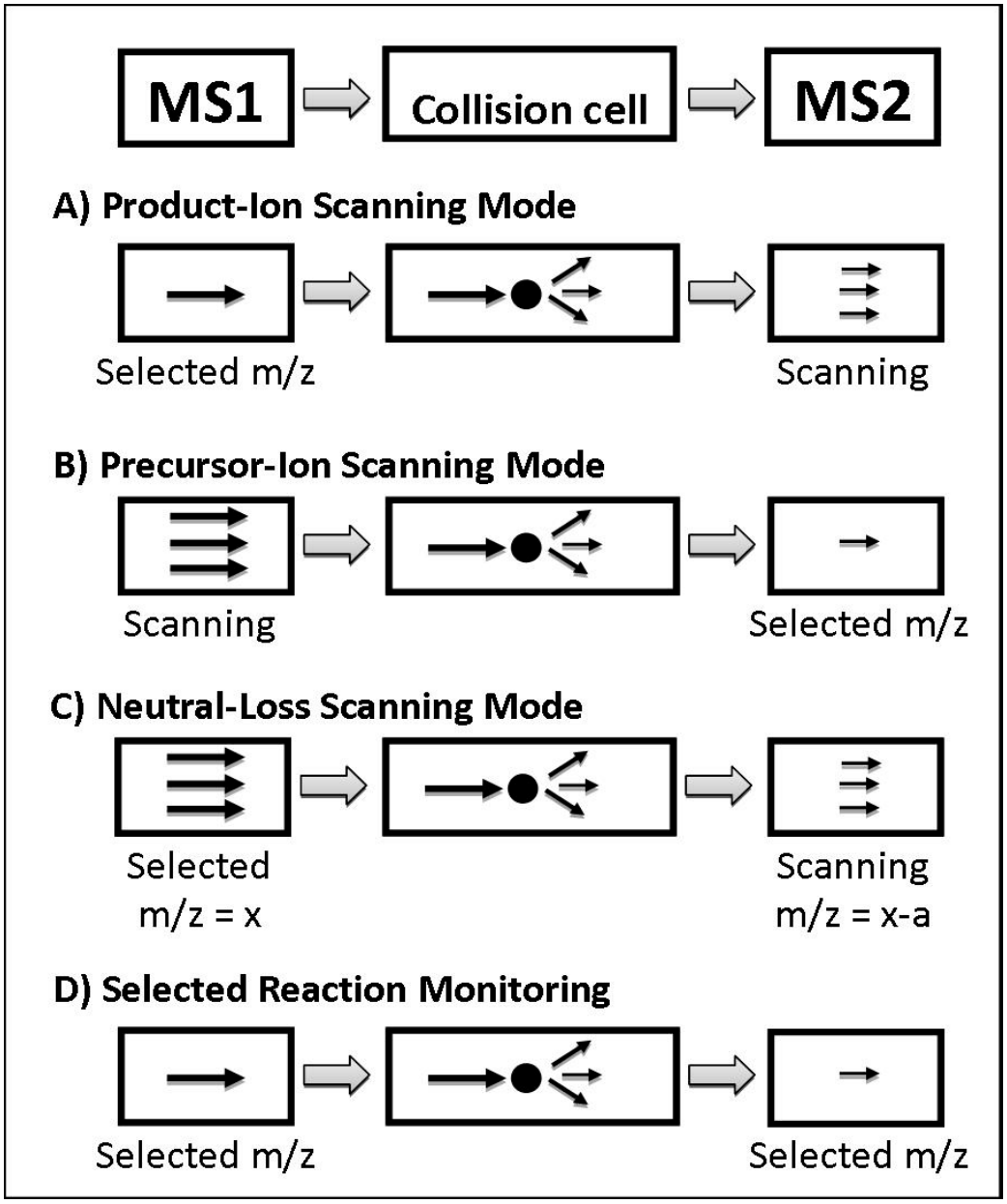

Figure 1.14: Four scan modes routinely used for MS/MS. A) Product-ion scanning mode. The first analyzer (MS1) selects a precursor ion of interest which is fragmented in the collision cell and the second analyzer (MS2) then measures m/z of all resultant product ions. **B)** Precursor-ion scanning mode. The MS1 detects all precursor ions and the MS2 focuses on a particular product ion of interest after ion fragmentation. **C)** Neutral-loss scanning mode. The MS1 and MS2 scan ions simultaneously but with a defined offset. A precursor ion transmitted to MS1 is recorded only if it yields a fragment (product) ion (x-a) in MS2 that is corresponding to the loss of a defined neutral fragment (a) from the precursor ion (x). **D)** Selected reaction-monitoring mode. The MS1 and MS2 both focus on the selected ions. When a set of selected ions are monitored for multiple reactions in one of the analyzers or both, the term "multiple reaction monitoring (MRM)" is used.

components. For this reason, proteomics has been the method of choice for studying the changes of sperm proteome during the maturation processes (Baker et al., 2012; Oliva et al., 2009). Although lipids are known to play important roles in a number of key physiological processes, including those in male reproduction, comprehensive analysis of lipids by MS has not been performed as extensively as that of proteins. This lack of analysis may be due to several reasons: While proteins are linear polymers with amino acids as their common basic component, lipids consist of many classes of different molecules (e.g., glycerols, fatty acids, sterols, sphingosines). Due to structural diversity, each lipid class has its own requirements for fragmentation and its specific ionization efficiency for MS analysis, therefore, the fragmentation of lipids cannot be standardized as that of proteins can be. This is one of the reasons why the development of standardized "all inclusive" methods for lipid analysis is a daunting challenge despite all the advances in MS technologies (Kofeler et al., 2012; Sandra and Sandra, 2013). Moreover, the data processing software for lipid identification and quantification is not commercially available and so far the data analysis has had to be manually performed (Kofeler et al., 2012). However, tremendous progress in MS-based lipidomics has been made for the past decade since the first shotgun lipidomics study was introduced by Han and Gross (Han and Gross, 1994). A number of lipidomic studies have revealed that changes in lipid profiles/levels are associated with several diseases, such as Alzheimer's disease, cancers, and atherosclerosis (Han et al., 2003; Rolim et al., 2014; Wenk, 2005). Despite the current technical challenges, it can be expected that MS-based lipidomics will continuosly develop into a high throughput technology and offer deeper insights into the understanding of molecular mechanisms underlying several diseases.

1.6 Research hypotheses, specific aims and experimental approaches

Specific Aim 1: To perform proteomic characterization of APM vesicles (SGG-associated membranes) isolated from non-capacitated (Non-cap) and capacitated (Cap) pig sperm

Hypothesis: *During capacitation the sperm APM undergoes biochemical changes that allow sperm to gain full ZP-binding ability. These changes may include recruitment of more ZP-binding proteins into the APM as well as formation of high molecular weight complexes with enhanced ZP-binding capacity*. The hypothesis was made based on our previous findings that sperm lipid rafts isolated as detergent resistant membranes (DRMs) from Cap sperm have higher ZP-binding capacity than DRMs from Non-cap sperm. Sperm APM vesicles are deemed to be sperm lipid rafts isolated by physical force. The proteomic characterization of sperm APM vesicles in this aim would provide a better understanding on how sperm gain their full fertilizing ability. The characterization of high molecular weight protein complexes with ZP-binding ability of APM vesicles would validate the existing concept in the field as to whether sperm APM proteins act together in ZP interaction.

Experimental Approaches: APM vesicles were isolated from Non-cap and Cap pig sperm by nitrogen cavitation at 650 psi. MS-based proteomic analyses of Non-cap and Cap APM vesicles were performed in a quantitative manner. The presence of APM proteins existing as high molecular complexes with ZP3 affinity was then validated by blue native gel electrophoresis and far western blotting. The identity of these proteins was then determined by gel-based MS analyses.

Specific Aim 2: To determine the fertility status and characterize the SGG levels and other lipid profiles of Sertoli cells and sperm of *Arsa* knockout (KO) mice with increasing age

Hypothesis: *SGG homeostasis is important for male fertility. Its degradation from the apoptotic germ cell remnants and residual bodies phagocytosed/engulfed into Sertoli cells is as important for sperm fertilizing ability as its synthesis in testicular germ cells.* This hypothesis is based on several previous findings of ours and of other investigators. First, SGG has a direct affinity for the ZP and sperm SGG is involved in sperm-egg binding. Second, SGG is integral in the formation of sperm lipid rafts (APM vesicles), which are the sperm head surface platforms of ZP binding. Third, engulfment/phagocytosis of residual bodies and apoptotic germ cells is an ongoing activity of Sertoli cells, which possess ARSA in their lysosomes, presumably involved in the first step of SGG degradation *(based on the fact that lysosomal ARSA is the enzyme that desulfates SGC, a sulfoglycolipid closely structurally related to SGG).* Of note is the fact that apoptosis occurs in >50% of total male germ cells produced during spermatogenesis. SGG degradation into a neutral lipid backbone is thus important for two purposes: to prevent cytotoxicity to Sertoli cells due to intracellular accumulation of the sulfoglycolipid and to provide a recycling pool of the neutral lipid backbone for a new round of SGG synthesis in testicular germ cells.

Experimental approaches: the fecundity, sperm production and morphology, *in vitro* sperm fertilizing ability and intactness of testicular and epididymal tissues of *Arsa* KO mice of various ages were compared with those of age-matched wild type (WT) mice following standard procedures. WT females (< 6 months old) were used for natural mating experiments (assessing fecundity) and also as sources of ovulated mature eggs used in *in vitro* sperm fertilizing ability. Quantitative ESI-MS/MS analysis was used to determine SGG levels from testis homogenates, sperm and Sertoli cells prepared from *Arsa* KO and age-matched WT mice. In some cases, where biological samples were limited,

immunofluorescence detection of SGG was used instead, and the values obtained from *Arsa* KO mice were compared with those from age-matched WT mice. The profiles and levels of other lipids (i.e., sulfolipids other than SGG, phospholipids, triacylglycerols, and cholesteryl esters) in Sertoli cells and sperm of both *Arsa* KO and age-matched WT mice were determined using quantitative ESI-MS/MS with the scan modes specific to each class of lipids. Cholesterol in these samples was quantified using the Amplex Red enzyme assay.

CHAPTER TWO

MATERIALS AND METHODS

2.1 Materials

Dulbecco's Modified Eagle Medium (DMEM) and Dulbecco's Modified Eagle Medium: Nutrient Mixture F-12 (DMEM/F12) were purchased from Life technologies, Inc. (Carlsbad, CA, USA). Fetal bovine serum (FBS), epidermal growth factor (EGF), 2.5% (w/v) trypsin solution, insulin, transferrin, gentamycin, and fungizone were also obtained from Life technologies, Inc. Petri dishes, culture chamber slides, and cell strainers were purchased from BD Biosciences (Bedford, MA, USA). Microscope glass slides and cover slips were obtained from VWR International, LLC. (Radnor, PA, USA). Sterile phosphate buffered saline (PBS) was purchased from Lonza (Walkersville, MD, USA). Percoll solution was obtained from GE Healthcare (Upsala, Sweden). Protease inhibitor cocktail was purchased from Roche Diagnostics (Laval, QC, Canada). The terminal deoxynucleotidyl transferase-mediated dUTP nick labeling (TUNEL) assay kit and anti-fluorescein Fab fragments conjugated with horseradish peroxidase (HRP) that were used for *in situ* cell death detection were also purchased from Roche Diagnostics. The 3, 3'-diaminobenzidine substrate kit was obtained from Vectorlabs (Burlingame, CA, USA). Diff-Quik^{TM} staining kit for assessment of sperm morphology was purchased from Siemens Healthcare Diagnostics Inc. (Newark, DE, USA). Peanut agglutinin conjugated with FITC was purchased from EY laboratories Inc. (San Mateo, CA, USA). Glutaraldehyde, paraformaldehyde, and sodium cacodylate buffer were obtained from Electron Microscopy Sciences (Hatfield, PA, USA). DRAQ5 was purchased from Biostatus Ltd. (Leicestershire,

UK). The Serva Blue/Coomassie blue G-250 used for blue native gel electrophoresis (BN-PAGE) was obtained from Helixx Technologies Inc. (Scarborough, ON, Canada). Pre-cast NativePAGE™ Novex® 3-12% Bis-Tris gradient gels and SilverQuest™ Silver Staining kit were purchased from Life Technologies, Inc. Coomassie blue RAPIDStain solution was obtained from G-biosicences (St Louis, MO, USA). Sequencing grade modified trypsin for in-gel tryptic digestion was obtained from Promega Corporation at two locations (Madison, WI, USA and Annandale, New South Wales, Australia). Purified pig ZP3 glycoprotein consisting of ZP3α and ZP3β was prepared from solubilized pig ZP as previously described (Yurewicz et al., 1987) and provided by Dr. E Yurewicz (Wayne State University, Detroit, MI, USA). Pierce sulfo-NHS-LC-biotin used for pig ZP3 biotinylation was obtained from Thermo Fisher Scientific Inc. HRP-conjugated streptavidin used for biotin detection was purchased from Calbiochem (San Diego, CA, USA). All primary antibodies used for indirect immunofluorescence and immunoblotting experiments are listed with details in Table 2.1. All secondary IgG antibodies conjugated with fluorophores used for indirect immunofluorescence were obtained from Molecular Probes (Eugene, OR, USA). All secondary IgG antibodies conjugated with HRP used for immunoblotting analyses were purchased from Bio-Rad Laboratories (Hercules, CA, USA). Coomassie blue dye reagent concentrate for Bradford assay and nitrocellulose membranes (0.45 μm) were also purchased from Bio-Rad Laboratories. Enhanced chemiluminescence (ECL) kit and Restore™ Western Blot stripping buffer were purchased from Thermo Fisher scientific, Inc. (Rockford, IL, USA). Paramagnetic Dynabeads Protein G kit for immunoprecipitation was obtained from Life Technologies Inc. HPK silica gel 60 Å plates (200 μm thickness, 10 × 10 cm dimension) were purchased from Whatman (Kent, UK). Lipid standards, including sphingomyelin, phosphatidylethanolamine and phosphatidylcholine, were purchased from

Table 2.1: List of primary antibodies used in my thesis research

#	Name of antibody	Antibody production	Source	Experiments
1	Affinity purified goat polyclonal anti-MFGM IgG antibody	This antibody was produced against mouse recombinant MFGM.	Purchased from R&D systems (Minneapolis, MN, USA)	Immunoblotting of pig APM proteins
2	The mouse monoclonal anti-MFGM IgG antibody	This antibody was directed against human recombinant MFGM.	Purchased from R&D systems	Indirect immunofluorescence of pig sperm
3	Rabbit polyclonal anti-proacrosin/acrosin IgG antiserum	This antibody was made against proacrosin purified from guinea pig testes as previously described (Hardy et al., 1987).	Provided by Dr. D Hardy (Texas Tech University Health Sciences Center, Lubbock, TX, USA)	Immunoblotting of pig APM proteins
4	Mouse monoclonal anti-proacrosin/acrosin IgG antibody (C2E5)	This antibody was produced against purified bovine proacrosin (Elce et al., 1986).	Provided by Dr. J Elce (Queen's University, Kingston, ON, Canada).	Indirect immunofluorescence of pig sperm
5	Rabbit polyclonal anti-AQN IgG antiserum	This antibody was produced against boar seminal plasma AQN spermadhesins and shown to recognize both AQN1 and AQN3 (Veselsky et al., 1999).	Provided by Dr. V Jonakova (Institute of Biotechnology AS, CR, v.v.i., Prague, Czech Republic)	Immunoblotting of pig APM proteins
6	Rabbit polyclonal anti-proacrosin binding protein (ACRBP) IgG antiserum	This antibody was made against the C-terminal sequence (Gln409-Tyr512) of mouse ACRBP (Tardif et al., 2012).	Provided by Dr. G Cornwall (Texas Tech University Health Sciences Center, Lubbock, TX, USA).	Immunoblotting of pig APM proteins & indirect immunofluorescence of pig sperm
7	Rabbit polyclonal anti-D1 domain of pig ZAN IgG antibody	This antibody was produced against the purified recombinant protein of von Willebrand factor (VWF) D1 domain of ZAN as previously described (Hickox et al., 2001). This anti-D1 antibody recognizes the p45 form of ZAN, containing VWF D0 and D1 domains (see diagram of ZAN structure in Figure 3.4C).	Provided by Dr. D Hardy	Immunoblotting of pig APM proteins
8	Rabbit polyclonal anti-D3 domain of pig ZAN IgG antibody	This antibody was produced against the purified recombinant protein of von Willebrand factor (VWF) D3 domain of ZAN as previously described (Hickox et al., 2001). The anti-D3 antibody recognizes the p105 form of ZAN, containing VWF D2, D3 and D4 domains (see Figure 3.4C).	Provided by Dr. D Hardy	Immunoblotting of pig APM proteins

Table 2.1 (continued): List of primary antibodies used in my thesis research

#	Name of antibody	Antibody production	Source	Experiments
9	Rabbit polyclonal anti-ZAN holoprotein IgG antibody	This antibody was made against pig ZAN holoprotein which was purified from the extracts of the pig sperm anterior head plasma membrane vesicles using anti-D3 antibody immunoaffinity column (Hickox et al., 2001); this anti-ZAN holoprotein antibody preferentially recognizes the high molecular weight forms (≥300 kDa) of ZAN, including the p105/45 multimeric forms (Hickox et al., 2001).	Provided by Dr. D Hardy	Immunoblotting of pig APM proteins
10	Mouse monoclonal anti-SGG/SGC IgM antibody or Oligodendrocyte marker (O4) antibody	This antibody was produced using white matter of corpus callosum from bovine brain as an immunogen. It is known to specifically react with SGC of oligodendrocytes.	Purchased from Neuromics (Edina, MN, USA)	Indirect immunofluorescence of mouse testicular germ cells and Sertoli cells
11	Mouse monoclonal anti-phosphotyrosine IgG antibody (clone 4G10)	This antibody was produced against phosphotyramine conjugated with KLH *in vitro* using mouse hybridoma 4G10® cells. This antibody recognizes tyrosine-phosphorylated proteins from all species.	Purchased from Millipore Canada Ltd. (Etobicoke, Ontario, Canada)	Immonoblotting of mouse sperm proteins
12	Mouse monoclonal anti-alpha tubulin IgG antibody	This antibody is derived from the hybridoma AA13 produced by the fusion of mouse myeloma cells and splenocytes from BALB/c mice immunized with rat brain tubulin.	Purchased from Sigma Aldrich (St. Louis, MO, USA)	Immonoblotting of mouse sperm proteins

Avanti polar lipids, Inc. (Alabaster, AL, USA). The Amplex Red cholesterol assay kit was obtained from Molecular Probes/Life technologies, Inc. Purified SGG was prepared in house from total pig testis lipid extracts as previously described (Kongmanas et al., 2010). SGG (C16:0/C16:0) with deuterium labels on the alkyl chain (D_3-SGG) was synthesized as previously described (Franchini et al., 2008) and used as the internal standard for SGG quantification by mass spectrometry. All chemicals and reagents other than those described above were obtained from Sigma-Aldrich (Mississauga, ON, Canada).

2.2 Animals

Mice: CF-1 female mice (6 – 8 weeks of age) and CD-1 male mice (10 weeks of age) were purchased from Charles Rivers (Montreal, QC, Canada). C57BL/6J (B6) male (retired breeders at the age of 5-6 months) and female wild type mice (8 weeks of age) were purchased from The Jackson Laboratory (Bar Harbor, ME, USA). A pair of male and female mice with null congenics for the *Arsa* allele was provided to us by Dr. Tony Rupar (University of Western Ontario) and they were used for breeding to retain the colony. The mice were housed in temperature and humidity controlled rooms with a 14:10 dark/light cycle and were provided with food and drink ad libitum. The use and handling of mice followed the protocols approved by the Animal Care Facility, Ottawa Hospital Research Institute or University of Ottawa Faculty of Medicine.

Pig: Pig sperm samples collected from fertile boars were from two sources. The first source was at the Animal Science Swine Facility, University of California, Davis through collaboration with Dr. Trish Berger; the boarding of the pig colony and the use of biological

samples collected from these pigs followed the protocols approved by the Animal Care Committee of this institution. The second source of boar sperm was commercially available from the Ontario Swine Improvement (Innerkip, ON, Canada). Boars ejaculate semen in sequential phases/fractions; the first fraction (~25 ml) contains mainly fluid from prostate gland, the second phase (40-100 ml), so called "sperm-rich fraction", includes mainly sperm, the third fraction is the largest by volume (70-400 ml) and usually discarded to avoid diluting the sperm sample, and the fourth fraction (20-40 ml) is the gelatinous phase. The sperm-rich fraction of pig ejaculates from both sources was collected at the appropriate time during ejaculation and subsequently filtered through two layers of miracloth to remove any small gelatinous particles. At the University of California, Davis, the pig sperm samples were kept in a temperature controlled cooler (~25 °C) and transported immediately to Dr. Berger's laboratory where I performed APM vesicle isolation. Pig sperm samples from the Ontario Swine Improvement (Innerkip, ON, Canada) were diluted in Minitube Androstar extender (Minitube Canada, Ingersoll, ON, Canada) at 1:4 volume ratio of semen: extender, cooled to 17°C prior to shipping to Dr. Tanphaichitr's lab in Ottawa. The pig sperm samples from this second source were used for APM vesicle isolation, lectin staining, indirect immunofluorescence and flow cytometry (see below).

2.3 Mating study for fecundity assessment of mice

The mating study was designed to evaluate the fecundity of *Arsa* knockout (KO) male mice in comparison with that of the age-matched wild type (WT) mice as a function of their age. Four B6 WT male mice and eight *Arsa* KO male mice at ~2 months of age were

used for the mating study over a period of 7 months. Each of these males was individually caged with an 8-week-old B6 WT female for approximately 2 months (a duration that the female could give birth to ~2 litters); afterwards this female was replaced with another 8-week-old WT female. The females that had been separated from the males were kept individually for an additional month to make sure that no live births were missed. All the females used were proven fertile by their ability to deliver pups following mating with WT males after this one-month waiting period. During the mating period, each female was checked for the presence of a vaginal plug (a sign of mating) every morning since the first day of caging with the male. The first day that the vaginal plug detected was counted as Day1 of gestation (for B6 mouse strain, the gestation period is ~20 days). Since the females of this strain sometimes eat their newborn pups, the pregnant females were monitored closely until the day that they delivered the pups and the numbers of pups were assessed immediately on the day of delivery.

2.4 Gamete collection and preparation

2.4.1 Preparation of caudal epididymal and vas deferens mouse sperm by a swim-up technique and Percoll gradient centrifugation

The caudal epididymis and vas deferens were dissected out from *Arsa* KO and age-matched WT mice, as well as CD-1 male mice. The caudal epididymis was longitudinally scored in the middle with a surgical blade and the epididymal luminal content was squeezed out from this incision using a pair of surgical forceps. The content in lumen of vas deferens was also collected by gently pressing the tubule along its length with a pair of surgical

forceps. The luminal content, containing mainly sperm, from both caudal epididymis and vas deferens was placed in a 1.5-ml microcentrifuge tube containing 0.5-1 ml of an appropriate medium (see below) that had been pre-warmed to 37°C.

For sperm preparation by the swim-up technique, the sperm-rich content collected from the caudal epididymis and vas deferens was first placed at the bottom of a microcentrifuge tube containing 500 µl of Krebs Ringers bicarbonate (KRB) supplemented with 0.3% bovine serum albumin (BSA) (KRB: 119.4 mM NaCl, 4.8 mM KCl, 1.7 mM $CaCl_2$, 1.2 mM KH_2PO_4, 1.2 mM Mg_2SO_4, 25 mM $NaHCO_3$, 25 mM sodium lactate, 1 mM sodium pyruvate, 5.6 mM glucose, 2.8 µM phenol red, pH 7.4). This 500-µl sperm suspension was then layered over with 1 ml of the same medium (KRB-BSA) into the same tube. This layering was done with care by having the medium released gently from the transfer pipet on the side of the tube wall. The tube was tilted 45° and then incubated for 30 min at 37°C under 5% CO_2. Due to the presence of BSA in the medium, sperm were capacitated; 600 – 800 µl of medium from the surface top containing sperm that swam up from the bottom layer was collected and referred to as the "swim-up" sperm fraction. The swim-up sperm fraction was immediately transferred into a new pre-warmed tube and used in the *in vitro* gamete functional assays (see below). The leftover medium (200-400 µl), which contained mainly immotile sperm and other epididymal/vas deferens luminal content, were also collected for further used in light microscopic assessment (see below).

For sperm preparation by Percoll gradient centrifugation (PGC), the sperm-rich content collected from caudal epididymis and vas deferens was resuspended in 2 ml of HEPES-buffered Krebs Ringers bicarbonate (KRB-HEPES) medium (KRB-HEPES: 119.4 mM NaCl, 4.8 mM KCl, 1.7 mM $CaCl_2$, 1.2 mM KH_2PO_4, 1.2 mM Mg_2SO_4, 21 mM HEPES,

5 mM $NaHCO_3$, 25 mM sodium lactate, 1 mM sodium pyruvate, 5.6 mM glucose, 2.8 µM phenol red, pH 7.4). This 2-ml sperm suspension was then loaded onto a discontinuous gradient of 45% and 90% Percoll prepared in KRB-HEPES. The gradient was centrifuged (800 x *g*, 28°C for 30 min), allowing motile sperm to sediment as a pellet and immotile sperm at the interface between the 45% and 90% layers of Percoll (Tanphaichitr et al., 1990). The immotile sperm were collected from the interface by aspiration with a transfer pipet, transferred into a new pre-warmed 15-ml falcon tube, and resuspended in 2 ml of KEB-HEPES. After removing other layers of the Percoll gradient, the motile sperm pelleted at the bottom of the gradient were resuspended in 1 ml of KRB-HEPES. Both interfaced sperm and PGC pelleted sperm were washed once with KRB-HEPES by centrifugation (500 x *g*, 28°C, 5 min). In some experiments (i.e., detection of protein tyrosine phosphorylation), the motile PGC pelleted sperm were resuspended in KRB-0.3% BSA at a concentration of 10 x 10^6 sperm/ml, and then allowed to capacitate in the same medium for 1 hour (h) at 37°C under 5% CO_2 (see below).

Prior to further use in lipid extraction and subsequent quantitative lipid analysis, sperm in the swim-up sperm fraction as well as sperm in the interfaced and PGC pelleted fractions were washed twice with PBS by centrifugation (500 x *g*, 28°C, 5 min). The numbers of total sperm in each sample/fraction prepared by swim-up or PGC technique was assessed as follows. An aliquot of each sperm suspension (~10 µl) was appropriately diluted (10-20X) in PBS and placed onto a hemocytometer, and sperm were counted under a Nikon inverted microscope (DIAPHOT-TMD, Nikon Canada, Mississauga, ON) at 200X magnification.

2.4.2 Preparation of mouse oocytes

Mouse oocytes were prepared from 8-week-old CF-1 female mice for sperm-egg binding and *in vitro* fertilization assays. Superovulation was induced by intraperitoneal injection of the female mice with 7.5 units of pregnant mare's serum gonadotropin (PMSG), and 7.5 units of human chorionic gonadotropin (hCG) (48 hours after PMSG injection). Following hCG injection for 14-15 hours, ovulated cumulus oocyte complexes were retrieved from the oviduct of the superovulated female mice and placed in KRB-HEPES containing 0.3% BSA using established procedures (Hogan et al., 1994). ZP–intact eggs were freed from the cumulus cells by treatment with 0.1% (wt/vol) bovine testicular hyaluronidase in KRB-HEPES for 1-2 min. The cumulus-free oocytes were thoroughly rinsed with KRB-HEPES-0.3% BSA medium and kept in KRB-0.3% BSA in an incubator (37°C, under 5% CO_2) prior to co-incubation with sperm. Note that only oocytes containing the first polar body with good morphology were selected for our experiments.

2.4.3 Mouse gamete functional assays

In vitro binding ability of sperm from WT and *Arsa* KO mice to ZP-intact eggs was determined using procedures described previously (Tanphaichitr et al., 1993). Briefly, ZP-intact eggs (n = 20–30) and capacitated swim-up sperm (6 x 10^4 sperm) prepared as described above were co-incubated in a 60-µl droplet of KRB-0.3% BSA (for 30 min, 37°C, under 5% CO_2). Following the co-incubation, sperm loosely bound to the ZP were removed by sequential transferring the sperm–egg complexes through 4 droplets of 60-µl of KRB-0.3% BSA using a drawn glass Pasteur pipette with an inner diameter of ~200 µm. The sperm-egg complexes were then placed into wells of glass depression slides (Thermo Fisher

Scientific Inc.) and over-layered with mineral oil. The number of sperm bound to the ZP of each egg was counted under a Nikon Diaphot inverted microscope. Since many sperm were bound to the ZP, only those in the same focal plane as the diameter of ZP were counted.

The *in vitro* fertilization assay was carried out as previously described (Tantibhedhyangkul et al., 2002). Briefly, capacitated swim-up sperm (~5 x 10^5 sperm) prepared from either WT or *Arsa* KO mice were incubated with 20–25 cumulus-free, ZP-intact eggs (37°C, under 5% CO_2) in 500 µl of KSOM medium supplemented with 0.3% BSA (KSOM: 95.0 mM NaCl, 2.5 mM KCl, 1.7 mM $CaCl_2$, 0.35 mM KH_2PO_4, 0.2 mM Mg_2SO_4, 25 mM $NaHCO_3$, 0.2 mM sodium pyruvate, 10 mM sodium lactate, 0.2 mM glucose, 0.01 mM sodium EDTA, 1.0 mM L-glutamine, 1 U/ml of penicillin G, 1 µg/ml of streptomycin sulfate, and 28 µM phenol red at pH 7.4). After 6 hours of gamete co-incubation, eggs were assessed for their fertilization status under a Nikon Diaphot inverted phase-contrast microscope at 400X magnification. Fertilized eggs were identified by the presence of two pronuclei. Level of parthenogenesis was also assessed by incubating eggs under the same conditions but without sperm addition and this level was consistently 0%.

2.4.4 Preparation of ejaculated pig sperm and capacitation

Pig sperm from both sources were washed free of seminal plasma or extender by centrifugation (500 x *g*, 28°C, 5 min). The washed sperm were resuspended in non-capacitating medium (0.1 M NaCl, 0.36 mM NaH_2PO_4, 8.6 mM KCl, 0.5 mM $MgCl_2$, 11 mM glucose, 23 mM HEPES, pH 7.6) at a concentration of 250 x 10^6 sperm/ml and subjected to centrifugation through 35/70% Percoll gradient to select the motile sperm population as previously described (Bou Khalil et al., 2006). The motile sperm fraction was

divided into two portions. The portion resuspended in non-capacitating medium was referred to as “non-capacitated (Non-cap) sperm”. The other portion which was referred to as “capacitated (Cap) sperm” was resuspended in capacitating medium (containing all components of the non-capacitating medium plus 10 mM $NaHCO_3$, 2 mM $CaCl_2$, 5 mM pyruvate and 0.3% BSA) and further incubated under 5% CO_2 at 39°C in this medium for 2 hours (minimum time for sperm to gain egg binding ability). Under microscopic examination, only Cap sperm possessed hyperactivated motility patterns. The Cap sperm were washed free of BSA in the non-capacitating medium prior to use in all experiments.

2.5 Preparation of testicular germ cells

Testicular germ cell mixture was prepared from testes of 5-month-old and 8-month-old *Arsa* KO mice and age-matched WT animals by sequential enzymatic digestion. The testes were dissected from the mice, weighed and carefully stripped off their tunica albuginea (capsule) and transferred into a siliconized 50-ml flask containing DMEM. The decapsulated testes were digested with 0.5 mg/ml collagenase in DMEM at 35°C for 15 min with constant shaking at 100 cycles per minute. This step allows the removal of interstitial cells and results in uncoiled seminiferous tubules. The resulting seminiferous tubules were allowed to sediment by gravity and washed 3 times with DMEM. The tubules were further digested with 0.5 mg/ml trypsin in DMEM supplemented with 1 µg/ml of DNase I at 35°C for 15 min with constant shaking at 130 cycles per minute. During the collagenase and trypsin treatments, the mixture of 5% CO_2 in air was directed into the flask via a large (18 G) needle. At the end of trypsin digestion, soybean trypsin inhibitor was added to the suspension to a

final concentration of 0.5 mg/ml. The suspension was gently pipetted with a large bore plastic transfer pipet to break up small clumps of tissues and filtered through a 70-µm nylon mesh cell strainer. The filtered cell suspension was centrifuged (450 x *g*, 28°C, 8 min) to pellet the testicular germ cell mixture and the cells were washed 3 times with washing buffer (0.5% BSA, 0.25 mg/ml soy bean trypsin inhibitor, 0.5 µg/ml DNase I in DMEM) by centrifugation as described above.

Alternatively, the testicular germ cell mixture prepared from 10-week-old CD-1 WT mice was further subjected to separation of each spermatogenic cell type using the STA-PUT method as previously described (Bellve, 1979). The STA-PUT method uses a linear BSA gradient and simple velocity sedimentation to separate testicular germ cells based on their masses and sizes. This cell isolation was performed by Dr. S Moss (University of Pennsylvania).

2.6 Preparation of primary cultured Sertoli cells isolated from different ages of mice

Sertoli cells were isolated from testes of 5-day-old, 20-day-old, 10-week-old CD-1 male mice as well as 8 to 11-month-old *Arsa* KO mice and age-matched WT mice (A flow chart showing major steps of Sertoli cell isolation is shown in Figure 2.1). The testes were dissected from these mice, decapsulated and transferred into a siliconized 50-ml Erlenmeyer flask containing DMEM/F12, which was supplemented with 20 µg/ml gentamycin, 10 µg/ml bacitracin, and 0.25 µg/ml Fungizone (Modified DMEM/F12). The decapsulated testes were washed three times with the modified DMEM/F12 medium to remove contaminating blood cells and allow to sediment by gravity. These washed testes were then digested by 0.5 mg/ml

collagenase in modified DMEM/F12 medium, containing 50 µg/ml DNase I, at 35°C for 15 min with constant shaking at 150 strokes per minute; this step results in loose seminiferous tubules. The tubules were subsequently washed once with modified DMEM/F12 medium and treated with a hypertonic solution (1M glycine, 2 mM EDTA (pH 7.4) and 50 µg/mL DNase I in modified DMEM/F12) at 35°C for 10 min with constant shaking at 150 strokes per minute to remove Leydig cells. Following washing with modified DMEM/F12 medium, the seminiferous tubules were digested into small pieces by incubating with 0.5 mg/ml trypsin in modified DMEM/F12 supplemented with 50 µg/mL DNase I at 37°C for 15 min. After the trypsin treatment, soybean trypsin inhibitor (0.5 mg/ml) was added to stop the enzyme reaction. The small fragments of seminiferous tubules and dispersed cells obtained from the trypsin digestion were then pelleted by centrifugation (800 x *g*, 28°C, 3 min). The pellet was washed once with modified DMEM/F12 medium and centrifuged under the same condition, and subjected to further digestion at 35°C for 30 min with constant shaking at 150 strokes per minute in modified DMEM/F12 containing 1 mg/mL collagenase, 2 mg/ml hyaluronidase, 0.1 mg/ml soybean trypsin inhibitor and 50 µg/mL DNase I to disperse Sertoli cells and germ cells from the tubule wall. Following this enzyme incubation, the cell mixture in this suspension was washed twice with modified DMEM/F12 and centrifugation (800 x *g*, 28°C, 3 min). The cell mixture was then filtered through a 100-µm nylon mesh cell strainer to remove any aggregates and the filtrate was then subjected to low speed centrifugation (57 x *g*, 28°C, 5 min) to pellet the Sertoli cells and separate the majority of the germ cells in the supernatant. The Sertoli cells in the pellet were washed twice and resuspended in “the complete Sertoli cell medium”, which is the modified DMEM/F12 supplemented with 10 µg/mL bovine insulin, 5 µg/mL human transferrin, and 2.5 ng/mL EGF. The cells were plated on a 60-mm Petri dish at density of 5 million cells/dish (for 5- and 20-day-old mice) or at density of 15-20 million

cells/dish (for 10-week-old and 8 to11-month-old mice); these cells were cultured in an incubator (35 °C, equilibrated with 5% CO_2). Once Sertoli cells have attached to the bottom of the Petri dish (i.e., Day 2 of culture for 5- and 20-day-old mice and Day 3 of culture for adult mice), any non-adhering germ cells that are co-isolated with Sertoli cells can be removed from the culture by gently rinsing the attached Sertoli cells with new complete Sertoli cell medium and this rinsing step was repeated every other day. On Day 8 of culture, Sertoli cells that are free of contaminating germ cells were harvested by incubating the cells in 3 ml of 0.25% trypsin and 0.53 mM EDTA in PBS for 3-4 min at 37 °C. The trypsin enzymatic reaction was stopped by the addition of DMEM/F12 medium containing 5% FBS (3 ml) to the culture dish. Sertoli cells in the suspension was collected by centrifugation (500 x *g*, 28°C, 5 min) and washed twice with PBS to remove FBS from the cells. The cells were then subjected to lipid extraction and MS analyses.

Our previous protocol for isolation of Sertoli cells, which were used for the immunofluorescence study (as previously shown in our publication (Xu et al., 2011)), was slightly different from the protocol described above. Namely, prior to cell filtration through 100-µm nylon mesh, the additional step of enzymatic digestion was performed by incubating cells in 1 mg/ml hyaluronidase in DMEM/F12 supplemented with 50 µg/mL DNase I at 35°C for 40 min with constant shaking at 200 strokes per minute. Also, the hypotonic solution (20 mM Tris-HCl, pH 7.4) was previously used to treat Sertoli cells to remove any contaminating germ cells on Day 3 of culture prior to harvesting Sertoli cells on Day 5 of culture. However, we omitted these steps in our modified Sertoli cell isolation protocol since we found out that these steps caused lower yield of isolated Sertoli cells.

1) Remove the tuniga albuginea (capsule) of the testes

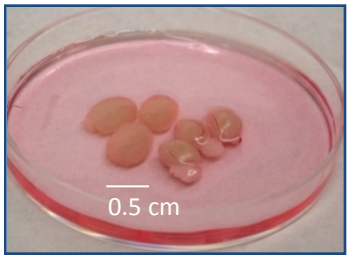

2) Treat decapsulated testes with collagenase to disperse interstitial cells of testes, yielding uncoiled seminiferous tubules

3) Treat seminiferous tubules with trypsin to digest the tubules into smaller fragments

4) Treat digested tubules with collagenase and hyaluronidase and gently pipette the tubules to disperse Sertoli and germ cells from the tubule walls

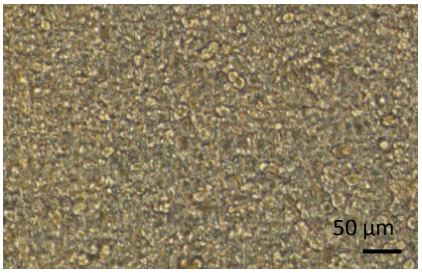

5) Filter mix cell suspension through 100 µm to remove any undigested tubules and collect the cell mixture in the filtrate

6) Pellet Sertoli cells from the cell mixture by low speed (57 g) centrifugation

7) Wash the cell pellet twice with medium, count the cell number and plate cell mixture on a 35-mm petridish at 15-18 million/dish

8) On Day 3 of culture, remove unattached cells (mainly contaminated germ cells) from the attached Sertoli cells by gently rinsing with the culture medium

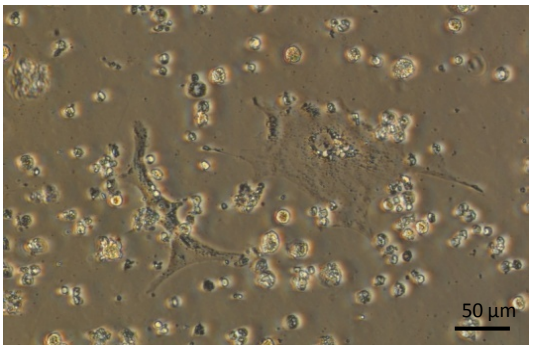

9) Remove any unattached cells everyday by rinsing with the culture medium. On Day 7 of culture, harvest the attached Sertoli cells (90-95% purity) by trypsination

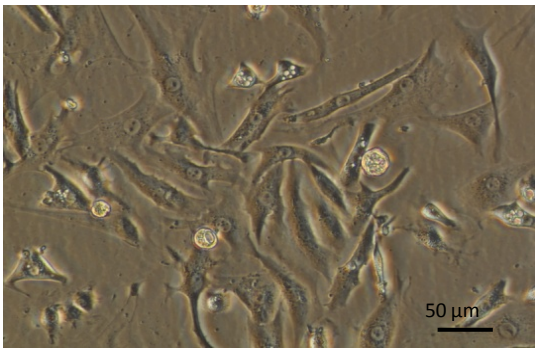

Figure 2.1: A flow chart showing procedure for isolation of Sertoli cells from adult mouse testes. The details of major steps and images of final products from certain steps are included.

2.7 Histological analyses of mouse testes, epididymis and sperm

2.7.1 Hematoxylin and eosin staining of testis and epididymis sections

Testes and epididymides collected from 5- and 8-month-old *Arsa* KO mice and age-matched WT animals were fixed in Bouin's solution at room temperature (RT) overnight. The fixed tissues were washed several times with 70% ethanol and stored in this solution before shipping to the Centre for Bone and Periodontal Research (McGill University, Montreal) for sectioning. Briefly, the tissues were serially dehydrated in increasing concentrations of ethanol and embedded in paraffin. The tissue paraffin blocks were cut into 6-µm-thick sections and the sections were mounted onto glass slides and heated to dryness at 60°C in an oven for 30 min. The tissue sections were deparaffinized in Xylene (3 min, 3 times) and then rehydrated through 100%, 95%, and 70% ethanol, and MilliQ water (5 min/each), respectively. The sections were stained with hematoxylin (nuclear staining) and eosin (cytoplasmic staining). The sections were dehydrated through 70%, 95%, and 100% ethanol (2 min/each), respectively. The sections were immersed in Xylene twice (3 min/each) and mounted with Permount, topped with a coverslip and viewed in bright field under a Zeiss IM35 epifluorescent microscope (Carl Zeiss Canada Ltd., Toronto, ON, Canada) and the images were captured at 100X and 400X magnification. Testes and epididymides collected from three animals of each age and each genotype were sectioned and viewed for histological analyses.

2.7.2 Quantitative analysis of seminiferous tubule profile areas

Quantitative analysis of the seminiferous tubule and epithelial areas of 5- and 8-month-old *Arsa* KO and WT mice was performed using a Zeiss MOP-3 image analyzer as previously described (Korah et al., 2003).

2.7.3 Electron microscopic analysis of testes

Two additional *Arsa* KO and WT mice at both 5 and 8 months of age were anesthetized with sodium pentobarbital, and were perfused via vascular system through the heart with normal saline (0.9% (w/v) NaCl) until the testes were clear of blood. Following the normal saline perfusion, the animals were then immediately perfused with a fixative containing 2.5% glutaraldehyde in 0.1 M sodium cacodylate buffer (pH 7.4) to fix the testes. The fixed testes were removed from animals, trimmed into small pieces (0.5 mm^3), and immersed in the above fixative solution containing 4% (w/v) sucrose at 4 ˚C, overnight. The tissues were sent to McGill University to be processed for electron microscopic analysis following the previously described protocol (Hermo et al., 1991).

2.7.4 Assessment of sperm morphology by Diff-Quik staining

Sperm retrieved from the caudal epididymal and vas deferens, which had been processed through the swim-up or PGC technique, were washed twice with PBS and gently applied onto a glass slide. After becoming air-dried, sperm were stained with Diff-Quik™ Stain kit following the manufacturer's protocol (Siemens Healthcare Diagnostics Inc.). The morphology of these cells in each fraction was assessed under a Zeiss Axioskop light microscope (Carl Zeiss Canada Ltd.) and the images were taken at 400X magnification.

2.8 Detection of apoptotic cells in the testis sections

The terminal deoxynucleotidyl transferase-mediated dUTP nick labeling (TUNEL) assay was performed on testis sections of 5- and 8-month-old WT and *Arsa* KO mice. Paraffin sections of the mouse testes (6-µm thick) were deparaffinized and rehydrated as described above. The sections were then permeabilized in freshly prepared 0.1% sodium citrate containing 0.1% Triton X-100 for 8 min at RT. After two rinses with PBS, the slides were treated with 1% hydrogen peroxide in 70% ethanol for 10 min to quench endogenous peroxidase. Following two washes in PBS, apoptotic cell staining was carried out using the in situ cell death detection kit containing TUNEL Enzyme and TUNEL Label Mix according to the supplier's instruction (Roche Diagnostics). The sections were then washed 3 times with PBS and viewed under the Zeiss IM35 epifluorescence microscope. The fluorescent signals of TUNEL-positive cells were subsequently converted into colorimetric signals by incubating the sections with anti-fluorescein Fab fragments conjugated with horseradish peroxidase for 30 min at 37^{o}C, followed by 3, 3'-diaminobenzidine substrate kit for 2-10 min at RT. The TUNEL-positive cells in the sections were finally stained brown. The sections were then washed 3 times with PBS, mounted with 50% glycerol in PBS under glass coverslips and analyzed under the Zeiss Axioskop light microscope.

2.9 Indirect immunofluorescence and flow cytometry

2.9.1 Indirect immunofluorescence and flow cytometric analyses of SGG on testicular germ cells

The SGG levels on mouse testicular germ cell populations were analyzed by flow cytometry. Approximately 2 x 10^6 of mouse testicular germ cells in 1 ml of DMEM were incubated with 20 µM DRAQ5 in the dark for 15 min at RT for DNA labelling. The cells were washed once with PBS by centrifugation (450 x *g*, 28°C, 5 min) and then fixed with 4% paraformaldehyde in PBS for 15 min at RT. After two washes with PBS supplemented with 0.3% BSA (PBS-BSA), the cells were blocked with 5% normal goat serum (diluted in PBS) for 15 min at RT. After centrifugation (450 x *g*, 28°C, 5 min), the pelleted cells were incubated (45 min, RT) with 5 µg/ml anti-SGG/SGC (Oligodendrocyte marker O4) mouse monoclonal IgM antibody or normal mouse IgM diluted in PBS-BSA. The cells were then washed in the same medium and incubated (30 min, RT) with 20 µg/ml goat anti-mouse IgM conjugated with the Alexa 488 fluorochrome. The cells were then washed twice with PBS-BSA, resuspended in 1 ml of the same buffer and analyzed on a Coulter EPICS XL flow cytometer (Beckman Coulter Ltd., Mississauga, ON, Canada) equipped with a 15 mW argon laser. Ten thousand cells from each sample were analyzed at a flow rate of 200 – 400 cells/second. Fluorescence emission of DRAQ5 (emission λ_{max} 681 nm / 697 nm) was quantified in FL4 after passage through a 675 nm bandpass filter (660 – 700 nm), while SGG fluorescence was quantified in FL1 after passage through a 525 ± 20 nm bandpass filter.

2.9.2 Indirect immunofluorescence and flow cytometric analysis of selected APM proteins on pig sperm

Indirect immunofluorescence of selected APM proteins was performed on either unfixed or aldehyde-fixed Non-cap and Cap pig sperm (prepared as described above), sperm incubated in capacitating medium for 30 and 60 min, and nitrogen-cavitated Cap sperm. In an alternate experiment, aldehyde-fixed Non-cap sperm were permeabilized by treating with

0.1% TritonX-100 in PBS (5 min, RT) prior to the staining. The fixed and unfixed sperm were incubated (30 min, RT) with either 5% normal rabbit serum or 5% normal goat serum in PBS to block non-specific binding of the secondary antibody. After blocking, the sperm were pelleted by centrifugation (500 x *g*, 28°C, 5 min) and incubated (30-60 min, RT) with the following primary antibodies: anti-ZAN holoprotein antiserum (1:2,000 dilution in 5% normal goat serum), anti-proacrosin/acrosin C2E5 antibody (1:100 dilution in PBS), anti-ACRBP antiserum (1:300 dilution in PBS) and anti-MFGM IgG (5 µg/ml in PBS). Normal rabbit serum or normal mouse IgG was used in place of the primary antibodies as negative controls. Sperm that were incubated with primary antibodies were washed once with PBS, and except for those sperm incubated with anti-MFGM, they were subsequently incubated (30 min, RT) in solution with the corresponding secondary antibody conjugated with Alexa-488 fluorophore (5 µg/ml in PBS). The sperm were then washed once with PBS and subjected to flow cytometry and/or fluorescence imaging. Pilot experiments indicated that MFGM may have come off the sperm surface following secondary antibody incubation and repeated centrifugation. Therefore, sperm pre-incubated with anti-MFGM were placed onto a slide in a moist chamber for the secondary antibody treatment.

Pisum sativum agglutinin (PSA) reacts with α-D-mannose and α-D-glucose, which exist abundantly in the acrosomal matrix. Therefore, PSA staining was used to detect the acrosomal status of Non-cap and sperm incubated in capacitating medium at different time points (Cap-30 min, 60 min, 120 min and 240 min) following the previously described protocol (Berger, 1990). Briefly, an aliquot of the sperm suspension from each group was smeared onto a coverslip and dried prior to treatment of sperm with 95% ethanol (30 min, 4°C) to allow the exposure of the acrosomal matrix. The ethanol-treated sperm were then

incubated (8 min, RT) with 100 µg/ml FITC-PSA followed by successive washing in PBS before mounting onto a slide in PBS/glycerol (1:1) for imaging. Sperm that still contained the acrosome were stained positive with FITC-PSA in the acrosome area, whereas those that had become fully acrosome reacted (significantly lost acrosomal content) showed no FITC-PSA staining in this area (Berger, 1990).

Sperm that were stained with anti-ZAN antibody and Alexa-488-secondary antibody were analyzed in the Coulter EPICS XL flow cytometer. The side and forward light scatter parameters were gated to include only cells with the light scatter characteristics of sperm for further fluorescence intensity analysis. Cell fluorescence was excited at 488 nm and the emission intensity per cell was detected in the logarithmic mode of FL1 (525 ± 20 nm band pass filter). Twenty thousand cells from each sample were analyzed at a flow rate of 200-400 cells/second. The data were further analyzed with FCS Express 4.0 (De Novo Software, Thornhill, ON, Canada).

2.10 Preparation of pig sperm APM vesicles

APM vesicles were prepared from both Non-cap and Cap sperm resuspended in Tris-Buffered Sucrose Solution (TBSS: 0.25 M sucrose in 5 mM Tris-HCl, pH 7.4) by nitrogen cavitation at 650 psi followed by differential centrifugation, as previously described (Flesch et al., 1998; Peterson et al., 1980). A diagram showing main steps of the APM vesicle preparation is shown in Figure 2.2. Briefly, Non-cap or Cap sperm were resuspended in Tris-Buffered Sucrose Solution (TBSS: 0.25 M sucrose in 5 mM Tris-HCl, pH 7.4) at a concentration of 400 $x10^6$ sperm/ml and placed under nitrogen pressure at 650 psi (4°C, 10

min) in a Parr cell disruptor (Parr Instrument Company, Moline, IL). The nitrogen-cavitated sperm suspension was added with protease inhibitor cocktail and then subjected to differential centrifugation, i.e., 1,000 x *g*, 4°C, 10 min to remove sperm particulates, and then 6,000 x *g*, 4°C, 10 min to remove sperm midpieces and tails. The nitrogen-cavitated Non-cap and Cap sperm particulates obtained from 1,000 x *g* centrifugation were collected to be examined for the intactness of their acrosomal structures (see below). APM vesicles in the final supernatant were pelleted by ultracentrifugation (200,000 x *g*, 4°C, 1 h) in a 70 Ti rotor, using a Beckman Optima^{TM} L-100 XP ultracentrifuge (Beckman, Palo Alto, CA, USA) and washed once with PBS by the same centrifugation force. A small aliquot of APM vesicles was treated with NaOH (1 N, 2 min, RT) and quantified for protein content by the Bradford assay, using similarly treated BSA as the protein standard.

Peanut agglutinin (PNA) lectin, which reacts with the Gal-β(1-3)-GalNAc carbohydrate sequence of the outer membrane of acrosome (Fazeli et al., 1997), was used to detect this membrane on nitrogen-cavitated pig sperm. Non-cap and Cap sperm collected before and after nitrogen cavitation were washed twice with PBS and treated with 4% paraformadehyde in PBS (15 min, RT). The paraformaldehyde-fixed sperm were incubated (15 min, RT) with the FITC-PNA (10 µg/ml) in PBS. Following successive washing in PBS, the sperm were resuspended in PBS/glycerol (1:1, v/v) solution and placed onto a glass slide for viewing under a Carl Zeiss Axiovert 200 epifluorescence microscope (Carl Zeiss Canada Ltd).

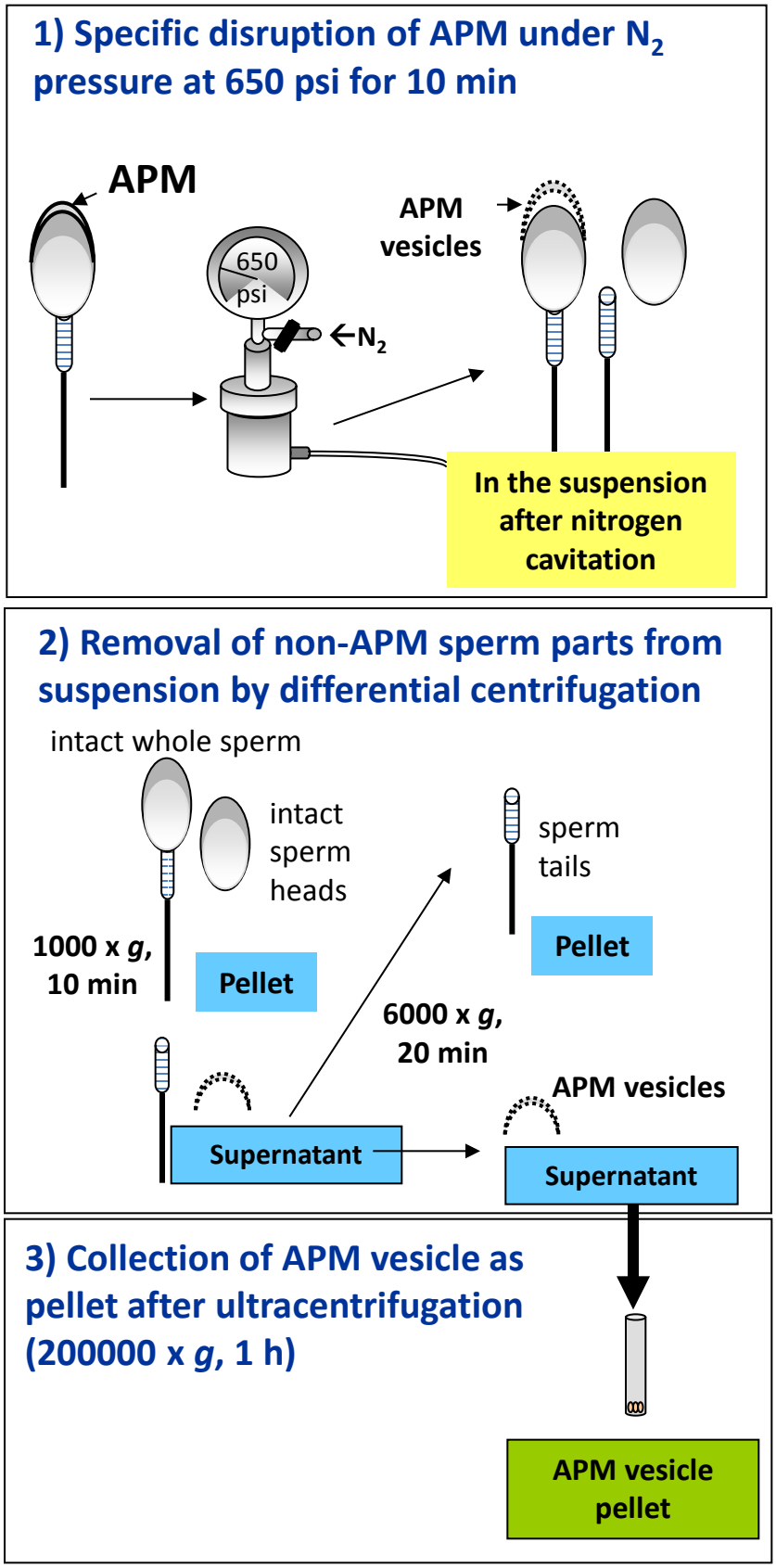

Figure 2.2: A diagram showing three main steps in the isolation of APM vesicles from pig sperm.

2.11 Protein biochemistry

2.11.1 SDS-PAGE, BN-PAGE and immunoblotting

Equal amounts of OG-extracted proteins prepared from Non-cap and Cap APM vesicles were subjected to reducing SDS-PAGE (10% polyacrylamide, 1.5 mm thick) (Laemmli, 1970), using Laemmli's sample buffer containing 2% SDS and 0.1 M dithiothreitol (DTT) for protein sample preparation (100°C, 5 min) prior to gel loading. Gels were stained with Coomassie blue RAPIDStain solution or alternatively subjected to electroblotting (250 mA, 1 h, 4°C) onto a nitrocellulose membrane (Towbin and Gordon, 1984). Immunoblotting was initiated by blocking proteins on the nitrocellulose membrane for 1 h with 5% fat-free powdered milk in Tris-Buffered Saline (TBS: 137 mM NaCl in 20 mM Tris-HCl, pH 7.6) containing 0.1% Tween 20 (TBST). The membrane was incubated (1 h, RT) with the following concentrations of primary antibodies, anti-MFGM IgG (1 μg/ml), anti-ACRBP antiserum (1:5,000 dilution), and anti-AQN-1/3 antiserum (1:1,000 dilution). Following the primary antibody incubation, the membrane was incubated with a corresponding secondary antibody conjugated with horseradish peroxidase (HRP) (1:5,000 dilution, 1 h, RT). Primary and secondary antibodies were prepared in blocking solution. Following incubation with each antibody, the membrane was washed extensively in TBST. The reactivity of antibody-antigen complex was detected by enhanced chemiluminescence (ECL) using a Thermo Fisher Scientific ECL kit. Specifically for immunoblotting of ZAN, 8% polyacrylamide SDS-PAGE was used and the nitrocellulose membrane containing the APM proteins was incubated first with anti-D1 domain IgG (recognizing the p45 form of ZAN; 1:5,000 dilution in TBST). Following the secondary antibody incubation and ECL detection of p45 ZAN band, the membrane was washed successively and then re-probed with

anti-D3 domain IgG (recognizing p105 form of ZAN; 1:10,000 dilution in TBST) and finally with anti-ZAN holoprotein antiserum (1:50,000 dilution in TBST) (Hickox et al., 2001). The secondary antibody used for anti-D1 domain, anti-D3 domain IgG and anti-ZAN holoprotein was diluted 1:10,000 in TBST. In an alternate experiment, OG-extracted APM proteins as well as nitrogen-cavitated sperm were solubilized in Laemmli's sample buffer and subjected to SDS-PAGE and immunoblotting for ZAN, using anti-ZAN holoprotein antiserum.

For BN-PAGE, proteins were extracted from APM vesicles in a solubilization buffer (50 mM NaCl, 50 mM imidazole/HCl, pH 7.0, 2 mM 6-aminohexanoic acid, 1 mM EDTA) containing either OG or digitonin with the weight ratio of proteins to the detergent of 6:1 (Wittig et al., 2006). APM proteins extracted by these two detergents were quantified by Bradford assay. Despite similar protein extraction abilities, digitonin gave a better resolution of APM proteins on BN-PAGE than OG. Therefore, digitonin-extracted APM proteins were used in all BN-PAGE analyses. BN-PAGE was performed according to the described protocol (Wittig et al., 2006). Prior to gel loading, the Coomassie blue G-250/Serva Blue (5% w/v) solution and glycerol were added to each sample to the final concentrations of 0.5% (w/v) and 10% (v/v), respectively. The proteins were separated at 4°C on a pre-cast NativePAGE™ Novex® 3-12% Bis-Tris gradient gel using a cathode buffer (0.02% Coomassie blue G-250, 50 mM Tricine, 15 mM Bis-Tris, pH 7.0) and an anode buffer (50 mM Bis-Tris-HCl, pH 7.0) with a constant voltage of 50 V for the first 30 min, and 150 V for another 4 h. The silver staining of BN gels was performed using SilverQuest™ Silver Staining Kit following the manufacturer's protocol (Life technologies, Inc.). Alternatively, the BN gels were subjected to destaining procedure to remove the background Coomassie blue dye from Cathode buffer and obtain the clear Coomassie blue-stained protein complex

bands following the manual of NativePAGE™ Novex® Bis-Tris Gel System (Life technologies, Inc.).

Immunoblotting of ZAN was also performed with APM proteins, separated on BN-PAGE, using anti-ZAN holoprotein antiserum, following the same protocol as described for SDS-PAGE separated proteins except that 3% BSA was used instead of 5% fat-free powdered milk in the blocking step.

2.11.2 Far western blotting of APM protein complexes with biotinylated pig ZP3

For preparation of biotinylated pig ZP3, two hundred micrograms of purified pig ZP3 were incubated (2 hours, 4ºC) with sulfo-NHS-LC-biotin at 1:22 molar ratio in 0.1 M sodium bicarbonate (pH 7.9), containing protease inhibitor cocktail in a siliconized glass tube. Excess free sulfo-NHS-LC-biotin was removed by filtration through a 3-kDa Amicon® Ultra-4 Centrifugal Filter Unit (Thermo Fisher Scientific Inc.). Biotinylated ZP3 was resuspended in PBS (5 µg/µl) and kept frozen until use.

The nitrocellulose membrane containing electroblotted APM HMW protein complexes (separated on BN-PAGE) was first blocked (30 min, RT) with 3% BSA in TBST and then incubated (1 h, RT) with 10 µg/ml of biotinylated ZP3 in TBST. After successive membrane washing with TBST, bound biotinylated ZP3 was detected by incubating (45 min, RT) the membrane with 200 ng/ml of HRP-conjugated streptavidin (Calbiochem, San Diego, CA, USA), followed by an ECL reaction using the Pierce kit. In an alternate experiment, the membrane containing protein complexes was pretreated (1 h, RT) with anti-ZAN holoprotein IgG antibody (1, 4 and 8 µg/ml) or normal rabbit IgG (8 µg/ml) prior to exposure to biotinylated pig ZP3.

2.11.3 Preparation of APM proteins and tryptic digestion for proteomic analyses

***Chloroform/methanol precipitation of APM protein extracts for gel-free proteomic analyses*:** OG-extracted APM proteins (50 µg/sample) prepared from Non-cap and Cap sperm of three different pigs were precipitated by chloroform and methanol using a modified Bligh-Dyer method (Furimsky et al., 2005). Briefly, chloroform and methanol were added into the extracted APM protein solution at a ratio of 1:1:0.9 (chloroform/methanol/protein sample). Following vigorous mixing and centrifugation (2000 x *g*, 3 min, RT), the chloroform (lower) phase was removed with care taken not to disturb the plaque at the interface. Fresh chloroform of the same volume was then added to the tube and the mixture was re-mixed vigorously and centrifuged as above. This procedure was repeated five times. Finally, the upper (methanol-aqueous) layer was removed, and methanol of an equal volume to the chloroform layer was added to the mixture to form a one-phase mixture. The protein precipitate was then pelleted by centrifugation (2,000 x *g*, 10 min) and air-dried. Sequencing grade modified trypsin (Promega, Annandale, New South Wales, Australia) in 25 mM ammonium bicarbonate, pH 7.0 containing 1 M urea was then added to the chloroform methanol precipitated proteins in a 1:50 ratio (w/w) of trypsin:protein and incubated with constant shaking overnight at 37 $^{\circ}$C. Following the incubation, the samples were then centrifuged (16,000 × *g*, 15 min, 4 $^{\circ}$C), and the supernatants were collected and acidified with 0.1% formic acid prior to subsequent proteomic analyses.

Preparation of 1D-SDS-PAGE resolved APM protein extracts for gel-based proteomic analyses: Samples extracted from Non-cap and Cap APM vesicles by 2% OG were resolved by one dimensional SDS-PAGE (10% polyacrylamide; 20 µg protein/lane). The samples from 2 pigs were loaded on two separated gels. Gels were stained with Rapid

Stain Coomassie blue solution (G-biosicences, St Louis, MO), and each lane was cut into 20 equal regions. Each region was diced into smaller pieces (1 x 2 mm), destained and then subjected to in-gel trypsin digestion. Briefly, the samples were dehydrated in acetonitrile before being rehydrated in 100 mM ammonium bicarbonate, and sequentially treated with 10 mM DTT in 100 mM ammonium bicarbonate for reduction, and 50 mM iodoacetamide in 100 mM ammonium bicarbonate for alkylation. The proteins within the gel slices were then digested with trypsin (overnight, 37°C) according to manufacturer's protocol (Promega, Madison, USA). The resulting peptides were extracted from the gel by twice repeated incubation in 25 mM ammonium bicarbonate and 5% formic acid in 50% acetonitrile solution, followed by incubation in acetonitrile. All the post-digestion extractions were pooled and dried in a speed vacuum centrifuge and resuspended in 0.1% formic acid prior to analyses by nano LC-ESI-MS/MS.

Preparation of APM HMW protein complexes from BN gels for proteomic analyses: The BN gel containing the HMW protein complexes of Non-cap and Cap APM vesicles was stained and de-stained using the Fast Coomassie G-250 Staining protocol as described in the NativePAGE™ manual (Life Technologies, Inc.). The Coomassie blue stained gel was aligned with the biotinylated pig ZP3-far-western blot of the Cap sperm APM sample. The protein complexes, which were in the same positions as the pig ZP3 binding areas, were arbitrarily divided into three complexes: Complex I, Complex II and Complex III (Figure 3.5). The Coomassie blue stained gel lane corresponding to each complex was then excised and diced into 1x2 mm pieces, which were then destained and subjected to trypsin digestion as described above.

2.11.4 Determination of protein-protein interaction by immunoprecipitation

Using a paramagnetic Dynabeads Protein G kit, anti-ZAN holoprotein IgG (1 µg) was captured onto Protein G Dynabeads (40 µl) followed by chemical cross-linking, according to the protocol provided by the manufacturer (Life Technologies Inc). The antibody-conjugated Protein G beads were incubated (45 min, RT, with rotation) with 25 µg of Cap APM vesicle protein extracts and diluted in Modified Dulbecco's PBS (8 mM NaH_2PO_4, 2 mM KH_2PO_4, 140 mM NaCl and 10 mM KCl, pH 7.4) to 700 µl. At the end of the incubation, the antibody-Protein G beads complexed with proteins were washed three times with RIPA buffer (25 mM Tris-HCl, pH 7.6, 150 mM NaCl, 1% (v/v) NP-40, 1% (w/v) sodium deoxycholate, 0.1% (w/v) SDS) to remove any non-specific binding. Bound proteins were then eluted from the beads with Laemmli's reducing SDS-PAGE sample buffer (95°C, 5 min) and subjected to immunoblotting for ZAN, proacrosin/acrosin and ACRBP, and MFGM. For comparison, the original APM protein extract of Cap sperm (5 µg) (input) was co-electrophoresed in a parallel lane. Restore™ Western Blot stripping buffer was used to remove the antibody in the previous detection round from the membrane.

2.12 Mass spectrometry for protein analyses

2.12.1 Combined liquid chromatography and tandem mass spectrometry (LC-MS/MS)

Proteomic analyses of chloroform-methanol precipitated APM proteins and HMW protein complexes from BN-gels were performed at University of Newcastle, Australia in collaboration with Drs. MA Baker and RJ Aitken. The tryptic peptides from these samples were subjected to liquid chromatography (LC) coupled with tandem mass spectrometry

(MS/MS). The peptide extracts were first applied onto an Ultimate3000 ultra high-pressure LC system (Dionex, Castle Hill, Sydney) consisting of two C18 PepMap 100 nanocolumns: a trapping column with 300 µm inner diameter × 5 mm, 5-µm particle size, 100-Å pore size, and a separating column with 75 µm inner diameter × 150 mm, 3-µm particle size, and 100-Å pore size. The LC separation was performed using 99.9% water + 0.1% FA (v/v) as Solvent A and 20/80 water/ACN (v/v) + 0.08% FA as Solvent B with the gradient of 2–40% B over 45 min, 90%B for 5 min, and 4% B for 30 min; the flow rate of sample through the nano column was 400 nl/min. The peptides eluted from the column were then analyzed in an AmaZon Ion Trap (Bruker Daltonik, Bremen, Germany) mass spectrometer using collision-induced dissociation (CID) and electron-transfer dissociation (ETD) as previously described (Baker et al., 2013).

Proteomic analyses of the APM proteins in 1D-SDS-PAGE gel pieces were performed at University of California, Los Angeles in collaboration with Drs. JP Whitelegge and KF Faull. Briefly, the tryptic peptides extracted from the gel pieces were injected (5 µl/injection at 5 µl/min) onto a loading column, then the flow was reversed and the analytical separation was achieved on a reverse phase column (100 µm x 3.5 cm containing Biobasic C18 resin, 5-µm particle size, 300-Å pore size, Microtech Scientific, Fontana, CA) equilibrated in Solvent A (water/formic acid, 100/0.1) and eluted (300 nl/min) with an increasing concentration of Solvent B (acetonitrile/formic acid, 100/0.1: min/%B; 0/2, 40/60, 50/80, 90/0). The eluate from the column was fed to nano-spray ion source (Thermo Fisher) connected to a hybrid linear ion trap Fourier Transform mass spectrometer (LTQ FT, Thermo Fisher, Waltham, MA, USA) operating in the positive ion, data-dependent mode (capillary temperature 220°C, tube lens 110 V, spray voltage of 2.5 kV; full precursor scan at

high-resolution (100,000 at m/z 400) and six MS/MS experiments at low resolution on the linear trap while the full scan was completed). For CID the intensity threshold was set to 5,000, where mass range was 350–2,000.

2.12.2 Protein and peptide identification

Acquired ETD or CID spectra from all analyses were processed in DataAnalysis 4.0, deconvoluted spectra were further analyzed with BioTools 3.2 software and submitted to Mascot database search (Mascot 2.3.02, Swissprot database against "other mammalia" (v57.15, 12,633 sequences; 181,334,896 residues, release date 2/03/2010) enzyme specificity trypsin with 2 missed cleavages considered. The following variable modifications were used: Deamidated (NQ), Oxidation (M), while carbomidomethylation was set to "fixed". It should be noted that both deamidation and oxidation are *in vitro* artefacts that can be introduced as a result of sample handling. Peptide mass tolerance ± 1.2 Da, fragment mass tolerance ± 0.7 Da; enzyme specificity trypsin with 2 missed cleavages considered.

To exclude false positive identifications, peptides with Mascot scores below 40 (chosen on the basis of manual evaluation of the MS/MS data of peptides with scores below this number) were rejected. The identified protein sequences were manually validated in BioTools (Bruker Daltonics) on a residue-by-residue basis using the raw data. Selected ions were only retained when they were greater than or equal to twice baseline noise intensity. A sequence was only accepted when the measured difference between any two assigned adjacent residues was ≤ 0.15 Da different from the calculated difference between the two residues, and ≥ 4 overlapping b and y or c and z ion series was evident. When run against a reversed database, and the spectra manually interpreted in a similar fashion, we found a false

discovery rate of less than 1%. Common contaminating proteins, such as keratins and trypsin were manually excluded from the list of identified proteins. In case of proteins that were assigned as non-pig species (e.g., bovine, sheep and horse), the peptide sequences were aligned with those of the corresponding pig protein from the Swiss-Prot database to determine their amino acid sequence similarity. If the amino acid sequences were identical or highly similar to one another, they were then re-assigned as of pig origin.

2.12.3 Bioinformatics analyses

The normalization of the spectral count of each APM protein identified in gel-free proteomic analysis was calculated following the method used in the Scaffold software (Proteome Software, Inc., Portland, OR, USA). Namely, the number of spectra assigned to an identified protein in each sample was multiplied by the ratio of the average spectrum counts of all proteins in the three pig samples over the total spectral counts of all proteins in that particular sample. Fold change calculations comparing Non-Cap and Cap samples were based on the average normalized spectral count values.

2.13 Lipid biochemistry

2.13.1 Lipid extraction

Lipids were extracted from pig sperm APM vesicles as well as cells and tissues of *Arsa* KO and WT mice following a modified Bligh-Dyer method as previously described (Bligh and Dyer, 1959; Kates, 1986; Kongmanas et al., 2010).

2.13.2 High performance thin layer chromatography (HPTLC)

HPTLC of lipid samples was performed according to our previously described protocol (Furimsky et al., 2005). Briefly, lipid extracts from APM vesicles (corresponding to 140 million sperm/sample) and Sertoli cells (1 million cells/sample) were separated on a HPK silica gel HTPLC plate using chloroform/methanol/water (65:25:4, v/v/v) as a developing solvent system. The plates were sprayed with orcinol solution (0.2% orcinol in 50% sulfuric acid) and heated at 120˚C for 3 min. After charring, glycolipid bands became purple, whereas phospholipid bands and cholesterol band became yellow brown and red, respectively (Kates, 1986). The orcinol-stained plate was further stained with 0.03% Coomassie Brilliant Blue G-250 in 30% methanol/100 mM NaCl and destained with the destaining solution (30% methanol in 100 mM NaCl) (Furimsky et al., 2005); the bands of all lipid types were stained blue with the this dye. Lipid standards (i.e., sphingomyelin, cholesterol, phosphatidylcholine, phosphatidylethanolamine, and SGG) were co-chromatographed with the lipid samples for lipid identification.

2.13.4 Cholesterol quantification by Amplex Red assay

Cholesterol in lipid extracts of Sertoli cells and sperm from WT and *Arsa* KO mice was quantified fluorometrically by the Amplex Red cholesterol assay, according to the manufacturer's instructions (Life technologies, Inc.). This assay is based on an enzyme-coupled reaction that can measure both free cholesterol and cholesteryl esters in the samples. Cholesteryl esters are first hydrolyzed by cholesterol esterase into cholesterol, which is then oxidized by cholesterol oxidase to yield H_2O_2 and the corresponding ketone product, 4-cholestene-3-one. The H_2O_2 then reacts with 10-acetyl-3,7-dihydroxyphenoxazine in the

presence of horseradish peroxidase in the Amplex Red reagent, resulting in the formation of highly fluorescent resorufin. The lipids extracts corresponding to 0.4 million sperm or 0.01 million Sertoli cells were used for each assay point. Each lipid sample was solubilized in 100% ethanol (25 µl) and mixed with 25 µl of 1X Reaction Buffer (100 mM potassium phosphate, pH 7.4, 50 mM NaCl, 5 mM cholic acid and 0.1% Triton X-100) in a well of a black 96-well plate (Corning, Inc., Corning, NY). To each well, 50 µl of Working Solution (1X Reaction Buffer containing 300 µM Amplex Red reagent, 2 U/ml HRP, 2 U/ml cholesterol oxidase, and 0.2 U/ml of cholesterol esterase) was added. A cholesterol standard curve was generated using different amounts of cholesterol (0 to 1 µg). The mixture of 1X Reaction Buffer and Working Solution without the lipid sample was used as the blank control. The plate was incubated for 30 min at 37^{o}C in the dark. The fluorescence was measured in a fluorescence microplate reader, SpectraMAX GeminiXS (Molecular Devices, Sunnyvale, CA), using excitation and emission wavelengths of 560 nm and 590 nm, respectively. Background fluorescence measured for the blank reaction was subtracted from each value for data analysis. Duplicates of each sample were used for the measurement of total cholesterol amount (free cholesterol + cholesteryl esters).

2.14 Mass spectrometry for lipid analyses

2.14.1 SGG quantification by LC-ESI-MS/MS-MRM

SGG levels in the whole testis homogenates and swim-up sperm of 5- and 8-month-old *Arsa* KO and age-matched WT mice as well as in pure populations of male germ cells from 10-week-old CD-1 WT mice were determined by LC-ESI-MS/MS and multiple

reaction monitoring (MRM) as described in our previous publications (Kongmanas et al., 2010; Xu et al., 2011). Briefly, the lipid extracts from testis (from 0.2 mg of testis wet weight) or germ cells (from 0.7 million cells) were redissolved in acetonitrile/methanol/ water/acetic acid (41/23/36/1, v/v/v/v, 180 μl) and added with the internal standard, D_3-SGG (100 pmol in 20 μl of chloroform/methanol, 1/1, v/v) prior to sample injection onto a reverse phase HPLC column (Supleco Ascentis® Express, C18, 150 x 2.1 mm). The column was equilibrated in buffer A (methanol/water, 95/5, v/v, containing 1 mM ammonium acetate), and eluted (100 μl/m) with an increasing concentration of buffer B (chloroform/water, 500/0.2, v/v, containing 1 mM ammonium acetate; min/%B, 0/0, 5/0, 55/100). The effluent from the column was passed to an Ionspray® source connected to a triple-quadrupole mass spectrometer (Sciex API III+ Perkin Elmer-Sciex Instruments, Thornhill, Ontario, Canada). Peak areas for the SGG and D_3-SGG signals were recorded using instrument manufacturer-supplied software (MacSpec version 3.3) and used for calculation of the SGG amounts.

2.14.2 Qualitative and quantitative analyses of different lipid species by flow injection ESI-MS/MS-MRM

Different lipid classes in isolated Sertoli cells and PGC pelleted sperm of 8 to 11-month-old *Arsa* KO and WT mice were analyzed by ESI-MS/MS and MRM using an Agilent 6460 triple quadrupole mass spectrometer (Agilent Technologies, Santa Clara, CA, USA). The molecular species of the following lipid classes were identified in different modes of tandem mass spectrometry (Table 2.2). Precursor ion scanning in the positive ion mode was used to identify phosphatidylcholine (PC) and sphingomyelin (SM) (precursors of m/z 184.1 of the choline group), and cholesteryl esters (CE) (precursors of m/z 369.4 of the cholesteryl group). Precursor ion scanning in the negative ion mode was performed for

identification of sulfolipids (precursors of m/z 97 of the sulfate group). Neutral loss scanning in the positive ion mode was used to identify phosphatidylethanolamine (PE) (neutral loss of 141 of the ethanolamine group) and triacylglycerol (TAG) (neutral loss of 273, 299 and 301, which correspond to C16:0, C18:1 and C18:0 of TAG's acyl chain, respectively). Identified lipid species were quantified using MRM. The data were collected and processed using instrument manufacturer-supplied software (Agilent Mass Hunter version B.05.00).

Prior to analyses of the lipid samples, MS/MS scan conditions were optimized for different classes of lipids using the following lipid standards: 1,2-dipalmitoyl-s*n*-glycero-3-phosphocholine (*m/z* 734.5); 1,2-dipalmitoyl, L-α-phosphatidylethanolamine (*m/z* 692.5); cholesteryl palmitate (*m/z* 643.3) and cholesteryl oleate (*m/z* 669.4); 1,2,3-trihexadecanoyl-glycerol (*m/z* 824.3); D3-SGG (*m/z* 798.5) and cholesteryl sulfate (*m/z* 465.7). Lipid standards were dissolved in the appropriate ion-pair reagents: chloroform:methanol: ammonium acetate (50:50:10 mM, v/v/c) for PC/SM, CE and TAG; chloroform:methanol: formic acid (50:50:0.1, v/v/v) for PE; chloroform:methanol: triethylamine (50:50:0.1, v/v/v) for sulfolipids. The lipid standard (20 pmole/µl) in 10 µl of the specific ion-pair reagent was applied into the mass spectrometer by flow injection through the Agilent Jet Stream ion source (gas temperature 300°C, gas flow 6L/min, nebulizer pressure 45psi, sheath gas temperature 50°C, sheath gas flow rate 10 L/min, capillary voltage 4500V, nozzle voltage 2000V) with chloroform:methanol (50:50, v/v) as the running solvent (100% with flow rate of 0.050 ml/min). The optimized MS parameters (Table 2.2) were then used for the Sertoli cell and sperm lipid analyses. An aliquot of the lipid extract corresponding to 0.04 million Sertoli cells or 0.8 million sperm was used for each MS/MS scan to obtain overall profile of

Table 2.2: Scan modalities for tandem mass spectrometric screens of major lipid classes.

Lipid Class	Ion-pair reagent	Polarity	Type of scan	Ion	Fragmentor voltage*	Collision energy
PC/SM	AA	Positive	Precursor of m/z 184 (choline group)	$[M+H]^+$	100	20
CE	AA	Positive	Precursor of m/z 369.4 (cholesteryl group)	$[M+NH_4]^+$	80	7
TAG	AA	Positive	Neutral loss of 273, 301, 299 (C16:0, C18:0, C18:1 acyl chain, respectively)	$[M+NH_4]^+$	140	10
PE	FA	Positive	Neutral loss of 141 (ethanolamine group)	$[M+H]^+$	141	10
S	TEA	Negative	Precursor of m/z 97 (sulfate group)	$[M-H]^-$	190	85

Abbreviations: PC - phosphatidylcholine; SM - sphingomyelin; PE - phosphatidyl ethanolamine; TAG - triacylglycerol; CE - cholesteryl ester; S - sulfolipids; FA - formic acid; TEA - triethyl ammonia; AA, -ammonium acetate.

*Fragmentor voltage of Agilent mass spectrometer is comparable to cone voltage in other MS instruments.

each lipid class in the sample. The major lipids obtained from MS/MS scanning of each lipid class were identified and selected for further quantitative analyses by MRM. For each MRM analysis, the lipid extract corresponding to 0.008 million Sertoli cells or 0.08 million sperm was used. The peak area of each lipid species obtained from in the MRM analyses was measured using instrument manufacturer-supplied software (Agilent Mass Hunter version B.05.00).

A set of lipid standard solutions (i.e., cholesterol sulfate and D_3-SGG) ranging in concentrations from 0.02-2 pmole/μl were used to construct standard curves plotted using peak area obtained from MRM of the analyte (Y axis) against the lipid concentration (X axis). These standard curves were used for determination of cholesterol sulfate and SGG levels in the lipid samples.

2.14.3 Imaging mass spectrometry

Sertoli cells and spermatogonia of 5-day-old mice and the testicular germ cell mixture from 20-day-old mice were prepared as described above. The cell suspension was coated onto indium-tinoxide-coated glass slides (Bruker Daltonics), frozen and shipped on dry ice to Dr. N Goto-Inoue's laboratory (Hamamatsu University, Japan). Imaging MS was then performed using a MALDI-time-of-flight (TOF)/TOF-type instrument, Ultraflex 2 TOF/TOF (Bruker Daltonics), in the negative mode with 2, 5-dihydroxybenzoic as a matrix, as previously described (Goto-Inoue et al., 2009). The spatial resolution of the obtained images was 25 μm.

2.14.4 Lipid identification

Identities of candidate lipids were assigned by manually comparing the *m/z* values obtained from the MS/MS analyses with those listed in the online lipid databases (i.e., http://www.lipidmaps.org and http://www.byrdwell.com/LipidAcademy) or previously described in the literature.

2.15 Detection of mouse sperm protein tyrosine phosphorylation

My MS-based lipidomic analysis revealed an increased level of cholesterol sulfate in 8-month-old *Arsa* KO mouse sperm, as compared with the WT level (see Figure 3.33). Cholesterol sulfate treatment has been shown to reduce sperm fertilizing ability and its inhibitory effect was suggested to occur during sperm capacitation (Fayrer-Hosken et al., 1987; Langlais et al., 1988; Nixon et al., 2011). I therefore performed this experiment to determine effects of cholesterol sulfate on ability of mouse sperm to undergo capacitation, which was assessed by the levels of sperm tyrosine phosphorylation (one of the key features of capacitated sperm). For determining endogenous and exogenous effects of cholesterol sulfate on capacitation, two sets of capacitated sperm were prepared as follows. The first set of sperm were prepared from 8-month-old *Arsa* KO mice, which have an increased level of endogenous cholesterol sulfate in sperm, and their age-matched WT mice. The motile PGC pelleted sperm were prepared from these mice as described above (see section 2.4.1) and subjected to capacitation induction by incubating in KRB-0.3%BSA (37°C, under 5%CO2 for 1h) at the concentration of 10 million sperm/ml. The second set of sperm were prepared from 10-week-old CD-1 WT mice by PGC (same as above) and used for determining effects

of exogenous cholesterol sulfate on capacitation. Different amounts of cholesterol sulfate(i.e., 0.15 and 75 µg for 10 million sperm), which were prepared from the concentrated stock solutions in dimethyl sulfoxide (DMSO), were used for sperm treatment; these amounts were selected based on the level of cholesterol sulfate detected in the 8-month-old *Arsa* KO PGC pellet sperm (i.e., 0.15 and 75 µg of cholesterol sulfate was equivalent to 2.5X and 1250X the amount of this lipid (0.06 µg) in the 10 million sperm of *Arsa* KO mice, respectively). Note that the treatment of sperm (10 million) with 100 µg/ml of cholesterol sulfate was previously demonstrated to have a significant effect on sperm fertilizing ability, but no effects on sperm viability (Fayer-Hosken et al., 1987). The treatment of sperm with cholesterol sulfate was performed either before capacitation or during capacitation. The former treatment was done by incubating the CD-1 WT PGC pellet sperm (37°C, for 1h) in KRB-HEPES, containing 0, 0.15, 75 µg of cholesterol sulfate, at the concentration of 10 million/ml prior to induction of capacitation in KRB-0.3%BSA as described above for the *Arsa* KO and WT sperm. The latter treatment was performed by incubating the sperm (37°C, under 5%CO_2 for 1h) in KRB-0.3%BSA containing, containing 0, 0.15, 75 µg of cholesterol sulfate, at the concentration of 10 million sperm/ml.

Following the induction of capacitation, all sperm samples from the two above-mentioned sets were washed twice with PBS to remove excess BSA prior to extraction of sperm proteins by solubilizing in Laemmli's reducing SDS-PAGE sample buffer. The solubilized sperm samples were sonicated and boiled (5 min each step), then centrifuged (14,000 x *g*, RT, 10 min) to pellet insoluble particulates. The supernatants containing sperm protein extracts (proteins corresponding to 1 million sperm were loaded in each lane) were subjected to SDS-PAGE and immunoblotting, following the procedure as described above

(see secton 2.11.1). Specifically for the antibody incubation steps, mouse monoclonal anti-phosphotyrosine IgG antibody (clone 4G10) (1 µg/ml) and goat-anti mouse IgG conjugated with HRP (1:5000 dilution) were used as primary and secondary antibodies, respectively. The reactivity of antibody-antigen complex was then detected by the enhanced chemiluminescence (ECL) as described above. To confirm the equal amount of proteins loaded in each lane, the nitrocellulose membrane probed with the 4G10 antibody was stripped using Thermo Fisher Scientific Restore™ Western Blot stripping buffer (following manufacturer's protocol), and re-probed with mouse monoclonal anti-alpha tubulin IgG antibody (1 µg/ml).

2.16 Statistical analyses

Student's *t*-test was used to determine a significant difference between Non-cap and Cap APM samples, or between WT and *Arsa* KO male mice. A *P* value of less than 0.05 was considered to be statistically significant.

CHAPTER THREE

RESULTS

3.1) Characterization of the SGG-associated membrane domains on the anterior sperm head surface, the initial site for sperm-egg interaction

3.1.1) Nitrogen-cavitated sperm still contain outer acrosomal membrane

In this study, prior to further use of APM vesicles as the source of SGG-associated membrane domains with ZP affinity, a quality control experiment was performed to ensure that nitrogen cavitation did not disrupt the sperm acrosomal structure, with a possible consequence of having acrosomal contents co-isolated with APM vesicles. Non-capacitated (Non-cap) and capacitated (Cap) sperm, subjected to nitrogen cavitation at 650 psi, were stained with FITC-PNA, a lectin that reacts specifically with glycoconjugates on the outer acrosomal membrane (Fazeli et al., 1997; Flesch et al., 1998). More than 80% of the unfixed nitrogen-cavitated sperm, both Non-cap and Cap, were stained intensely with FITC-PNA (Figure 3.1). In contrast, Non-cap and Cap sperm which were not subjected to nitrogen cavitation showed negative staining with FITC-PNA (Figure 3.1). This result indicated that nitrogen cavitation at 650 psi did not remove the outer acrosomal membrane or damage the overall acrosomal structure, but the removal of APM vesicles allowed FITC-PNA to react with the outer acrosomal membrane of nitrogen-cavitated sperm.

3.1.2) HPTLC lipid profiles of APM vesicles from Non-cap and Cap sperm

HPTLC analysis of lipids extracted from the APM vesicles of Non-cap and Cap sperm revealed that both samples contained similar lipid components, including cholesterol,

phosphatidylcholine, phosphatidyl ethanolamine, sphingomyelin, and SGG, and that the levels of these lipids (based on Coomassie blue staining intensity) did not seem to be drastically different in the two samples (Figure 3.2). For this reason, we started to refocus our efforts towards proteomic characterization of APM vesicles isolated from Non-cap and Cap sperm.

3.1.3) Proteomic profiles of APM vesicles from Non-cap and Cap sperm

Overall properties: Bradford assay showed that the total APM protein content per million sperm was significantly higher in Cap sperm than that in Non-cap sperm (0.12 ± 0.06 versus 0.08 ± 0.03 $\mu g/10^6$ sperm) (Figure 3.3A). SDS-PAGE/Coomassie blue staining of APM protein extracts of Non-cap and Cap sperm also revealed that a number of protein bands in the Cap APM vesicles had increased intensity as compared with the Non-cap samples, when the same total protein amounts in each sample were loaded for PAGE (Figure 3.3B).

Identities and relative amounts of proteins in APM vesicles of Non-cap and Cap sperm: The identities and levels of proteins in the APM vesicles of Non-cap and Cap sperm were further determined and compared by MS and subsequent immunoblotting analyses. Chloroform-methanol precipitated proteins of Non-cap and Cap APM vesicles prepared from 3 different pigs were subjected to tryptic digestion and MS analysis. Proteomic analysis revealed a total of 149 proteins in both types of APM vesicles. While 59 proteins were present in common between the Non-cap and Cap sperm samples, 22 and 68 proteins were found only in the Non-cap or Cap sample, respectively. All proteins identified in both APM

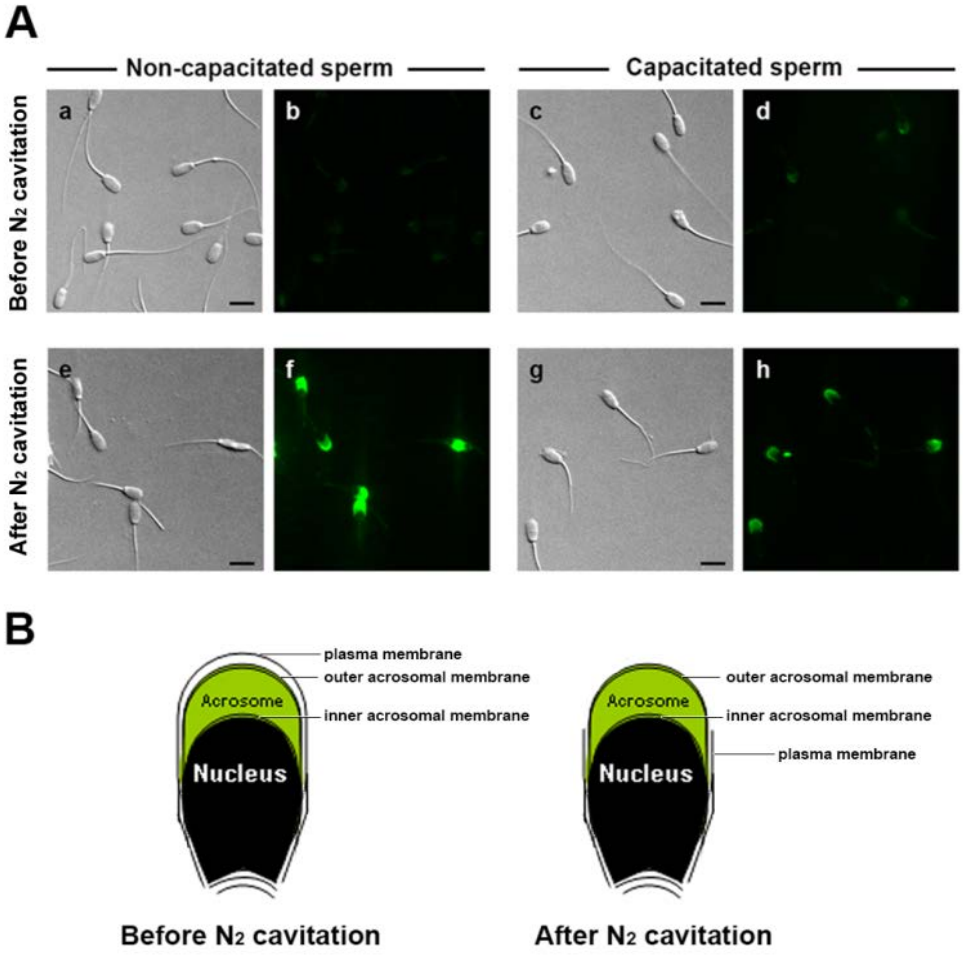

Figure 3.1: Nitrogen cavitation does not remove the acrosome from sperm. A) Intact (a, b, c, d) and nitrogen-cavitated (e, f, g, h) non-capacitated (Non-cap) and capacitated (Cap) sperm were fixed with paraformaldehyde and incubated with FITC-PNA, a lectin that stains the outer acrosomal membrane. Differential interference contrast (DIC) images (a, c, e, g) were shown with corresponding fluorescence images (b, d, f, h). Bar = 20 µm. Note the FITC-PNA staining on the surface of nitrogen-cavitated sperm, but not on intact sperm, indicating that: 1) the plasma membrane of the majority of Non-cap and Cap sperm was intact without permeabilization/disruption for the entry of FITC-PNA to stain the outer acrosomal membrane; 2) After nitrogen cavitation, the acrosome with the outer acrosomal membrane remained on nitrogen-cavitated sperm. **B)** Illustration showing the structure of pig sperm head before and after N2 cavitation.

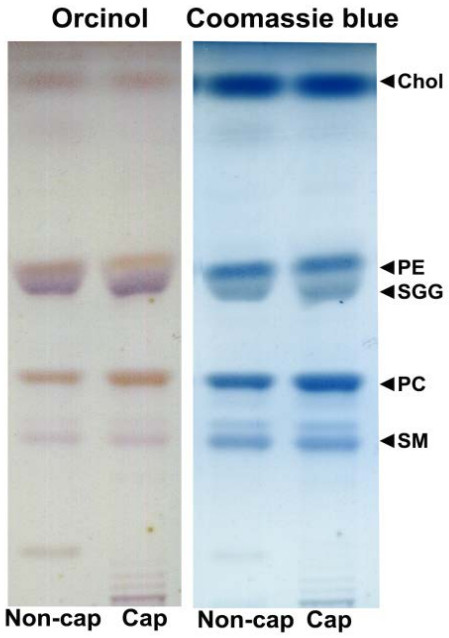

Figure 3.2: Similar lipid profiles of APM vesicles isolated from Non-cap and Cap sperm. Lipids extracted from APM vesicles isolated from 200 million of Non-cap or Cap sperm were loaded onto a HPTLC plate, which was developed using chloroform/methanol/water (65:25:4,v/v/v) as a running solvent. The developed HPTLC plate was stained with Orcinol solution (left panel), which gives specific stained colors for different lipids (i.e., glycolipids purple, phospholipids yellow-brown). The plate was then post-stained with Coomassie blue solution (right panel), which stains all lipids blue. Lipid standards, including cholesterol (Chol), phosphatidylethanolamine (PE), sulfogalactosylglycerolipid (SGG), phosphatidylcholine (PC) and sphingomyelin (SM) were used as markers. The HPTLC shown in the figure is a representative of 3 replicate experiments.

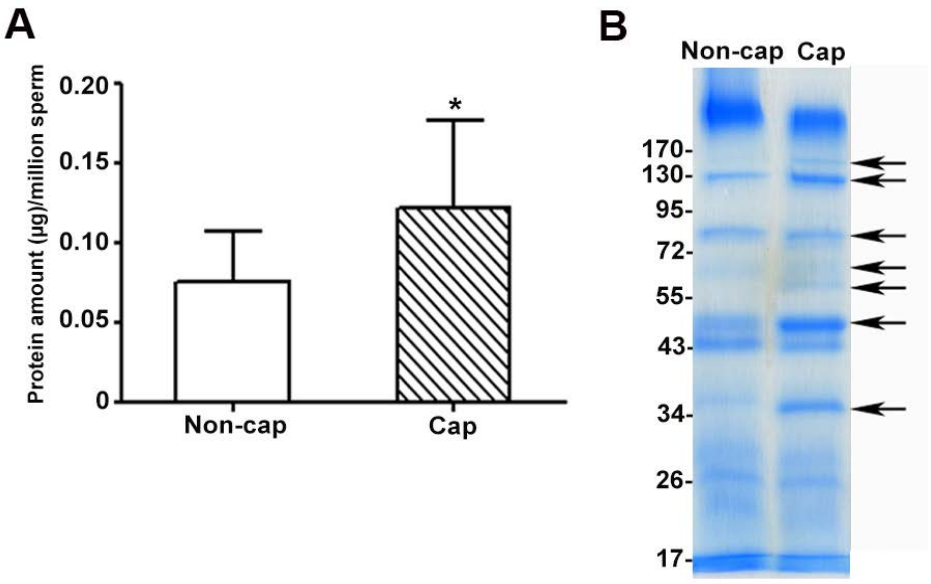

Figure 3.3: Protein levels and profiles of APM vesicles isolated from Non-cap and Cap sperm. A) Levels of proteins in NaOH-solubilized Non-cap and Cap APM vesicles were determined using Bradford assay. The protein level per sperm in the Cap samples was significantly higher than that of the Non-cap counterparts (* $P < 0.05$). Data are expressed as mean ± S.D. from 8 sets of APM vesicle samples. **B)** An equal amount of proteins (20 µg) extracted from APM vesicles of Non-cap and Cap sperm by 2% (w/v) octylglucoside was subjected to SDS-PAGE and Coomassie blue staining. The result revealed a number of protein bands with increased intensity (arrows indicated) in Cap APM vesicle extracts, as compared with the Non-cap samples. The gel shown in this figure is a representative of 5 replicate experiments.

samples are listed in Appendix Table 1. Of note was the higher abundance (based on spectral counts) of proteins found in common between both types of vesicles, as compared with proteins present in only one type of the vesicles (Appendix Table 1). APM vesicles of both sperm samples contained proteins with diverse functions, including those involved in sperm-egg interactions, chaperones, enzymes (mainly kinases), and cell adhesion/cell-signaling (Table 3.1). Interestingly, proteins known for their functions in sperm-egg interactions were the most enriched among all APM vesicle proteins (details about functions of these proteins are shown in Table 1.2 in the INTRODUCTION). Consistently, milk fat globule-EGF factor 8 (MFGM or SED1), previously described as a ZP-binding molecule (Ensslin and Shur, 2003), was present with the highest spectral counts in both Non-cap and Cap samples, but its levels were significantly higher in the latter (Figure 3.4A). Other identified APM proteins with functions relevant to sperm-egg interactions included zonadhesin (ZAN), carbohydrate binding proteins (AQN-3 and AWN), ZP-binding protein 1 (ZPBP1 or sp38), angiotensin-converting enzyme (ACE), proacrosin/acrosin, and proacrosin-binding protein (ACRBP) (Table 3.1). Importantly, the levels of ZAN and ACRBP significantly increased in the Cap sperm samples (Figure 3.4A). ZAN, proacosin/acrosin, and ZPBP1 have been previously shown to be present in the acrosome of Non-cap sperm (Bi et al., 2003; De los and Barros, 2000). The presence of these three proteins in APM vesicles may thus reflect the possibility that they were transported to the Cap sperm head surface during the capacitation process.

In order to validate the changes in the amounts of APM proteins involved in gamete interaction in Non-cap and Cap sperm as revealed by the proteomic data, immunoblotting analyses of selected APM proteins were performed. Based on the immuno-reactive band

intensity, MFGM, ZAN, and ACRBP levels were increased in the Cap samples, whereas the AQN3 level was decreased (Figure 3.4B), results that were consistent with the proteomic analyses (Table 3.1). Immunoblotting analyses also revealed molecular masses of these APM proteins to be similar to those previously described. For MFGM, the mature form (~47 kDa) (Ensslin and Shur, 2003) was present in both APM samples, although an extra band at 39 kDa (possibly a degraded or processed product) was also present in the Cap samples. For ZAN, immunoblotting with sequential exposure to its three antibodies (anti-D1, anti-D3 and then anti-ZAN holoprotein) revealed the p45 and p105 bands, both previously described as major ZAN forms in isolated pig sperm membrane fractions (Bi et al., 2003; Hickox et al., 2001), as well as a broad band of an average molecular mass of 300 kDa. These bands were present with higher intensity in the Cap APM sample, as compared with the Non-cap APM sample (Figure 3.4B). Under our reducing SDS-PAGE conditions, it was unlikely that the p45 and p105 ZAN forms could form a complex, which could then form a dimer of a 300 kDa molecular mass (Hickox et al., 2001). Furthermore, the 300 kDa band was not the MAM-containing p300 form of ZAN, since this MAM-containing ZAN fragment does not contain D1 and D3 domains (see Figure 3.4C for the structural diagram of ZAN precursor protein and its processed forms). Therefore, the 300 kDa forms were simply the D1 and D3 containing ZAN fragments. For ACRBP, both the 32 and 28 kDa forms (Baba et al., 1994b) were detected in both Non-cap and Cap APM samples.

Another proteomic analysis was performed using the gel-based approach, involving 1-D SDS-PAGE of APM proteins, Coomassie-blue staining of protein bands, in gel tryptic digestion and proteomic analysis. Proteins identified by this approach were similar to those obtained from the unfractionated APM extract (Tables 3.2 and 3.1, respectively).

Table 3.1: Quantitative LC-MS/MS analyses of Non-cap and Cap APM vesicle proteins[1,2]

#	Protein name/Function Category[3]	Swiss-Prot Accession	Av. Spec. Count[4]		Fold difference (Cap/Non-cap)
			Non-cap[3]	Cap	
	Sperm-egg interaction				
1	Milk fat globule-EGF factor 8 (SED1)	MFGM	67	106	1.6
2	Carbohydrate-binding protein AQN-3	AQN3	12	6	0.5
3	Carbohydrate-binding protein AWN	AWN	8	6	0.8
4	Proacrosin/acrosin	ACRO	8	9	1.1
5	Angiotensin-converting enzyme	ACE	4	5	1.3
6	Proacrosin-binding protein precursor (sp32)	ACRBP	2	8	4.0
7	Zona pellucida-binding protein 1 (sp 38)	ZPBP1	1	2	2.0
8	Zonadhesin	ZAN	0	8	∞
	Chaperone				
9	Heat shock 70 kDa protein 1-like	HS71L	11	5	0.5
10	Heat shock protein HSP 90-alpha (HSP 86)	HS90A	4	4	1.0
	Enzyme				
11	Adenylate kinase isoenzyme 1	KAD1	38	20	0.5
12	Phosphoglycerate mutase 2	PGAM2	11	8	0.7
13	Hexokinase-1	HXK1	5	4	0.8
14	Phosphoglycerate kinase, testis specific	PGK2	5	3	0.6
	Cell Signalling/Cell adhesion/Other				
15	Tubulin polymerization-promoting protein family member 2	TPPP2	12	7	0.6
16	14-3-3 protein zeta/delta	1433Z	11	5	0.5
17	Ubiquitin	UBIQ	8	3	0.4
18	Calmodulin (CaM)	CALM	7	10	1.4
19	Vesicle-associated membrane protein 3	VAMP3	4	3	0.8
20	Glucose transporter type 3	GTR3	4	3	0.8
21	Phosphatidylethanolamine-binding protein 1	PEBP1	3	1	0.3
22	Major seminal plasma glycoprotein PSP-I	PSP1	1	2	2.0

[1]An equal amount (50 µg) of proteins extracted from APM vesicles of non-capacitated (Non-cap) and capacitated (Cap) sperm from each of the 3 pigs was used for MS analyses.
[2]Only highly abundant APM proteins, showing at least 5 spectral counts in one of the three replicates, were listed in this table.
[3]The APM proteins identified are grouped based on their known biological functions and individual proteins in each group were ranked from the highest to the lowest abundance in Non-cap samples using normalized spectral counts as relative indexes.
[4]Average normalized spectral counts for proteins identified in Non-cap and Cap APM samples of the 3 animals. All data from individual pigs are in Appendix Table 1.

Table 3.2: Non-cap and Cap sperm APM vesicle proteins identified by gel-based proteomic analysis[1,2]

#	Protein name/Function Category[4]	Swiss-Prot Accession[5]	Total spectral counts[3]	
			Non-cap	Cap
	Sperm-egg interaction			
1	Milk fat globule-EGF factor 8	**MFGM**	338	378
2	Proacrosin/acrosin	**ACRO**	105	126
3	Carbohydrate-binding protein AWN	**AWN**	65	27
4	Acrosin-binding protein precursor	**ACRBP**	27	27
5	Carbohydrate-binding protein AQN-3	**AQN3**	24	9
6	Angiotensin-converting enzyme	**ACE**	17	31
7	Zonadhesin	**ZAN**	1	25
	Epididymal fluid/seminal plasma protein			
1	Epididymal sperm-binding protein 1	**ESPB1**	60	46
2	Clusterin precursor	**CLUS**	31	14
3	Seminal plasma sperm motility inhibitor precursor	SPMI	20	10
4	Seminal plasma acrosin inhibitor A1	IACA	18	7
5	Seminal plasma protein pB1	**PB1**	10	11
	Chaperone			
1	Heat shock protein HSP 90-alpha	**HS90A**	47	23
2	Heat shock 70 kDa protein 1-like	**HS71L**	12	24
	Cytoskeleton protein			
1	Tubulin alpha-3 chain	**TBA3**	15	8
2	Tubulin beta-2C chain	**TBB2C**	14	11
3	Tubulin beta-4 chain	**TBB4**	2	12
	Enzyme			
1	Gamma-glutamyltranspeptidase 1 precursor	GGT1	38	9
2	Adenylate kinase isoenzyme 1	**KAD1**	22	22
3	Hexokinase-1	**HXK1**	21	23
4	Aldose reductase	**ALDR**	20	6
5	Malate dehydrogenase	MDHC	17	0
6	Alkaline phosphatase	PPBT	15	2
7	Aspartate aminotransferase	**AATC**	14	6
8	Aminopeptidase N	AMPN	14	1
9	Phosphoglycerate mutase 2	**PGAM2**	13	12
10	Alpha-enolase	**ENOA**	12	7
11	Dipeptidyl peptidase 4 soluble form	**DPP4**	11	11
	Other proteins			
1	Leukocyte surface antigen CD47 precursor	**CD47**	20	12
2	Ubiquitin	**UBIQ**	18	12
3	14-3-3 protein zeta/delta	**1433Z**	14	13
4	Ezrin (p81) (Cytovillin) (Villin-2)	**EZRI**	14	0
5	Brain acid soluble protein 1	BASP1	12	3

[1]An equal amount (20 µg) of proteins extracted from APM vesicles of non-capacitated (Non-cap) and capacitated (Cap) sperm was resolved on 1D-SDS-PAGE and stained with Coomassie blue solution. Each gel lane containing either Non-cap or Cap APM proteins was cut into 20 pieces and subjected to in-gel tryptic digestion and MS/MS analyses.

[2]Only highly abundant APM proteins, showing at least 10 spectral counts in either Non-cap or Cap sample, were listed in this table. All proteins identified by gel-based proteomic analysis can be found in Appendix Table 2.

[3]Total spectral counts represented sum of all spectral counts of each identified protein in all 20 protein bands prepared from Non-cap or Cap sample.

[4]The identified APM proteins are grouped based on their known biological functions and individual proteins in each group were ranked from the highest to the lowest abundance in Non-cap samples using total spectral counts as relative indexes.

[5]Proteins with Swiss-Prot accession in bold blue fonts are those identified commonly by both gel-free and gel-based proteomic analyses.

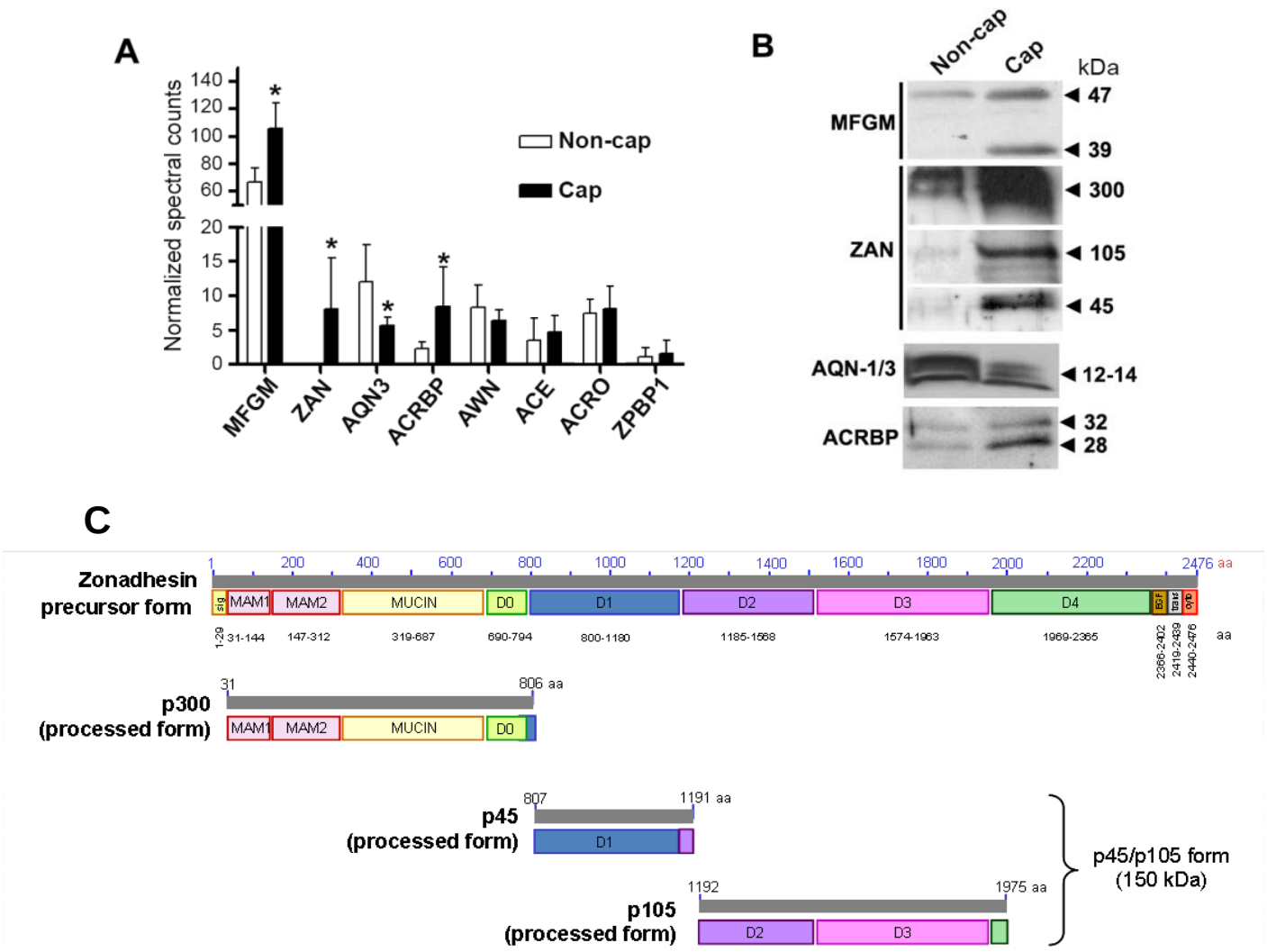

Figure 3.4: Levels of proteins with known functions in sperm-egg interaction in Non-cap and Cap sperm APM vesicles. A) Normalized spectral counts of selected APM proteins with significance in sperm-egg interactions. The spectral counts used in this analysis were those shown in Table 1. Note ACRO denotes sequences in both proacrosin and acrosin. Data were expressed as mean ± S.D. of spectral counts from 3 replicates. Asterisks indicate significance difference (P<0.05) between Non-cap and Cap sperm APM samples. **B) Immunoblotting analyses of selected APM proteins.** An equal amount of proteins (20 µg), prepared from Non-cap and Cap APM vesicles, was loaded in each lane. The molecular mass of each protein was indicated on the right. Similar to the proteomic results (A), immublotting analyses revealed that the amounts of MFGM, ZAN, and ACRBP were increased in the Cap APM vesicles, whereas the amount of AQN-1/3 was decreased. **C) Structural domains of zonadhesin (ZAN).** Peptide domains of precursor and processed forms of ZAN are shown based on Bi et al. (2003) and Herlyn and Zischler (2008). The precursor form contains a signal peptide, 2 MAM domains (MAM = meprin/A5 antigen/mu receptor tyrosine phosphatase), von Willebrand factor (VWF) D domains (partial D0, D1, D2, D3 and D4 domain), an EGF-like domain, a transmembrane domain and a cytoplasmic domain. The processed forms include p300, p45 and p105. The p45 and p105 forms contain D1 and D3 domains, respectively and these two forms have been shown to bind to ZP (Hickox et al., 2001). Under a non-reducing SDS-PAGE condition, p150 which contains both p45 and p105 forms can be detected (Hickox et al., 2001).

Namely, the proteins with known functions in sperm-egg interactions (i.e., MFGM, ZAN, AQN3, and AWN) were found with the highest spectral counts. The gel-based analyses also revealed other protein types, including chaperones, cytoskeleton proteins, enzymes, and cell adhesion molecules, similar to those identified by the gel-free approach. All proteins identied through the gel-based proteomic approach are listed in Appendix Table 2. Overall, there were 90 proteins in common between the two approaches. The total number of proteins from the gel-based approach was higher than that of the gel-free counterpart (200 vs 149, respectively), likely due to the reduced complexity of the samples following electrophoretic separation, thus allowing for enhanced detection of low abundant species (Aitken and Baker, 2008).

The existence of many ZP-binding proteins on the sperm APM leads to a question of which proteins are essential for the sperm-ZP interaction and thus for male fertility. Recent studies suggest that these ZP-binding proteins on the sperm head may act together as a complex and/or as backups for one another during ZP interaction (Redgrove et al., 2012; Tanphaichitr et al., 2007a).

3.1.4) Presence of high molecular weight protein complexes in isolated APM vesicles: preferential pig ZP3 affinity of the complexes from capacitated sperm

Blue native gel electrophoresis (BN-PAGE) and silver staining revealed the presence of HMW protein complexes in both Non-cap and Cap APM vesicles (Figure 3.5A, left panel). The sizes of these HMW protein complexes ranged from ~200 to 1300 kDa. In both samples, the complexes in the 600-800 kDa range had the highest silver staining intensity

and the complexes in the 1000-1300 kDa range appeared as diffuse bands. The complexes in the 200-800 kDa range from Non-cap sperm showed stronger silver staining intensity than those of the Cap counterpart, whereas those with mass >1000 kDa had lower staining intensity in the Non-cap sample.

Pig ZP3 glycoprotein is a hetero-oligomer of pigZP3α and pigZP3β, constituting about 75% of total pig ZP glycoproteins. Pig ZP3 is a sperm receptor, shown previously to bind to isolated pig APM vesicles (Bou Khalil et al., 2006; Yurewicz et al., 1993; Yurewicz et al., 1998). Far western blotting of APM HMW complexes with biotinylated purified pig ZP3 indicated that the protein complexes in the range of 750-1300 kDa of Non-cap and Cap APM vesicles had affinity for the pig ZP3, but the affinity was significantly higher in the Cap APM sample (Figure 3.5A, right panel). These complexes were arbitrarily grouped into three units: Complex I ranging from 1000-1300 kDa, Complex II from 850-1000 kDa and Complex III from 750-800 kDa. (Figure 3.5A, right panel). None of these complexes had affinity for biotinylated ovalbumin (Figure 3.5B), indicating their specific affinity for pig ZP3.

Complexes I, II and III from the Coomassie-blue stained gel were excised and trypsin-digested for proteomic analyses. In both sperm samples, the results indicated that proteins with known functions in sperm-egg interaction were their most abundant components (Table 3.3), a finding consistent with the MS analysis results from the whole APM vesicle extracts (Tables 3.1 and 3.2). However, ZAN was the most abundant component in the Complex I of Non-cap and Cap samples (Table 3.3) and its spectral count was higher than that of MFGM, which showed the highest spectral count when the whole APM vesicle extracts were used for the analysis (Tables 3.1 and 3.2). The spectral counts of

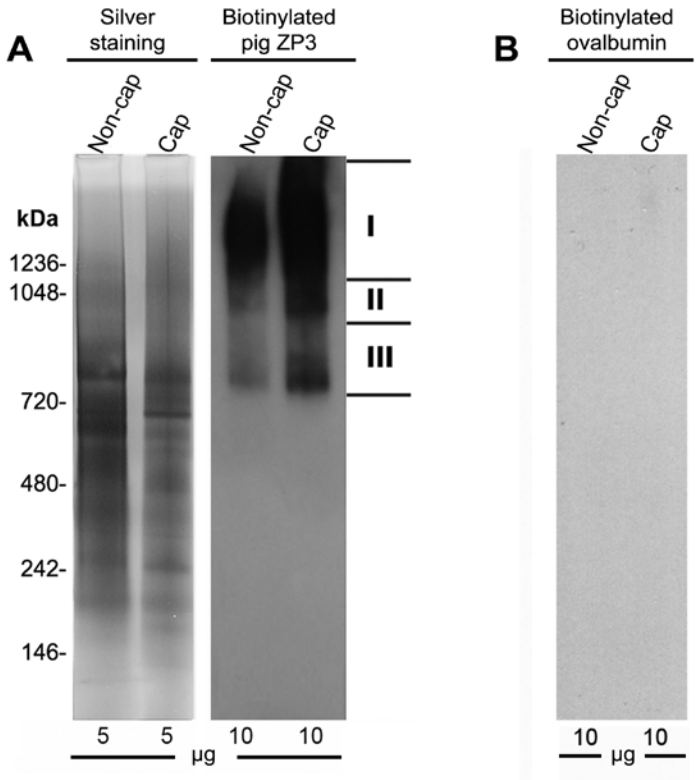

Figure 3.5: A) Silver staining and far western blotting with biotinylated pig ZP3 of APM proteins separated on blue native gel electrophoresis. High molecular weight (HMW) protein complexes ranging from 200-1300 kDa were detected in both Non-cap and Cap sperm APM vesicle extracts. HMW protein complexes of Non-cap and Cap APM samples (750-1300 kDa) showed affinity for pig ZP3 but the stronger pig ZP3 affinity was observed in the Cap APM HMW complexes. These HMW protein complexes were designated as Complex I (1000-1300 kDa), Complex II (850-1000 kDa) and Complex III (750-850 kDa) and prepared from Coomassie blue-stained gels for proteomic analyses. Molecular masses (kDa) of protein standards were listed on the left of the gel panel. **B) Far western blotting of HMW APM protein complexes with biotinylated ovalbumin.** HMW protein complexes of Non-cap and Cap APM samples showed no binding to biotinylated ovalbumin.

Table 3.3: Identity and spectral counts of proteins in the three HMW protein complexes of Non-cap and Cap sperm APM samples[1]

#	Protein name/Function Category	Swiss-Prot Accession	Total spectral counts of identified peptides in HMW protein complexes[2]					
			Complex I		Complex II		Complex III	
			Non-cap	Cap	Non-cap	Cap	Non-cap	Cap
	Sperm-egg interaction							
1	Zonadhesin	ZAN	83	137	7	12	2	18
2	Milk fat globule-EGF factor 8 (SED1)	MFGM	7	15	6	4	15	12
3	Proacrosin/acrosin	ACRO	4	17	3	4	10	3
4	Proacrosin-binding protein precursor (sp32)	ACRBP	5	17	1	2	3	1
5	Sperm acrosomal protein (SP-10)	ASPX	3	6	0	2	0	4
6	Carbohydrate-binding protein AWN	AWN	5	3	3	1	4	0
7	Zona pellucida-binding protein 1 (Sp 38)	ZPBP1	0	4	0	0	0	0
	Chaperone							
8	T-complex protein 1 subunit gamma	TCPG	0	23	0	6	0	9
9	T-complex protein 1 subunit eta	TCPH	0	16	0	1	0	8
10	T-complex protein 1 subunit beta	TCPB	0	8	0	3	0	6
11	T-complex protein 1 subunit alpha	TCPA	0	7	0	4	0	3
12	T-complex protein 1 subunit delta	TCPD	0	3	0	2	0	5
13	T-complex protein 1 subunit theta	TCPQ	0	3	0	0	0	0
14	T-complex protein 1 subunit zeta	TCPZ	0	2	0	1	0	4
15	T-complex protein 1 subunit zeta-2	TCPW	0	3	0	1	0	1
16	Heat shock 70 kDa protein 1-like	HS71L	3	7	2	1	2	3
17	Heat shock-related 70 kDa protein 2	HSP72	0	2	0	1	0	0
18	Heat shock protein HSP 90-alpha	HS90A	0	1	0	2	0	2
	Cytoskeleton proteins							
19	Tubulin beta-4 chain	TBB4	2	0	1	0	0	4
20	Tubulin alpha-8 chain	TBA8	3	0	0	0	0	2
21	Tubulin beta-2C chain	TBB2C	7	32	0	3	0	6
22	Tubulin alpha-3 chain	TBA3	3	5	0	0	0	2
23	Tubulin beta-3 chain	TBB3	0	6	0	0	0	0
24	Dynein light chain 1, cytoplasmic	DYL1	0	1	0	2	0	1
	Epididymal fluid/seminal plasma proteins							
25	Clusterin precursor	CLUS	17	2	4	0	1	0
26	Seminal plasma acrosin inhibitor A1	IACA	0	2	1	1	5	1
27	Seminal plasma sperm motility inhibitor precursor	SPMI	1	3	0	0	0	0
28	Sperm-associated acrosin inhibitor	IACS	2	0	2	0	2	0
	Enzymes							
29	Superoxide dismutase [Cu-Zn]	SODC	2	1	3	2	8	8
30	ATP-citrate synthase (EC 2.3.3.8)	ACLY	0	3	0	3	0	9
31	Aspartyl aminopeptidase	DNPEP	0	4	0	2	0	2
32	Phosphoglycerate kinase, testis specific	PGK2	1	1	0	0	0	2
	Other proteins							
33	Ferritin heavy chain	FRIH	0	5	0	3	0	5
34	Peroxiredoxin-5	PRDX5	1	1	3	0	3	2
35	Fibronectin	FINC	1	0	3	0	1	0
36	Ubiquitin domain-containing protein 1	UBTD1	4	3	2	1	3	3
37	Ubiquitin	UBIQ	0	2	0	2	0	7
38	26S protease regulatory subunit 7	PRS7	0	2	0	1	0	0
39	26S proteasome non-ATPase regulatory subunit 2	PSMD2	0	1	0	2	0	0
40	Proteasome subunit beta type 1 precursor	PSB1	0	0	0	0	0	4

[1]Equal amount of APM vesicle proteins (25 µg/sample) from Non-cap and Cap sperm were separated on a blue native gel and stained with Coomassie blue dye. The gel areas corresponding to the three designated three Complexes (I, II, III) that showed pig ZP3 affinity (as shown in Figure 3.5) were excised and subjected to MS analyses.

[2]The number of spectral counts in each column is the sum of peptides of each protein in each HMW protein complexes. Data shown were representative of two replicate experiments.

ZAN were higher in Complex I than in Complexes II and III. Other proteins with relevance to sperm-egg interactions, including MFGM, proacrosin/acrosin, ACRBP, ASPX, AWN and ZPBP1, were also enriched in these complexes. Except for AWN, the spectral counts of these proteins were higher in the Complex I of Cap APM vesicles than those in the Non-cap counterpart. Notably, the higher levels of these proteins in Complex I corresponded with the higher ZP capacity of Complex I as compared with that of Complex II and Complex III. ZAN, which has the highest spectral count in Complex I from Cap APM vesicles, may contribute significantly to the binding of APM vesicles to pig ZP3.

Chaperone proteins were also present in the HMW complexes, particularly in the Cap samples. Eight subunits of chaperonin-containing T-complex polypeptide-1 (TCP-1) were detected in the Cap protein complexes (Table 3.3). In contrast, TCP-1 proteins were found in relatively low abundance when the whole APM preparation was used (Appendix Table 1). Other molecular chaperones, including Hsp72 and Hsp90α, were similarly found selectively in the Cap APM HMW protein complexes. Cytoskeleton proteins, i.e., tubulin α and β, were another group of proteins present in the APM HMW protein complexes. In particular, tubulin β-2C showed a distinct increase in spectral counts in the Cap sperm samples. Proteins known for their presence in epididymal fluid and seminal plasma, such as clusterin precursor and acrosin inhibitor (Davidova et al., 2009; Griffiths et al., 2009), were also present in the APM HMW complexes, with decreased levels in the Cap samples. In addition, enzymes (i.e., superoxide dismutase, ATP-citrate synthase) and other proteins, including ubiquitin, peroxiredoxin 5 and proteosomal proteins were detected in the HMW protein complexes, and most were present at higher levels in the Cap APM sample.

3.1.5) Localization of ZAN and other selected acrosomal proteins, which were present as APM components, on intact and nitrogen-cavitated sperm

Previous electron microscopic studies indicate that ZAN is localized in the outer acrosomal membrane and acrosomal matrix of Non-cap sperm from pigs and hamsters (Bi et al., 2003; Olson et al., 2004). Our finding that ZAN was present preferentially in isolated APM vesicles of Cap sperm, especially as a component of the HMW protein complexes (Tables 3.1, 3.2 and 3.3), implicated that ZAN trafficked to the anterior surface of the sperm head during capacitation. Immunofluorescence and flow cytometry of aldehyde-fixed pig sperm indicated that about 20% of the Non-cap sperm stained positively for ZAN (Figure 3.6A, panels b & h). In contrast, ~70% of sperm that had been incubated in capacitating medium for 30 min showed ZAN positive staining, and this percentage rose slightly to 75-78% following incubation for 60 to 120 min (Figure 3.6A, panels c & i, d & j, e & k, respectively). The intensity of the fluorescent ZAN labeling on the sperm head surface was increased during the course of capacitation; after 60 min incubation in capacitating medium, the ZAN fluorescence intensity on the sperm surface was maximal and ten-fold higher than that in the Non-cap sperm (Figure 3.6A, panels j & k versus h). The majority of Cap sperm showed ZAN staining at the periphery of the acrosome on the sperm discoid plane, although in a small Cap sperm population the staining was over the entire region of the acrosome (Figure 3.6A, panels c-e). Similar results were observed when intact live (unfixed) pig sperm were used in the parallel immunofluorescence experiment (Figure 3.7), confirming that the ZAN fluorescence signals on aldehyde-fixed sperm were on the sperm surface. During the 2-h course of capacitation, only 20% of the sperm were acrosome-reacted (showing negative staining with FITC-PSA), indicating that the majority of these Cap sperm

had an intact acrosome (Figure 3.6B). After 4 h incubation in capacitation medium, a similar percentage of sperm with FITC-PSA negative staining was observed (data not shown). Therefore, it was not surprising that the ZAN fluorescence signal in Cap sperm increased ten-fold in aldehyde-fixed sperm that were post-treated with 0.1% Triton X-100 to permeabilize the plasma membrane (Figure 3.6A, panel l). The staining in aldehyde-fixed/Triton X-100 permeabilized sperm covered the entire acrosome in both Non-cap (data not shown) and Cap sperm (Figure 3.6A, panel f), results indicating that this staining corresponded to ZAN in the acrosome. This interpretation is further supported by the observation that a similar staining pattern of ZAN over the acrosome region was present in >90% of nitrogen-cavitated sperm, both Cap (Figure 3.6C) and Non-cap (data not shown). As observed in aldehyde-fixed/Triton X-100 permeabilized sperm, the ZAN staining on the acrosome of nitrogen-cavitated sperm was ten-fold higher than the staining on the surface of aldehyde-fixed Cap intact sperm (Figure 3.6C).

Besides ZAN, proacrosin/acrosin and ACRBP, known to localize in the acrosome of Non-cap sperm (Baba et al., 1994), were found as components of the Cap APM vesicles and the HMW protein complexes (Tables 3.1, 3.2 and 3.3). Therefore, immunofluorescent labeling for these two proteins was performed on aldehyde-fixed Non-cap and Cap sperm (Figure 3.8). The same trend for ZAN immunofluorescent staining was also observed for proacrosin/acrosin staining (Figure 3.8, panels e & f). Minimal immunofluorescent staining of proacrosin/acrosin was present in ~4% of Non-cap sperm as revealed by flow cytometry (Figure 3.8, panel i) or 8% by manual counting (Table 3.4). Conversely, a stronger staining of proacrosin/acrosin over the acrosomal region was apparent in ~35% of sperm after 2 h of incubation in capacitating medium (Figure 3.8, panels f & j). In contrast to results obtained

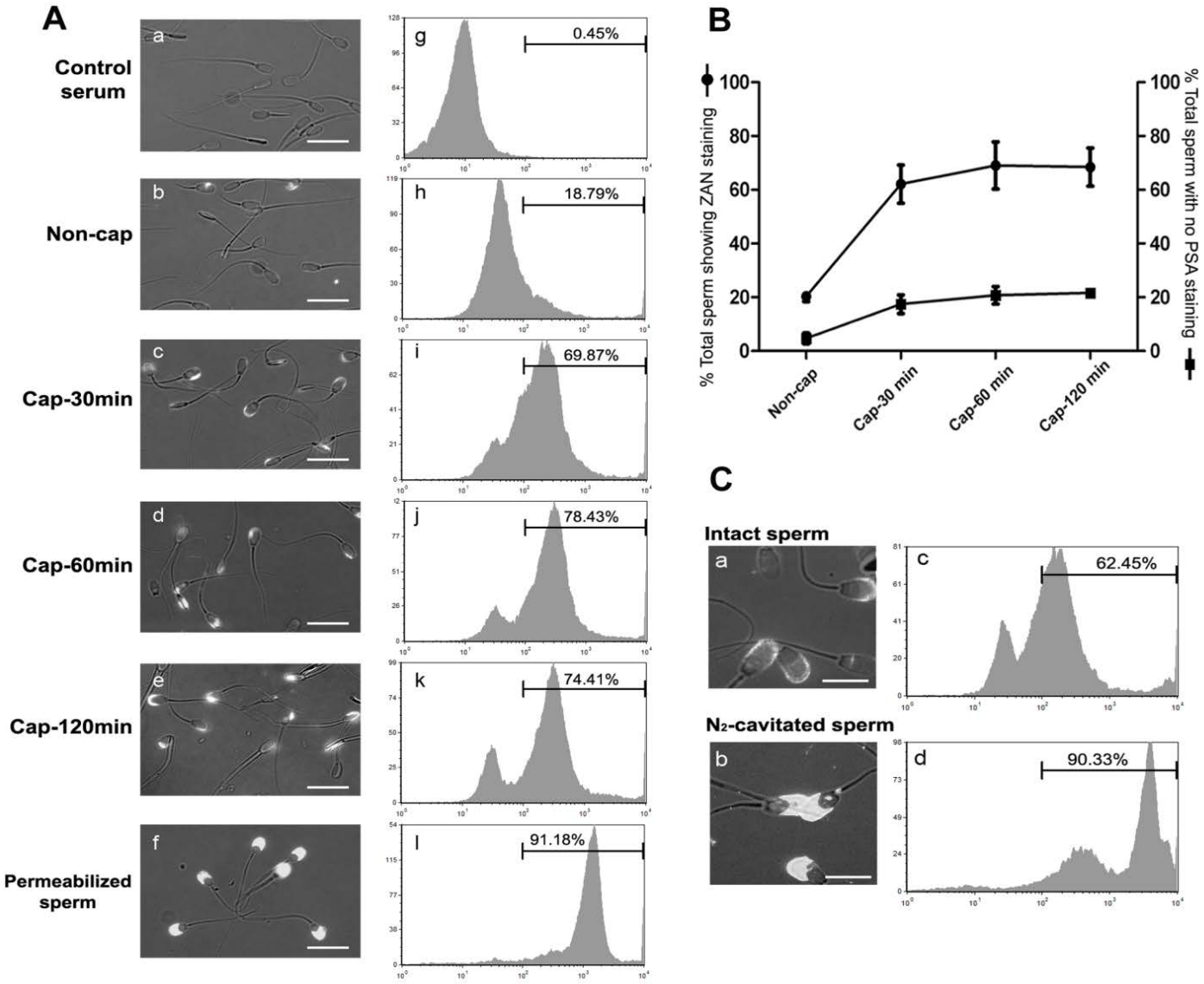

Figure 3.6: Increased exposure of ZAN on the sperm head surface during capacitation. A) Merged fluorescent-phase contrast images (a-f) and flow cytometry histograms (g-l) showing anti-ZAN staining signals of Non-cap sperm and sperm incubated for various times in capacitating medium (Cap-30 min, Cap-60 min, Cap-120 min). Aldehyde-fixed sperm were used for anti-ZAN antibody and secondary antibody incubation. Aldehyde-fixed sperm incubated with control rabbit antiserum (a) in place of anti-ZAN antibody served as a negative control to set the background level for flow cytometry (g). Aldehyde-fixed sperm permeabilized with TritonX-100 were also analyzed (f, l) to detect overall ZAN signals, both on the surface and inside the cell. Flow cytometry histograms and micrographs shown were representative from 3 replicate experiments. Bar = 20 μm. **B)** Kinetics of sperm numbers showing ZAN exposure to the cell surface during incubation in capacitating medium. Sperm were fixed and treated with antibodies as in **A.** An aliquot of sperm at each time point was also assessed for the acrosomal status by PSA staining (see Materials and Methods). Note the low percentages of acrosome-reacted sperm (showing no PSA staining) over the course of capacitation (120 min). Data shown are mean ± S.D. from 3 replicate experiments. **C)** Merged fluorescent-phase contrast images (a, b) and flow cytometry histograms (c, d) of ZAN staining of aldehyde-fixed intact and nitrogen-cavitated capacitated sperm. Bar = 20 μm.

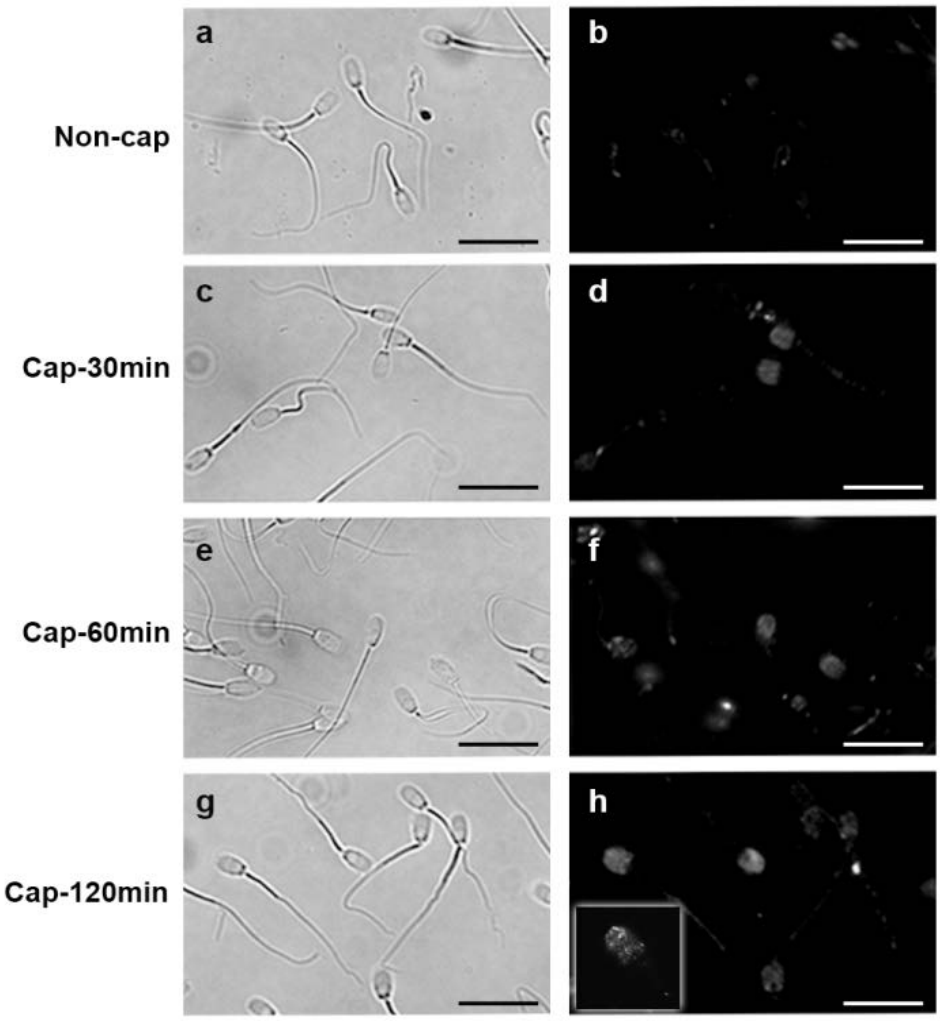

Figure 3.7: Immunofluorescent staining of ZAN on intact live (unfixed) pig sperm also showed a gradual increase in ZAN level on the sperm head surface over the course of capacitation. The immunofluorescent staining was performed using anti-ZAN holoprotein antibody as described in Materials and Methods. Phase contrast (a, c, e, g) and fluorescent (b, d, f, h) images of ZAN staining on unfixed Non-cap sperm (a, b) and sperm incubated in capacitating medium for 30 min (Cap-30 min) (c, d), 60 min (Cap-60 min) (e, f), and 2 hours (Cap-120 min) (g, h). Bar = 20 μm. Inset in panel h: A close-up image of ZAN staining on the head of a Cap sperm incubated in capacitating medium for 120 min.

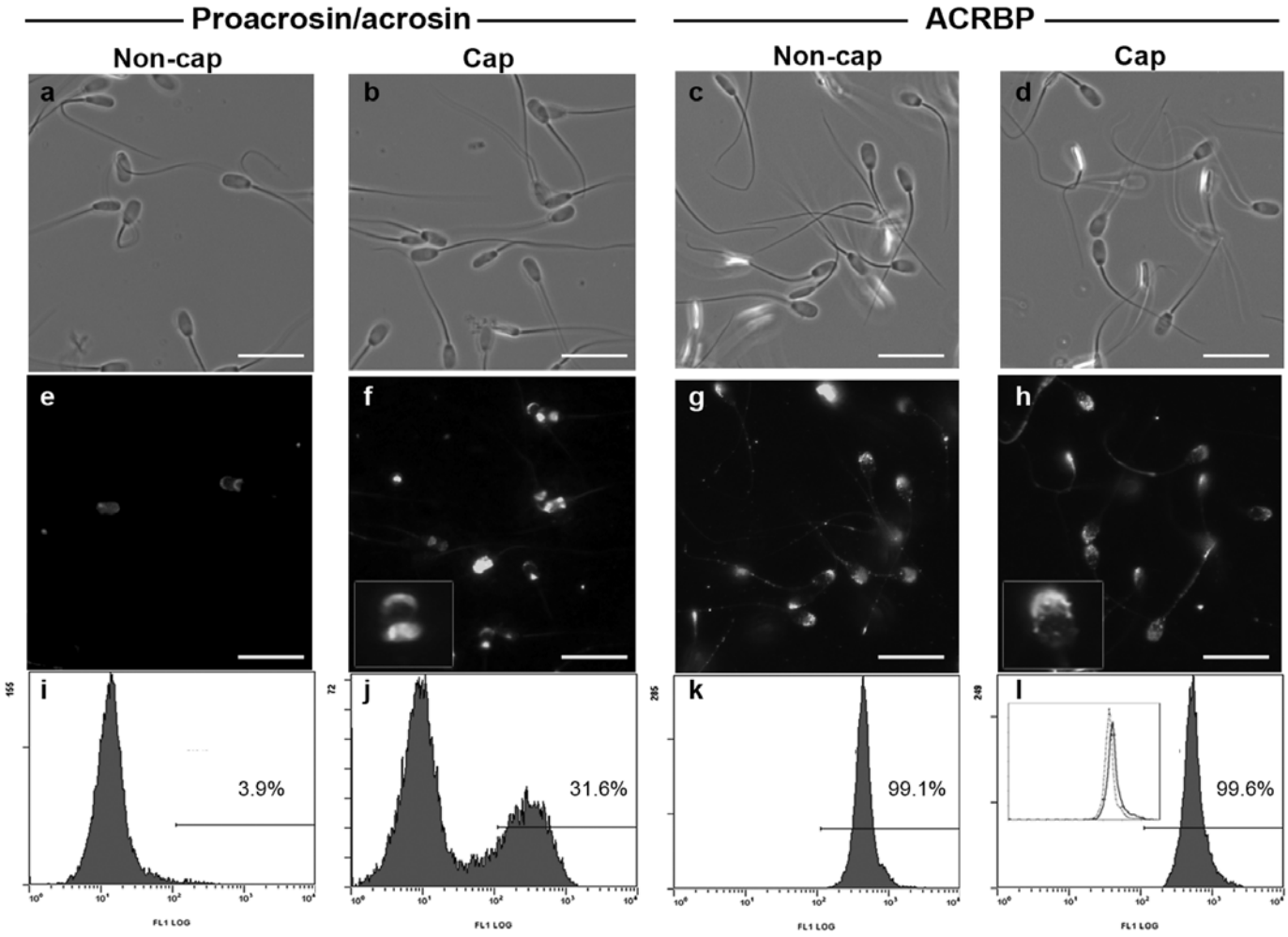

Figure 3.8: Localization of proacrosin/acrosin and ACRBP on the sperm head surface. Phase contrast (a-d), immunofluorescent (e-h) images and flow cytometry histograms (i-l) show staining signals for proacrosin/acrosin and ACRBP on aldehyde-fixed Non-cap and Cap sperm. The staining was performed as described in Materials and Methods. Minimal number of Non-cap sperm had positive staining for proacrosin/acrosin (a, e, i), but after 2-h incubation in capacitating medium, the number of sperm with proacrosin/acrosin staining was increase to ~30% of the total Cap sperm population (b, f, j). In contrast to proacrosin/acrosin, positive staining for ACRBP was detected in almost 100% of the Non-cap (c, g, k) and Cap (d, h, l) sperm populations. However, Cap sperm showed slightly higher fluorescence staining for ACRBP as compared with Non-cap sperm. The shift of ACRBP signal in the Cap sperm is shown in the inset of panel l. Close-up fluorescent images of Cap sperm heads with positive staining for proacrosin/acrosin and ACRBP on their surface are shown in insets of panel f and panel h, respectively. Bar =20 µm.

Table 3.4: Numbers of Non-cap sperm and Cap-120 min sperm that were stained positively with anti-ZAN, anti-proacrosin, and anti-ACRBP antibodies

Protein	Percentage of positive stained cells		
	Non-cap	**Cap-120 min**	**Δ**
ZAN	27.9 ± 8.0	73.0 ± 8.6	45.1
Proacrosin/acrosin	8.9 ± 0.1	34.3 ± 0.1	25.4
ACRBP	99.5 ± 0.0	98.8 ± 0.0	0.7

Data were obtained by manual counting and are shown as mean ± S.D. from 3 replicate experiments.

for ZAN and proacrosin/acrosin, 99% of Non-cap sperm analyzed by either flow cytometry (Figure 3.8, panel k) or by manual counting (Table 3.4) already stained positively for ACRBP with a punctate pattern over the whole acrosomal region (Figure 3.8, panel g). Following incubation in capacitating medium for 2 h, the same number of sperm showed positive staining for ACRBP (Figure 3.8, panels h & l), although the staining intensity at the anterior periphery was increased in the Cap sperm (Figure 3.8, inset of panel l), indicating the transport of additional ACRBP (possibly in the proacrosin-bound form) from the acrosome to the sperm head surface. Immunofluorescent staining of MFGM, another ZP-binding protein identified in the APM vesicles, was also observed at the sperm anterior head surface of the majority (~80-90%) of intact unfixed sperm, both Non-cap and Cap, and the fluorescence intensity of MFGM labeling in those two sperm types was similar. However, after nitrogen cavitation, the sperm showed no MFGM staining, indicating that MFGM was exclusively localized on the sperm head plasma membrane (Figure 3.9).

3.1.6) Contribution of ZAN to the pig ZP3 binding ability of APM high molecular weight protein complexes

The results from our proteomic and immunofluorescence analyses suggested that a fraction of ZAN present on the Cap sperm surface may be the main factor contributing to the ZP affinity of APM HMW protein complexes. Immunoblotting results of APM HMW protein complexes, as separated by BN-PAGE, indicated that the ZAN bands (Figure 3.10A, left panel) were at the same positions as the pig ZP3-reactive bands in all three Complexes (Figure 3.5A). Under DTT-reducing SDS-PAGE conditions, immunoblotting using anti-

ZAN holoprotein antibody revealed ZAN forms in the 275-420 kDa and 420-645 kDa ranges, and even higher molecular masses (evident in the stacking gel) in the APM vesicle samples (Figure 3.10A, right panel, lane a). Of note was the observation that ZAN HMW forms in nitrogen-cavitated sperm were not larger than 420 kDa (Figure 3.10A, right panel, lane b).

Direct contribution of ZAN to the ZP-binding ability of the Cap HMW protein complexes was further demonstrated by pre-treating the complexes with various concentrations (1, 4 and 8 µg/ml) of anti-ZAN-holoprotein IgG or with 8 µg/ml of normal rabbit IgG prior to incubation with biotinylated pig ZP3. HMW complexes treated with normal rabbit IgG showed similar ZP3 affinity to those untreated with any IgG (Figure 3.10B and 3.5A, respectively). At 1 µg/ml of anti-ZAN IgG, the level of pig ZP3 binding of Cap HMW Complexes (I, II and III) was decreased to ~70% of parallel HMW complexes treated with normal rabbit IgG (Figure 3.10B). The inhibition of pig ZP3 binding of Cap HMW complexes was further enhanced when 4 µg/ml of anti-ZAN IgG was used, with Complex II showing a minimum binding level to pig ZP3, and Complex I and III exhibiting ~40% ZP3 binding compared with the control HMW complexes (treated with 8 µg/ml normal rabbit IgG) (Figure 3.10B). Similar inhibition of Cap HMW complexes were observed upon treatment with 8 µg/ml of anti-ZAN IgG, indicating that the inhibition of ZP3 interaction reached a plateau upon treatment with anti-ZAN IgG treatment at 4 µg/ml (Figure 3.10B).

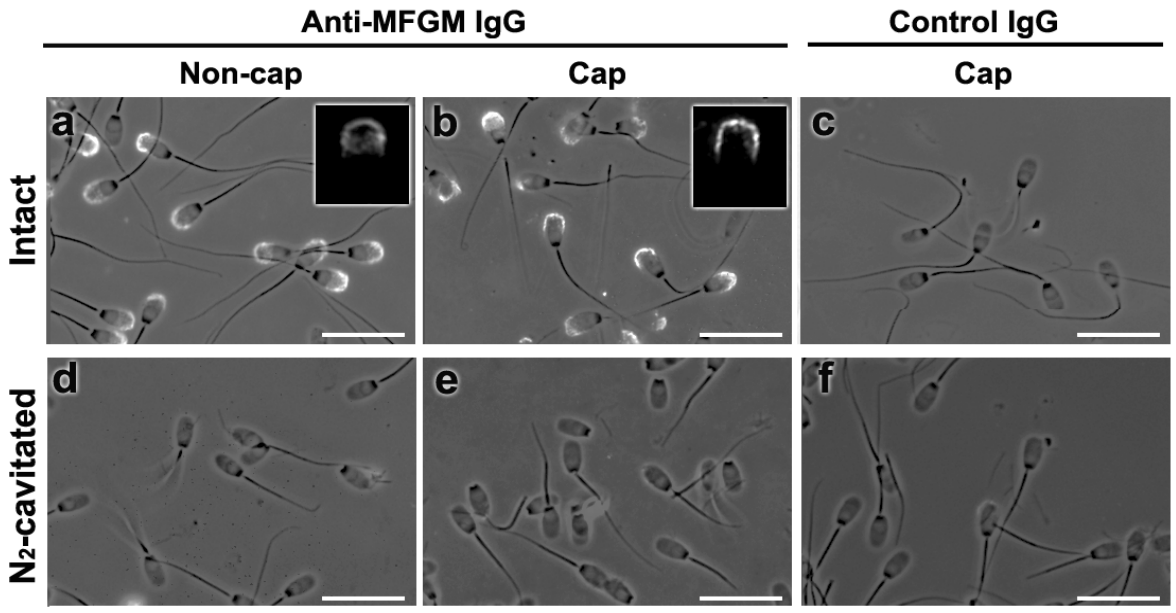

Figure 3.9: Immunofluorescence of MFGM on intact and nitrogen-cavitated Non-cap and Cap pig sperm. Both intact (a, b, c) and nitrogen-cavitated (d, e, f) sperm were incubated with either anti-MFGM IgG (a, b, d, e) or control mouse IgG (c, f) (both at 5 µg/ml) in solution. After washing, the sperm were put on glass slides prior to incubation with Alexa-488 conjugated secondary antibody. Insets in panel a and b show close-up fluorescent images of MFGM staining on intact Non-cap and Cap sperm heads, respectively. Bar = 20 µm. The merged fluorescent-phase contrast images presented were representative of 3 replicate experiments.

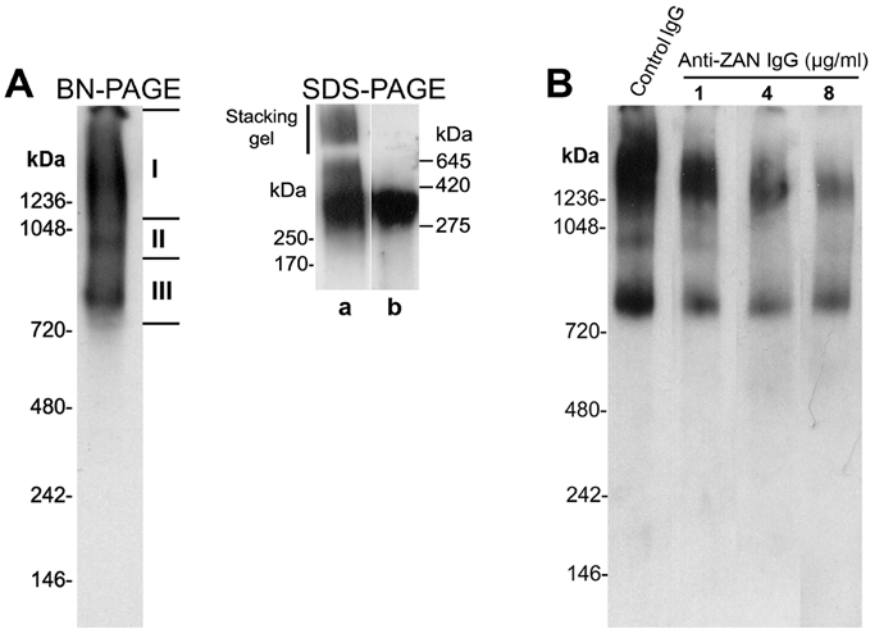

Figure 3.10: Significance of ZAN on ZP affinity of APM HMW protein complexes. A) Immunoblotting of ZAN in Cap sperm samples. *Left panel:* HMW protein complexes of Cap sperm APM were separated by BN-PAGE and probed for ZAN. Right panel: Protein extracted from Cap APM vesicles (lane a) and nitrogen-cavitated Cap sperm (lane b) were resolved by SDS-PAGE and probed for ZAN. Anti-ZAN holoprotein antiserum was used for ZAN detection by immunoblotting. **B) Pre-incubation of HMW protein complexes with anti-ZAN antibody could inhibit the complexes' ZP binding ability.** Pre-treatment of APM HMW protein complexes with anti-ZAN IgG resulted in their decreased ability to bind to biotinylated pig ZP3, as shown by far western blotting. Purified anti-ZAN holoprotein IgG at 1, 4 and 8 µg/ml, as well as normal rabbit IgG at 8µg/ml, was used for the treatment.

3.1.7) Interaction of ZAN with proacrosin/acrosin and ACRBP

ZAN is a mosaic protein with a number of domains known for molecular adhesion, including MAM, mucin-like and von Willebrand factor D domains (see Figure 3.4C for ZAN structure), and this adhesion property may be the basis of ZAN contribution to the affinity of APM HMW protein complexes for pig ZP3. In addition, it was possible that ZAN might interact with other acrosomal proteins, forming a cohort during trafficking to the sperm head surface. I tested this possibility by co-immunoprecipitation of proteins extracted from the Cap APM vesicles with anti-ZAN holoprotein IgG, crosslinked with protein G paramagnetic beads. The results of this experiment revealed that the 300 kDa form of ZAN was successfully captured from the Cap APM protein extracts (Figure 3.11). Proacrosin/acrosin with predominant bands of 53, 43, and 35 kDa (Baba et al., 1989) and ACRBP of 32 and 28 kDa (Baba et al., 1994b) were also captured by the anti-ZAN immunobeads, implicating their interaction with ZAN in the Cap sperm APM vesicles (Figure 3.11). In contrast, MFGM, another ZP-binding protein which was present at high levels in the Cap APM vesicles, was not immunoprecipitated by the anti-ZAN antibody (Figure 3.11). This result suggested that ZAN formed complexes with the other two acrosomal proteins, proacrosin/acrosin and ACRBP.

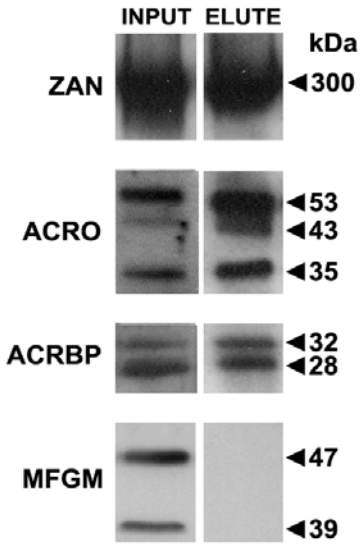

Figure 3.11: Interaction of ZAN with proacrosin/acrosin (ACRO) and ACRBP in the Cap sperm APM vesicle extracts. Proteins (25 µg) extracted from Cap APM vesicles were incubated with protein G Dynabeads conjugated with anti-ZAN holoprotein IgG. Loosely bound proteins were washed off with RIPA buffer, and the bound proteins (ELUTE) were eluted from the beads with SDS-PAGE sample buffer prior to being subjected to immunoblotting. The whole APM protein extracts (INPUT) (5 µg) were included in immunoblotting for identification of the pulled-down proteins. Molecular masses (kDa) of the ZAN, ACRO, ACRBP and MFGM bands were indicated on the right side. Immunoblotting results revealed that ZAN, ACRO, ACRBP, but not MFGM interacted with each other in the Cap APM sample. Results shown were representative of 3 replicate experiments.

3.2) Importance of SGG homeostasis in male fertility

Homeostasis of SGG in the male reproductive system is regulated mainly through its synthesis and degradation pathways. The SGG synthesis pathway involves CGT and CST enzymes. Lack of these enzymes causes no SGG production in the testicular germ cells and results in infertility due to a spermatogenesis arrest at primary spermatocyte stages of *Cgt* and *Cst* knockout mice (Fujimoto et al., 2000; Honke et al., 2002). The SGG degradation pathway starts with the desulfation of SGG by ARSA. Since *Arsa* KO mice have been produced, we investigated their fecundity along with SGG quantification in testes, testicular germ cells and mature sperm, with a plan to correlate the changes of SGG levels with male infertility/subfertility. Besides this objective, we wanted to investigate the *in vivo* roles of sperm ARSA, which we have shown for its relevance, independent of its enzymatic activity (Xu et al., 2012), in sperm fertilizing ability *in vitro* (Carmona et al., 2002a; Tantibhedhyangkul et al., 2002).

3.2.1) Reduced fecundity and abnormal sperm morphology of aging *Arsa* knockout males

Fecundity of *Arsa* KO mice was evaluated as a function of age (from 2 to 9 months). Natural mating of *Arsa* KO males or age-matched WT males with fertile females was performed in parallel. I performed these experiments in collaboration with Dr. Hongbin Xu (a former Ph.D. student in Dr. Tanphaichitr's lab). The results demonstrated that *Arsa* KO males at 2-5 months of age produced the same accumulated numbers of pups/mating pair as age-matched WT males. However, after 5 months of age, *Arsa* KO males started to show lower fecundity as compared with WT males. Specifically, when the *Arsa* KO males were 8

months old (equivalent to 40-year-old men), their accumulated number of pups/pair was only 65% of the WT values (Figure 3.12A). During the 6 months of the mating study, the *Arsa* KO males produced an average litter size of 6.2 ± 2.4 pups/litter, which was significantly smaller than the average litter size produced by the WT males (7.9 ± 1.3 pups/litter). The fertilizing ability of motile swim-up sperm retrieved from 5-month-old and 8-month-old *Arsa* KO mice was further compared *in vitro* with sperm from age-matched WT mice. Corroborating the mating study results, sperm of 8-month-old *Arsa* KO mice showed significantly lower ZP binding and fertilizing ability *in vitro*, as compared with sperm from WT males of the same age, while sperm of 5-month-old *Arsa* KO mice showed no difference in their ZP binding and fertilizing ability as compared with sperm from the WT mice (Figure 3.12B). The minimal sperm fertilizing ability of the 8-month-old *Arsa* KO males may be partly attributed to a high population (30-40%) of sperm with abnormal morphology, despite the fact that they were already selected by the swim-up technique (Figure 3.12C). The abnormal morphology included irregular head shapes and 180° folding of sperm tails. In contrast, 90% of the swim-up sperm from WT animals of the same age were normal in their morphology (Figure 3.12C).

Subsequently, I further characterized the morphology of 8-month-old *Arsa* KO and WT mouse sperm prepared by Percoll gradient centrifugation, which separates sperm populations based on density and motility. Following centrifugation through a discontinuous (45%/90%) Percoll gradient, sperm with higher motility and density sediment as a pellet at the bottom of the 90% Percoll layer, whereas sperm with lower motility and density stay at the interface between the 45% and 90% Percoll gradient layers; the epididymal fluid and the majority of round cells remain at the top of the 45% Percoll layer (Figure 3.13A). In the WT

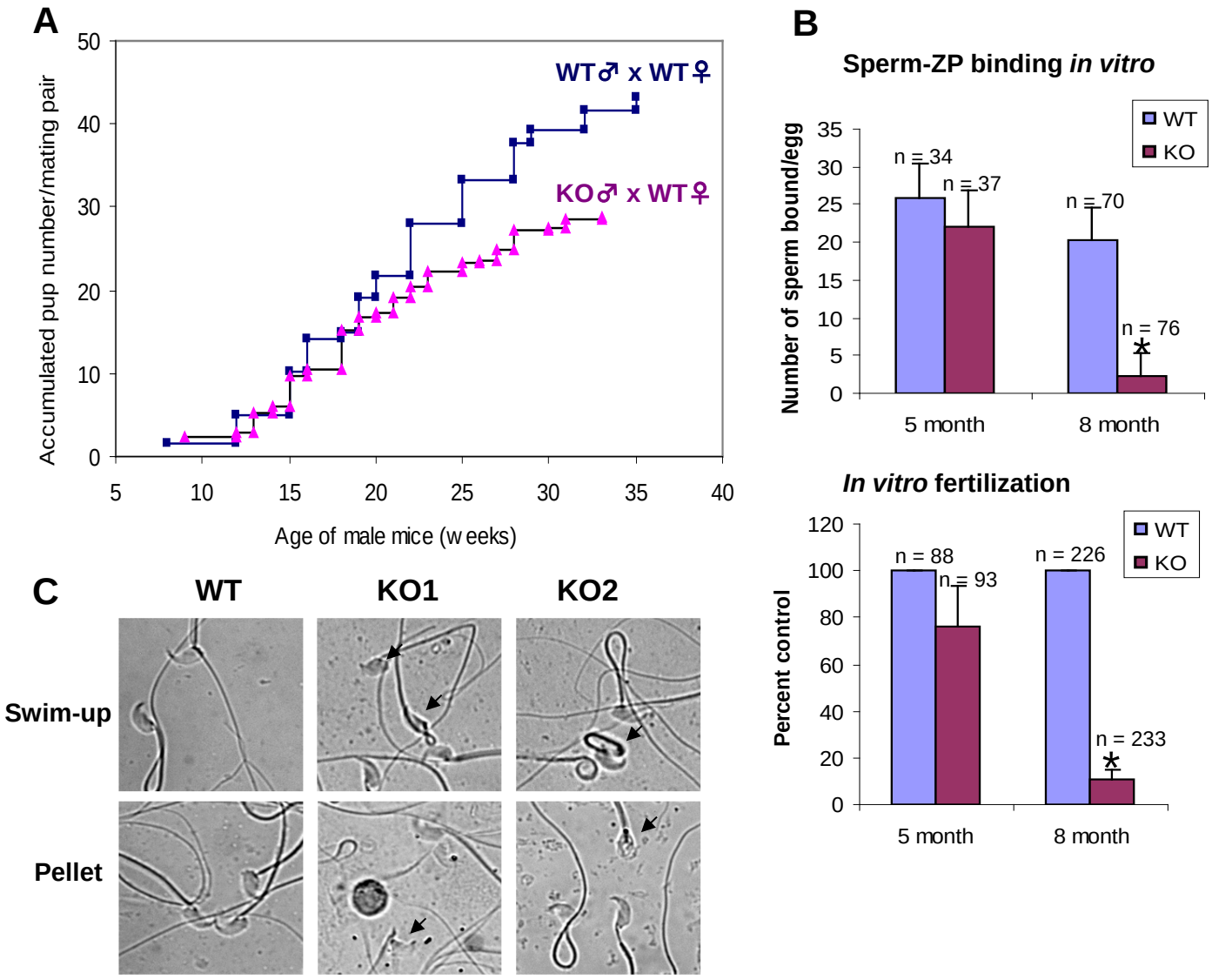

Figure 3.12: Reduced fecundity of older *Arsa* knockout (KO) males. A) The fecundity of *Arsa* KO males was evaluated by natural mating studies with wild type (WT) females starting when the males were 2 months of age for a duration of 7 months. The average accumulated numbers of pups produced by 4 pairs of WT ♂x WT ♀ (blue line with squares) and 8 pairs of KO ♂x WT ♀ (pink line with triangles) were presented. Note the lower accumulated pup numbers from *Arsa* KO fathers, when they were older than 5 months of age. The total number of litters produced by WT and *Arsa* KO males during the whole mating period was 5.5 and 4.6, respectively. The average litter size produced by *Arsa* KO males (6.2 ± 2.4 pups/litter) was significantly lower ($P < 0.05$) than that of the WT males (7.9 ±1.3 pups/litter). **B)** Near zero fertilizing ability of 8-month-old *Arsa* KO sperm. Caudal epididymal and vas deferens sperm were collected from *Arsa* KO and WT mice, each at 5 months and 8 months of age. The motile sperm population was prepared by the swim up technique and was used for co-incubation with mature mouse eggs. The number of sperm bound to the egg ZP was then counted after 30 min of co-incubation (top panel). Data were expressed as mean ± S.D. of numbers of sperm bound per egg from 3 experiments. In alternate experiments, gamete co-incubation was prolonged to allow sperm to enter the egg proper and fertilize the eggs. The fertilization rate was scored by the presence of two pronuclei. Fertilization ability of *Arsa* KO sperm was expressed as mean ± S.D. of percent control (WT) values from 3 experiments (bottom panel). n = Total number of eggs analyzed for each sample. Asterisk indicates significance difference (P <0.05) between KO and WT values. **C)** Abnormal morphology of both swim-up and non-swim-up (pellet) sperm were obvious in 8-month-old *Arsa* KO mice. These abnormalities (arrows indicated) include irregular sperm head shapes and 180º folding of the tails.

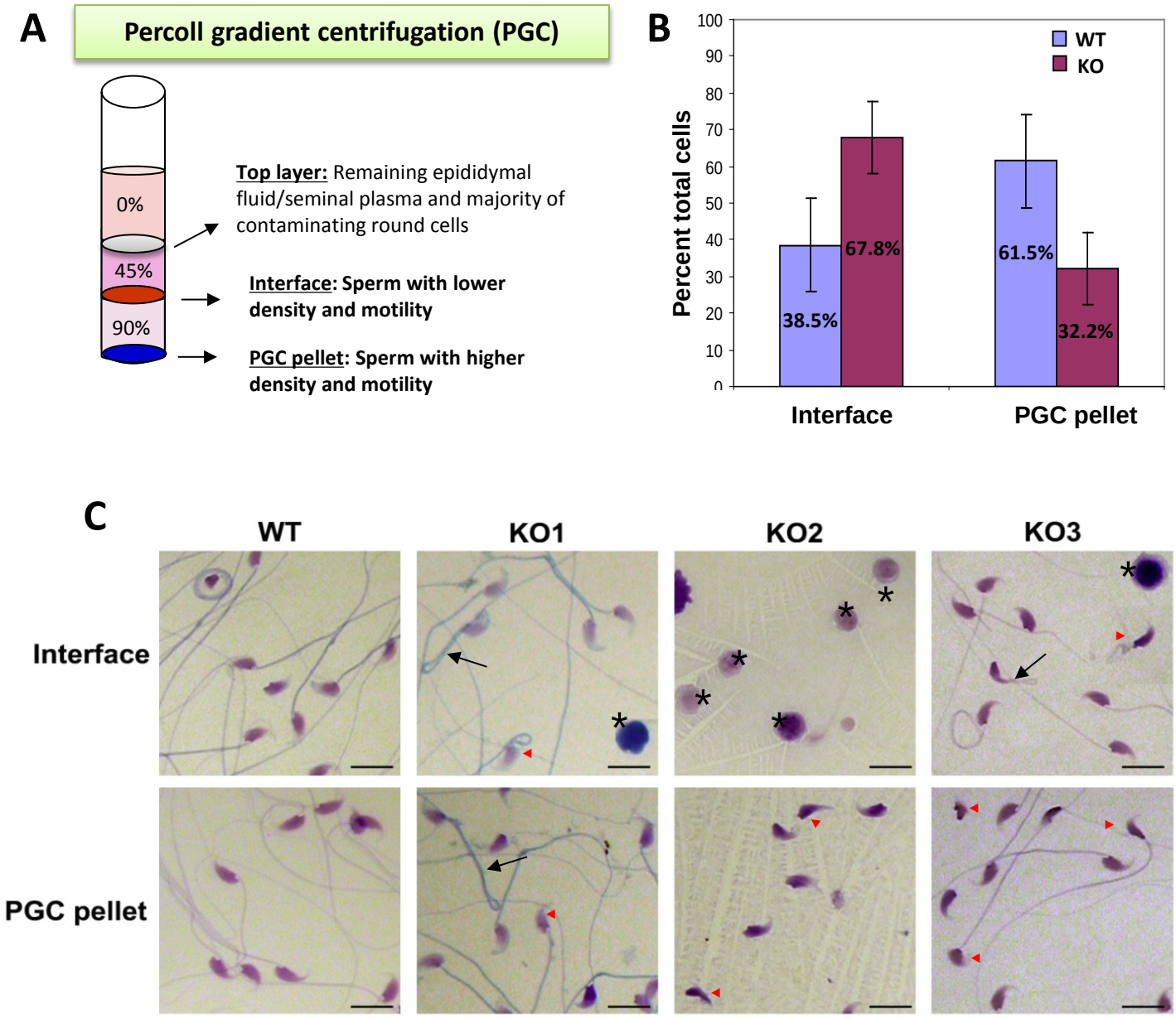

Figure 3.13: Analyses of epididymal sperm prepared from 8- to 11-month-old *Arsa* KO and age-matched WT mice using Percoll gradient centrifugation. A) Diagram showing Percoll gradient centrifugation (PGC), a sperm separation technique that gives a great yield of motile and morphologically normal sperm. The PGC method is significantly effective in selecting sperm with high fertilizing ability. **B)** Distribution of sperm from WT and *Arsa* KO mice (8-11 months of age) retrieved from the interface and PGC pellet fractions following the centrifugation. Data were expressed as mean ± S.D. of percentages of total cells in the interface and PGC pellet fractions. In contrast to the WT sperm, the majority of the KO sperm were found in the interface fraction, indicating that motility and cell density of KO sperm were lower than those of the WT sperm. **C)** Morphology of WT and *Arsa* KO mouse cells found in the interface and PGC pellet fractions. The PGC pellet fractions of *Arsa* KO samples contained only sperm populations, but the interface fractions consisted of both sperm and round cells (asterisks), which may be round spermatids sloughed off from the seminiferous epithelium. A number of *Arsa* KO sperm in both interface and PGC pellet fractions showed abnormal sperm morphology, including misshaped heads (red arrowheads) and 180˚ folding of the tails (arrows). Bar = 10 µm.

sperm populations retrieved from 8-month-old WT mice, 61.5% of the total sperm was found in the PGC pellet, whereas the other 38.5% stayed at the interface between 45% and 90% Percoll solutions (Figure 3.13B). In contrast, only 32.2% of the total sperm from 8-month-old *Arsa* KO mice was in the PGC pellet and the other 67.8% of *Arsa* depleted sperm was at the Percoll gradient interface (Figure 3.13B). Consistent with previous observations in swim-up sperm, the PGC pellet and interfaced sperm prepared from 8-month-old *Arsa* KO mice had a number of abnormalities in their morphology, including irregular head shapes, broken heads and tails, 180° folding of the sperm tails, as compared with those corresponding fractions of WT sperm (Figure 3.13C). In addition, there appeared to be a number of round cells co-existed with sperm at the interface, varying from 10-80% of total cells at this gradient position. These round cells were likely spermatids sloughed off from the seminiferous tubules, as observed in the epididymis section (see below). However, in the corresponding interfaced fraction of cells collected from the lumen of caudal epididymis and vas deferens of WT animals, only sperm (no round cells) were present. But as expected, only sperm constituted the PGC pellet fractions for both *Arsa* KO and WT samples. These PGC pellet sperm from WT and KO animals were further used for lipid characterization (see the results in section 3.2.5).

3.2.2) Reduced spermatogenesis rate of 8-month-old *Arsa* knockout mice

Histological analyses of testis sections revealed that the germ cell layers in the seminiferous tubule epithelia of 8-month-old *Arsa* KO mice were disorganized, with sporadic empty spaces that never appeared in WT seminiferous tubules (Figure 3.14A). Morphometric analyses of the areas of seminiferous tubule epithelium indicated a significant decrease of this area in 8-month-old *Arsa* KO mice, as compared with that of age-matched

WT animals (i.e., the epithelial areas were 37297 ± 8501 and 24189 ± 6587 μm^2 in WT and *Arsa* KO mice, respectively) (Figure 3.14B). In addition, there was a very distinct increase in the number of apoptotic germ cells (mainly primary spermatocytes) in the KO mice of this age (i.e., 12.3 ± 2.5 versus 196.3 ± 20.5 apoptotic cells per 100 tubules of WT and KO mice, respectively) (Figure 3.14C). These changes may be the cause of germ cell layer disorganization in the seminiferous tubules of the 8-month-old KO animals as described above, as well as a reduction in the testicular weights of the 8-month-old KO mice to about half of the WT values (64.5 ± 8.5 versus 105.7 ± 5.0 mg/testis of KO and WT mice, respectively) (Figure 3.14D). Obviously, spermatogenesis in KO mice of this age occurred at a reduced rate, a phenomenon further confirmed by the presence of only 50% of sperm in their epididymis and vas deferens, compared with the values in the counterpart wild types (total numbers of sperm were 21.5 ± 3.5 versus 45.3 ± 6.0 million from each KO and WT mouse, respectively) (Figure 3.14E). The lower rate of spermatogenesis together with the disorganization of germ cell layers in the seminiferous tubules (as described above) may result in the sloughing of immature germ cells into the lumen, which eventually migrate into the epididymal lumen, as shown in Figure 3.14A (lower right panel). However, the caudal epididymal epithelial cell morphology (Figure 3.14A) and caput epididymis weight (Figure 3.14F) of these old *Arsa* KO mice were normal, implicating that circulating and topical testosterone was at functional levels (epididymis are the known targets of the hormone). This implication would in turn suggest that the decrease in the spermatogenesis rate and the presence of a substantial population of sperm with abnormal morphology were from testicular defects which were not regulated by the testosterone actions. In contrast to the aberrancy in the testis and sperm from 8-month-old *Arsa* KO mice, all processes of

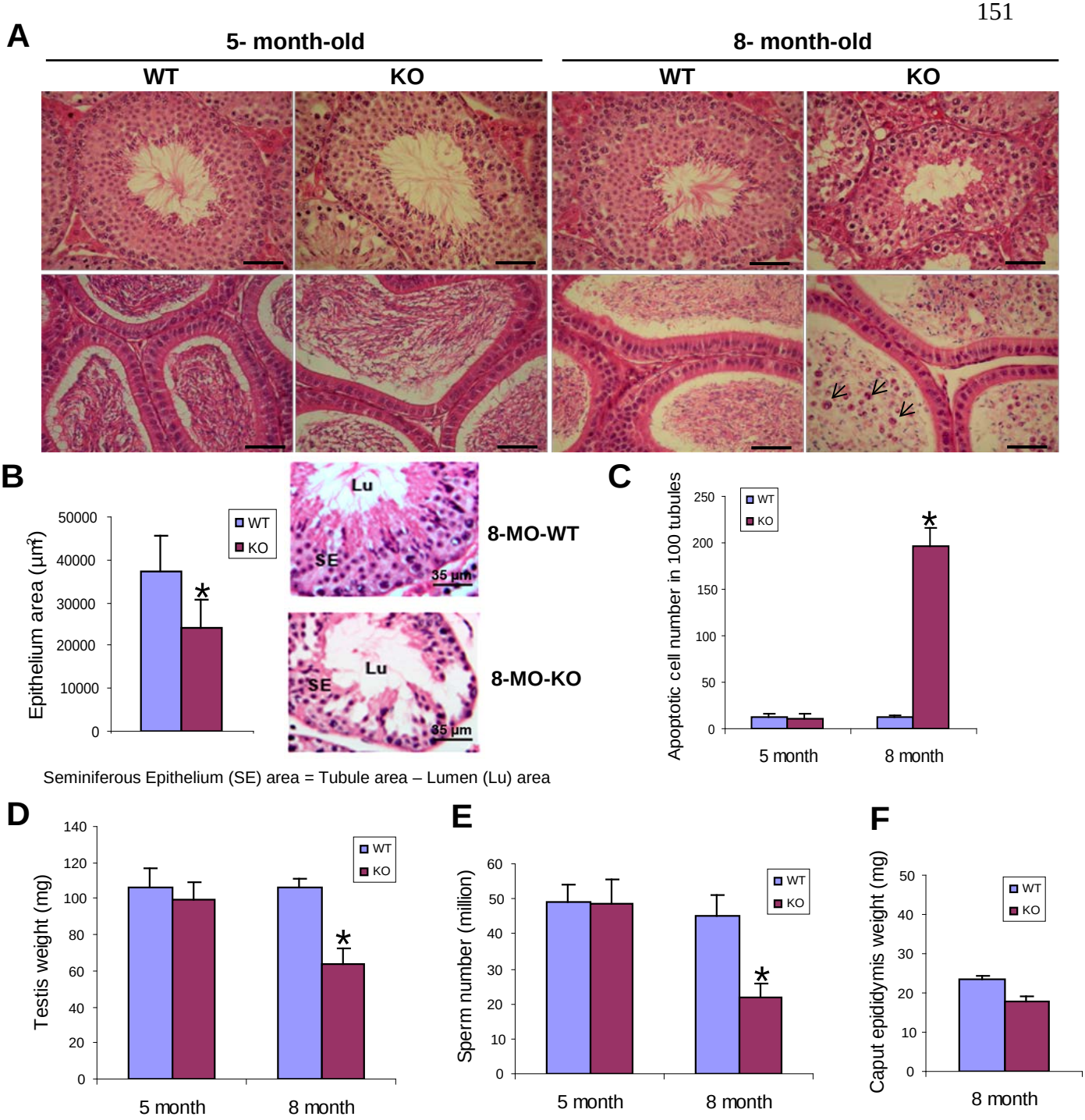

Figure 3.14: Reduced spermatogenesis rate in 8-month-old *Arsa* KO males. A) Histology of testes (top row) and epididymis (bottom row) of WT and KO mice at 5 months and 8 months of age. Note the disorganization of testicular germ cells in the seminiferous tubules of 8-month-old *Arsa* KO mice, and the presence of immature round germ cells (arrows) in their epididymis. In contrast, 5-month-old *Arsa* KO mice showed normal morphology of cells in seminiferous tubules and normal morphology of sperm in the epididymal lumen. Bar = 25 µm. **B)** The epithelial area of the seminiferous tubules of 8-month-old *Arsa* KO mice was significantly thinner than that of the age-matched WT mice. Quantification of profile areas was done in 80 WT and 80 *Arsa* KO seminiferous tubules. **C)** Higher number of apoptotic testicular germ cells in 8-month-old *Arsa* KO mice. TUNEL staining was performed on testis sections of WT and KO mice of 5 months and 8 months of age. The total number of apoptotic germ cells was counted on randomly selected 100 tubules of each mouse. Reduced spermatogenesis rate in 8-month-old *Arsa* KO males was confirmed by a decrease in their testis weights **(D)** and a low number of sperm retrieved from the cauda epididymis and vas deferens **(E)**. **F)** Caput epididymis weights of 8-month-old *Arsa* KO mice were similar to those of WT mice, suggesting no changes in testosterone levels of KO mice. Results in **A and B** are representative from 3 replicate experiments, whereas data in **C, D, E and F** were mean ± S.D. of values obtained from 5 WT and 5 KO mice at each age. Asterisk indicates significance difference (P<0.05) between KO and WT values.

spermatogenesis and sperm maturation appeared to be normal in the KO mice 5 months of age (Figures 3.14A, C, D, and E).

3.2.3) Levels of SGG in testis, germ cells, sperm and Sertoli cells in wild type and *Arsa* knockout mice of various ages

Since ARSA is important for SGG desulfation, lack of ARSA may lead to disruption of SGG homeostasis, which likely results in the observed reduction of the spermatogenesis rate and sperm fertilizing ability in aging *Arsa* KO mice. However, background information of SGG levels in the male reproductive system of WT animals first needs to be determined for a better understanding of the effects on male fertility of SGG level changes in *Arsa* KO mice. The experimental results of this study in WT mice were therefore put forth at the beginning of the section below.

3.2.3.1) SGG levels in primary spermatocytes, round spermatids and sperm of wild type mice

To date, SGG is known to be synthesized in primary spermatocytes (Kornblatt, 1979; Letts et al., 1978). However, it is not known whether there are additional rounds of synthesis in round spermatids or whether some amounts of SGG, which are synthesized and targeted to the testicular germ cell surface, are shed as part of cellular differentiation during spermiogenesis and transport of sperm through the epididymis. Quantification of SGG in primary spermatocytes, round spermatids, and mature sperm (collected from cauda epididymis and vas deferens) in wild type animals should give information towards the changes of SGG levels during these physiological events. Pure populations of primary spermatocytes (mainly pachytene stage) and round spermatids were isolated from mixed

testicular germ cells of 50 WT mice (10 weeks of age) using the STAPUT technique, which separated different types of germ cells based on their differential sedimentation at unit gravity on a continuous BSA gradient (STAPUT technique, reference); these purified germ cells were prepared by Dr. Stuart Moss (University of Pennsylvania). SGG quantification was performed using a highly specific and sensitive LC-ESI-MS/MS-MRM method (Kongmanas et al., 2010), which I established in collaboration with Dr. Kym F. Faull, Pasarow Mass Spectrometry Laboratory, University of California, Los Angeles. Quantitative analysis revealed that levels of SGG (C16:0/C16:0) in primary spermatocytes, round spermatids and sperm from caudal epididymis and vas deferens were 1.912 ± 0.591, 0.712 ± 0.036, and 0.120 ± 0.006 nmole/million cells, respectively (Figure 3.15). It is known that one primary spermatocyte gives rise to 4 round spermatids (Kiersenbaum, 2002). SGG in round spermatids should be about ¼ of that in primary spermatocytes (i.e., 0.478 nmol/million cells) if there is no synthesis in germ cells post the primary spermatocyte stage. My results showing 0.712 nmole of SGG/million round spermatids suggested that there must be another round of SGG synthesis in either the secondary spermatocytes or the round spermatids. However, SGG levels in mature sperm were decreased to ~17% of the round spermatid level. This reduction suggested that the majority of SGG in the spermatids was possibly removed as part of the residual bodies, cytoplasmic fractions that are extruded from elongating spermatids and engulfed by Sertoli cells.

3.2.3.2) Detection of SGG in Sertoli cells of 5-day-old, 20-day-old and 10-week-old mice

Sertoli cells are responsible for the phagocytosis and degradation of residual bodies and apoptotic germ cells (Igdoura and Morales, 1995; Mruk and Cheng, 2004; Wang et al., 2006; Xiong et al., 2009). Notably, 50% of developing testicular germ cells becomes

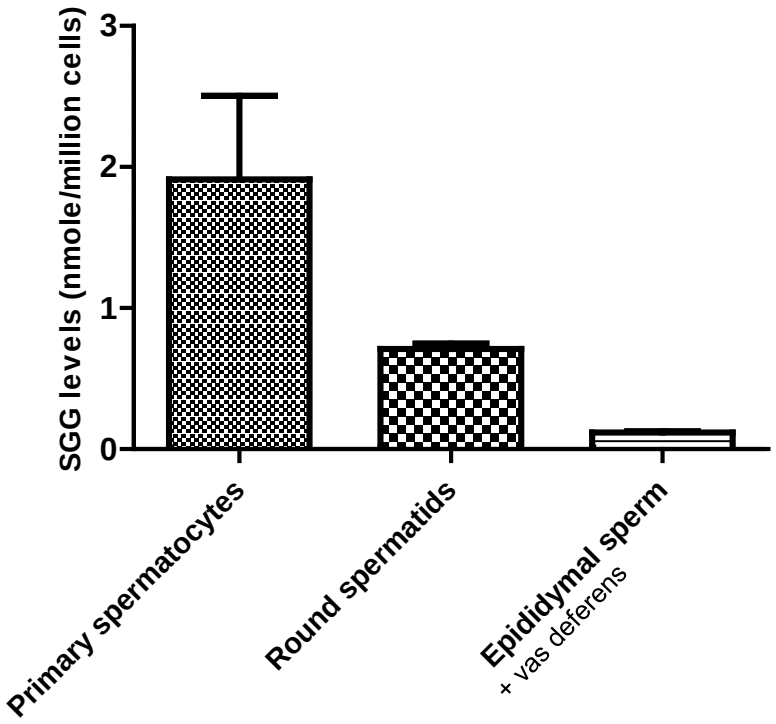

Figure 3.15: SGG levels in testicular germ cells and sperm of CD-1 WT mice. Purified populations of primary spermatocytes, round spermatids and caudal epididymal/vas deferens sperm isolated from wild type mice were subjected to lipid extraction and SGG quantification by ESI-MS/MS MRM. The data were expressed as mean ± S.D. of results from triplicate experiments.

apoptotic. Therefore, from the onset of spermatogenesis Sertoli cells are constantly challenged with the processing of SGG in the residual bodies and apoptotic corpses. Thisstatement is supported by my HPTLC results, revealing that Sertoli cells isolated from 5-day-old neonatal mice did not contain SGG. In contrast, Sertoli cells isolated from 20-day-old mice, where the first round of spermatogenesis has started and round spermatids are already produced, contained a significant amount of SGG (Figure 3.16A). Imaging MS performed in collaboration with Dr. N Goto-Inoue (Hamamatsu University, Japan) further supported my statement above. SGG (C16:0/C16:0) with *m/z* 795 was absent from the Sertoli cells and spermatogonia of 5-day-old mice but it was present in the testicular germ cells of 20-day-old mice (Figure 3.16B). The existence of SGG in the Sertoli cells of 20-day-old pubertal mice was further confirmed by precursor ion scanning of m/z 97 (sulfate) of Sertoli cell lipid extracts. The same analysis also revealed SGG existence in the Sertoli cells of 10-week-old adult mice. In the Sertoli cells of mice of both ages, SGG was the most abundant sulfolipid species (Figure 3.16C, panel a). However, subsequent MRM analyses revealed that SGG levels were at a double amount in the Sertoli cells of 10-week-old mice, compared with those in 20-day-old animals (1.383 and 0.663 nmole/million cells, respectively) (Figure 3.16C, panel b). Higher SGG levels in Sertoli cells of adult mice may reflect a higher number of phagocytosed apoptotic corpses of germ cells. With the degradation activities of lysosomes (Igdoura and Morales, 1995; Igdoura et al., 1996) and the presence of ARSA in these organelles, Sertoli cells should be responsible for SGG degradation (see more below under the results from *Arsa* KO Sertoli cells). Nonetheless, the presence of SGG in Sertoli cells following the onset of spermatogenesis indicated that the degradation of the sulfoglycolipid was not highly efficient.

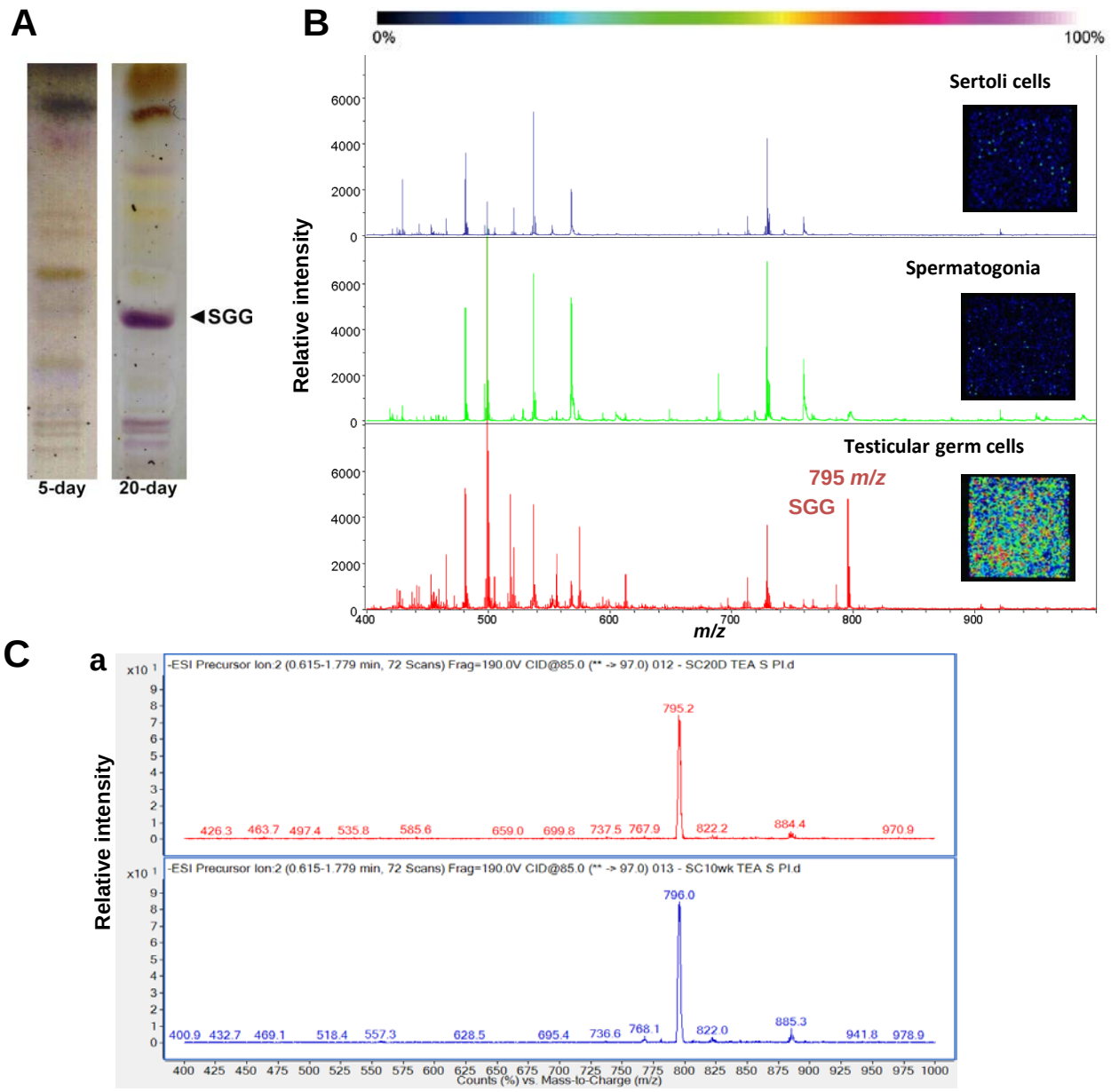

b

Samples	nmole of SGG/million cells
Sertoli cells from 20-day-old mice	0.663 ± 0.016
Sertoli cells from 10-week-old mi ce	1.383 ± 0.054

Figure 3.16: Presence of SGG in Sertoli cells in mice of different ages. **A)** HPTLC showing the presence of SGG in Sertoli cells of 20-day-old mice but not in those of the 5-day-old animals. Lipids extracted from 2 million Sertoli cells isolated from 5-day-old or 20-day-old mice were loaded onto a HPTLC plate, and stained with Orcinol solution which specifically reacts with glycolipids to yield purple bands. SGG was found as the major glycolipid in the Sertoli cells of 20-day-old mice (where the first round of spermatogenesis has initiated) but it was not detectable in Sertoli cells of neonatal 5-day-old mice. **B)** Mass spectra and reconstructed ion images (insets) from imaging MS showing absence of SGG (*m/z* 795) in Sertoli cells (top panel) and spermatogonia cells (middle panel) isolated from 5-day-old mice, but its presence in testicular germ cells of 20-day-old mice (bottom panel). **C)** *Panel a*: Mass spectra from precursor ion scanning of m/z 97 (sulfate group) showing the presence of SGG (*m/z* 795) as the major sulfolipid in Sertoli cells isolated from 20-day-old (top) and 10-week-old (bottom) mice. *Panel b*: Table showing the amounts of SGG in Sertoli cells of 20-day-old and 10-week-old mice quantified by ESI-MS/MS-MRM analysis; the analysis was performed using one set of isolated Sertoli cell sample from each animal age and the data shown were the mean ± S.D. of SGG amounts obtained from triplicate MS analyses of the same sample.

3.2.3.3) SGG levels in testes, sperm and testicular germ cells of 5-month-old and 8-month-old *Arsa* knockout and age-matched wild type mice

We hypothesized that a lack of ARSA may lead to SGG accumulation in the testis and sperm of *Arsa* KO mice, and the buildup of SGG over time likely results in the reduced fecundity observed in the old *Arsa* KO mice. To verify this hypothesis, lipid extracts were prepared from testis homogenates and swim-up sperm and used for SGG quantification by ESI-MS/MS-MRM. As expected, SGG levels in the testes of the KO mice at both 5 months and 8 months of age were significantly higher than the corresponding WT values (i.e., 1.139 ± 0.392 versus 0.717 ± 0.160 nmole/mg of testis weight of 5-month-old mice; 0.934 ± 0.194 versus 0.645 ± 0.032 nmole/mg of testis weight of 8-month-old animals) (Figure 3.17A). Unexpectedly, SGG levels of swim-up sperm showed no significant difference in *Arsa* KO and WT males at 5 months of age (0.219 ± 0.026 and 0.200 ± 0.026 nmole/million sperm, respectively). The sperm SGG levels in the 8-month-old *Arsa* KO animals were even markedly lower than those in the age-matched WT males (i.e., 0.170 ± 0.031 and 0.092 ± 0.048 nmole/million sperm of WT and KO males, respectively) (Figure 3.17B).

SGG levels in the testicular germ cells of *Arsa* KO mice at both 5 and 8 months of age were also compared with those of WT mice by flow cytometry following indirect immunofluorescence with the anti-SGG antibody. In this experiment, the use of flow cytometry for SGG analysis in place of MS allowed us to obtain comparative SGG levels in each type of germ cell without the need for isolation of pure germ cell populations, which would have required a large number of mice. Following quantitative DNA staining, different types of testicular germ cells in the mixed populations (including primary spermatocytes, round spermatids, highly condensed elongated spermatids, and spermatogonia) could be

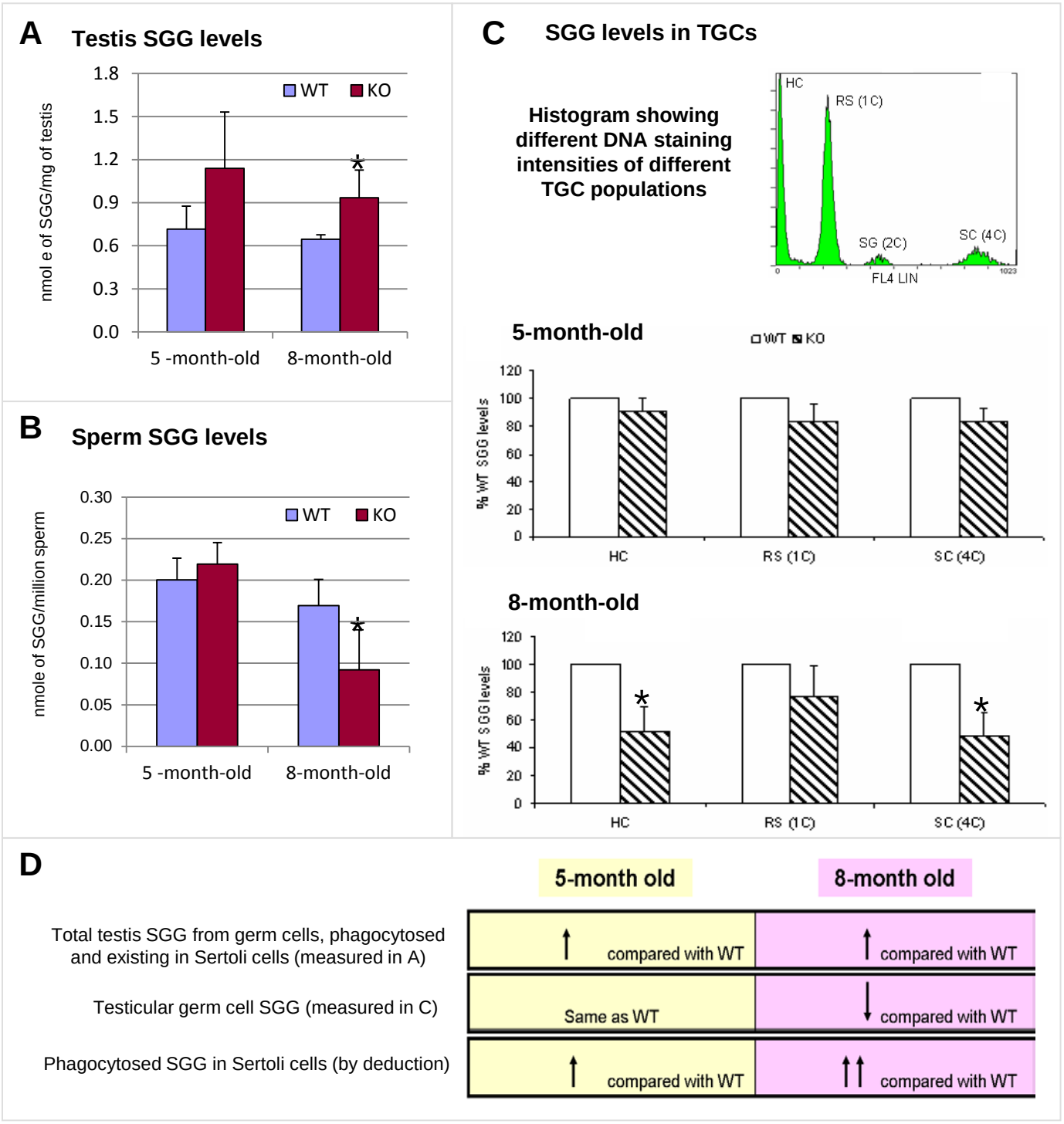

Figure 3.17: SGG levels in whole testes, sperm and testicular germ cells (TGCs) from WT and *Arsa* KO mice at 5 months and 8 months of age. SGG quantification by ESI-MS/MS-MRM was performed to determine SGG levels in lipids extracted from whole testes **(A)** and sperm prepared by swim-up technique **(B)** of 5-month-old and 8-month-old WT and *Arsa* KO mice. Data are expressed as absolute SGG amounts per one milligram testis weight or one million sperm. **C)** SGG levels in various TGC types of *Arsa* KO mice, expressed as percentages of corresponding WT values as determined by immunofluorescence and flow cytometry. Histogram from flow cytometric analysis revealed that different TGC populations could be detected as separated peaks based on differential amounts and/or compactness of their DNA. Namely, primary spermatocytes (SC, mainly pachytene spermatocytes, 4X DNA content (4C)), spermatogonia + Sertoli cells (SG + S, 2X DNA content (2C)), round spermatids (RS, 1X DNA amount (1C)) and highly condensed elongated spermatids (HC, 1X compact DNA) could be detected and further assessed for SGG staining intensities. Three WT and three *Arsa* KO mice of both ages were used in A, B, and C, and all data are expressed as mean ± S.D. of the values. Asterisk indicates significant difference between WT and KO samples ($P < 0.05$). **D)** Deduction of results in A, B and C suggests that SGG accumulation occurs in Sertoli cells of *Arsa* KO mice.

differentiated from each other in flow cytometry (see the histogram in Figure 3.17C). When each germ cell population was analyzed for anti-SGG reactivity and by setting the SGG staining intensity of WT germ cells to 100%, the staining intensities of germ cells in 5-month-old *Arsa* KO mice were as follows: 84 ± 8% for primary spermatocytes, 84 ± 12% for round spermatids, and 91 ± 11% for elongated spermatids; all results showing no significant difference from the corresponding WT values (Figure 3.17C). In contrast, the SGG intensities on the primary spermatocytes, and elongated spermatids of 8-month-old *Arsa* KO mice were significantly decreased to 49 ± 16% and 52 ± 17% of the age-matched WT values, respectively (Figure 3.17C). The SGG intensity on the round spermatids of 8-month-old *Arsa* KO mice was also reduced to 77 ± 21% of the WT value, but the difference between KO and WT samples was not statistically significant (Figure 3.17C). Round spermatids have a number of developmental steps (steps 1-8 in mouse), and these cells may contain various amounts of SGG. Although decreases in SGG levels may indeed occur in various round spermatid steps in *Arsa* KO males relative to the corresponding WT round spermatids, the inability to separate the different spermatid steps may make the differences statistically insignificant.

The results so far have revealed that SGG levels in the whole testis homogenate, which contained both the Sertoli cells and testicular germ cells of *Arsa* KO mice, were increased but SGG levels in the testicular germ cells of *Arsa* KO mice were either unchanged or decreased as compared with the corresponding WT values. By deduction, accumulation of SGG would be in the Sertoli cells of *Arsa* KO mice (Figure 3.17D). Ideally, Sertoli cells purely isolated from *Arsa* KO and WT mice should be used for SGG quantification by the ESI-MS/MS-MRM approach. Unfortunately, at the time that we performed this work, we

were faced with two problems. First, we did not have enough *Arsa* KO mice (at ≥ 8 months of age) from which we could isolate Sertoli cells for primary culturing. Second, our method of isolating Sertoli cells from adult animals at that time was far from efficient. Only 0.09 million cells could be obtained from 10 mice and quite often they were contaminated (25% or more) with testicular germ cells. Therefore, we took an alternative indirect immunofluorescence approach to compare SGG levels in the Sertoli cells of *Arsa* KO and WT animals. Sertoli cells co-isolated with testicular germ cells were prepared by Dr. Suraj Kadunganattil (a former postdoctoral fellow in Dr. Tanphaichitr's lab) and placed on a chamber slide. The isolated Sertoli cells were gently treated with 0.1% Triton X-100 in order to remove any residual SGG from the plasma membrane of germ cells that attached to the Sertoli cell surface and to permeabilize the cells for the access of the anti-SGG antibody to react with intracellular SGG. SGG staining was at a much higher intensity and in larger clumps in 8-month-old *Arsa* KO Sertoli cells as compared with the staining in the WT Sertoli cells, a result strongly suggesting that SGG was accumulated in Sertoli cells (Figure 3.18).

We also performed transmission electron microscopy of testis thin sections from *Arsa* KO and WT mice. Our results revealed details of abnormality in the Sertoli cells of 8-month-old *Arsa* KO mice. In normal Sertoli cells from WT animals of the same age, the lysosomes were small, dense structures and not very numerous (Figure 3.19A, panel a), whereas in the *Arsa* KO mice, some Sertoli cells had numerous lysosomes with irregular shapes and a heterogeneous content (Figure 3.19A, panel b). In other seminiferous tubules, lipid droplets were also apparent in *Arsa* KO Sertoli cells and were especially abundant at Stages I-VII of the cycle (Figure 3.19A, panel c); such droplets were not found at these stages of the cycle in WT Sertoli cells. The number of large-sized lipid droplets (with

diameter of ≥3 μm) detected in these *Arsa* KO mice was about 40% of the lipid droplet population; this number was higher than that previously found in the WT mice (17% of the whole lipid droplet population) (Wang et al., 2006). In some tubules of *Arsa* KO mice, a number of very large lysosomes appeared in the Sertoli cells (Figure 3.19A, panel d). All these appearances in the *Arsa* KO Sertoli cells were typical of a lysosomal storage disorder (Schulze et al., 2009; Xu et al., 2011), likely contributing to Sertoli cell dysfunction. In normal testes, Sertoli cells provide spatial support and cyto-organization to developing testicular germ cells, localizing more advanced germ cells closer to the tubal lumen and positioning the heads of elongated spermatids vertical to the basement membrane (Griswold and McLean, 2006). In the tubules of 8-month-old *Arsa* KO mice, several elongated spermatid heads were disoriented, lying horizontal to the basement membrane (Figure 3.19B, top panel). Apoptotic germ cells were also frequently present in the *Arsa* KO tubules (Figure 3.19B, bottom panel), while they were not abundant in the WT testes. These results suggested that the ability to support germ cells as well as the phagocytic function of Sertoli cells to "clear up" apoptotic germ cells were likely impaired in 8-month-old *Arsa* KO mice. All electron microscopy work was performed in collaboration with Dr. Louis Hermo at McGill University.

Results from indirect immunofluorescence of SGG in the Sertoli cells of aging *Arsa* KO mice suggested that ARSA was involved in the SGG degradation process. In other words, SGG was a natural substrate of ARSA *in vivo*. While our finding could be a significant contribution to the field of sulfoglycolipid metabolism, the results still need to be confirmed by another experimental approach that allows specific and quantitative detection of SGG within Sertoli cells. ESI-MS/MS-MRM would be an ideal method for this

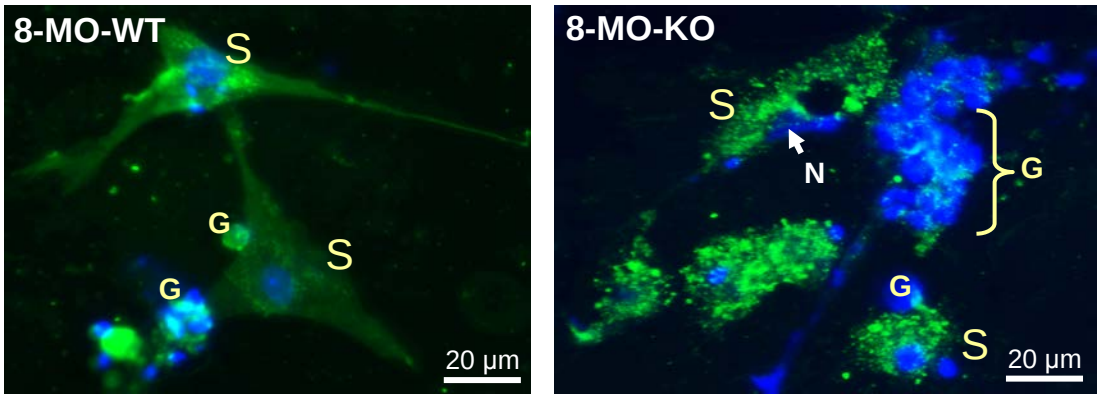

Figure 3.18: SGG is highly accumulated in Sertoli cells of 8-month-old *Arsa* KO mice. Sertoli cells (S) were isolated from decapsulated testes of 8-month-old WT and KO mice by sequential enzyme treatments and plated onto chamber slides. After two days of culturing in DMEM/F-12 with 7.5% FBS, the attached cells were further cultured in the same medium without FBS, and subjected to two hypotonic treatments during this period to remove as many germ cells as possible. At the end of Day 5 in culture, attached Sertoli cells and co-isolated germ cells (G) were washed in PBS and fixed with 4% paraformaldehyde (15 min, room temperature) followed by treatment with 0.1% Triton X-100 (10 min, RT). The fixed cells were then incubated with anti-SGG/SGC antibody followed by Alexa 488-labeled secondary antibody. While SGG on the plasma membrane of co-isolated germ cells was mostly extracted, intracellular SGG staining was observed in Sertoli cells of both WT and KO mice. However, the SGG staining was more intense, with clumping patterns in the KO mice. Note that the nucleus (N) of *Arsa* KO Sertoli cells was often positioned at a wrong site (white arrow).

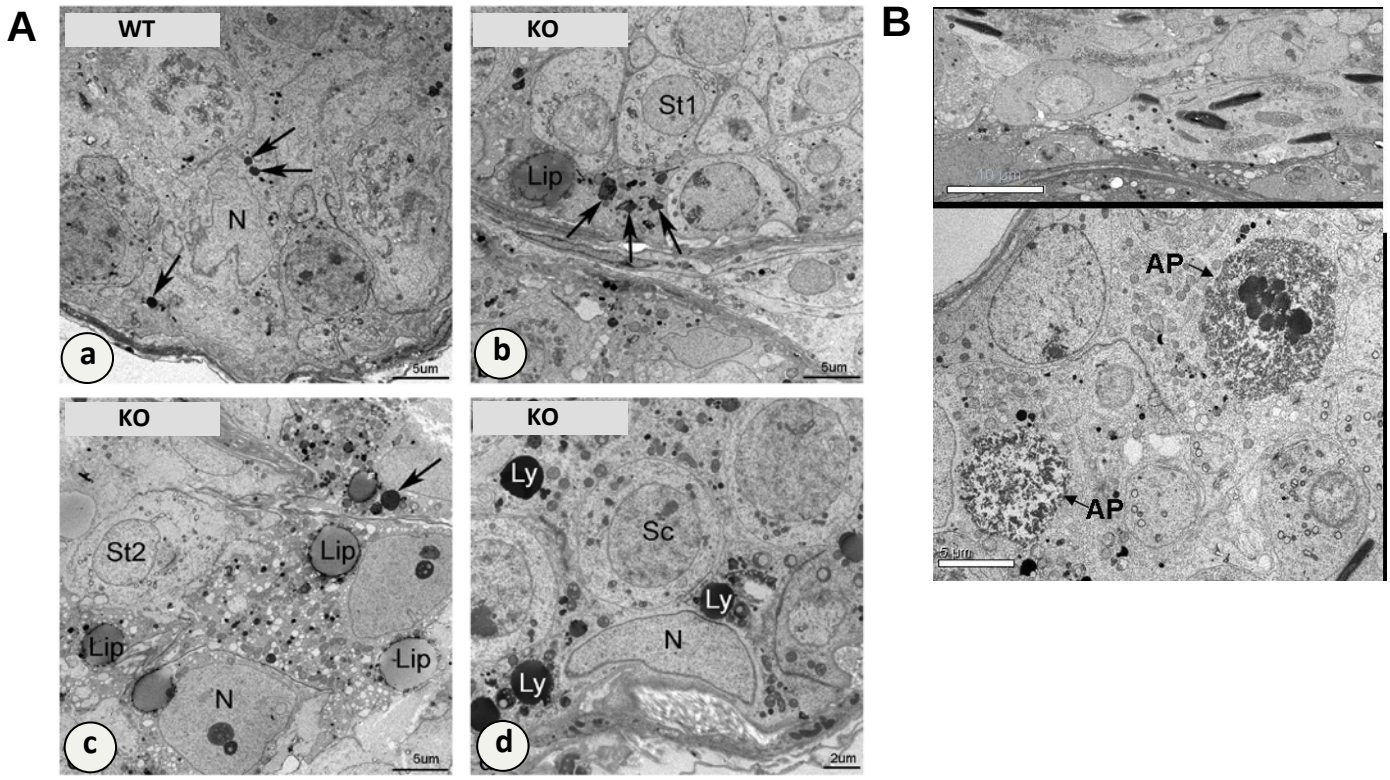

Figure 3.19: A) Electron microscopy of testis sections of 8-month-old WT and *Arsa* KO mice. Note that in WT mice (a), lysosomes of Sertoli cells (arrows) were small dense structures and were not that numerous, whereas in KO mice (b), some Sertoli cells had numerous lysosomes (arrows) that were irregular in shape and contained a heterogeneous content, a situation typical of lysosomal storage disorders (LSD). In other tubules (c), lipid droplets (Lip) were also apparent in KO Sertoli cells, and were especially abundant at stages I-VII of the cycle; such droplets were not found in WT Sertoli cells. In some tubules (d), lysosomes (Ly) of KO mice were very large, more or less spherical and numerous. In (b) and (c), round spermatids were present (St1 and St2). In (c), the nucleus (N) of Sertoli cells of *Arsa* KO mice was displaced in its position within the seminiferous epithelium. Sc = primary spermatocyte. **B)** *Upper panel:* The heads of several deeply stained elongated spermatids were disoriented in *Arsa* KO seminiferous tubules. Instead of being vertical to the basement membrane of Sertoli cells as in the wild type mice, they lay horizontal to this membrane. *Lower panel*: Note the presence of apoptotic germ cells (AP) in the seminiferous tubules which revealed a pyknotic nuclear morphology.

validation, provided that a relatively pure population of Sertoli cells from *Arsa* KO and WT mice can be isolated from their seminiferous tubules. The method previously used in the isolation of Sertoli cells for indirect immunofluorescence experiments was based on the published protocol of Dr. CY Cheng's group, which involves 4 steps of enzyme digestion as well as hypotonic treatment, and has been shown to provide >90% purity for 20-day-old Sertoli cells (Li et al., 2001). However, when this method was applied for isolation of adult mouse Sertoli cells, it failed to provide the same purity as that of 20-day-old Sertoli cells. Therefore, I assisted Dr. Arpornrad Sae Wu, a postdoctoral fellow in Dr. Tanphaichitr's lab, in establishing a new method for preparing a pure population of Sertoli cells from adult mice by reducing the enzyme digestion steps and omitting the hypotonic treatment (see details in Materials and Methods). With these modifications, we have improved the yield of Sertoli cells isolated from 8- to11-month-old mice from 0.009 ± 0.004 to be 0.189 ± 0.110 million cells/mouse, as well as the purity of Sertoli cells to 90-95% (Figure 3.20A). The numbers of Sertoli cells isolated from 8- to 11-month-old *Arsa* KO mice and age-matched WT mice were 0.096 ± 0.037 and 0.179 ± 0.069 million cells/mouse, respectively (Figure 3.20B). The Sertoli cell number isolated from *Arsa* KO mice was significantly lower than that of the WT mice. It is possible that accumulated abnormalities in the aging *Arsa* KO mice lead to dysfunction and a reduced ability of Sertoli cells to survive *in vivo* and/or *in vitro* during the isolation/culture process.

3.2.3.4) Analyses of SGG and other sulfolipids in Sertoli cells of *Arsa* knockout mice.

Our newly established method of purifying Sertoli cells from adult animals allowed me to validate SGG accumulation in Sertoli cells by ESI-MS/MS. In this procedure, precursor ion scanning for m/z 97 (sulfate) was initially used to screen for the SGG ion

A

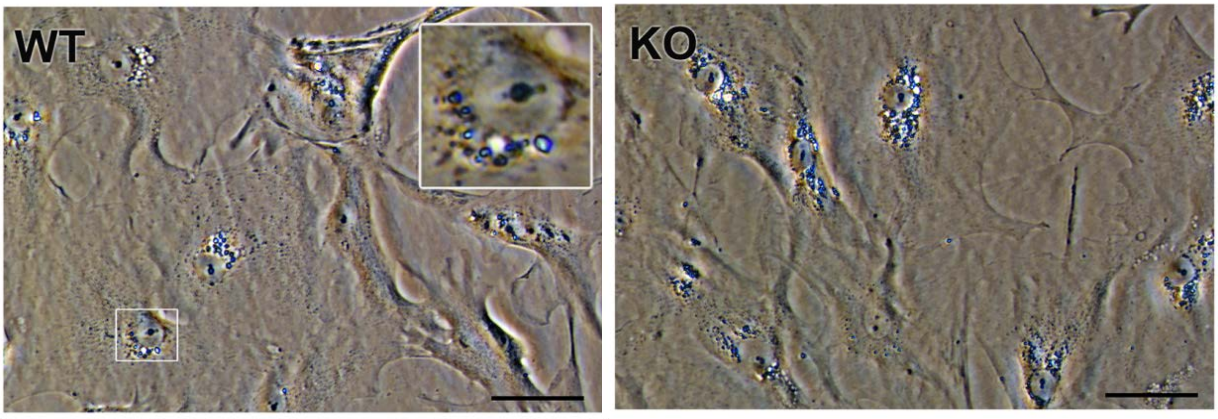

B

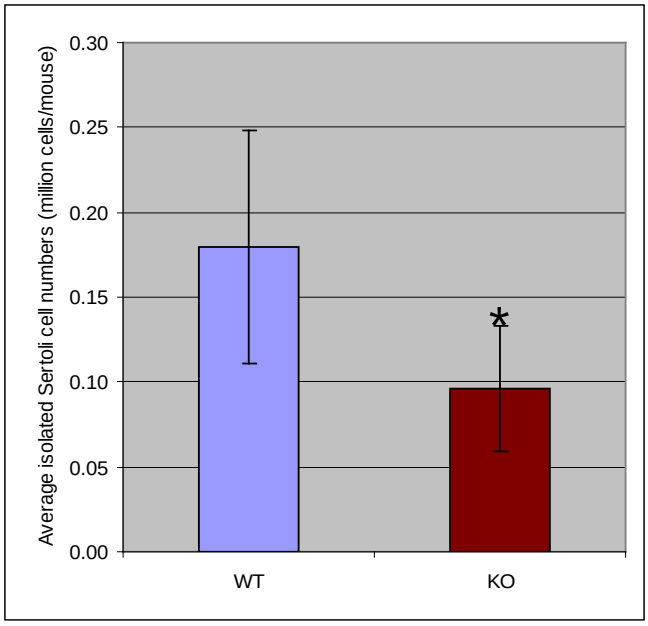

Sample (No. of mice used)	Number of Sertoli cells (million) obtained per mouse
WT (n=16)	0.18 ± 0.07
KO (n=29)	0.10 ± 0.04

Figure 3.20: Morphology and numbers of primary cultured Sertoli cells isolated from 8- to 11-month-old *Arsa* KO and age-matched WT mice. **A)** Phase contrast images showing morphology and purity of the WT and KO Sertoli cells on the last day (Day 7) of culture. The cultured cells had multiple long processes and tripartite nucleolus (inset), which are characteristics of Sertoli cells, and they were free from any attached round germ cells. Bar = 20 µm. **B)** Plots showing average numbers of Sertoli cells obtained from individual WT and KO mice. Asterisk indicates a significant difference ($P< 0.05$) between WT and KO samples. Data are expressed as mean ± S.D. of Sertoli cell numbers obtained from four isolations performed on different days. The total number of mice (n) used for four Sertoli cell isolations are shown in the table. Testes from four WT mice were used for each experiment. However, since the KO mouse testis size was ~50% of that of the WT animal, testes from 4-10 KO mice were used for each preparation of Sertoli cells. These isolated Sertoli cells were used for lipid analyses.

peaks. This scanning revealed that the SGG molecular species (C16:0/C16:0) with m/z 795 was the most abundant sulfolipid in the *Arsa* KO and WT Sertoli cell samples from 8- to 11-month-old animals (Figure 3.21A). Other sulfolipids with m/z 768, 778, 822, 823, 843 were also detected in the Sertoli cell samples, but their relative signal intensities were much lower than that of the m/z 795 (Figure 3.21B). Interestingly, lipids with m/z 778, 823 and 843 were present selectively in the KO Sertoli cells (Figure 3.21B). Based on the previous MS analyses of sulfolipids predominantly found in mouse testes (Goto-Inoue et al., 2009), the lipids with m/z 768, 822, 823, and 843 were likely representing SGG molecular species with C16:0/C14:0, C18:1/C16:0, C18:0/C16:0 and C20:4/C16:0, respectively (Figure 3.22A). However, a sulfolipid with m/z 778 was previously identified by our ESI-MS/MS analysis to be SGC with C16:0 (aka palmitoylsulfatide) (Xu et al., 2011) (Figure 3.22A). Quantitative MRM analyses of these identified sulfolipids further revealed that the levels of SGG molecular species with C16:0/C16:0, C20:4/C16:0, C18:0/C16:0, C18:1/C16:0 and SGC with C16:0 were significantly increased in *Arsa* KO Sertoli cells (Figure 3.22B). By comparing peak areas with a standard curve of different concentrations of deuterated SGG standard (m/z 798), SGG (C16:0/C16:0) levels in the Sertoli cells of *Arsa* KO and WT mice were determined to be 4.400 ± 1.765 and 1.791 ± 0.728 nmole/million cells, respectively (Figure 3.23). These results directly indicated that a lack of ARSA led to the accumulation of C16:0/C16:0 SGG and other SGG molecular species, as well as to a new appearance of C16:0 SGC in the Sertoli cells of 8-month-old *Arsa* KO mice. These results validated that SGG was a substrate of ARSA *in vivo*.

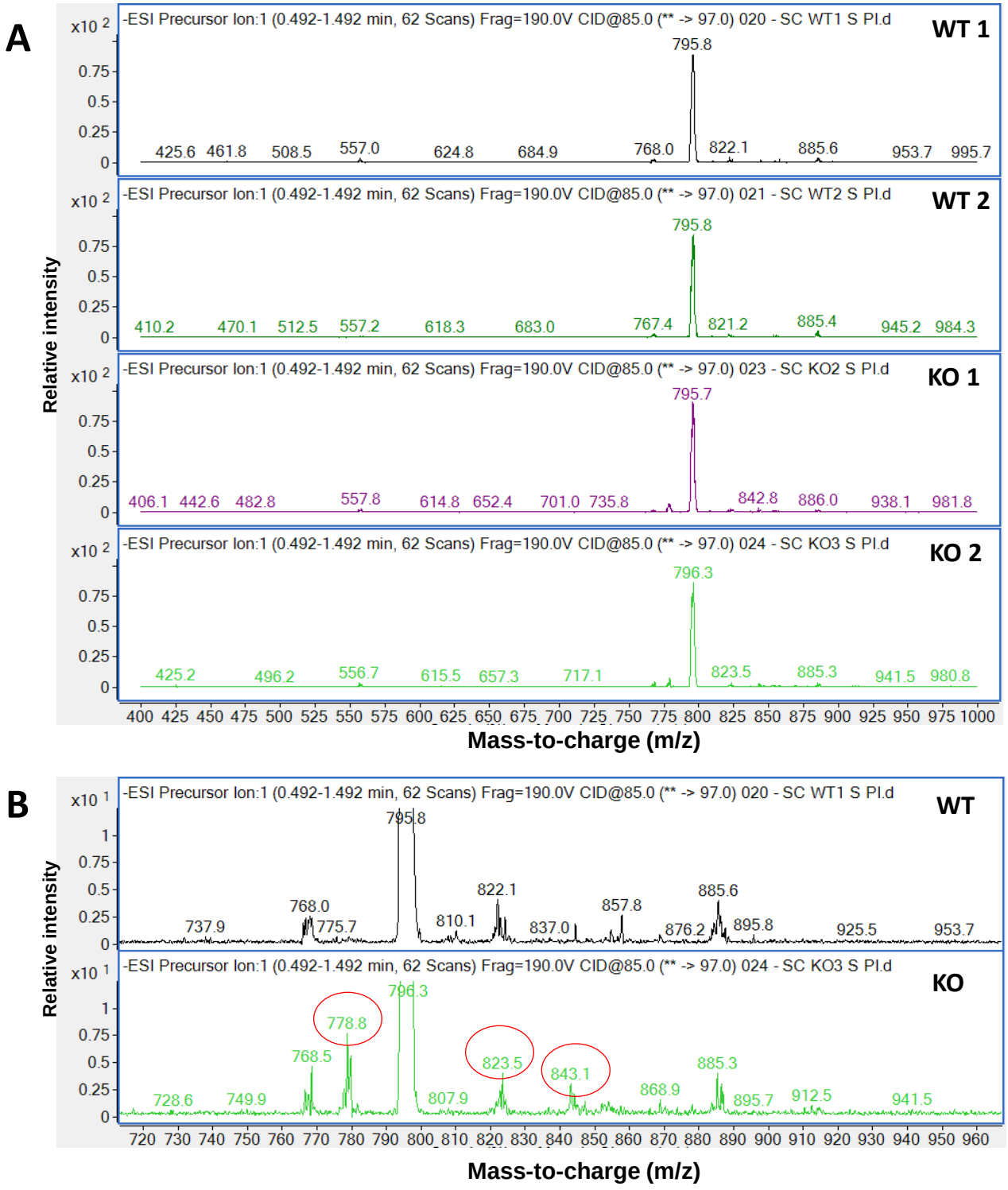

Figure 3.21: Precursor ion scanning of m/z 97 showing major sulfolipids in Sertoli cells of 8- to 11-month-old WT and *Arsa* KO mice. A) Representative mass spectra from two out of four sets of WT and KO samples were shown. Note that SGG (C16:0/C16:0) with m/z 795 was the most abundant sulfolipid in WT and KO Sertoli cell samples. **B)** Magnified view of the mass spectra in the range of m/z 720-960 showing selective presence of sulfolipids with m/z 778, 823, 843 (red circles) in the KO sample; these lipids were identified as SGC (C16:0) and SGG molecular species with C18:0/C16:0 and C20:4/C16:0, respectively.

A

#	Lipid classes	m/z	Ion	Possible identities	Formula of lipid ion
1	Sulfolipid	843.5	$[M-H]^-$	SGG C20:4/C16:0	$C_{45}H_{79}O_{12}S$
2	Sulfolipid	823.5	$[M-H]^-$	SGG C18:0/C16:0	$C_{43}H_{83}O_{12}S$
3	Sulfolipid	821.5	$[M-H]^-$	SGG C18:1/C16:0	$C_{43}H_{81}O_{12}S$
4	Sulfolipid	809.5	$[M-H]^-$	SGG C17:0/C16:0	$C_{42}H_{81}O_{12}S$
5	Sulfolipid	795.5	$[M-H]^-$	SGG C16:0/C16:0	$C_{41}H_{79}O_{12}S$
6	Sulfolipid	767.5	$[M-H]^-$	SGG C16:0/C14:0	$C_{39}H_{75}O_{12}S$
7	Sulfolipid	778.5	$[M-H]^-$	SGC C16:0	$C_{40}H_{76}NO_{11}S$
8	Sulfolipid	465.3	$[M-H]^-$	Cholesterol-3-sulfate	$C_{27}H_{45}O_4S$

B

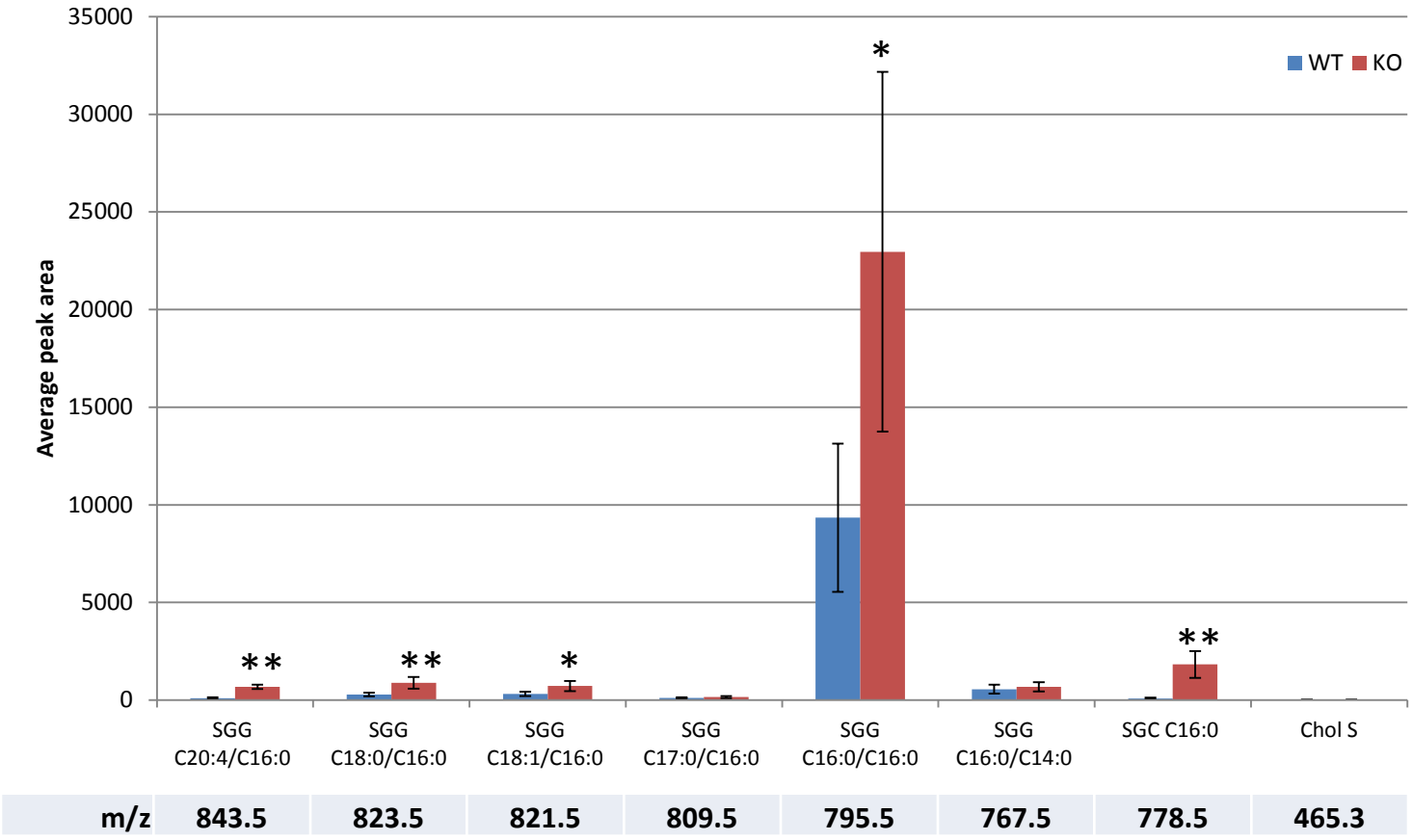

Figure 3.22: Quantitative ESI-MS/MS-MRM analyses of major sulfolipids present in the Sertoli cells of WT and *Arsa* KO mice. A) Table showing a list of major sulfolipids identified and selected for quantitative analysis. **B)** Relative abundance of selected sulfolipids was assessed based on peak area of ion signals. Data are expressed as mean ± S.D. from four sets of the isolated Sertoli cell samples. Asterisks indicate significance differences (* $P<0.05$; ** $P<0.005$) between WT and KO samples.

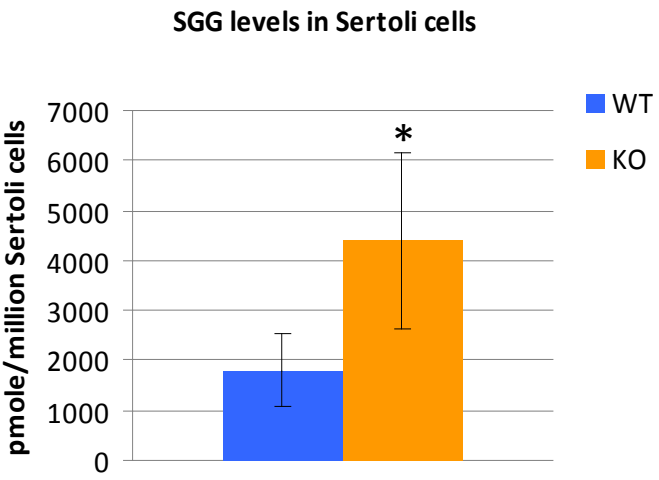

nmole of SGG/million Sertoli cells	
WT	1.79 ± 0.73
KO	4.40 ± 1.76

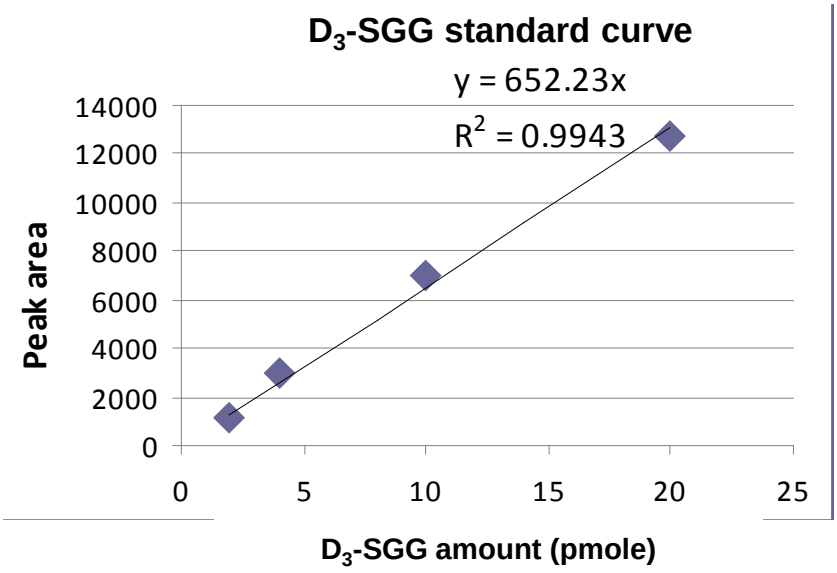

Figure 3.23: Absolute amounts of SGG (C16:/C16:0) in the Sertoli cells of 8- to 11-month-old WT and *Arsa* KO mice. A standard curve of deuterated SGG (D3-SGG) was built and used for the absolute SGG amount calculation. Data are expressed as mean ± S.D. from 4 sets of the isolated Sertoli cell samples. Asterisk indicates a significant difference (* $P<0.05$) between WT and KO samples.

3.2.4) Profiles of other lipids in Sertoli cells of 8- to 11-month-old *Arsa* knockout mice

Since SGG is known to associate with cholesterol and saturated phospholipids/sphingolipids (Attar et al., 2000) and they co-existed in lipid raft membranes (Bou Khalil et al., 2006), the aberrant level of SGG may affect levels of its associated lipids in the Sertoli cells of 8- to 11-month-old *Arsa* KO mice. Moreover, the presence of large lipid droplets in the Sertoli cells of 8-month-old *Arsa* KO mice (Figure 3.19) suggested that neutral lipids, such as triacylglycerols (TAGs) and cholesteryl esters (CEs), known as lipid droplet components, may be increased in the *Arsa* KO mice. For these reasons, the profiles of phosphatidylcholines (PCs), phosphatidylethanolamines (PEs), sphingomyelins (SMs), triacylglycerols (TAGs) and cholesteryl esters (CEs) were determined by ESI-MS/MS analyses with different scan modalities specific for each type of lipid (see Materials and Methods). As well, cholesterol levels were biochemically determined by the Amplex Red assay.

Both PCs and SMs contain a choline head group (m/z 184). The precursor ion scanning of m/z 184 revealed that Sertoli cells of *Arsa* KO and WT mice contained similar PC and SM molecular species, including PCs with m/z, 676, 704, 734, 836 and SM with m/z 703, 761, 783, 811 (Figure 3.24). The candidate PC and SM molecular species were assigned based on lipid database and literature searches (Figure 3.25A) and selected for further quantitative MRM analyses. The relative amounts of all major PC and SM molecular species selected for quantification appeared to be lower in the *Arsa* KO Sertoli cell samples, as compared with the WT values. However, statistical analyses showed no significant differences in the levels of major PC/SM molecular species between the WT and KO samples and this lack of statistical difference was likely due to the high variation of

major PC/SM levels in different animals (Figures 3.25B&C). The precursor ion scanning of m/z 184 also revealed a lipid with m/z 496, which was identified based on the database searching to be a lysoPC with C16:0. By HPTLC analysis, a lipid band corresponding to the lysoPC standard cannot be detected in the total lipid extracts from mouse testes and sperm (Appendix Figure 2), suggesting the low abundance of lysoPC in these biological samples, although they could be detected by a more sensitive method – ESI-MS/MS (Figure 3.24 and Figure 3.35). These MS/MS quantitative analyses revealed that the levels of lysoPC with C16:0 in *Arsa* KO Sertoli cells were lower than those in the corresponding WT samples (Figure 3.25B).

Neutral loss scanning of m/z 141 (ethanolamine group) was used to obtain the PE profile. My results revealed the presence of different PE molecular species with m/z 718, 740, 744, 766, 768, 792 in both the WT and *Arsa* KO Sertoli cell samples (Figure 3.26). Identification of the candidate PE molecular species was determined as described for PC/SM (Figure 3.27A). The MRM analysis results showed that the relative amounts of major PE molecular species found in *Arsa* KO Sertoli cells were slightly higher but not significantly different from those of the WT samples (Figure 3.27B).

CE was detected by precursor ion scanning of m/z 369.4 (cholesterol without the hydroxyl group). This procedure revealed that Sertoli cells of *Arsa* KO and WT mice contained CE with m/z of 643, 669, 691, 715 (Figure 3.28) and these lipids were further identified as CE containing C16:0, C18;1, C20:4, and C22:6, respectively (Figure 3.29A). The relative amounts of these CEs seemed to be higher in the KO samples, although not significantly different from those in the WT Sertoli cells (Figure 3.29B).

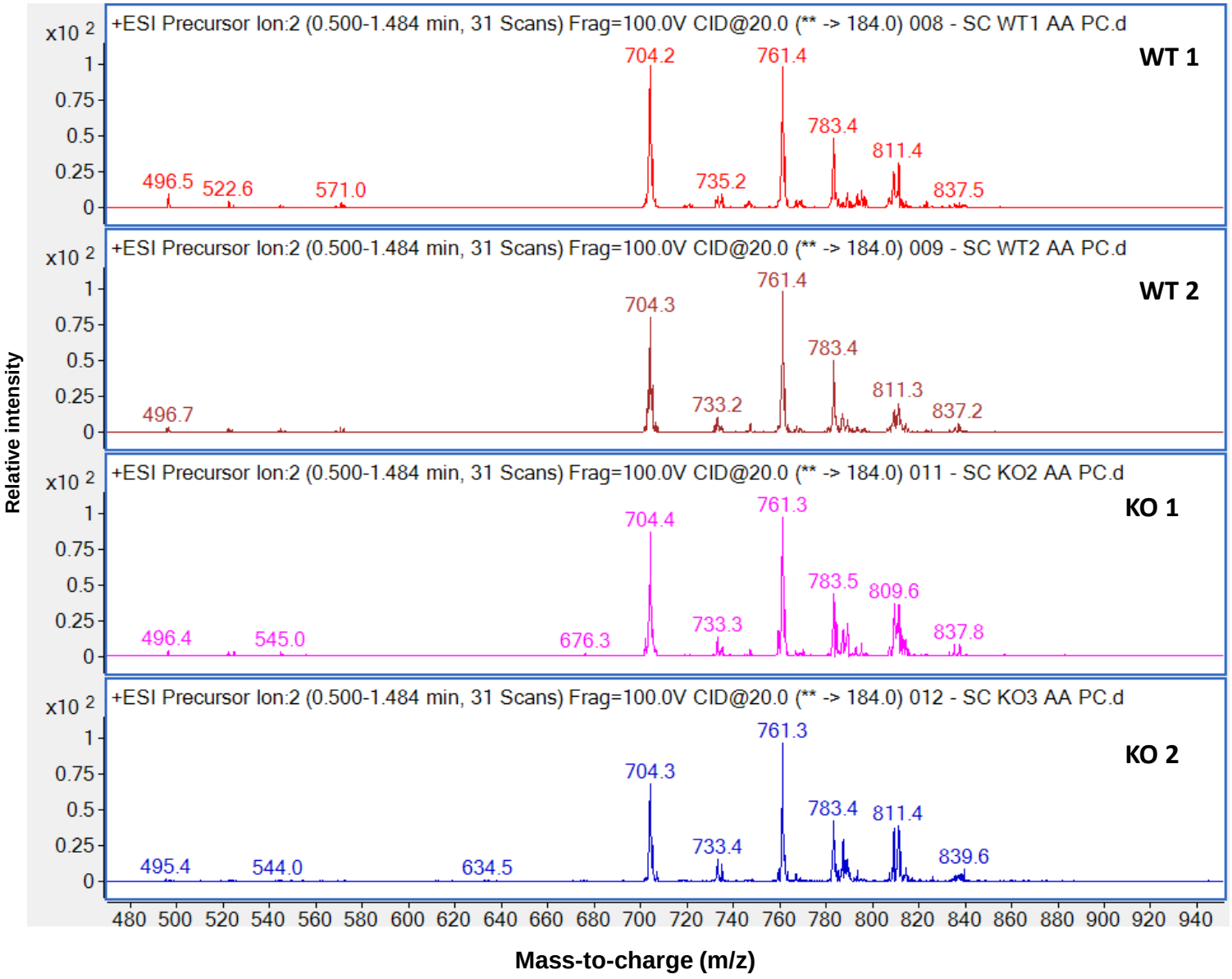

Figure 3.24: Mass spectra from precursor ion scanning of m/z 184 (choline ion) showing molecular species of phosphatidylcholines and sphingomyelins present in the Sertoli cells of WT and *Arsa* KO mice (8-11 months of age). Representative spectra from two out of four sets of the isolated WT and KO Sertoli cell samples were shown.

A

#	Lipid classes	m/z	Ion	Possible identities	Formula of lipid ion
1	PC	676.4	$[M+H]^+$	28:1 PC	$C_{36}H_{70}NO_8P + H$
2	PC	704.5	$[M+H]^+$	30:1 PC	$C_{38}H_{74}NO_8P + H$
3	PC	734.5	$[M+H]^+$	32:0 PC	$C_{40}H_{80}NO_8P + H$
4	PC	836.5	$[M+H]^+$	40:5 PC	$C_{46}H_{78}NO_{10}P + H$
5	LysoPC	496.3	$[M+H]^+$	LysoPC (16:0)	$C_{24}H_{50}NO_7P + H$
6	SM	675.5	$[M+H]^+$	32:1 SM	$C_{37}H_{75}N_2O_6P + H$
7	SM	703.5	$[M+H]^+$	34:1 SM	$C_{39}H_{79}N_2O_6P + H$
8	SM	761.6	$[M+H]^+$	38:0 SM	$C_{43}H_{89}N_2O_6P+H$
9	SM	783.6	$[M+H]^+$	40:3 SM	$C_{45}H_{87}N_2O_6P +H$
10	SM	811.6	$[M+H]^+$	42:3 SM	$C_{47}H_{91}N_2O_6P +H$

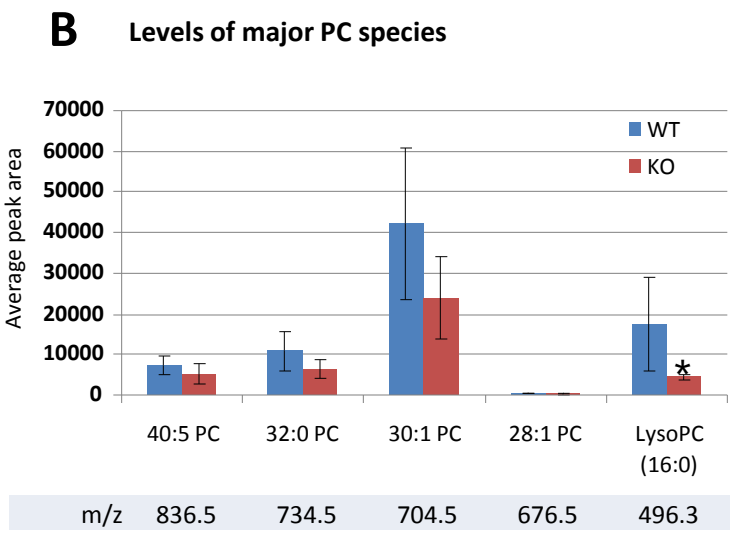

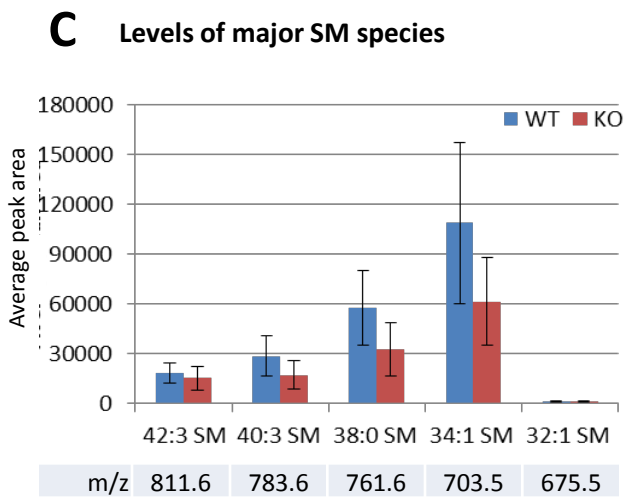

Figure 3.25: Quantitative ESI-MS/MS-MRM analyses of major phosphatidylcholine and sphingomyelin molecular species present in Sertoli cells of 8- to 11-month-old WT and *Arsa* KO mice. A) List of major phosphatidylcholine (PC) and sphingomyelin (SM) candidates identified and selected for quantitative analyses. **B)** Plots showing average peak areas of signals of major PC molecular species. **C)** Plots showing average peak areas of major SM species. Data are expressed as mean ± S.D. from 4 sets of the isolated Sertoli cell samples. An asterisk indicates statistical difference ($P < 0.05$) between KO and WT samples.

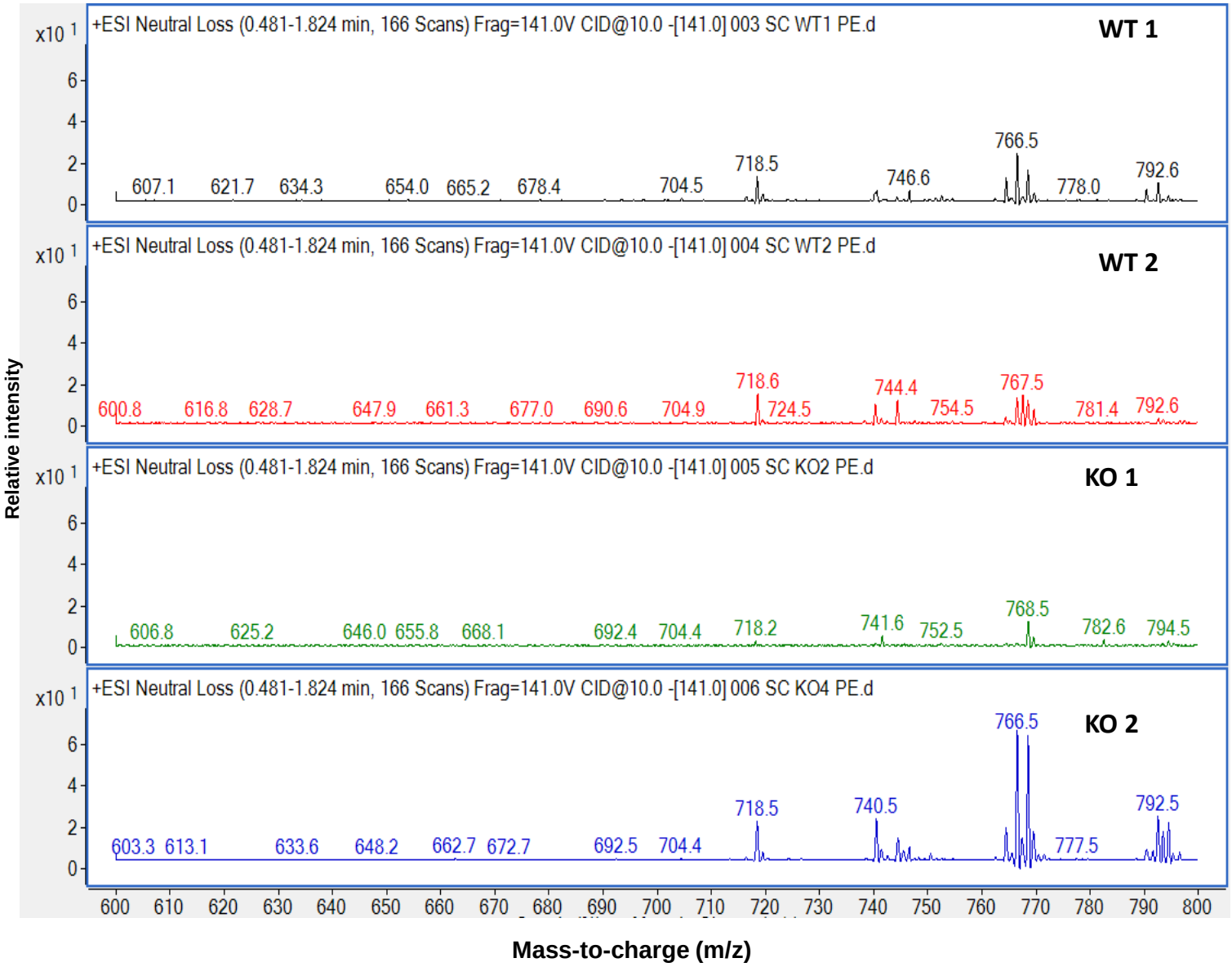

Figure 3.26: Neutral loss scanning of 141 (ethanolamine group) showing major molecular species of phosphatidylethanolamines (PE) in the Sertoli cells of 8- to 11-month-old WT and *Arsa* KO mice. Representative spectra from two sets of the isolated Sertoli cells samples were shown.

A

#	Lipid classes	m/z	Ion	Possible identities	Formula of lipid ion
1	PE	718.5	$[M+H]^+$	34:1a PE	$C_{39}H_{76}NO_8P$ +H
2	PE	740.5	$[M+H]^+$	36:4a PE	$C_{41}H_{74}NO_8P$ +H
3	PE	744.5	$[M+H]^+$	36:2a PE	$C_{41}H_{78}NO_8P$ +H
4	PE	766.5	$[M+H]^+$	38:5a PE	$C_{43}H_{76}NO_8P$ +H
5	PE	768.5	$[M+H]^+$	38:4a PE	$C_{43}H_{78}NO_8P$ +H
6	PE	792.5	$[M+H]^+$	40:6a PE	$C_{45}H_{78}NO_8P$ +H

B

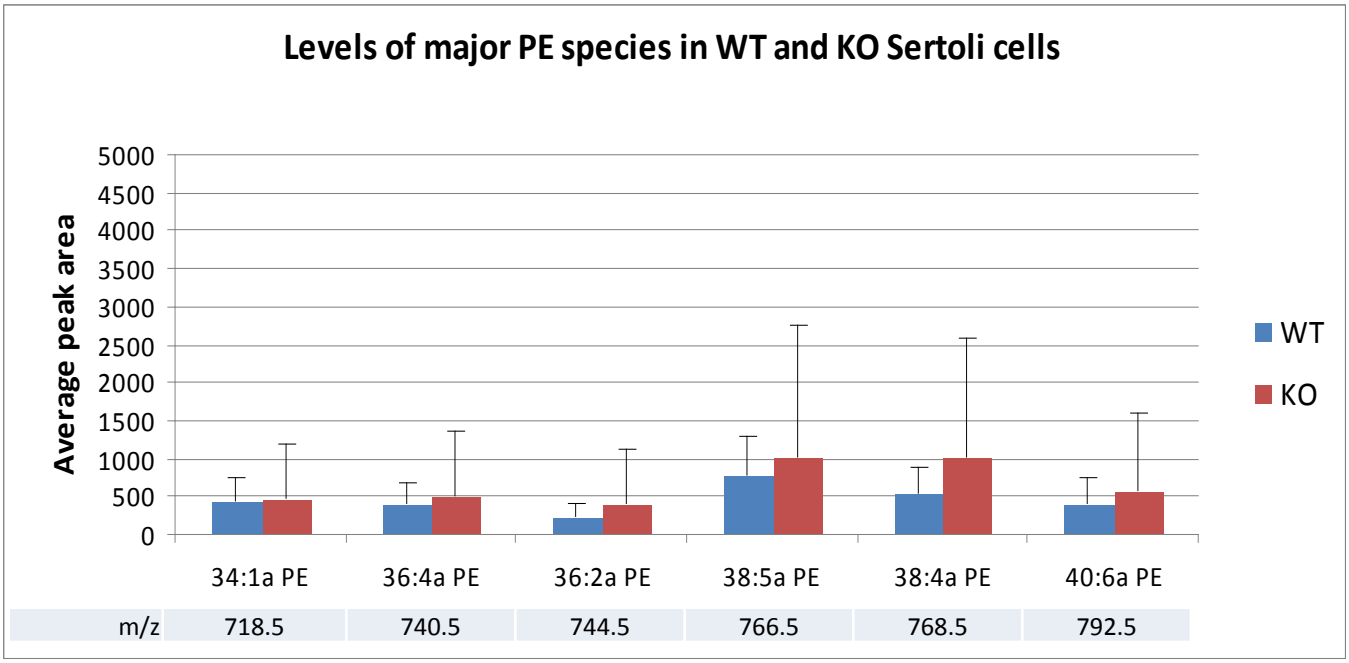

Figure 3.27: Quantitative ESI-MS/MS-MRM analyses of major PE molecular species present in Sertoli cells of WT and *Arsa* KO mice. A) Table showing list and details of major phosphatidylethanolamines (PE) selected for quantitative analysis. **B)** Relative abundance of major PE species (listed in A) was quantified based on the peak area of each m/z ion signal. Data are expressed as mean ± S.D. from 4 sets of samples.

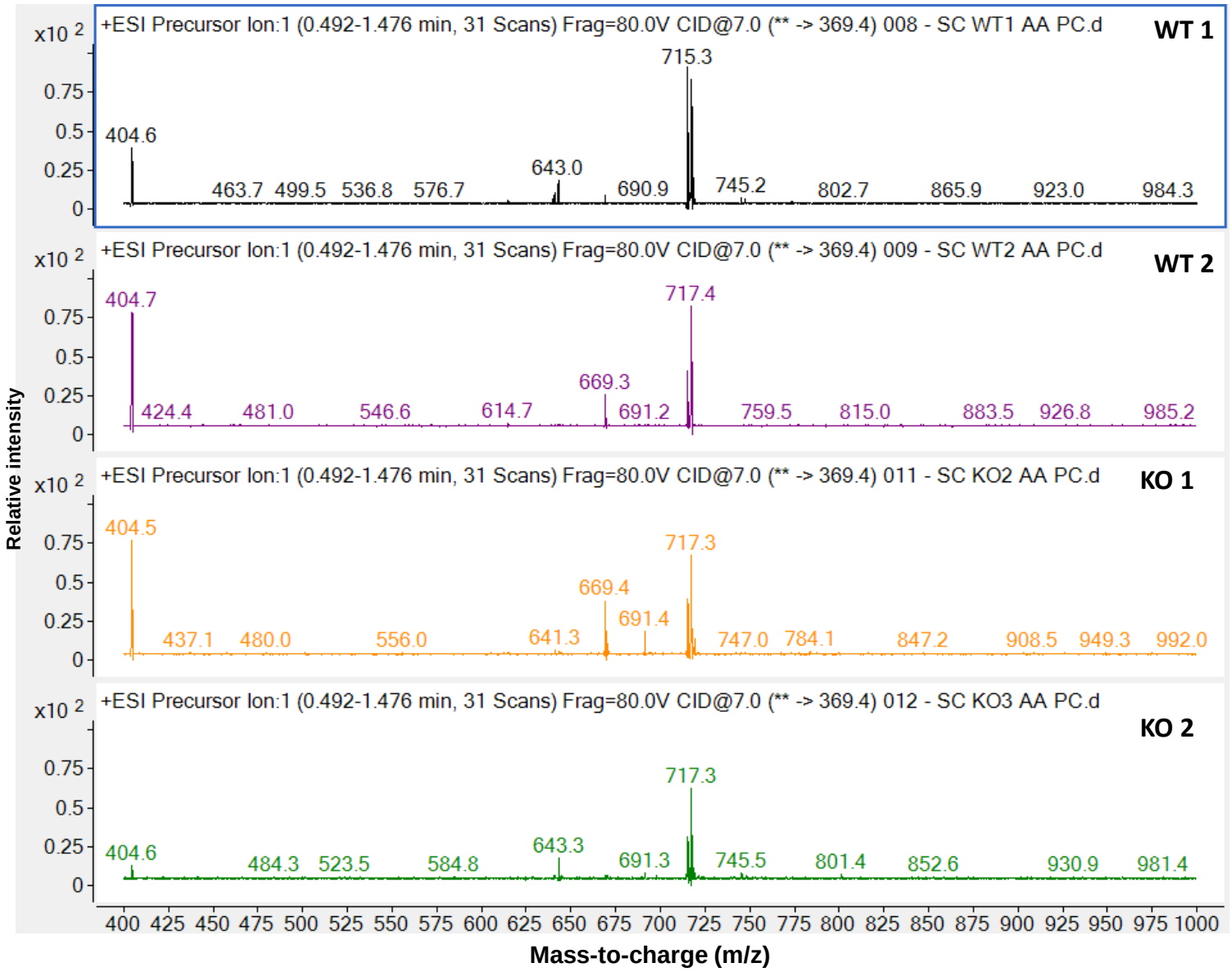

Figure 3.28: Precursor ion scanning of m/z 369.4 showing cholesteryl ester profiles of WT and *Arsa* KO Sertoli cells. Representative spectra from two sets of the isolated WT and KO Sertoli cell samples were shown.

A

#	Lipid classes	m/z	Ion	Possible identities	Formula of lipid ion
1	CE	643.6	$[M+NH_4]^+$	CE (16:0)	$C_{43}H_{76}O_2 + NH_4$
2	CE	669.6	$[M+NH_4]^+$	CE (18:1)	$C_{45}H_{78}O_2 + NH_4$
3	CE	691.6	$[M+NH_4]^+$	CE (20:4)	$C_{47}H_{76}O_2 + NH_4$
4	CE	715.6	$[M+NH_4]^+$	CE (22:6)	$C_{49}H_{76}O_2 + NH_4$
5	CE	717.6	$[M+NH_4]^+$	CE (20:5)	$C_{49}H_{78}O_2 + NH_4$

B

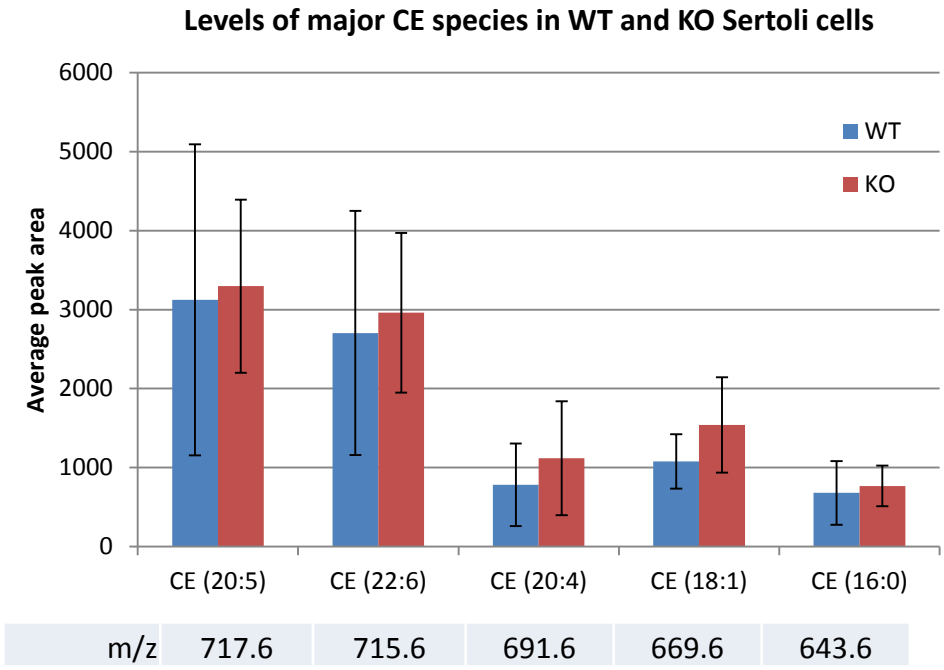

Figure 3.29: Quantitative ESI-MS/MS-MRM analyses of major cholesteryl ester (CE) species present in the Sertoli cells of WT and *Arsa* KO mice (8-11 months of age). A) Table showing list of major CE selected for quantitative analyses. **B)** Relative abundance of major CE species was quantified based on the peak area of each m/z ion signal. Data are expressed as mean ± S.D. from 4 sets of isolated Sertoli cell samples.

Unlike other described lipid types, the TAG of all molecular species (containing various fatty acids) cannot be obtained using only one assigned ion product for MS/MS scanning. Therefore, in this study, only TAG molecular species containing common fatty acids (i.e., C16:0, C18:0, and C18:1) were selected for MS/MS analyses. Neutral loss scanning of m/z 273, 301, 299 (corresponding to the loss of C16:0, C18:0 and C18:1 acyl chains of TAGs) showed relatively low peak intensities of these TAG molecular species in both WT and KO Sertoli cell samples (Figure 3.30) as compared with those in the sperm samples (Figure 3.36), suggesting a low abundance of these TAG molecular species in Sertoli cells. Among the TAGs detected in the Sertoli cell samples, the TAG with m/z 874.7, which likely corresponded to 16:0/18:1/18:2 TAG, showed the strongest intensity (Figure 3.30) and its level appeared to be higher in *Arsa* KO Sertoli cells as compared with that in the WT samples (Figure 3.31). However, we cannot exclude the possibility that there might be other TAG molecular species (without C16:0, C18:0 and C18:1 as their acyl chains) present in Sertoli cells, but they were missing from our MS analyses.

Absolute amounts of total cholesterol in *Arsa* KO and WT Sertoli cells, as measured by the Amplex Red assay, revealed significantly lower levels in *Arsa* KO Sertoli cells (164.22 ± 20.20 versus 204.02 ± 45.45 nmole/million cells for the KO and WT sample, respectively) (Figure 3.32). Summary of the lipid analysis results of Sertoli cells from *Arsa* KO and age-matched WT mice is shown in Table 3.5.

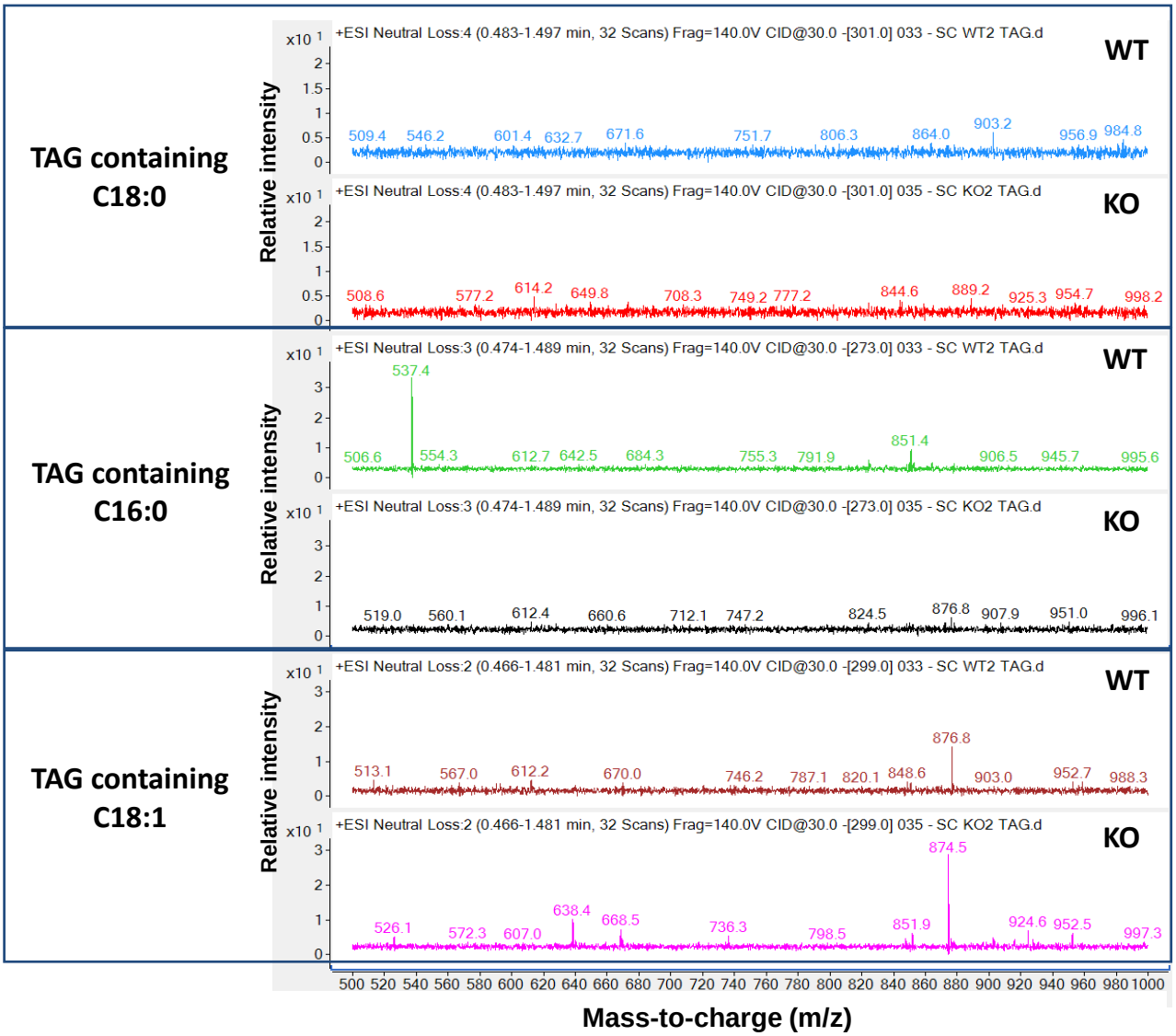

Figure 3.30: Mass spectra from neutral loss scanning of 301, 273, and 299 showing major triacylglycerol (TAG) species containing C18:0, C16:0, and C18:1 respectively, in WT and *Arsa* KO Sertoli cells. Representative spectra of each TAG molecular species from one set of the WT and KO Sertoli cell samples were shown.

A

#	Lipid classes	m/z	Ion	Possible identities	Formula of lipid ion
1	TAG	874.7	$[M+NH_4]^+$	16:0/18:1/18:2 TAG	$C_{55}H_{100}O_6 + NH_4$
2	TAG	900.8	$[M+NH_4]^+$	18:0/18:1/18:3 TAG	$C_{57}H_{102}O_6 + NH_4$
3	TAG	874.7	$[M+NH_4]^+$	16:0/18:1/18:2 TAG	$C_{55}H_{100}O_6 + NH_4$
4	TAG	900.8	$[M+NH_4]^+$	18:0/18:1/18:3 TAG	$C_{57}H_{102}O_6 + NH_4$

B

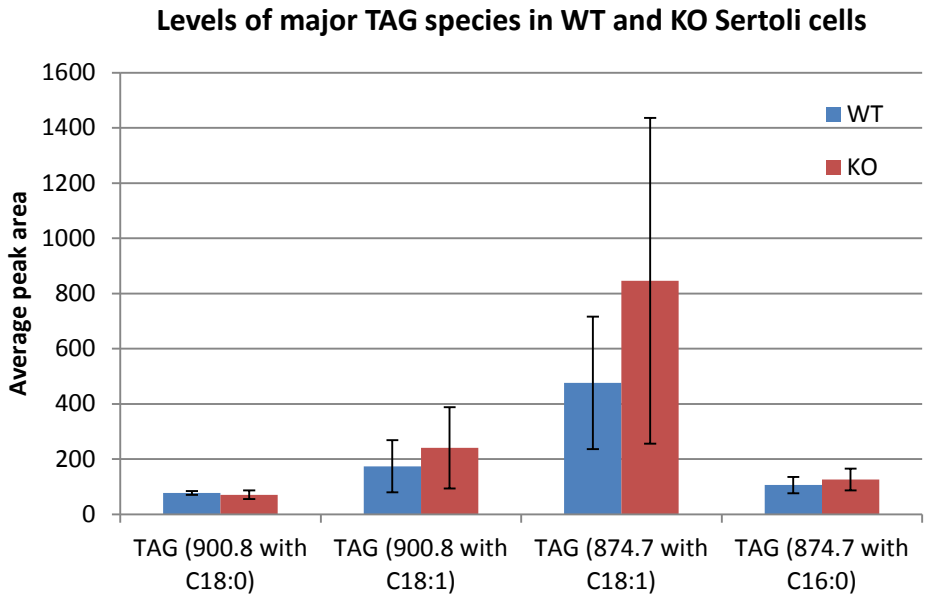

Figure 3.31: Quantitative ESI-MS/MS-MRM analyses of major triacylglycerol (TAG) species present in Sertoli cells of WT and *Arsa* KO mice (8-11 months of age). A) Table showing a list of major TAG molecular species selected for quantitative analyses. **B)** Relative abundance of the major TAG species (listed in A) was quantified based on the peak area of each m/z ion signal. Data are expressed as mean ± S.D. from 4 sets of the isolated Sertoli cell samples.

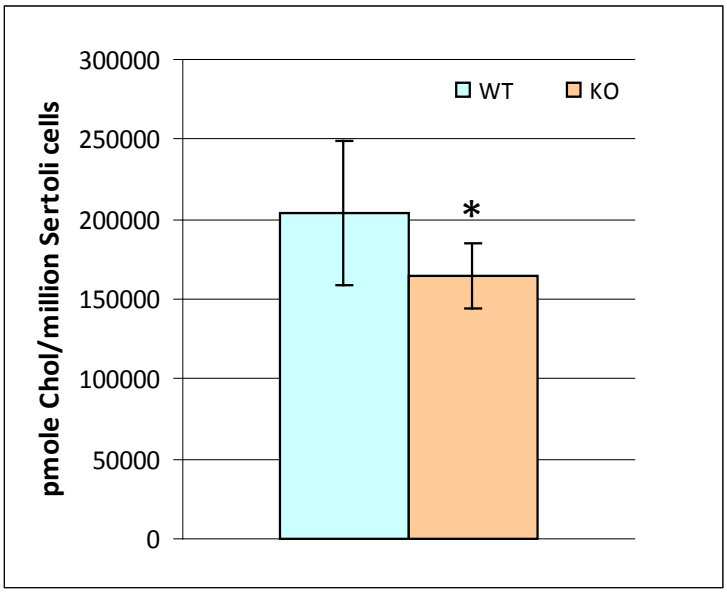

Sample	nmole of cholesterol/million Sertoli cells
WT	204.01 ± 45.45
KO	164.21 ± 20.20

Figure 3.32: Absolute amounts of total cholesterol in Sertoli cells of WT and *Arsa* KO mice, as measured by Amplex Red assay. Data are expressed as mean ± S.D. from 4 sets of the isolated Sertoli cell samples. An asterisk indicates a statistically significant decrease (P<0.05) of cholesterol level in the KO samples.

Table 3.5: Quantitative comparison of Sertoli cell lipid profiles from 8- to 11-month-old *Arsa* KO and WT mice

Lipid types	Summary of changes
SGG and other sulfolipids	- Significant increases of SGG molecular species (i.e., C16:0/16:0, C24:0/C16:0, C18:1/16:0, C18:0/16:0) and SGC (C16:0) amounts were observed in *Arsa* KO Sertoli cells. - Level of SGG (C16:0/16:0), the most abundant sulfolipid species, in *Arsa* KO Sertoli cells was increased to 2.5 times of the WT value (4400 vs 1790 pmole/million cells, respectively). -Cholesterol sulfate level was minimal (below the detection limit) in both *Arsa* KO and WT Sertoli cells.
Triacylglycerol (TAG)	No statistically significant changes but an increasing trend, especially for TAG with m/z 874.7, was observed in *Arsa* KO Sertoli cells.
Cholesterol ester (CE)	No statistically significant changes but an increasing trend was observed in *Arsa* KO Sertoli cells.
Phosphatidylcholine (PC) & Shingomyelin (SM)	- Levels of all identified major PC and SM species showed a decreasing trend in *Arsa* KO Sertoli cells, although these decreases were not statistically significant as compared with corresponding values of the WT lipids. A high variation of PC and SM levels in both *Arsa* KO and WT samples from different animals was likely the cause of the lack of statistical differences. - Lyso PC (C16:0) showed a statistically significant decrease in *Arsa* KO Sertoli cells.
Phosphatidylethanolamine (PE)	No statistically significant changes but a slight increasing trend in PE levels was observed in *Arsa* KO samples.
Cholesterol	A statistically significant decrease was detected in *Arsa* KO Sertoli cells.

3.2.5) Lipid analyses of Percoll gradient centrifuged sperm from 8- to 11-month-old *Arsa* knockout and wild type mice

Instead of the swim-up sperm previously used in this study, the Percoll gradient centrifuged (PGC) sperm prepared from *Arsa* KO and WT mice were used for further lipid analyses because the PGC sperm was free from the remnants of epididymal/vas deferens epithelial cells. During the swim-up sperm preparation, most of these cell remnants sedimented at the bottom of the tube, but some of them often floated into the upper part of the medium which was collected as the swim-up sperm fraction (see Materials and Methods and Figure 3.12). This contamination would make it impossible to use the swim-up sperm preparation for specifically quantifying some sperm lipid classes expected to be present in these remnants from epithelial cells (e.g., PC, SM, cholesterol and TAG).

Sulfolipid profiling revealed that other than SGG (C16:0/C16:0) with m/z 795 (which appeared as the major peak), the PGC sperm of 8-month-old *Arsa* KO and WT mice contained another sulfolipid with m/z 464.3, which was identified as cholesterol sulfate (Figure 3.33A). ESI-MS/MS-MRM analyses revealed that 8-month-old *Arsa* KO mouse sperm showed a significant reduction of SGG (C16:0/16:0) level to ~50% of the WT sperm (Figure 3.33B), which was consistent with our previous result obtained from sperm in the swim-up fraction (Figure 3.17B). In contrast, the cholesterol sulfate level in the *Arsa* KO PGC sperm was significantly increased as compared with the corresponding WT sperm (Figure 3.33B). Absolute amounts of SGG (C16:0/C16:0) and cholesterol sulfate were determined using the standard curves built from different concentrations of the purified lipid standards. In one million *Arsa* KO sperm and WT sperm, SGG (C16:0/C16:0) levels were

0.053 ± 0.015 and 0.097 ± 0.032 nmole, respectively (Figure 3.34), whereas cholesterol sulfate levels were 0.014 ± 0.004 and 0.008 ± 0.002 nmole, respectively (Figure 3.34).

The abnormal morphology of *Arsa* KO sperm suggested the possibility that in addition to a change in sulfolipid levels, levels of other major lipids, including PC, SM, TAG and cholesterol in the sperm of 8-month-old *Arsa* KO mice, may be affected. Therefore, relative amounts of these lipids in PGC sperm from 8-month-old *Arsa* KO and WT animals were also determined using the same methods described for the analyses of Sertoli cell lipids. Mass spectra from precursor ion scanning of m/z 184 (choline ion) revealed that PGC sperm of *Arsa* KO and WT mice contained similar PC and SM molecular species, including PC with m/z 676, 704 and SM with m/z 675 and 703 (Figure 3.35A). The identities of these candidate lipids were shown in the readout table in Figure 3.25. The PCs containing polyunsaturated fatty acids (i.e., PC 16:0/22:6 with m/z 807, PC 18:0/22:6 with m/z 835) have been previously described in sperm (Lenzi et al., 1996), and these PC molecular species may also exist in our PGC sperm samples as shown in the zoom-in mass spectrum of the PC profile (Figure 3.35B); however, due to their relatively low levels in the PGC pellet sperm samples, they were not selected for further quantification. All PC and SM molecular species selected for MRM analysis showed a decreasing trend in their levels in the *Arsa* KO sperm as compared with those in the WT samples (Figure 3.35C) although no statistical differences between the WT and KO levels were observed. The lipid with m/z 496, likely corresponding to a lysoPC with C16:0, was also observed in the WT and *Arsa* KO sperm samples and the level of this lipid showed a statistiscally significant decrease in the *Arsa* KO sperm, as compared with that in the WT sperm.

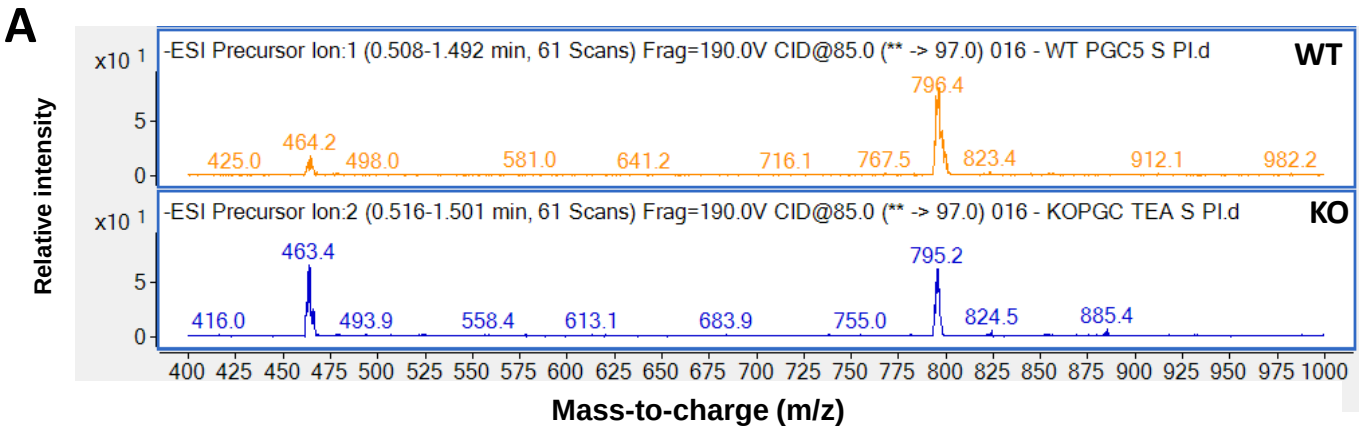

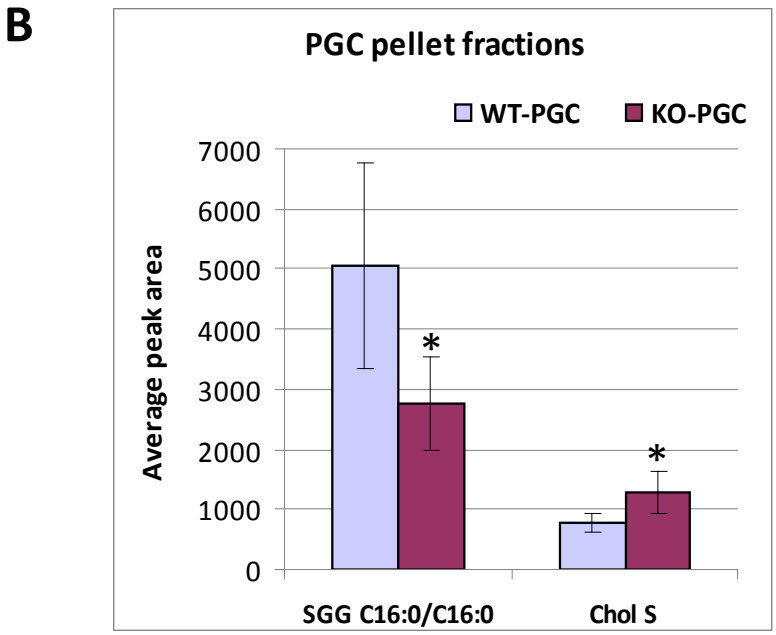

Figure 3.33: A) Precursor ion scanning of m/z 97 showing major sulfolipids present in PGC pellet sperm fractions of WT and *Arsa* KO mice (8-11 months of age). **B)** Relative abundance of SGG (C16:0/C16:0 with m/z 795.5) and cholesterol-3-sulfate (Chol S with m/z 465.3) in the PGC pellet fractions of WT and KO sperm. Data are expressed as mean ± S.D. of 3 sets of sperm samples. Asterisks indicate significance differences (P<0.05) between WT and KO sperm samples.

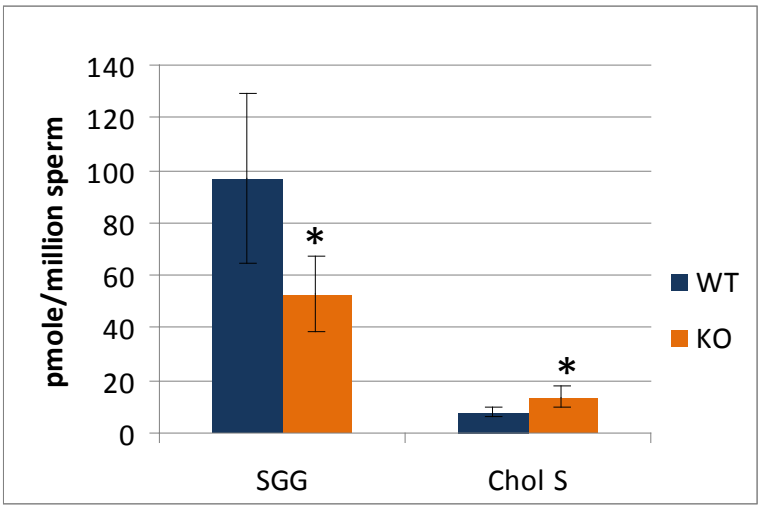

pmole of lipid/million sperm		
Sample	**SGG**	**Cholesterol sulfate (Chol S)**
WT	96.9 ± 32.5	8.2 ±1.7
KO	52.8 ± 14.7	13.9 ±3.9

Figure 3.34: Absolute amounts of SGG and cholesterol sulfate in PGC pellet sperm fractions of WT and *Arsa* KO mice. The average peak areas as shown in the Figure 3.33 were used for the calculation of the absolute amounts of SGG and cholesterol sulfate, based on the known amounts of the lipid standards analyzed in the parallel ESI-MS/MS run. Data are expressed as mean ± S.D. of 3 sets of sperm samples. Asterisks indicate significance differences (P<0.05) between WT and KO samples.

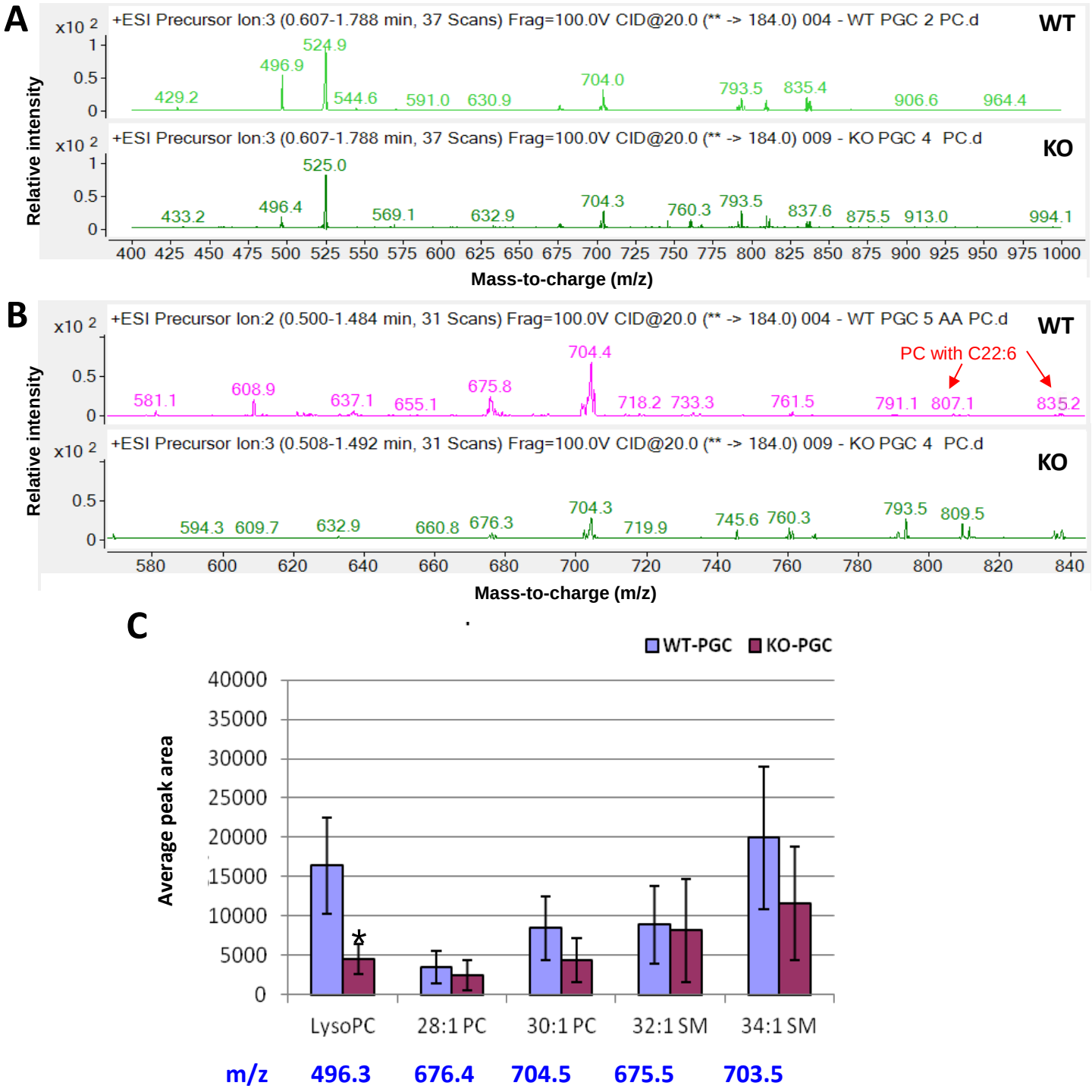

Figure 3.35: A) Mass spectra from precursor ion scanning of m/z 184 in the range of m/z 400-1000 showing major phosphatidylcholine (PC) and sphingomyelin (SM) species present in PGC pellet sperm fractions of WT and *Arsa* KO mice (8-11 months of age). **B)** Magnified view of PC and SM ions in the range of m/z 570-840. Note that the PC containing polyunsaturated fatty acids (i.e., C22:6) that have been previously described in sperm were also detected in our PGC sperm samples. The PC with m/z 807 and 835 likely correspond to the PC 16:0/22:6 and PC 18:0/22:6, respectively. **C)** Relative abundance of selected lipid candidates, including major PC (m/z 676.4, 704.5), lysoPC (m/z 496.3), and SM (m/z 675.5, 703.5) species, in the PGC pellet fractions of WT and KO sperm. The possible identities of these major PCs and SMs are listed here as well as in the readout table in Figure 3.25A. Data are expressed as mean ± S.D. of 3 sets of sperm samples. The asterisk indicates a significant difference (P<0.05) between WT and KO sperm samples.

Neutral loss scanning for TAG revealed two major TAG molecular species in *Arsa* KO and WT sperm, including TAG containing C16:0 and C18:1 with m/z 874 and TAG containing C18:0 and C18:1with m/z 900 (Figure 3.36); the levels of these TAGs appeared to be higher in the *Arsa* KO samples but no statistically significant difference in their levels between the KO and WT sperm samples was detected (Figure 3.37). Levels of total cholesterol in the KO and WT sperm samples were also similar (Figure 3.38). Summary of the lipid analyses of sperm from *Arsa* KO and age-matched WT mice is shown in Table 3.6.

3.2.6) Effects of increased cholesterol sulfate level on sperm function

Treatment of sperm with cholesterol sulfate (100 μg/ml) has been previously shown to significantly reduce rabbit sperm fertilizing ability (Fayrer-Hosken et al., 1987). Direct binding of cholesterol sulfate to the surface of human sperm (Langlais et al., 1981) resulting in retardation of sperm capacitation has also been implicated (Langlais et al., 1988; Nixon et al., 2011). Therefore, it is possible that the increased cholesterol sulfate level in *Arsa* KO sperm affects the ability of sperm to undergo capacitation, and this contributes in part to the observed defect in their fertilizing ability (Figure 3.12B). Sperm protein tyrosine phosphorylation, one of the major signaling events associated with capacitation (Visconti and Kopf, 1998), was then assessed for the first time on mouse sperm associated with increased levels of cholesterol sulfate. The direct effect of cholesterol sulfate was first evaluated by treating WT sperm with different amounts of cholesterol sulfate (i.e., 0, 0.15, 75 μg of cholesterol sulfate for 10 million sperm) either before or during induction of capacitation. The amount of cholesterol sulfate used was based on the level of cholesterol

sulfate found in the 8-month-old *Arsa* KO PGC pellet sperm (i.e., the amount of cholesterol sulfate in the *Arsa* KO sperm was 0.06 µg per 10 million sperm, so 0.15 µg of cholesterol sulfate used was equivalent to 2.5X the amount of cholesterol sulfate in the *Arsa* KO sperm suspension – 1 ml of 10 million). The results demonstrated that cholesterol sulfate could indeed inhibit sperm tyrosine phosphorylation in a dose-dependent manner regardless of whether the cholesterol sulfate treatment was done before or during capacitation (Figure 3.39A). In addition, sperm of 8-month-old *Arsa* KO mice showed a lower level of protein tyrosine phosphorylation upon incubation in a capacitating medium, as compared with the corresponding level in WT sperm (Figure 3.39B). All these results strongly suggested that the increased cholesterol sulfate level could be another factor contributing to the reduced sperm fertilizing ability of *Arsa* KO mice.

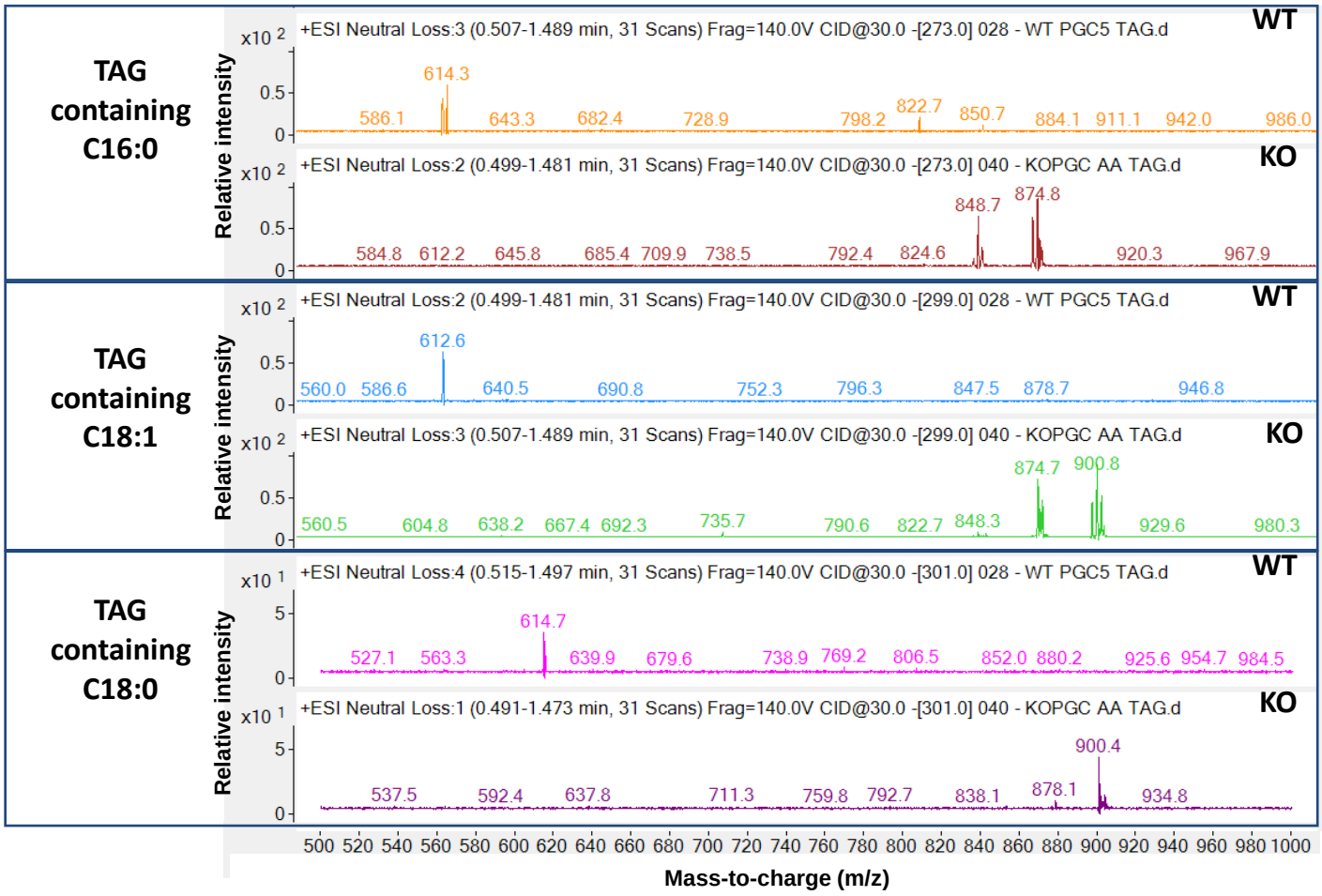

Figure 3.36: Mass spectra from neutral loss scanning of 273, 299, and 301 showing major triacylglycerol (TAG) species containing C16:0, C18:1 and C18:0, respectively, in the PGC pellet sperm fractions of WT and *Arsa* KO mice (8-11 months of age).

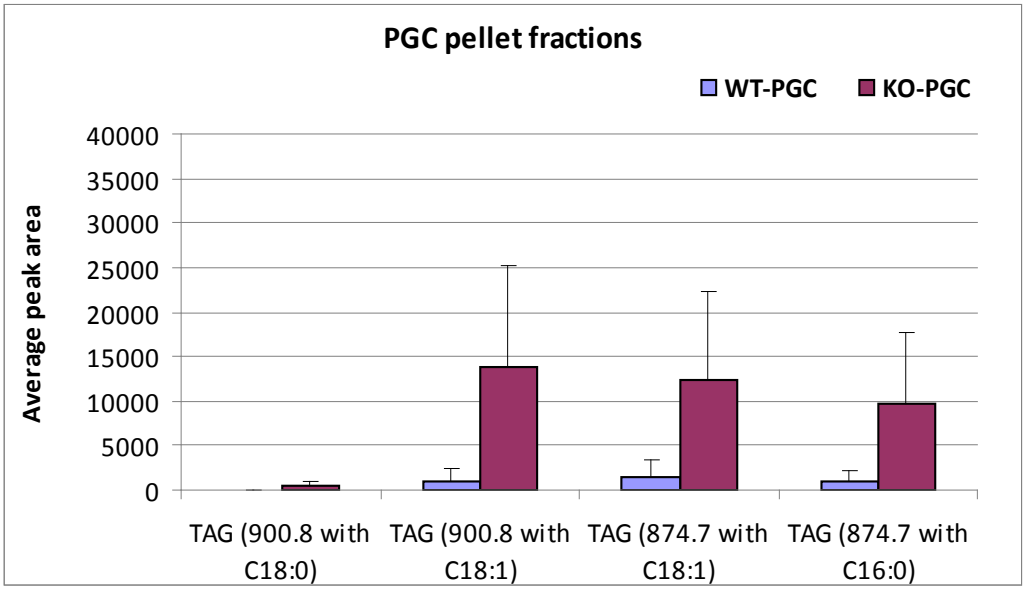

Figure 3.37: Relative abundance of major triacylglycerols (TAG) (m/z 874.7 and 900.8) in PGC pellet sperm fractions of WT and *Arsa* KO mice (8-11 months of age). Details on identities of these TAGs are included in the Table in Figure 3.31A. Although there are no statistical differences, there is a trend in the increased levels of a number of TAG species in the KO sperm.

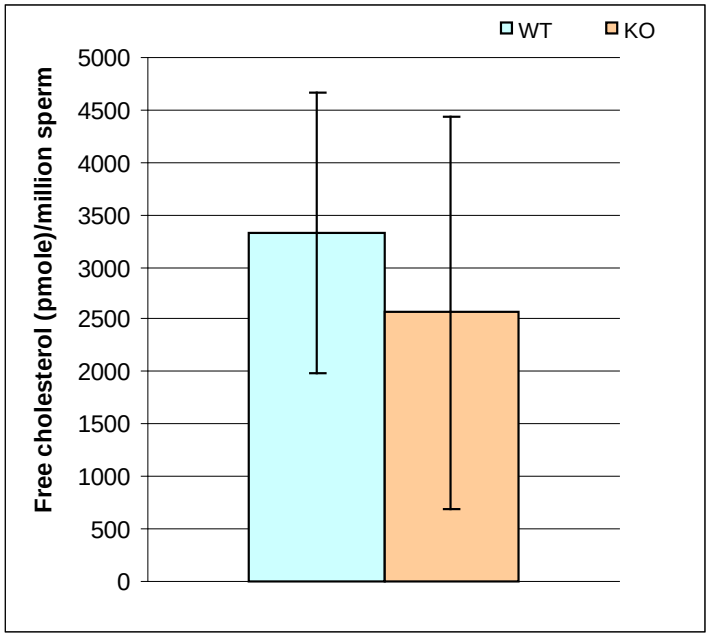

nmole of cholesterol/million sperm	
Sample	**PGC**
WT	3.324 ± 1.345
KO	2.565 ± 1.879

Figure 3.38: Absolute amounts of total cholesterol in PGC pellet sperm fractions of WT and *Arsa* KO mice, as measured by the Amplex red assay. Data are expressed as mean ± S.D. of 3 sets of sperm samples. No statistically significant difference in total cholesterol levels was detected between WT and KO sperm samples.

Table 3.6: Quantitative comparison of sperm lipid profiles from 8- to 11-month-old *Arsa* KO and WT mice

Lipid types	Summary of changes
SGG and other sulfolipids	-*Arsa* KO sperm showed a significant decrease of SGG (C16:0/16:0) level to ~50% of the WT value -Other SGG molecular species as well as SGC (C16:0) levels were minimal (below the detection limit) in both *Arsa* KO and WT sperm samples. -*Arsa* KO sperm showed a significant increase of cholesterol sulfate level to ~200% of the WT value.
Triacylglycerol (TAG)	All identified TAG species showed an increasing trend in *Arsa* KO sperm, although these increases were not statistically different from those of the WT samples; this was possibly because of the high variation among sperm samples from different animals.
Cholesterol ester (CE)	Minimal (below the detection limit)
Phosphatidylcholine (PC) & Shingomyelin (SM)	- Levels of all identified major PC and SM species showed a decreasing trend in *Arsa* KO sperm, although these decreases were not statistically significant as compared with corresponding values of the WT lipids. A high variation of PC and SM levels in both *Arsa* KO and WT samples from different animals was likely the cause of the lack of statistical differences. - Lyso PC (C16:0) showed a statistically significant decrease in *Arsa* KO sperm.
Phosphatidylethanolamine (PE)	Minimal (below the detection limit)
Cholesterol	No statistically significant changes.

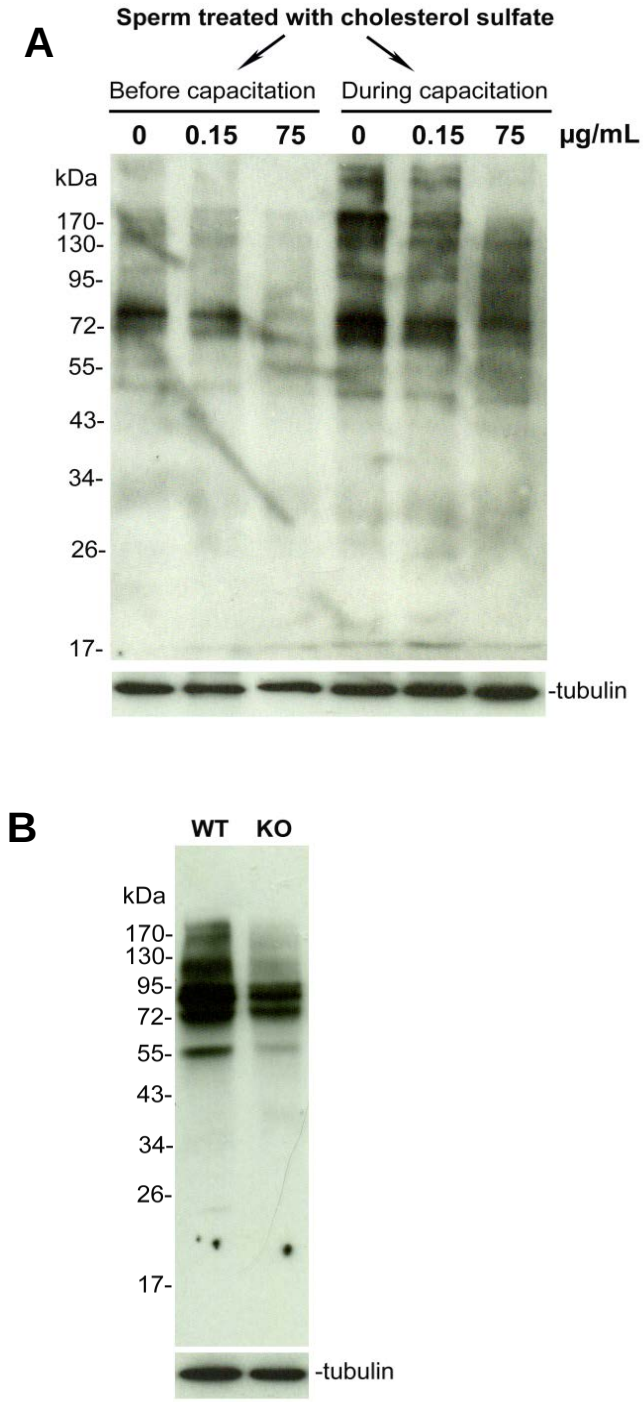

Figure 3.39: Cholesterol sulfate retards sperm capacitation as detected by sperm protein tyrosine phosphorylation. **A)** Sperm from CD-1 WT mice were treated with different concentrations of cholesterol sulfate (0, 0.15, 75 µg/mL) either before or during induction of capacitation by incubating sperm in 0.3% BSA-containing medium (1 h, 37˚ C, under 5% CO2). Equal numbers of sperm (1 million) from each treatment were solubilized in Laemmli's SDS sample buffer for protein extraction and the protein samples were subjected to SDS-PAGE and immunoblotting with anti-phosphotyrosine antibody (4G10). The level of sperm tyrosine phosphorylation was decreased in a concentration-dependent manner in response to the cholesterol sulfate treatment. The representative blot from three experiments is shown. **B)** Sperm prepared from 8-month-old WT and *Arsa* KO mice were also assessed for their tyrosine phosphorylation levels after incubation in capacitation medium. Lower levels of protein tyrosine phosphorylation were evident in the KO sperm, as compared with that of the WT sample. Alpha-tubulin immunoblotted signals were also shown to confirm similar amounts of proteins loaded in each lane.

CHAPTER FOUR

DISCUSSION

4.1) SGG and SGG associated membranes on sperm: relevance in sperm fertilizing ability

Defining the molecular mechanisms underlying the species-specific interaction between a spermatozoon and ZP has been a challenge in the field. A number of sperm molecules, including those existing on the sperm head plasma membrane and those localized in the acrosome, have been shown to possess ZP affinity. Emerging evidence suggested that sperm-ZP interaction requires the coordinated action of several sperm surface molecules rather than relying on a single receptor-ligand interaction. How a number of ZP-binding molecules act together for ZP adhesion is still elusive. However, it is very likely that sperm surface remodeling during capacitation plays an important role in the coordination of these molecules. Our lab has previously demonstrated that after capacitation the levels of sperm lipid rafts isolated as DRMs were increased and a number of ZP-binding molecules were found as components of the DRMs of Cap sperm (Bou Khalil et al., 2006). We have also shown that specifically to the sperm, the formation of lipid rafts is based on the interaction of SGG, an ordered lipid present selectively on the sperm head surface, with cholesterol and saturated phospholipids (Bou Khalil et al., 2006). Based on the known roles of lipid rafts in somatic cells, the sperm lipid raft may likewise serve as the organizing center which allows the coordinated action of several ZP-binding molecules in sperm-ZP interaction.

The use of detergents for the isolation of lipid rafts was first introduced by a pioneer in the field (Schroeder et al., 1994; Simons and Ikonen, 1997) and has been commonly used

for lipid raft studies; however, recent findings suggest that the detergents may cause reorganization of raft protein or lipid components (Pike, 2009). People in the rafts field are now moving towards using a milder detergent or a physical force for isolating rafts (Smart et al., 1995; Sprenger and Horrevoets, 2007). Fortunately, in the sperm field, the method for APM vesicle isolation by using a physical force, namely nitrogen cavitation, has been established and used widely (Peterson et al., 1980; Flesch et al., 1998). We have also demonstrated that the DRMs and APM vesicles have similar binding ability to the ZP (Bou Khalil et al., 2006). Therefore, in this study, to avoid any problems that might occur from using DRMs, we have used the APM vesicles isolated from Non-cap and Cap sperm for comparative analyses of their lipid and protein components. Results from this study have demonstrated a new mechanism involving the recruitment of acrosomal proteins onto sperm surface during capacitation for further ZP interaction.

4.1.1) Changes in molecular components of APM vesicles after capacitation

HPTLC analysis showed that APM vesicles contained a number of lipids, including SGG, PC, SM, cholesterol and TAG, but no drastic difference in their levels was observed between Non-cap and Cap APM vesicles (Figure 3.2). However, our APM lipid characterization by HPTLC was still fundamental and the quantitative analysis of sperm APM lipids would be needed in order to gain more conclusive results. Quantification of SGG and cholesterol can be performed using our established ESI- MS/MS-MRM method and the Amplex Red assay, respectively but quantitative analyses of other lipids are not simple. Among the identified APM lipids, only SGG is present specifically in sperm and has been

shown for its ZP affinity (White et al., 2000; Tanphaichitr et al., 2003). Nonetheless, it is unlikely that SGG alone is involved in ZP binding, considering the accumulated findings on sperm head surface proteins with ZP affinity. For this reason, the focus of this study was shifted toward characterizing the protein profiles of Non-cap and Cap APM vesicles.

Our proteomic results indicated an increase in a number of proteins that are involved directly or indirectly in sperm-ZP interactions (i.e., MFGM, ZAN and ACRBP) in the Cap APM vesicles as compared with the Non-cap APM samples (Figure 3.4A). The increased amounts of these proteins in Cap APM samples corroborated the higher efficiency of ZP binding of Cap sperm (Melendrez et al., 1994), and also explained the higher amounts of total proteins determined in the Cap APM samples (Figure 3.3A). Sperm are unable to synthesize new proteins due to their highly condensed chromatin structure. The sperm surface proteins with ZP affinity found in the APM vesicles of Cap sperm are also present in the Non-cap sperm samples (Table 3.1). Therefore, changes during capacitation that allow these proteins to function at the highest capacity in ZP binding must be attained through their reorganization to the proper structural form and/or relocalization to the proper domain in the APM. Cholesterol is known to be released from the sperm plasma membrane during capacitation; this cholesterol efflux leads to an increase in global membrane fluidity, thus allowing rearrangement of more sperm surface proteins into lipid raft microdomains (Bou Khalil et al., 2006). The increase in global membrane fluidity may explain in part how the protein amounts of APM vesicles were increased following capacitation. Additionally, proteins known for their localization in the acrosome of Non-cap sperm (i.e., ZAN, proacrosin/acrosin, ACRBP, and ZPBP1) were found at higher levels in the APM vesicles of Cap sperm; therefore, the increase in the APM vesicle proteins of Cap sperm may reflect

relocalization of the proteins from the acrosome to the sperm head plasma membrane. Another possibility could be from the looseness of the plasma membrane after capacitation, making it possible to isolate more APM vesicles. However, the proteins found specifically in the Cap APM vesicles showed low spectral counts (1-2 counts per protein) and the increase in the protein amounts in the Cap APM vesicles mainly belonged to the proteins that existed in both the Non-cap and Cap sperm samples (Appendix Table 1). This means that even though the looseness of the plasma membrane after capacitation allowed better APM vesicle isolation, nitrogen cavitation still occurred at similar sites in the Cap sperm as compared with the Non-cap sperm.

Our findings that ZP-binding proteins and other proteins relevant for male fertility, such as MFGM, ACRBP, AQN3, AWN, were the most abundant types of proteins in isolated APM vesicles (Tables 3.1&3.2) are in agreement with the previous proteomic studies of 2-D gel separated APM proteins that show ZP affinity (Van Gestel et al., 2007). In addition to this similar list of proteins, our proteomic analyses of total protein extracts of APM vesicles specifically revealed ZP-binding molecules, including ZAN and ZPBP1 that were not detected in the previous study. This finding could be due to the fact that these extra ZP-binding proteins did not have a strong ZP affinity under the denatured conditions required for the 2-D gel electrophoresis (Van Gestel et al., 2007). This postulate was supported by the fact that these proteins were major components of the APM HMW protein complexes (with native conformation) that showed ZP affinity (Figure 3.5, Table 3.3). Moreover, since our proteomic analyses were performed on the total APM vesicle protein extracts (not limited to those with ZP affinity), other types of proteins, including chaperone proteins, kinases and cell signaling and adhesion proteins, were also revealed from our analyses (Tables 3.1&3.2).

Among these proteins, the cell signaling/binding proteins that have been shown to be involved in the capacitation process, such as calmodulin (a calcium-binding protein) (Gonzalez-Fernandez et al., 2013) and PSP-I (a major seminal plasma protein) (Caballero et al., 2009), were found at higher levels in the Cap APM vesicles.

In this present study, we further demonstrated that APM vesicles shared similar lipid and protein components to those of the DRMs. The lipid components of Non-cap and Cap APM vesicles (i.e., cholesterol, SGG, PC, SM) were similar to those of DRMs isolated from Non-cap and Cap pig sperm (Bou Khalil et al., 2006). Proteins previously identified in Cap pig sperm DRMs, such as MFGM, ACRBP, and AQN-3 (Van Gestel et al., 2005) were also found as components of our Cap APM vesicles (Tables 3.1&3.2). All these findings strongly indicated that APM vesicles are the SGG associated membrane domains, representing the sperm lipid rafts with specific localization to the anterior sperm head region, and they can be used in place of DRMs for studying the functions of lipid rafts in sperm-ZP interaction.

4.1.2) Formation of high molecular weight protein complexes with ZP affinity on the APM

The existence of a number of proteins with known *in vitro* ZP affinity on the sperm surface raises the question of how these proteins function during sperm-egg interaction. Based on several lines of evidence in the field, a new concept that these ZP-binding molecules act together as functional complexes for ZP binding has been proposed (Redgrove et al., 2012; Tanphaichitr et al., 2007a). Our BN-PAGE and far western blotting analyses demonstrated that APM vesicles isolated from Cap pig sperm contained HMW protein

complexes (in the range of 750-1300 kDa) with preferential affinity for the pig ZP3 (Figure 3.5A). While these results were similar to those previously described for mouse and human sperm (Dun et al., 2011; Redgrove et al., 2011), the pig APM HMW complexes were in the higher mass range and contained more components. For example, pig Complex I (1000-1300 kDa) contained six ZP-binding proteins (i.e., ZAN, MFGM, proacrosin/acrosin, ASPX, AWN and ZPBP1). In contrast, the HMW protein complexes from mouse sperm plasma membrane extracts contained fewer ZP-binding proteins, particularly only ZPBP2 in the 900 kDa complex, and ARSA and SPAM1 in the 220 kDa complex (Dun et al., 2011). Only ZPBP1, ZPBP2 and ZP3R were found in the 820 kDa complex from human sperm plasma membrane extracts (Redgrove et al., 2011). These dissimilarities may be due to species differences, but may also reflect the sources of materials used in the work. Here APM vesicles of pig sperm were used as the source for the HMW protein complexes with ZP affinity, whereas the total plasma membrane extracted from both the head and tail of mouse and human sperm were used in the previous studies. However, because of their specific location on the sperm head, the APM vesicles are more enriched in ZP-binding proteins than the total plasma membrane extracts, and thus would serve as an ideal source for HMW complexes for ZP binding studies.

Proteomic analyses in this study also demonstrated that the APM HMW complexes of Cap pig sperm contained a number of chaperone proteins, including TCP-1 subunits (gamma, eta, beta, alpha, theta, zeta), and heat shock 70 kDa protein-1 like (HS71L) (Table 3.3). Our finding is consistent with the reported identification of TCP-1 in the HMW complexes (700-900 kDa) from mouse and human sperm plasma membrane extracts (Dun et al., 2011; Redgrove et al., 2011). These previous studies also revealed that the chaperones

found in the HMW complexes of mouse and human sperm played a role in the HMW protein complex formation but did not have direct ZP-binding ability (Dun et al., 2011; Redgrove et al., 2011), suggesting that the chaperone proteins in the pig APM HMW complex may function in the same manner. In addition, cytoskeleton proteins, especially TBB2C, showed a preferential presence in the Cap pig APM HMW complexes. Association between chaperone and cytoskeleton proteins has been previously described (Quinta et al., 2011), and may explain the co-presence of these two types of proteins in the Cap pig APM HMW complexes. The functions of cytoskeleton proteins in sperm capacitation have yet to be determined.

4.1.3) Zonadhesin and other acrosomal proteins are major components of high molecular weight protein complexes with ZP affinity on the APM

In the total protein extracts from APM vesicles, the spectral count for ZAN was lower than that of MFGM, showing the highest spectral count (Table 3.1). Therefore, it is surprising to see that ZAN was the most abundant component in the Cap APM HMW complexes (Table 3.3). Nonetheless, the abundance of ZAN in the Cap APM HMW complexes strongly suggested its contribution to the ZP-binding ability of these complexes, which was further confirmed by the decrease in ZP-binding ability when these complexes were pretreated with anti-ZAN holoprotein IgG (Figure 3.10B).

ZAN is a mosaic protein with a number of domains previously implicated in cell-adhesion (including MAM, mucin and von Willebrand factor (VWF) D domains, see Figure 3.4C). During spermatogenesis, ZAN is synthesized as a precursor protein in the spermatid

stage, but after epididymal maturation the processed forms of ZAN and their multimers are detected in the mature sperm (Bi et al., 2003; Hickox et al., 2001). Significantly, the p45 and p105 forms, containing VWF D domains, have been shown to bind to the homologous pig ZP particulates (Hickox et al., 2001). Our analyses of ZAN peptide sequences identified by MS also revealed enrichment of the VWF D domains in both the whole APM vesicle extracts and the HMW protein complexes with ZP affinity of the Cap pig sperm (Appendix Table 1). Moreover, the existence of p105 and p45 forms of ZAN as well as its higher mass forms (300-500 kDa and higher) was further confirmed by SDS-PAGE/immunoblotting (Figures 3.4B & 3.10A). Since the VWF D domain has been shown for its role in multimerization of VWF (Rosenberg et al., 2002), this domain may drive the ZAN polypeptide to multimerize and/or interact with other proteins on the sperm head surface. Sequences of the MAM domain at the N-terminal region of ZAN were also detected, indicating that ZAN fragments other that those containing VWF D domains (Appendix Figure 3) may also be present in our isolated APM vesicles. Since MAM domains are known to function in cell adhesion (Cismasiu et al., 2004), they might contribute to the ZP recognition of the APM HMW complexes. However, the direct binding of MAM domain with ZP has not yet been shown. Based on the adhesion property of several ZAN domains, it is not surprising to see that ZAN interacted with other APM proteins, including proacrosin/acrosin and ACRBP, as observed in our immunoprecipitation experiments (Figure 3.11). ZAN may scaffold these acrosomal proteins and facilitate their transportation from the acrosome to the head surface of Cap sperm, allowing the formation of APM HMW protein complexes for ZP interaction. Proacrosin/acrosin and ACRBP in acrosome have been shown for their affinity for each other (Baba et al., 1994b); therefore, the possibility that ZAN may interact directly only with proacrosin/acrosin, but not with all of the co-precipitated ACRBP, cannot be excluded. We

observed three forms of proacrosin/acrosin (i.e., 53, 43, and 35 kDa) in the Non-cap and Cap APM samples (Figure 3.11). ACRBP is known to bind to the proacrosin (53 kDa) form but not to the intermediate (43 kDa) and mature (35 kDa) forms of acrosin (Baba et al., 1994b). Therefore, there would be a pool of ACRBP unbound to acrosin and this free ACRBP may have the ability to traffic from the acrosome to the sperm head surface by itself. The trafficking of free ACRBP from the acrosome to the sperm surface may occur even before capacitation. This assumption is derived from results demonstrating the presence of ACRBP on the head surface of >90% of both Non-cap and Cap sperm (Figure 3.8). However, the fact that the ACRBP staining intensity on the sperm head surface was increased after capacitation (Figure 3.8, inset of panel l) indicated the additional transport of ACRBP to the sperm head surface during capacitation.

In contrast to proacrosin/acrosin and ACRBP, MFGM was not co-precipitated with ZAN by the anti-ZAN antibody, indicating no affinity between MFGM and any of these three proteins (Figure 3.11). This result was expected, considering that MFGM deposits onto the sperm head surface during the sperm transit in the epididymis (Ensslin and Shur, 2003), whereas ZAN, ACRBP and proacrosin/acrosin originally reside in the acrosome (Hickox et al., 2001; Howes et al., 2001; Baba et al., 1994). The fact that MFGM is acquired onto the sperm head surface before capacitation would also explain the similar intensity of anti-MFGM antibody staining on the head surface of Non-cap and Cap pig sperm as revealed by immunofluorescence (Figure 3.9). Although a difference in the MFGM distribution among the three APM HMW Complexes was detected after capacitation, the total spectral counts of MFGM in the three complexes of the Cap APM did not markedly increase as compared with those of the Non-cap complexes (31 vs 28 spectral counts, respectively) (Table 3.3).

ZAN, proacrosin/acrosin, ZP3R/sp56, ZPBP1, and ASPX/SP-10 have been shown for their ZP affinity and their location in the acrosome of Non-cap sperm (Hickox et al., 2001; Tardif et al., 2010; Howes et al., 2001; Cheng et al., 1994; Mori et al., 1993; Yu et al., 2006; Coonrod et al., 1996). The presence of these acrosomal proteins in the Cap APM HMW complexes with pig ZP3 affinity (Table 3.3) indicated that they re-localized from the acrosome to the sperm head surface during capacitation prior to the sperm-ZP interaction. This finding was in contrast to the paradigm that the acrosomal proteins are released from the acrosome upon the binding of the capacitated sperm to the ZP, which is known as an inducer of acrosomal exocytosis (Berger et al., 1989). However, a recent study has demonstrated the initiation of acrosomal exocytosis in mouse sperm during their movement through the cumulus cell layers (i.e., prior to their binding to the ZP) (Jin et al., 2011), suggesting that transportation of acrosomal proteins to the sperm surface during capacitation is possible. In fact, ZAN was shown to be on the surface of Cap mouse sperm (Tardif et al., 2010), and previous results also implicate the presence of proacrosin/acrosin (De los and Barros, 2000) and ZP3R (Cheng et al., 1994) on the sperm surface after capacitation. In this report, our immunofluorescence results indicated that a portion of ZAN, proacrosin/acrosin and ACRBP was localized on the surface of intact Cap sperm, whereas the majority of these proteins was still in the acrosome (Figures 3.6 & 3.8). Gerton et al. have shown that acrosomal exocytosis occurs in a gradually continuous manner (Kim and Gerton, 2003; Tanphaichitr et al., 2007a) and the acrosomal proteins with ZP-binding ability likely play an important role in keeping acrosome-reacting/reacted sperm adhered to the ZP during sperm penetration through this egg vestment. Therefore, the acrosomal proteins with ZP affinity that we have shown here for their presence on the Cap sperm surface likely contribute to the initial phase of sperm-ZP

interaction, whereas the same proteins remaining in the acrosome still play roles in the continuing adhesion of acrosome-reacting sperm to the egg ZP (see our model, Figure 4.1).

4.1.4) Possible mechanisms for the acrosomal protein trafficking to the sperm surface

While our results clearly demonstrated that a number of acrosomal proteins target to the sperm head surface during capacitation, the mechanisms underlying this protein trafficking are not known. Acrosin plays a role in the dispersal of the acrosomal matrix (Yamagata et al., 1998), and this dispersal may be the beginning step in the movement of acrosomal proteins to the sperm surface. The autoactivation of proacrosin to generate the active form of acrosin has been shown to occur during capacitation (Polakoski and Parrish, 1977; Puigmule et al., 2011) and acrosome reaction (Noland et al., 1989). Our results showing that the mature active form of acrosin (35 kDa) was detected in both APM vesicles and nitrogen-cavitated sperm (Appendix Figure 4) corroborate this finding. During the course of capacitation, apposition of the outer acrosomal membrane to the plasma membrane has been observed in pig sperm (Tsai et al., 2010), which may initiate the exposure of acrosomal proteins (especially those on the outer acrosomal membrane) to the sperm surface. This membrane apposition may be driven by trans SNARE protein assembly, which would result in the formation of fusion pores (Tsai et al., 2012), thus facilitating the transport of acrosomal proteins to the sperm surface. Alternatively, the plasma membrane and outer acrosomal membrane apposition may be part of the “kiss and run” mechanism with transient fusion pore formation (Rizzoli and Jahn, 2007) that would also allow the movement of acrosomal proteins to the sperm surface (Tardif and Cormier, 2011). However, our results

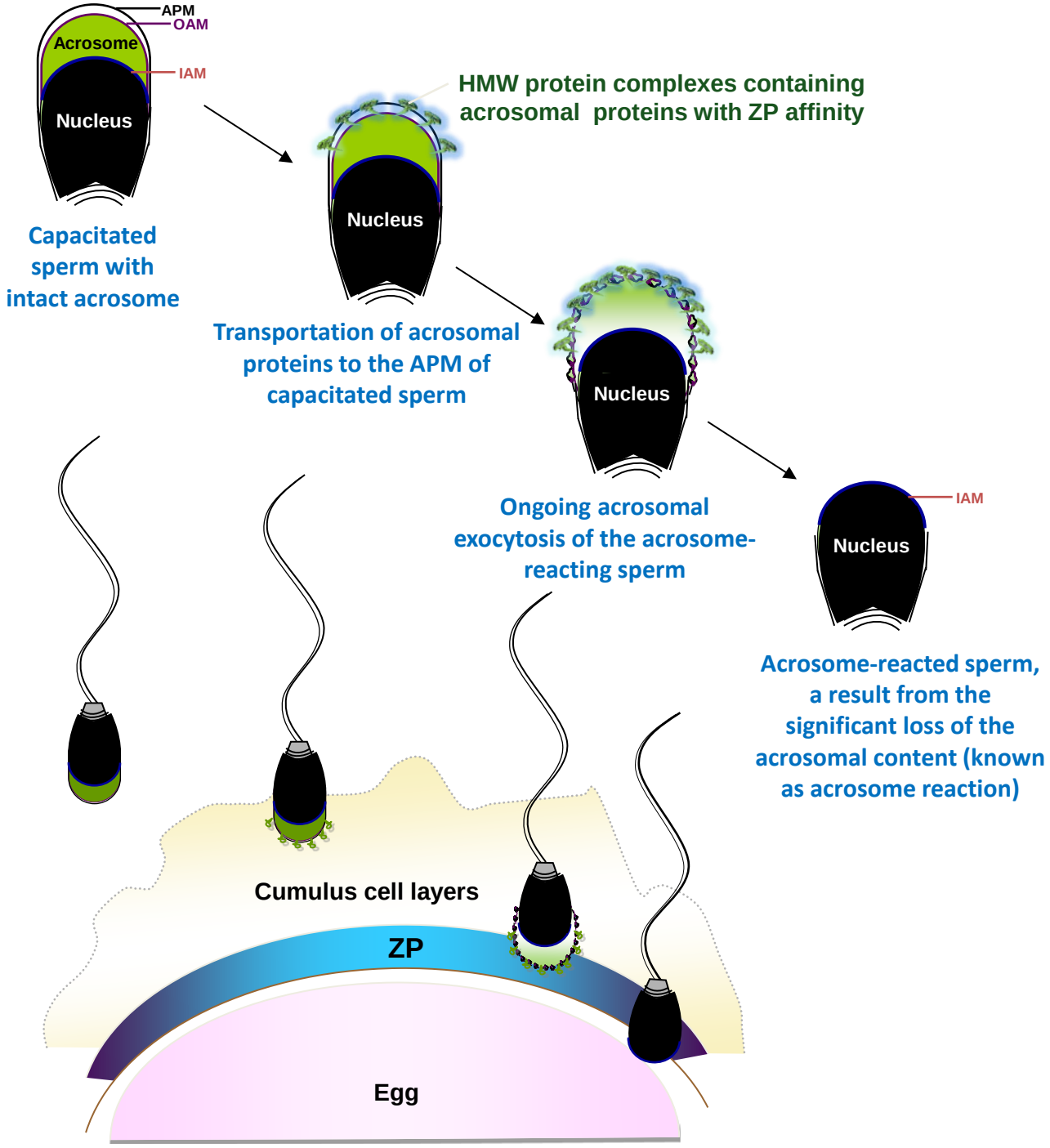

Figure 4.1: Proposed model of acrosomal protein involvement in initial binding of sperm to the ZP. During capacitation, a fraction of acrosomal proteins with ZP affinity traffics to the APM possibly in the form of HMW protein complexes, which likely then contribute to the ability of capacitated sperm to bind to the ZP during the initial phase of sperm-ZP interaction. Following the initiation of acrosomal exocytosis, the majority of the same proteins remaining in the acrosome continue to play roles in the adhesion of acrosome-reacting sperm to the egg ZP. The acrosome-reacted sperm, which have completed the acrosome reaction occurring on the ZP, further bind to the egg plasma membrane.

Abbreviations: APM – anterior head plasma membrane; OAM-Outer acrosomal membrane; IAM-Inner acrosomal membrane; ZP-zona pellucida; HMW – high molecular weight.

showed that the completion of acrosomal exocytosis, as a result of SNARE-driven apposition between the sperm plasma membrane and outer acrosomal membrane (De Blas et al., 2005), was not observed at a high rate during the 4 h course of pig sperm capacitation. Therefore, the transportation of acrosomal proteins to the pig sperm APM by the "kiss and run" mechanism may be more plausible than the SNARE-driven apposition. Besides the postulated mechanisms described above for acrosomal proteins, the trafficking of ZAN from the acrosome to the sperm APM during capacitation may be specifically dependent on its VWF D domains. This postulation is based on the known mechanism that the VWF D domain plays a role in the secretion of VWF from its multimeric complexes in an intracellular storage and this secretion is triggered by the rise of $[Ca^{2+}]_i$, intracellular cAMP level and pH_i (Rosenberg et al., 2002), all of which are physiological changes that also occur during capacitation (Baldi et al., 1991; Vredenburgh-Wilberg and Parrish, 1995; Wertheimer et al., 2013). In addition, the possibility that chaperone proteins such as TCP-1 subunits are involved in the re-localization of these acrosomal proteins to the sperm APM cannot be ruled out. Regardless of the acrosomal protein transport mechanism, our results described herein provide a new perspective on the roles of acrosomal proteins in the acquisition of sperm ZP-binding ability during capacitation.

4.1.5) SGG may serve as a binding ligand for proteins in the high molecular weight protein complexes on the APM

A number of acrosomal proteins identified in the APM HMW protein complexes of Cap sperm (i.e., ZAN (p45 and p105 forms), proacrosin/acrosin, ACRBP) do not contain

transmembrane domains. Therefore, once transported out from the acrosome, they may need a specific ligand on the sperm head surface to hold onto for further interaction with the ZP. SGG may serve as such a ligand for these proteins because it exists at a high amount on the APM and plays a role in lipid raft formation. Also, SGG and its analog SGC are known for their adhesion property to a number of molecules, including VWF (see Table 1.2 in INTRODUCTION). Since ZAN contains VWF domains, it is possible that ZAN may interact with SGG on the sperm surface after its re-localization from the acrosome. Moreover, my preliminary results from SGG liposome binding experiments showed that the ACRBP from pig sperm homogenates had specific affinity for the SGG liposomes (Appendix Figure 5). Therefore, it is possible that SGG might serve as the binding ligand on the sperm surface for these acrosomal proteins.

4.2) Importance of SGG homeostasis in male fertility: a study using *Arsa* KO mice

As indicated above, SGG on the sperm surface plays an important role in sperm fertilizing ability. Its direct relevance includes its affinity for the ZP and its structural property for the formation of sperm lipid rafts and APM domains, which can be isolated as vesicles by nitrogen cavitation. These SGG associated sperm membranes are in turn platforms for ZP binding. Therefore, the SGG levels on the sperm plasma membrane must be within a proper range, which reflects homeostasis of its synthesis in developing testicular germ cells and its shedding from the surface membrane during spermiogenesis and sperm maturation. The SGG synthesis rate in testicular germ cells is dependent on the availability of its backbone lipid, alkylacylglycerol (e.g., palmitylpalmitoylglycerol). While de novo

synthesis of this lipid is expected in testicular germ cells (Kornblatt et al., 1974), the recycling pool of alkylacylglycerol from Sertoli cells due to the processing of SGG from phagocytosed apoptotic corpses of germ cells and residual bodies would also be substantial, considering that apoptosis of testicular germ cells occurs at a 50% rate and residual bodies have to be removed from all elongating spermatids to become testicular spermatozoa (Cheng and Mruk, 2010; Dym, 1994; Huckins, 1978). As neutral lipids, alkylacylglycerol should readily traffic from Sertoli cells to adjacent primary spermatocytes or spermatids for the new round of SGG synthesis. Therefore, the SGG degradation steps in Sertoli cells contribute to SGG biosynthesis and must also be considered as part of SGG homeostasis; perturbation of any of the SGG degradation steps, like those in its biosynthesis pathway (Fujimoto et al., 2000; Honke et al., 2002) would lead to abnormal levels of SGG on testicular germ cells and/or sperm and subsequent male infertility. Results from wild type and *Arsa* KO mice presented in my thesis have confirmed the physiological importance of SGG degradation in Sertoli cells in keeping a homeostasis of this lipid, which in turn is relevant in male fertility. In addition, our results indicated for the first time the cytotoxic effects of SGG accumulation in Sertoli cells, a phenomenon typical of a lysosomal storage disorder. This disorder was likely the cause of the decrease in spermatogenesis and the abnormality of sperm produced in *Arsa* KO mice. Furthermore, my lipidomic analyses indicated that the lipid profiles of both the Sertoli cells and the sperm of aging *Arsa* KO mice were significantly different from those of age-matched WT animals, a result suggesting the importance of SGG homeostasis in keeping proper lipid composition of Sertoli cells and sperm.

4.2.1) SGG levels in germ cells and Sertoli cells during normal spermatogenesis

It is known that SGG is synthesized in pachytene primary spermatocytes, and once synthesized it is targeted to the cell surface and remains there throughout the developing stages of testicular germ cells. However, whether SGG levels on testicular germ cells changed during spermatogenesis (e.g., through shedding/degradation or additional synthesis) was unknown. In this study, I employed the recently established quantitative ESI-MS/MS-MRM analysis (Kongmanas et al., 2010) to demonstrate the changes of SGG levels in male germs cells at various development stages, i.e., in primary spermatocytes, round spermatids, and mature sperm retrieved from the caudal epididymis and vas deferens. My results (Figure 3.15) indicated that the SGG level in pachytene spermatocytes was 2.6 times higher than the corresponding value in spermatids, which in turn was 5.9 times higher than the level in sperm. Although the decrease in SGG level in round spermatids as compared with that in primary spermatocytes is expected, this decrease should be 4 times lower, considering that one pachytene spermatocyte gives rise to four spermatids through meiosis. Since my results showed only a 2.6-fold lower SGG level in round spermatids, this suggested that there may be another round of SGG synthesis in round spermatids. Notably, the surface area of a pachytene spermatocyte is approximately 2.6 times higher than that of a round spermatid (i.e., 706.5 μm^2 and 254.3 μm^2 with cell diameter of 15 and 9 μm, respectively). The additional round of SGG synthesis in round spermatids may therefore be needed for keeping a constant distribution level of SGG on the germ cell surface. Considering that SGG is an ordered lipid (Attar et al., 2000), a similar membrane rigidity may be required to maintain the physiological properties of these two spermatogenic cells. The area of a mature mouse sperm head is about 28 μm^2, based on the estimation that the mouse sperm head is a cone

shape with a radius and length of 1.25 and 7 μm, respectively. The surface area of a mouse sperm head (where SGG is localized) is about 9-fold decreased, as compared with that of a round spermatid, but the SGG level of mouse sperm was only ~6-fold lower than that of the round spermatid. Therefore, the higher density of SGG per area of sperm head would likely reflect a somewhat increased rigidity of the sperm head plasma membrane as compared with the entire plasma membrane of round spermatids. The summary of SGG amounts per cell surface area of primary spermatocyte, round spermatid, and sperm is shown in Table 4.1. SGG is known to localize mainly at the anterior head plasma membrane of sperm, the ZP-binding site (White et al., 2000; Bou Khalil et al., 2006). Based on the roles of SGG as the structural lipid raft component and ZP adhesion molecule, the higher concentration of SGG at the egg-binding site of the sperm surface would be beneficial for the sperm-egg interaction processes.

The remodeling of round spermatids into elongated spermatids occurs in a stepwise manner starting in the adluminal compartment between Sertoli cells in the seminiferous tubules. However, spermatids of elongating steps impregnate their heads into the apical membrane of Sertoli cells. Part of the cellular substance (the so called residual body), likely containing SGG, of the elongated spermatids is then pushed into one side of the posterior region of the spermatid head (i.e., in the same direction of the spermatid tail, but as a separate entity). Sertoli cells then pull off this residual body structure, transforming the elongated spermatids into anatomically developed testicular sperm, which then are ejected into the seminiferous lumen. This phenomenon may explain the reduction of SGG levels in sperm relative to those in round spermatids and implicate Sertoli cells in the handling of SGG in the phagocytosed residual bodies.

Table 4.1: Distribution of SGG per μm^2 in primary spermatocytes, round spermatids, and epididymal/vas deferens sperm

Cell types	Femto mole of SGG per cell	cell surface area (μm^2)	Femto mole of SGG per 1 μm^2
Primary spermatocytes (pSc)	1.912	706.5	2.7×10^{-3}
Round spermatids (RS)	0.712	254.3	2.8×10^{-3}
Caudal epididymal/vas deferens sperm (sp)	0.120	28.0	4.3×10^{-3}

In addition to the SGG-containing residual bodies, apoptotic corpses of testicular germ cells are the other SGG-comprising substances that Sertoli cells phagocytose. Of note is the 50% rate of apoptosis of developing testicular germ cells in normal spermatogenesis (Cheng and Mruk, 2010; Dym, 1994; Huckins, 1978). Therefore, degradation of SGG derived from the phagocytosed apoptotic cells and/or residual bodies would be one of the high responsibility tasks of Sertoli cells. Supporting this postulation, the MS analysis of lipid extracts from Sertoli cells of 20-day-old and 10-week-old mice showed that SGG (C16:0/C16:0; *m/z* 795) was the major sulfolipid found in these cells (Figure 3.16). Moreover, HPTLC analysis and imaging MS results showing the presence of SGG in Sertoli cells of 20-day-old mice but not in 5-day-old animals (where spermatogenesis has not yet occurred) strongly suggested that SGG in Sertoli cells was originated from the SGG-containing germ cell remnants and residual bodies, both phagocytosed by Sertoli cells (Figure 3.16). The finding that the SGG level in Sertoli cells was increased from 0.663 nmole/million cells in 20-day old animals to 1.383 nmole/million cells in 10-week-old mice agrees with the increased numbers of phagocytosed SGG-containing substances that Sertoli cells have to cope with in the older mice (Note that the first round of spermatogenesis has not even completed in 20-day old mice). However, the existence of SGG at these relatively high levels in Sertoli cells of 20-day-old and 10-week old mice indicated that the degradation of SGG did not occur or occurred but not at a high efficiency. However, the first possibility was unlikely, considering that lysosomes of Sertoli cells contained ARSA (Weerachatyanukul et al., 2003) with activities that can be measured in vitro (see below); our *Arsa* KO mouse studies described below also indicated that SGG was a substrate of Sertoli cell lysosomal ARSA. Previous studies from our lab and from the research group of Dr. Arvan L Fluharty (our colleague at UCLA) have shown that ARSA can desulfate SGG pre-solubilized with a detergent or

saposin B *in vitro*, but the desulfation is at a low efficiency (i.e., about 20% of SGG in the reaction mixture within 16 hours at 37°C) (Schenk et al., 2009; Fluharty et al., 1974). These results would explain the existence of SGG in Sertoli cells in 20-day-old and adult mice. Also, it was noted that the SGG level in Sertoli cells of 10-week-old mice was comparable to that in the primary spermatocytes (i.e., 1.383 and 1.912 nmole/million cells, respectively). This finding suggested that a feedback inhibition on the SGG degradation process might take place once there was equilibrium of SGG levels in Sertoli cells and testicular germ cells. This putative inhibition might be an avenue to regulate optimal SGG levels on testicular germ cells.

4.2.2) SGG is a physiological substrate of ARSA in lysosomes of Sertoli cells and its intracellular accumulation in Sertoli cells of *Arsa* null mice leads to a lysosomal storage disorder

We have previously shown that ARSA is localized in the lysosomes of Sertoli cells and the acrosomal granules of spermatogenic cells (Weerachatyanukul et al., 2003). However, my preliminary results showed that ARSA enzymatic activity, assayed *in vitro* by using NCS as an artificial substrate, was much higher in Sertoli cells than in spermatogenic cells (0.138 vs 0.002 units/million cells, respectively). These results suggested that Sertoli cell lysosomal ARSA played an active role in SGG desulfation, likely on the remnants of apoptotic germ cell corpses and residual bodies, both of which are phagocytosed by Sertoli cells. My MS-based SGG quantification indeed revealed that SGG in Sertoli cells of *Arsa* KO mice (8-11 months of age) was ~2.5x higher than that in Sertoli cells of age-matched

wild types (4.400 ± 1.765 and 1.791 ± 0.728 nmole/million cells, respectively), a result indicating that SGG was a substrate of ARSA *in vivo*. Interestingly, a sulfolipid with m/z 778.5 previously identified to be C16:0 SGC (Xu et al., 2011), a known substrate of ARSA (Takahashi and Suzuki, 2012), was also uniquely detected in Sertoli cells of 8- to11-month-old *Arsa* KO mice. In contrast, Sertoli cells of age-matched WT males showed only background levels of SGC, in accordance with our previous report on the lack of a detectable amount of SGC in the mouse testis homogenates (Kongmanas et al., 2010). However, this m/z 778.5 ion peak was not present in sperm from either aging WT or *Arsa* KO mice (Figure 3.33). These findings therefore suggested that C16:0 SGC was synthesized in testicular germ cells, utilizing the same pathway as SGG, and along with SGG, this SGC molecular species was likely reduced in amounts during spermiogenesis and sperm migration through the epididymis. Possibly, the level of C16:0 SGC on epididymal/vas deferens sperm was so minimal that it could not be detected by our ESI-MS/MS. Future experiments are required to determine the levels of C16:0 SGC in testicular germ cells, whether it can be detectable by ESI-MS/MS or not. Regardless, the level of C16:0 SGC in the germ cells must be much lower than that of SGG and when the apoptotic germ cell corpses are phagocytosed into Sertoli cells of WT animals, ARSA and GALC can completely degrade this SGC down to the backbone lipid (ceramide). The postulation that C16:0 SGC is synthesized in testicular germ cells at a level much lower than SGG is supported by the finding that the amount of C16:0 SGC accumulated in Sertoli cells of aging *Arsa* KO mice was only 9% of the SGG (C16:0/C16:0) accumulated (Figure 3.22). At this time, it is not clear why a low amount of SGC has to be synthesized in testicular germ cells. However, the co-presence of a low amount of SGC with SGG in human male germ cells has been documented (Levine et al., 1976).

In the previous section we reported that there was still SGG in the Sertoli cells of pubertal and adult WT mice, suggesting that a certain level of intracellular SGG was not toxic to Sertoli cells. However, when these intracellular SGG amounts rise above a threshold level, Sertoli cells become dysfunctional due to cytotoxicity induced by the accumulated SGG. This statement is based on the apparent aberrancy of Sertoli cell morphology/histology observed in aging *Arsa* KO mice as well as the analogous lysosomal storage disorders observed in other tissues (especially the brain) of human beings and mice that lack enzymes to degrade various glycolipids, including SGC and GC (e.g., MLD, Krabbe's disease). The most apparent aberrant changes in the Sertoli cell morphology of aging *Arsa* KO mice include the swelling of lysosomes (they could be up to 2-3 μm, which are unusually larger than the normal lysosome size (0.1-1 μm) in WT animals) and the accumulation of lipid droplets/globules with sizes significantly larger than those in WT mice (Xu et al., 2011). The former is likely due to the over-storage of SGG in the lysosomes, leading to lysosomal dysfunctions. The increased number and size of lipid droplets/globules may then be a consequence of the inability of the swollen lysosomes in *Arsa* KO mice to allow further entry of SGG. In turn, SGG would remain in the cytoplasm. Its association with saturated tri/di-acylglycerol (see more below) would then result in the increasing formation of lipid droplets/globules of larger sizes. We have also noted that in aging *Arsa* null mice, some Sertoli cells were smaller than usual and dislocation of the nuclei just above the basement membrane did occur in certain Sertoli cells. In the male reproductive system, the lack of β-hexosaminidase (expressed at a high level in epididymis) in the gene targeted null mice (animal models for Tay-Sachs and Sandhoff diseases), resulting in the accumulation of G_{M2} gangliosides. Epididymal epithelial cells of these mice, which are subfertile/infertile at older ages (Trasler et al., 1998), exhibit morphological aberrancies

similar to those observed in Sertoli cells of *Arsa* KO mice as described above. All of these aberrancies are typical of lysosomal storage disorders described in other organs (Cox and Cachon-Gonzalez, 2012), and our studies on aging *Arsa* KO male mice demonstrate for the first time a lysosomal storage disorder in the seminiferous tubules, which is associated with subfertility. This disorder observed in the *Arsa* KO male mice was unlikely to be secondary to the defects of the operation of the hypothalamus-pituitary-testis (HPT) axis for the following reasons. First, the testosterone action (part of the HPT axis) appeared to be functioning in all adult and aging *Arsa* KO male mice, since the weight of epididymis (target organs of testosterone) of these KO mice was similar to that in the age-matched WT mice (Figure 3.14F). Furthermore, the morphology of Leydig cells, which secrete testosterone, of *Arsa* KO male mice of all ages was as normal as that in WT mice. It should also be noted that *Arsa* KO mice have mild MLD phenotype despite the intracellular accumulation of SGC (a known substrate of ARSA) in the brain (Hess et al., 1996; our unpublished data in Appendix Figure 1). Perhaps this mild symptom is due to a better ability of the mouse brain, as compared with the human brain, to cope with the surplus amounts of intracellular SGC, and it is likely that the hypothalamus and pituitary continue to secrete GnRH and FSH/LH. This situation observed in *Arsa* KO mice appears to be different from that manifesting in Twitcher mice, natural mutant mice with defects in the *Galc* gene that is responsible for degalactosylation of GC and GG (Luddi et al., 2005; Tohyama et al., 2000); Twitcher mice, which are animal models of Krabbe's disease in humans, show very obvious neurological disorders and usually die young (Tohyama et al., 2000). Only one Twitcher mouse colony can live up to the onset of spermatogenesis; obviously the Leydig cells of these mutant mice show an apparent morphological aberrancy (Piomboni et al., 2014). The spermatogenic arrest observed in these Twitcher mice could be a combination of the lack of proper levels of

testosterone and LH, as well as FSH, together with the accumulation of GG in the testes (Luddi et al., 2005). The latter putative cause would be analogous to the SGG accumulation in Sertoli cells of *Arsa* KO mice. However, information on the lipid profiles in Sertoli cells (and also their morphology) and in other parts of reproductive system of Twitcher mice is not available.

Any aberrancy in Sertoli cells would lead to their suboptimal functionality, which includes spatial and nutritional support of adjacent developing germ cells in the adluminal compartment and elongating spermatids whose heads are penetrated through the apical membrane as part of the ectoplasmic specialization junctions (Cheng and Mruk, 2010). Abnormal orientation of many spermatid heads impregnated in Sertoli cells, as well as a high number of sperm with abnormal morphology in 8-month-old *Arsa* KO mice (Figures 3.12, 3.13, & 3.19), may reflect defective formation of the apical ectoplasmic specialization in Sertoli cells, a device for anchoring and shaping of the elongated spermatid heads. Furthermore, the phagocytic activity of Sertoli cells of 8-month-old *Arsa* KO mice may be compromised, as shown by a significant increase in apoptotic germ cells detected in the seminiferous tubules of these mice (Figure 3.14C). These abnomalities would have a "domino" effect, resulting in a reduced rate of spermatogenesis. Future research to characterize functional activities, such as secretion of proteins/factors essential to the spermatogenesis (Androgen Binding Protein (ABP), various growth factors (IGF-I/II), lactate and pyruvate) of Sertoli cells in these KO mice, is needed to validate this postulate. In a number of lipid-induced lysosomal storage disorders, toxicity to cells with the intracellular accumulated lipids is attributed to the overproduction of reactive oxygen species (ROS) (Vitner et al., 2010). Therefore, our ongoing research is to determine whether Sertoli cells of

Arsa KO mice (≥ 8 months old) have increased levels of ROS and of proteins involved in ROS production as compared with the age-matched WT animals. Regardless, I hope that the research studies presented in my thesis will stimulate reproductive biologists to invest deep thought into the significance of Sertoli cells in male fertility. To date, assessment of Sertoli cell functionality is not at all a part of male infertility diagnosis.

Being able to characterize the fertility status and lipid profiles of the reproductive system in metachromatic leukodystrophy (MLD) males would be helpful. However, MLD is closely associated with severe neurological/behavioral disorders in humans and true MLD individuals die young or are too sick to engage in sexual activities (Barth et al., 1993). It would be interesting to follow the fecundity status and reproductive physiology of males who are not true MLD patients (carrying less severe *Arsa* mutations) that can live to their reproductive age. I hope that our studies in *Arsa* KO mice will inspire the scientific community to conduct such fertility related studies.

4.2.3) Sperm from aging *Arsa* null mice also have aberrant levels of SGG and reduced fertilizing ability

Sperm that have undergone epididymal maturation have virtually all the machinery necessary for specific binding and penetration of the egg. The initial egg ZP-binding site of capacitated sperm is the APM or the acrosomal region of sperm head plasma membrane (Burkin and Miller, 2000; Kerr et al., 2002). SGG is localized at this site and involved in sperm-ZP binding in two ways. SGG itself has an affinity for the ZP (White et al., 2000; Bou Khalil et al., 2006). Furthermore, as a structural lipid, SGG is important for the

formation of ordered lipid membranes in sperm APM, which can be isolated as DRMs (aka lipid rafts) and APM vesicles. As described in our published articles (Bou Khalil et al., 2006; Kongmanas et al., 2014; Tanphaichitr et al., 2007b), these SGG associated membranes on the sperm head surface are platforms for ZP binding as they contain a number of proteins having direct affinity for the ZP. Therefore, the question of whether SGG levels on mature sperm were altered in *Arsa* KO mice (in particular in animals with ≥ 8 months of age, with reduced fecundity) was addressed.

At first glance, the existence of ARSA at two sites in mature sperm (on the APM as a peripheral plasma membrane protein, and in the acrosome as part of the acrosomal content) gave the impression that SGG levels in sperm may be partly controlled by these two ARSA sources. However, careful analyses of the properties and localization of these ARSA sources eliminated this possibility. Since the sperm chromatin is highly condensed, the transcriptional activity is very low and it is impossible without the presence of endoplasmic reticuli in the sperm. Therefore, acrosomal ARSA is originated from that synthesized in primary spermatocytes. In fact, our unpublished EM immunogold labeling results revealed the presence of ARSA in acrosomal granules in round spermatids (Appendix Figure 6). Acrosomal ARSA is compartmentalized from SGG on the sperm head surface. Furthermore, as indicated above, the activity of ARSA in testicular germ cells was minimal (as compared with that in Sertoli cells). The localization and property of this acrosomal ARSA make it unlikely to be involved in SGG degradation. On the other hand, sperm head surface ARSA is originated from the epididymal lumen. Caudal epididymal epithelial cells secrete ARSA into the lumen, and ARSA, as a peripheral plasma membrane protein, in turn deposits onto the head surface of transit sperm (Weerachatyanukul et al., 2003) through its high affinity for

SGG (K_d = 9 nM) (Carmona et al., 2002b). This SGG binding, however, does not occur at the enzymatically active site pocket of ARSA but likely takes place at a cleft containing a positively charged amino acid (Arg) on the surface of ARSA's 3-D structure (Xu et al., 2012). In fact, sperm surface ARSA can still desulfate a small artificial substrate, NCS, although its activity is very minimal (0.00035 U/1 million sperm). It is not surprising therefore that despite the fact that ARSA and SGG co-exist on the sperm head surface, SGG remains intact with no evidence of GG formation (Carmona et al., 2002b). We have shown that purified ARSA has direct affinity for mouse and pig ZP (Carmona et al., 2002a; Tantibhedyangkul et al., 2002), and that sperm ARSA is involved in sperm-ZP binding (Rattanachaiyanont et al., 2001; Tantibhedyangkul et al., 2002). Considering that ARSA is dually localized on the sperm head surface and in the acrosome, the involvement of the protein in ZP binding is for both acrosome-intact and acrosome-reacting sperm. The fact that ARSA has affinity for mouse ZP3 and ZP2 glycoproteins (Xu et al., 2012), both known to be relevant in interaction with acrosome-intact and acrosome-reacting/reacted sperm, supports the preceding statement. Nonetheless, like a number of other sperm surface proteins with ZP affinity, ARSA was not essential for sperm-ZP binding. Sperm from 5-month-old *Arsa* KO mice showed the same *in vitro* fertilizing ability as sperm from WT mice of the same age (Figure 3.12B) and our natural mating studies revealed that *Arsa* KO males had the same fecundity as WT males up to 5 months of age (Figure 3.12A).

In 5-month-old *Arsa* KO mice, SGG levels of testicular germ cells and mature epididymal/vas deferens sperm were the same as those of age-matched wild types. In contrast, when the KO mice were 8 months old, SGG levels became ~50% of the corresponding WT values for both testicular germ cells and epididymal/vas deferens sperm.

As indicated above, in wild type mice, SGG levels in epididymal/vas deferens sperm decrease to 17% of the levels in testicular germ cells. Since the SGG levels in 8-month-old *Arsa* KO mice was decreased to 50% WT levels in both testicular germ cells and sperm, the SGG reduction process when testicular germ cells develop into sperm was not altered in the *Arsa* KO mice. Note that the *Cgt* and *Cst* expression levels were unchanged in *Arsa* KO mouse testicular germ cells as compared with those of the WT mice, indicating that the reduction of SGG levels in these cells is not due to decreased levels of enzymes for SGG synthesis (Appendix Figure 7). The reduced SGG levels in testicular germ cells and sperm in these *Arsa* KO mice could therefore be explained by the lower rates of SGG biosynthesis in spermatogenic cells due to insufficient amounts of lipid backbones for SGG. The synthesis of SGG starts with the backbone ether lipid, PPG, or other akylacylglycerols (AAG), which can be synthesized de novo by testicular germ cells (primary spermatocytes, round spermatids) (Komljenovic et al., 2009; Rodemer et al., 2003). Also, PPG/AAG generated from the degradation of SGG in Sertoli cells is likely recycled to testicular germ cells for the new round of SGG synthesis. This statement is based on the current concept that lysosomal degradation of lipids serves not only for preventing intracellular accumulation of such lipids that can cause cytotoxicity but also for providing the molecular building blocks for the re-synthesis of the lipids (Dugail, 2014; Platt et al., 2012). Obviously, using the recycling pool of the building blocks for the lipid synthesis would significantly saves cellular energy. Since SGG exists at a substantial amount in testicular germ cells (Tanphaichitr et al., 2003), it is logical that the PPG/AAG produced from the SGG degradation pathway would be recycled for the synthesis purpose. However, the situation of SGG in the seminiferous tubules is unique. The degradation and synthesis of SGG do not occur in the same cell, the former occurs in Sertoli cells and the latter in primary spermatocytes and round spermatids

(adjacent to Sertoli cells). PPG/AAG has to exit the Sertoli cells to enter the cytoplasm of spermatocytes/spermatids. This transport of PPG/AAG should be possible, considering that they are neutral lipids, and our unpublished results also revealed that mouse testicular germ cells could uptake diacylglycerol from the surrounding medium. Regardless, production of PPG/AAG from SGG in Sertoli cells of *Arsa* KO mice would not be possible and the ongoing synthesis of SGG in testicular germ cells had to be totally dependent on the de novo synthesis of PPG/AAG in these cells. In the early part of their lives (up to 5 months), primary spermatocytes and round spermatids of *Arsa* KO mice may be able to increase the de novo synthesis rate of PPG/AAG to make up for the unavailability of the recycling pool. However, when the KO mice became older with more SGG accumulated in their Sertoli cells, the cytotoxicity exerted by the sulfoglycolipid on Sertoli cells would be escalated over the threshold level. This elevated level resulted in Sertoli cell dysfunctions, which included the support of the development of testicular germ cells. At this time, functional activities, including PPG/AAG de novo synthesis in primary spermatocytes and round spermatids, would also be negatively affected, with the observed consequence of a 50% reduction of SGG level in 8-month-old *Arsa* KO mice (Figure 3.17). The model explaining link between SGG synthesis and degradation processes in WT and *Arsa* KO mice (at both 5 and 8 months of age) is shown in Figure 4.2.

When the ZP-binding and fertilizing ability of sperm from 8-month-old *Arsa* KO mice were assessed *in vitro*, these parameters were nearly zero, a strikingly different result from that in the age-matched WT animals (Figure 3.12). The 50% reduction of SGG level may be a partial cause of the minimal fertilizing ability of these ARSA depleted sperm. Reduced SGG amounts would contribute to the decrease in the ZP-binding ability of these

Figure 4.2: A model showing relationship between SGG synthesis and degradation in WT and *Arsa* KO mice (5 and 8 months of age). In testes of normal WT mice, Sertoli cells can degrade SGG from apoptotic germ cells and residual bodies by the enzymatic action of lysosomal ARSA, resulting in GG which is further degraded to PPG by GALC. The generated PPG may be recycled to new generations of testicular germ cells (TGCs), mainly at the stage of pachytene primary spermatocytes (pSc), for new round of SGG synthesis. Moreover, the pSc would have PPG from its de novo synthesis. In *Arsa* KO mice, Sertoli cells fail to degrade SGG leading to accumulation of SGG in the lysosomes, which then become swollen, a phenomenon typical of a lysosomal storage disorder. In 5-month-old *Arsa* KO mice, Sertoli cells can still function in maintaining normal spermatogenesis although SGG accumulation is already observed in their Sertoli cells. Despite of no PPG recycling, the SGG levels in TGCs of 5-month-old *Arsa* KO mice are also unaffected and this normal SGG level may be attributed to the compensation of PPG de novo synthesis (possibly in the pSc) of these mice. In 8-month-old *Arsa* KO mice, SGG accumulation becomes more pronounced and this may result in cytotoxicity and subsequent decrease in functionality of Sertoli cells, including reduced ability to phagocytose apoptotic germ cells and to support development of germ cells in the adluminal compartment. The cytotoxicity of accumulated SGG in Sertoli cells of 8-month old *Arsa* KO mice may also lead to the observed displacement of the Sertoli cell nucleus. The SGG levels in TGCs of 8-month-old *Arsa* KO mice are decreased to 50% of the wild type values and this reduction in SGG level may be a result from the insufficient de novo synthesis of PPG in pSC together with the lack of recycling PPG pool from Sertoli cells.

Abbreviations: BTB = blood-testis barrier, SG = spermatogonium, lSc = leptotene primary spermatocyte, pSC = pachytene primary spermatocyte, RS = round spermatid, ES = elongated spermatid. Ly = lysosome, N = nucleus, Rb = residual body, SGG = sulfogalactosylglycerolipid, GG = galactosylglycerolipid, PPG = palmitylpalmitoylglycerol, CGT = ceramide galactosyltransferase, CST = cerebroside sulfotransferase, ARSA = arylsulfatase, GALC = galactosylceramidase.

Figure 4.2

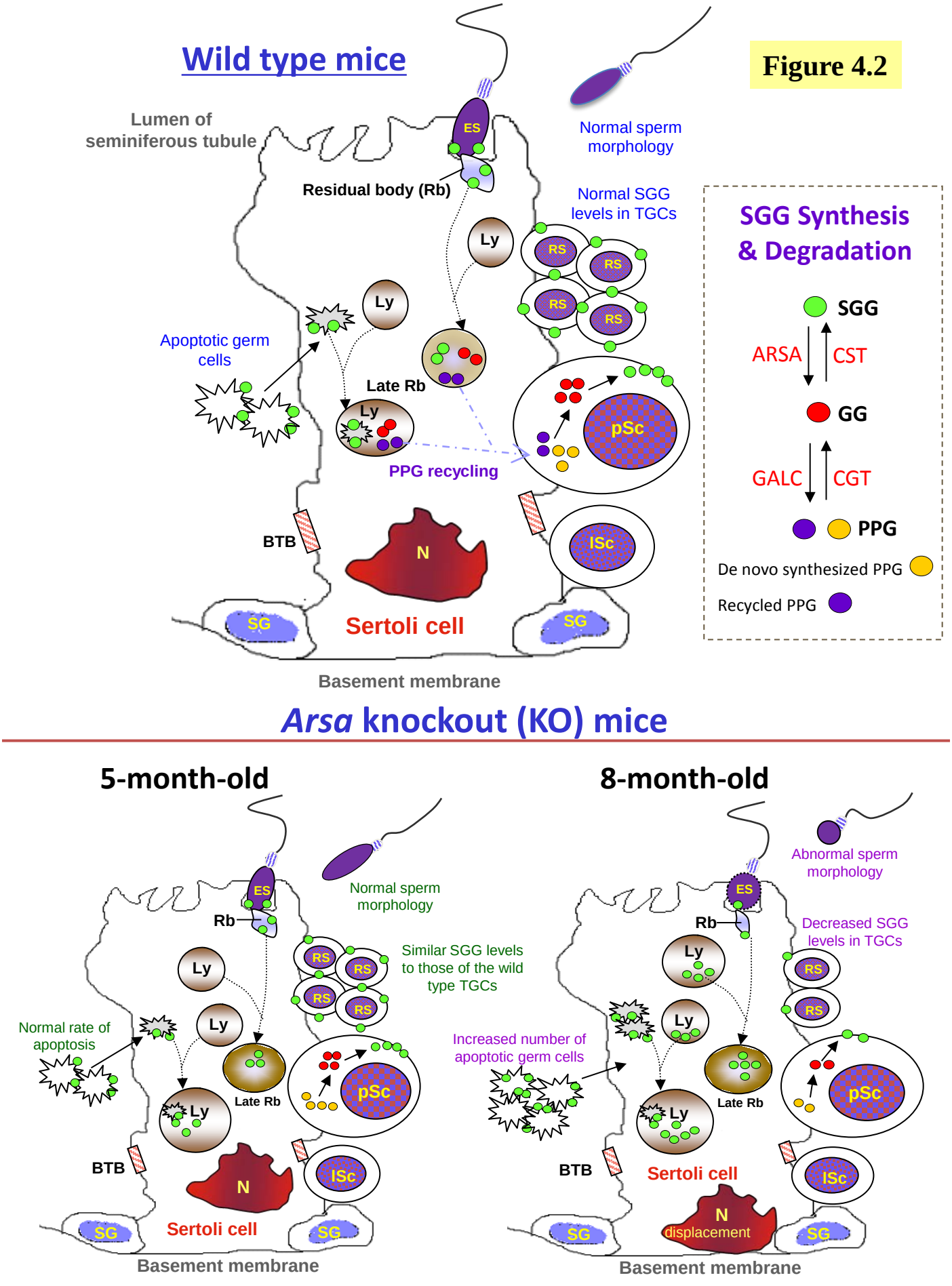
Wild type mice
Lumen of seminiferous tubule
ES
Normal sperm morphology
Residual body (Rb)
Normal SGG levels in TGCs
Ly
RS
Apoptotic germ cells
Late Rb
pSc
PPG recycling
BTB
N
ISc
SG
Sertoli cell
Basement membrane
SGG Synthesis & Degradation
SGG
ARSA
CST
GG
GALC
CGT
PPG
De novo synthesized PPG
Recycled PPG
Arsa knockout (KO) mice
5-month-old
Rb
Similar SGG levels to those of the wild type TGCs
Normal rate of apoptosis
Sertoli cell
8-month-old
Abnormal sperm morphology
Decreased SGG levels in TGCs
Increased number of apoptotic germ cells
N displacement

sperm, since SGG has a direct affinity for ZP. However, the more drastic decrease in the sperm fertilizing ability in these aging KO mice needs additional explanation. Besides its ZP adhesion property, SGG has a structural role in the formation of ordered lipid membranes (sperm lipid rafts, APM vesicles), which house a number of ZP-binding proteins. The 50% decrease in SGG level may negatively impact the formation of these ordered membranes in a significant manner; ZP-binding proteins may not be recruited to stay together as high molecular weight complexes, which I have shown in pig sperm (Kongmanas et al., 2014), to be the fundamental units on the sperm head surface in ZP binding. Results from ongoing proteomic analyses and lipid raft/APM characterizations of sperm from *Arsa* KO mice may give a better understanding of how the drastic loss of their fertilizing ability occurs. In addition, I have demonstrated that the lipid profiles from sperm of these aging *Arsa* KO mice were dissimilar from those in the WT counterpart (Figures 3.33-3.37). One such change is the increase in cholesterol sulfate, which may cause retardation of sperm capacitation (see more below) and thus contribute to the minimal sperm fertilizing ability in these KO animals. Whether changes of other lipid profiles in 8-month-old *Arsa* KO mice were closely associated with a decrease in SGG level is a matter for further investigation. Since SGG is an ordered lipid, the decrease in its level in testicular germ cells may also have an impact on the formation of a proper head shape of testicular sperm during spermiogenesis, resulting in the observed increase in the number of sperm with abnormal morphology (in particular in the head) (Figures 3.12C & 3.13C). This abnormality would also attribute to the lower fertilization rate of sperm from older *Arsa* KO mice.

The decrease in fecundity of aging *Arsa* KO mice was observed in our natural mating study using WT females paired with either *Arsa* KO males or WT males for a period of 7

months (Figure 3.12A). At 8 months of age, the accumulated pups produced by *Arsa* KO males were ~65% of those sired by WT males. This decrease was much less than that observed for the in vitro fertilizing ability of sperm retrieved from 8-month-old *Arsa* KO mice. This striking difference may be simply explained by the fact that embryos developed from eggs fertilized by *Arsa* null sperm progressed in their development at a normal rate and the number of embryos was enough to sustain ongoing fecundity at a 65% rate. Alternatively, the sperm fertilizing ability of *Arsa* KO mice may be corrected in vivo by secretions from uterine epithelial cells, a situation demonstrated in *Prss21* null mice (Yamashita et al., 2008). It remains to be seen whether the uterine secretion in a woman with a defined menstrual cycle has these correcting factors for sperm with reduced fertilizing ability. Also, as one egg is ovulated at a time in humans, even a slight decrease in sperm fertilizing ability may result in a no pregnancy outcome.

4.2.4) Disrupted SGG homeostasis leads to changes in other lipids and subsequent dysfunction of Sertoli cells of *Arsa* knockout mice

In addition to the expected accumulation of SGG and SGC in Sertoli cells of 8- to11-month-old *Arsa* KO mice, my results indicated that a number of TAG and CE molecular species, both being neutral lipids known as components of lipid droplets, showed a trend to be increased, as compared with Sertoli cells of age-matched WT males (Figures 3.29 & 3.31). The increasing trend of these neutral lipids corroborates increases in the size and number of lipid droplets in Sertoli cells of the KO animals (Figure 3.19A), and these increases may reflect an elevated amount of SGG accumulated in the cytoplasm in these KO

mice, as discussed above. It should be mentioned here that lipid droplets exist in functioning Sertoli cells in WT animals and, as in other somatic cells, they are intracellular reservoirs enriched in CE and TAGs, which can be "recycled" into cholesterol, phospholipids and free fatty acids. The first two lipids would be structurally relevant (i.e., in formation of new membranes), whereas the free fatty acids would be the source of energy. Lipid droplets in Sertoli cells provide important nutritional support in this recycling process not only to themselves but also to the adjacent developing germ cells (Keber et al., 2013). Early and recent work indicates that lipid droplets are formed inside the cytoplasm of Sertoli cells after the phagocytosis of apoptotic germ cells and residual bodies (Kerr and De Kretser, 1975; Wang et al., 2006; Xiong et al., 2009). A time period is required following the phagocytic event for the formation of lipid droplets, indicating that the phagocytosed cellular remnants have to be first molecularly degraded/processed by Sertoli cell lysosomes. A number of metabolites (such as PPG), which are generated from the degradation processes and can be recycled for the new molecular syntheses, may then be shuttled to the synthesis sites, including adjacent spermatogenic cells and the cytosol of Sertoli cells themselves. The extra metabolites (including TAGs and CEs) would then be stored as lipid droplets for future demand by both germ cells and Sertoli cells. Previous findings suggest that lipid components in the lipid droplets are transported to spermatogenic cells (Gillot et al., 2005; Kerr and De Kretser, 1975). This shuttling event would likely regulate the size of lipid droplets in WT animals to be constant (in mice, the size of the majority of lipid droplets is mainly ≤ 1 μm, Wang et al., 2006). However, in the case of Sertoli cells of aging *Arsa* KO mice, lipid droplets enlarged and increased in number, suggesting that metabolite/lipid transport to the molecular synthesis sites may be hindered. Eventually, the functionality and health of spermatogenic cells of these *Arsa* KO mice would be at a sub-optimum state due to

the insufficiency of the recycling metabolites from Sertoli cells. In addition, Sertoli cells from these KO mice would suffer from a lysosomal storage disorder and would secrete at a reduced rate proteins (e.g., growth factors) and metabolites (e.g., pyruvate, lactate) necessary for spermatogenic cell development. Under these suboptimum conditions, autophagy may occur in these Sertoli cells and explain why certain Sertoli cells from aging *Arsa* KO mice became smaller. However, the breakdown of lipid droplets, a phenomenon occurring as part of autophagy following their sequestration into autophagosomes and delivery to lysosomes for molecular degradation is likely to be futile in Sertoli cells of these KO mice due to the dysfunction of the lysosomes (Dugail, 2014; Singh et al., 2009). This failure may lead to apoptosis/necrosis of Sertoli cells in the aging *Arsa* KO mice (8-11 months of age) and explain why a significantly lower number of Sertoli cells were isolated from these mice as compared with those obtained from the age-matched WT animals (Figure 3.20). Nonetheless, little information on the mechanisms of autophagy and its relationship with lyososomal functions in Sertoli cells is available and further investigation on this topic is required for a better understanding of these processes.

All identified PC and SM species seemed to have lower amounts in *Arsa* KO Sertoli cells, as compared with those of the WT Sertoli cell samples. However, the lyso PC with C16:0 showed a statistically significant decrease in its amount in *Arsa* KO Sertoli cells. *In vivo*, lysoPC is produced by the enzymatic action of phospholipase A_2 (PLA_2), which hydrolyzes the fatty acyl chain at the *sn*-2 position of PC. In somatic tissues and cells, PLA_2 is found to localize inside the cell or as a secreted enzyme in the surrounding environment. In macrophages, PLA_2 is localized in the lysosomes and its high activity is presumably responsible in degrading phospholipids of the phagocytosed materials into the lyso forms

(Abe et al., 2004). The enzymatic activity of PLA_2 in Sertoli cells has been described (Janini et al., 1994; Meroni et al., 2003). Although further verification for the existence of this enzyme in the Sertoli cell lysosomes is required, it is tempting to speculate that Sertoli cells depend on their lysosomal PLA2 to hydrolyze phospholipids to the lyso forms as part of their phagocytic duty, so that the phospholipid building blocks can be recycled for the new round of synthesis (as in my argument of the SGG degradation). In the case of *Arsa* KO mouse Sertoli cells, the intracellular accumulation of SGG might lead to a decreased activity of PLA_2 and consequently the observed reduced amounts of lysoPC (C16:0) (Figure 3.25B).

Total cholesterol (including CE and free cholesterol) in Sertoli cells of aging *Arsa* KO mice was significantly decreased to 80% of the WT level. However, a slight increase in CEs of the KO Sertoli cells (~10-20% higher than the WT values) indicated that the level of free cholesterol in these cells was decreased somewhat more than 20%, as compared with the WT level. This reduction could reflect a decrease in the de novo synthesis and/or the transport of cholesterol from an external source (Keber et al., 2013). For the former possibility, the decreased synthesis may include that of cholesterol precursors, one of which, the so called T-MAS (testis meiosis activating sterol, 4,4-dimethyl-5α -cholest-8,24-diene-3β-ol), is relevant for meiosis (Keber et al., 2013). The concentration of T-MAS required for meiosis stimulation may be relatively small and a slight decrease in its concentration may have a significant impact on the meiotic steps, resulting in the reduced rate of spermatogenesis as observed in aging *Arsa* KO mice.

4.2.5) Altered levels of lipids may be the cause of abnormal morphology and reduced fertilizing ability of *Arsa* knockout mouse sperm

Besides the 50% decrease in sperm SGG level, a significant increase in cholesterol sulfate was detected in sperm from 8- to 11-month-old *Arsa* KO mice (Figure 3.34). As mentioned above, the decrease of SGG levels in spermatogenic cells and sperm is likely due to the reduced supply of PPG recycled from the Sertoli cells. The lack of SGG's lipid precursor would result in an over-supply of the sulfate donor (PAPS-3'-phosphoadenosine-5'-phosphosulfate), and its possible shunting towards the synthesis of cholesterol sulfate in testicular germ cells and its eventual existence in sperm of *Arsa* KO mice. The shunting of sulfate donor to the cholesterol sulfate synthesis pathway may be a mechanism whereby *Arsa* KO male germ cells attempt to compensate for the loss of SGG, a major sulfolipid that is essential for male fertility. An analogous phenomenon was observed in *Cgt* knockout mice which could not produce SGC; in these mice, the levels of alternative sulfolipids (i.e., lactosylceramide II^3-sulfate, gangliotetraosylceramide II^3, IV^3-*bis*-sulfate) were increased in the kidney, which appeared to function normally (Tadano-Aritomi et al., 2000). The enzymes responsible for cholesterol sulfate synthesis (i.e., steroid sulfotransferase) and degradation (i.e., steroid sulfatase, aka cholesterol sulfate sulfatase or arylsulfatase C) have previously been characterized in the testis (Cui and Iwamori, 1997; Roberts, 1987). My result showing no accumulation of cholesterol sulfate in *Arsa* KO Sertoli cells suggested that steroid sulfatase was in fact present and active in these cells.

The presence of cholesterol sulfate and desmosterol sulfate has previously been shown in the sperm of various species, including human and hamster (Legault et al., 1979; Sion et al., 2001). Previous studies have revealed that very low concentrations of sterol

sulfate can inhibit the egg penetration ability of hamster sperm (Bleau et al., 1975). Also, sperm treated with cholesterol sulfate showed deposition of cholesterol sulfate onto their head surface (Langlais et al., 1981), and cholesterol sulfate treated sperm had a lower ability to fertilize eggs as compared with the control untreated sperm (Fayer-Hasken et al., 1987). Cholesterol sulfate is generally assumed to affect sperm fertilizing ability by retarding the sperm capacitation process (Langlais et al., 1988), and cholesterol sulfate has been used to inhibit capacitation *in vitro* (by adding it into a suspension of sperm in a capacitating medium) (Nixon et al., 2011). However, my study shown herein demonstrated for the first time that the signature signaling event of sperm capacitation – the increase in sperm tyrosine phosphorylation- was retarded in sperm containing an increased level of cholesterol sulfate (i.e., sperm from aging *Arsa* KO mice, Figure 3.39) and WT sperm that were treated with cholesterol sulfate *in vitro*. A consequence of the retardation of sperm capacitation in 8- to 11-month-old *Arsa* KO mice was the minimal ability of these sperm to bind to the ZP and the nearly zero rate to fertilize the eggs in vitro (Figure 3.12). These results suggested that the increase in cholesterol sulfate was another factor contributing to the reduced fecundity of *Arsa* KO males. Further investigation is required to discern the molecular mechanisms through which cholesterol sulfate inhibits sperm capacitation. However, since the level of cholesterol sulfate in mouse sperm is very low (8 pmole/million sperm of WT mice) and even though there was ~100% increase in *Arsa* KO sperm, the increased level of this lipid was still very small. Therefore, the retardation of capacitation in *Arsa* KO sperm is unlikely to be from the membrane stabilization property of cholesterol sulfate. It is possible that cholesterol sulfate inhibits the signaling events relevant to sperm capacitation. One of the known properties of cholesterol sulfate is its inhibition of serine protease activity, including

acrosin, which is known for its role in fertilization (Burck and Zimmerman, 1980; Yamagata et al., 1998).

An increase in the number of sperm with abnormal morphology is obvious in *Arsa* KO males at 8 months of age or older (Figures 3.12C and 3.13C). This observation suggests that structural lipid contents in these morphologically and functionally defective sperm are altered. Since SGG is a structural and ordered lipid constituting 10 mole% of total lipids in sperm and since it is localized in clusters in the sperm head anterior, it may play a role in shaping the sperm head during spermiogenesis. Therefore, the significant decrease of the SGG level to 50% of the WT value in testicular germ cells of *Arsa* KO mice could be a cause of abnormal sperm head formation. Moreover, PC and SM, other major structural lipid components of sperm plasma membrane, also appeared at lower levels (50-80% of the WT values) in sperm of *Arsa* KO mice (Figure 3.35). These reduced levels might reflect a decreased ability of Sertoli cells to shuttle lipids such as diacylglycerol, alkylacylglycerol, free fatty acids and TAGs to adjacent testicular germ cells (due to the presence of "abnormal" lipid droplets and their sub-optimum functionality as discussed above). Although the overall cholesterol levels in *Arsa* KO and WT sperm showed no significant difference (Figure 3.38), the drastic change in the overall composition of major lipids (i.e., lower amounts of SGG and phospholipids) in *Arsa* KO mouse sperm would affect the overall plasma membrane biophysical property, resulting in abnormal morphology and dissociation between sperm head and tail. It is also known that SGG interacts with saturated phospholipids and cholesterol for the formation of sperm lipid raft microdomains. Altered levels of these lipids in *Arsa* KO sperm may therefore affect the formation of lipid rafts

("APM vesicle" domains), which house a number of ZP-binding proteins, resulting in decreased sperm fertilizing ability.

Like PCs, the level of lysoPC with C16:0 was significantly reduced in caudal epididymal/vas deferens sperm of the aging *Arsa* KO mice (to 25% of the WT sperm value). This decrease may be a consequence of the lower levels of the precursor PCs in these ARSA depleted sperm (as described above). In addition, the activity of PLA_2 present in the epididymal fluid may be compromised in aging *Arsa* KO mice, leading to a lower production of lysophospholipids and a further decrease in the lysoPC (C16:0) level. In fact, the role of PLA_2 in epididymal fluid in lipid remodeling during sperm maturation has been described (Sato et al., 2010). Lysophospholipids are fusogenic and they will thus accelerate fusion events during sperm-egg interaction, i.e., the acrosome reaction and sperm-egg plasma membrane fusion (Florman and Duibella, 2006). My observation that sperm from aging *Arsa* KO mice had a markedly decreased ability to fertilize eggs might therefore be partly attributed to the reduced level of lysoPC in these sperm.

4.3 Conclusions

Capacitation is a post-synthesis maturation process that allows sperm to gain their maximal capacity in ZP binding. This process involves reorganization of the sperm surface, especially on the APM, the initial ZP-binding site. The results of this study revealed a new mechanism on how sperm gain full fertilizing ability during capacitation. This mechanism is based on the movement of proteins with significant functions in sperm-ZP interaction from the acrosome to the sperm head surface at the APM region, and the recruitment of these acrosomal proteins as part of the APM HMW protein complexes with ZP affinity. Our lipid

of interest, SGG, is also an integral component of the ZP-binding platforms on the APM. Levels of SGG on the sperm are likely important for the sperm function. In this study using *Arsa* KO mice the physiological significance of SGG homeostasis in male fertility is revealed. SGG is shown for the first time as a natural substrate for ARSA desulfation activity. Lack of ARSA causes SGG accumulation in Sertoli cells, leading to lysosomal storage disorder in these cells. The buildup of SGG in Sertoli cells over time leads to Sertoli cell dysfunction and the production of sperm with abnormal morphology and decreased SGG levels. The decrease in sperm SGG level may be due to a lack of the recycling pool of PPG (SGG's lipid precursor) generated in Sertoli cells through the SGG degradation pathway. Disruption of SGG homeostasis also leads to aberrant levels of other lipids, including PC, SM, lysoPC, TAG, CE, and cholesterol sulfate in aging *Arsa* KO mice (≥ 8 months of age) and the usual changes in levels of these lipids may be another factor attributed to subfertility in these *Arsa* KO mice. Overall, these findings indicated that homeostasis of SGG is important for male fertility.

4.4 Scientific Significance and Future Directions

The results from proteomic characterization of APM vesicles presented in this study have provided a better understanding of the molecular mechanisms underlying capacitation and sperm-ZP interaction. The presence of acrosomal proteins with ZP affinity on Cap sperm APM should be used as a sperm capacitation bio-index. In addition, instead of targeting a single protein, a conglomerate of APM proteins with their proper balances as HMW complexes should be used as biomarkers of sperm fertilizing ability. Significantly,

the proteins found in the ZP-binding HMW complexes of pig sperm APM are known for their presence in human sperm, suggesting their potential application for clinical analysis of human sperm function. However, prior to potential application of this finding into clinical analysis, we have to further prove whether ZP-binding protein complexes are formed on capacitated human sperm APM. Therefore, the next step is to characterize the ZP-binding protein complex formation on human sperm APM before and after capacitation. Nitrogen cavitation will first be optimized for the specific isolation of human sperm APM vesicles. Overall protein profiles of APM vesicles isolated from Non-cap and Cap human sperm will be quantitatively compared using stable-isotope dimethyl labeling and LC-MS/MS analyses. The HMW protein complexes isolated from human sperm APM samples separated by BN-PAGE will be subjected to far western blotting with recombinant human ZP3 (sperm receptors, already provided to us by Dr. Jeffrey Harris, Zonagen) for the detection of human sperm APM proteins with ZP affinity. We anticipate that proteins relevant to human fertility will be revealed. The findings from our *Arsa* KO mouse study also demonstrate that disruption of SGG homeostasis is correlated with a decline in male fertility. Levels of sperm SGG are another promising bio-index for male fertility. Aberrant levels of SGG in sperm may also reflect abnormal functions of Sertoli cells; therefore, determining changes in sperm SGG levels should be considered as a new approach for diagnosis of male infertility and/or subfertility. Quantifying SGG in sperm samples from infertile and fertile men is the first step towards the use of SGG levels for sperm fertilizing ability assessment in clinical application.

The development of non-hormonal contraceptives with fewer systemic side effects than those of the widely used birth control pills is also needed. The better understanding of

the molecular mechanisms of mammalian sperm-ZP interaction and SGG functions provided in this study is useful for this development. The use of antibodies/inhibitors generated against a group of ZP-binding molecules should effectively interfere with sperm-egg binding. Alternatively, since SGG is the male germ cell specific glycolipid with significance in male fertility, non-hormonal contraceptives can also be developed based on SGG functions. Moreover, since SGG can bind to gp120, a surface HIV glycoprotein (Gadella et al., 1998), the use of specific antibodies/inhibitors to mask or interfere with SGG functions may also help in preventing HIV infection.

CONTRIBUTION STATEMENT

The mating study and gamete functional assays in the experiments of figures 3.12A and B were performed by Dr. Hongbin Xu with the help from me. The histological analysis shown in figure 3.14A and analysis of apoptotic cells on testis sections by TUNEL staining shown in figure 3.14C were performed by Dr. Hongbin Xu. The profile analysis of seminiferous tubules shown in figure 3.14B was performed by Dr. Charles E. Smith, McGill University. Isolation of pure male germ cell populations used in experiment of figure 3.15 was performed by Dr. Stuart Moss, University of Pennsylvania. Imaging mass spectrometry in experiment of figure 3.16B was performed by Dr. Naoko Goto-Inoue, Hamamatsu University, Japan. The flow cytometric analyses of SGG in mixed testicular germ cell populations in the experiment of figure 3.17C were performed by Dr. Hongbin Xu. The indirect immunofluorescence experiment of figure 3.18 was performed by Dr. Suraj Kadunganattil. The electron microscopic analysis in the experiment of figure 3.19 was performed by Dr. Louis Hermo, McGill University. The Sertoli cells used in this study were isolated and cultured by Dr. Arpornrad Sae-wu with the help from me. The quantitative proteomic analyses of APM proteins and components of HMW protein complexes were performed by Dr. Mark Baker, University of New Castle, Australia. The gel-based proteomic analyses of APM proteins were performed by Mr. Puneet Souda and Dr. Julian Whitelegge at Pasarow Mass Spectrometry Laboratory, University of California, Los Angeles (UCLA), USA. However, I have prepared all the protein samples and mined all the data generated by proteomic analyses. All MS-based lipid analyses of testicular germ cells, Sertoli cells and sperm from wild type and *Arsa* knockout mice were performed by me under the supervision of Dr. Kym F. Faull at the Pasarow Mass Spectrometry Laboratory, University of California, Los Angeles, USA.

REFERENCES

Abe, A., Hiraoka, M., Wild, S., Wilcoxen, S.E., Paine, R., 3rd, and Shayman, J.A. (2004). Lysosomal phospholipase A2 is selectively expressed in alveolar macrophages. The Journal of biological chemistry *279*, 42605-42611.

Ahn, V.E., Faull, K.F., Whitelegge, J.P., Fluharty, A.L., and Prive, G.G. (2003). Crystal structure of saposin B reveals a dimeric shell for lipid binding. Proceedings of the National Academy of Sciences of the United States of America *100*, 38-43.

Ahnonkitpanit, V., White, D., Suwajanakorn, S., Kan, F.W., Namking, M., Wells, G., Kamolvarin, N., and Tanphaichitr, N. (1999). Role of egg sulfolipidimmobilizing protein 1 on mouse sperm-egg plasma membrane binding. Biology of reproduction *61*, 749-756.

Ahuja, K.K., and Gilburt, D.J. (1985). Involvement of sperm sulphatases in early sperm-zona interactions in the hamster. Journal of cell science *78*, 247-261.

Aitken, R.J. (1995). Free radicals, lipid peroxidation and sperm function. Reproduction, fertility, and development *7*, 659-668.

Aitken, R.J., and Baker, M.A. (2008). The role of proteomics in understanding sperm cell biology. International journal of andrology *31*, 295-302.

Aitken, R.J., and Nixon, B. (2013). Sperm capacitation: a distant landscape glimpsed but unexplored. Molecular human reproduction *19*, 785-793.

Alberts, B., Johnson, A., Lewis, J., Raff, M., Roberts, K., and Walter, P. (2002). Molecular Biology of the Cell, Vol 4 (New York: Garland).

Alvarez, J.G., Storey, B.T., Hemling, M.L., and Grob, R.L. (1990). High-resolution proton nuclear magnetic resonance characterization of seminolipid from bovine spermatozoa. Journal of lipid research *31*, 1073-1081.

Alves, M.G., Rato, L., Carvalho, R.A., Moreira, P.I., Socorro, S., and Oliveira, P.F. (2013). Hormonal control of Sertoli cell metabolism regulates spermatogenesis. Cellular and molecular life sciences : CMLS *70*, 777-793.

Anakwe, O.O., Sharma, S., Hardy, D.M., and Gerton, G.L. (1991). Guinea pig proacrosin is synthesized principally by round spermatids and contains O-linked as well as N-linked oligosaccharide side chains. Molecular reproduction and development *29*, 172-179.

Arcelay, E., Salicioni, A.M., Wertheimer, E., and Visconti, P.E. (2008). Identification of proteins undergoing tyrosine phosphorylation during mouse sperm capacitation. The International journal of developmental biology *52*, 463-472.

Argraves, W.S., and Morales, C.R. (2004). Immunolocalization of cubilin, megalin, apolipoprotein J, and apolipoprotein A-I in the uterus and oviduct. Molecular reproduction and development *69*, 419-427.

Arvanitis, D.N., Min, W., Gong, Y., Heng, Y.M., and Boggs, J.M. (2005). Two types of detergent-insoluble, glycosphingolipid/cholesterol-rich membrane domains from isolated myelin. Journal of neurochemistry *94*, 1696-1710.

Asquith, K.L., Baleato, R.M., McLaughlin, E.A., Nixon, B., and Aitken, R.J. (2004). Tyrosine phosphorylation activates surface chaperones facilitating sperm-zona recognition. Journal of cell science *117*, 3645-3657.

Attar, M., Kates, M., Bou Khalil, M., Carrier, D., Wong, P.T., and Tanphaichitr, N. (2000). A Fourier-transform infrared study of the interaction between germ-cell specific sulfogalactosylglycerolipid and dimyristoylglycerophosphocholine. Chemistry and physics of lipids *106*, 101-114.

Attar, M., Wong, P.T., Kates, M., Carrier, D., Jaklis, P., and Tanphaichitr, N. (1998). Interaction between sulfogalactosylceramide and dimyristoylphosphatidylcholine increases the orientational fluctuation of their lipid hydrocarbon chains. Chemistry and physics of lipids *94*, 227-238.

Auharek, S.A., Avelar, G.F., Lara, N.L., Sharpe, R.M., and Franca, L.R. (2011). Sertoli cell numbers and spermatogenic efficiency are increased in inducible nitric oxide synthase mutant mice. International journal of andrology *34*, e621-629.

Austin, C.R. (1951). Observations on the penetration of the sperm in the mammalian egg. Australian journal of scientific research Ser B: Biological sciences *4*, 581-596.
Austin, C.R. (1952). The capacitation of the mammalian sperm. Nature *170*, 326.

Avella, M.A., Baibakov, B., and Dean, J. (2014). A single domain of the ZP2 zona pellucida protein mediates gamete recognition in mice and humans. The Journal of cell biology *205*, 801-809.

Avella, M.A., and Dean, J. (2011). Fertilization with acrosome-reacted mouse sperm: implications for the site of exocytosis. Proceedings of the National Academy of Sciences of the United States of America *108*, 19843-19844.

Baba, D., Kashiwabara, S., Honda, A., Yamagata, K., Wu, Q., Ikawa, M., Okabe, M., and Baba, T. (2002). Mouse sperm lacking cell surface hyaluronidase PH-20 can pass through the layer of cumulus cells and fertilize the egg. The Journal of biological chemistry *277*, 30310-30314.

Baba, T., Azuma, S., Kashiwabara, S., and Toyoda, Y. (1994a). Sperm from mice carrying a targeted mutation of the acrosin gene can penetrate the oocyte zona pellucida and effect fertilization. The Journal of biological chemistry *269*, 31845-31849.

Baba, T., Kashiwabara, S., Watanabe, K., Itoh, H., Michikawa, Y., Kimura, K., Takada, M., Fukamizu, A., and Arai, Y. (1989). Activation and maturation mechanisms of boar acrosin zymogen based on the deduced primary structure. The Journal of biological chemistry *264*, 11920-11927.

Baba, T., Niida, Y., Michikawa, Y., Kashiwabara, S., Kodaira, K., Takenaka, M., Kohno, N., Gerton, G.L., and Arai, Y. (1994b). An acrosomal protein, sp32, in mammalian sperm is a binding protein specific for two proacrosins and an acrosin intermediate. The Journal of biological chemistry *269*, 10133-10140.

Baker, M.A., Naumovski, N., Hetherington, L., Weinberg, A., Velkov, T., and Aitken, R.J. (2013). Head and flagella subcompartmental proteomic analysis of human spermatozoa. Proteomics *13*, 61-74.

Baker, M.A., Nixon, B., Naumovski, N., and Aitken, R.J. (2012). Proteomic insights into the maturation and capacitation of mammalian spermatozoa. Systems biology in reproductive medicine *58*, 211-217.

Baker, M.A., Witherdin, R., Hetherington, L., Cunningham-Smith, K., and Aitken, R.J. (2005). Identification of post-translational modifications that occur during sperm maturation using difference in two-dimensional gel electrophoresis. Proteomics *5*, 1003-1012.

Baldi, E., Casano, R., Falsetti, C., Krausz, C., Maggi, M., and Forti, G. (1991). Intracellular calcium accumulation and responsiveness to progesterone in capacitating human spermatozoa. Journal of andrology *12*, 323-330.

Barros, C., Capote, C., Perez, C., Crosby, J.A., Becker, M.I., and De Ioannes, A. (1992). Immunodetection of acrosin during the acrosome reaction of hamster, guinea-pig and human spermatozoa. Biological research *25*, 31-40.

Barth, M.L., Fensom, A., and Harris, A. (1993). Prevalence of common mutations in the arylsulphatase A gene in metachromatic leukodystrophy patients diagnosed in Britain. Human genetics *91*, 73-77.

Battistone, M.A., Alvau, A., Salicioni, A.M., Visconti, P.E., Da Ros, V.G., and Cuasnicu, P.S. (2014). Evidence for the involvement of proline-rich tyrosine kinase 2 in tyrosine phosphorylation downstream of protein kinase A activation during human sperm capacitation. Molecular human reproduction *20*, 1054-1066.

Baum, H., Dodgson, K.S., and Spencer, B. (1959). The assay of arylsulphatases A and B in human urine. Clinica chimica acta; international journal of clinical chemistry *4*, 453-455.

Bavister, B.D. (1973). Capacitation of golden hamster spermatozoa during incubation in culture medium. Journal of reproduction and fertility *35*, 161-163.

Bellve, A.R. (1979). Purification, culture, and fractionation of spermatogenic cells. In Guide to Techniques in Mouse Development, P.M. Wassarman, ed. (San Diego, CA: Academic Press, Inc.), pp. 84-112.

Berger, T. (1990). Pisum sativum agglutinin used as an acrosomal stain of porcine and caprine sperm. Theriogenology *33*, 689-695.

Berger, T., Turner, K.O., Meizel, S., and Hedrick, J.L. (1989). Zona pellucida-induced acrosome reaction in boar sperm. Biology of reproduction *40*, 525-530.

Bi, M., Hickox, J.R., Winfrey, V.P., Olson, G.E., and Hardy, D.M. (2003). Processing, localization and binding activity of zonadhesin suggest a function in sperm adhesion to the zona pellucida during exocytosis of the acrosome. The Biochemical journal *375*, 477-488.

Bianchi, E., Doe, B., Goulding, D., and Wright, G.J. (2014). Juno is the egg Izumo receptor and is essential for mammalian fertilization. Nature *508*, 483-487.

Bleau, G., Vandenheuvel, W.J., Andersen, O.F., and Gwatkin, R.B. (1975). Desmosteryl sulphate of hamster spermatozoa, a potent inhibitor of capacitation in vitro. Journal of reproduction and fertility *43*, 175-178.

Bleil, J.D., and Wassarman, P.M. (1980). Structure and function of the zona pellucida: identification and characterization of the proteins of the mouse oocyte's zona pellucida. Developmental biology *76*, 185-202.

Bleil, J.D., and Wassarman, P.M. (1990). Identification of a ZP3-binding protein on acrosome-intact mouse sperm by photoaffinity crosslinking. Proceedings of the National Academy of Sciences of the United States of America *87*, 5563-5567.

Bligh, E.G., and Dyer, W.J. (1959). A rapid method of total lipid extraction and purification. Canadian journal of biochemistry and physiology *37*, 911-917.

Boerke, A., Tsai, P.S., Garcia-Gil, N., Brewis, I.A., and Gadella, B.M. (2008). Capacitation-dependent reorganization of microdomains in the apical sperm head plasma membrane: functional relationship with zona binding and the zona-induced acrosome reaction. Theriogenology *70*, 1188-1196.

Boggs, J.M., Koshy, K.M., and Rangaraj, G. (1988). Influence of structural modifications on the phase behavior of semi-synthetic cerebroside sulfate. Biochimica et biophysica acta *938*, 361-372.

Boggs, J.M., Menikh, A., and Rangaraj, G. (2000). Trans interactions between galactosylceramide and cerebroside sulfate across apposed bilayers. Biophysical journal *78*, 874-885.

Boivin, J., Bunting, L., Collins, J.A., and Nygren, K.G. (2007). International estimates of infertility prevalence and treatment-seeking: potential need and demand for infertility medical care. Hum Reprod *22*, 1506-1512.

Bond, C.S., Clements, P.R., Ashby, S.J., Collyer, C.A., Harrop, S.J., Hopwood, J.J., and Guss, J.M. (1997). Structure of a human lysosomal sulfatase. Structure *5*, 277-289.

Bou Khalil, M., Chakrabandhu, K., Xu, H., Weerachatyanukul, W., Buhr, M., Berger, T., Carmona, E., Vuong, N., Kumarathasan, P., Wong, P.T., *et al.* (2006). Sperm capacitation induces an increase in lipid rafts having zona pellucida binding ability and containing sulfogalactosylglycerolipid. Developmental biology *290*, 220-235.

Breitbart, H. (2002). Intracellular calcium regulation in sperm capacitation and acrosomal reaction. Molecular and cellular endocrinology *187*, 139-144.

Brogi, A., Presentini, R., Piomboni, P., Collodel, G., Strazza, M., Solazzo, D., and Costantino-Ceccarini, E. (1995). Human sperm and spermatogonia express a galactoglycerolipid which interacts with gp120. Journal of submicroscopic cytology and pathology *27*, 565-571.

Brogi, A., Presentini, R., Solazzo, D., Piomboni, P., and Costantino-Ceccarini, E. (1996). Interaction of human immunodeficiency virus type 1 envelope glycoprotein gp120 with a galactoglycerolipid associated with human sperm. AIDS research and human retroviruses *12*, 483-489.

Brown, D.A., and London, E. (1998). Structure and origin of ordered lipid domains in biological membranes. The Journal of membrane biology *164*, 103-114.

Brown, D.A., and London, E. (2000). Structure and function of sphingolipid- and cholesterol-rich membrane rafts. The Journal of biological chemistry *275*, 17221-17224.

Buffone, M.G., Foster, J.A., and Gerton, G.L. (2008). The role of the acrosomal matrix in fertilization. The International journal of developmental biology *52*, 511-522.

Buffone, M.G., Wertheimer, E.V., Visconti, P.E., and Krapf, D. (2014). Central role of soluble adenylyl cyclase and cAMP in sperm physiology. Biochimica et biophysica acta *1842*, 2610-2620.

Burck, P.J., and Zimmerman, R.E. (1980). The inhibition of acrosin by sterol sulphates. Journal of reproduction and fertility *58*, 121-125.

Burkin, H.R., and Miller, D.J. (2000). Zona pellucida protein binding ability of porcine sperm during epididymal maturation and the acrosome reaction. Developmental biology *222*, 99-109.

Caballero, I., Vazquez, J.M., Mayor, G.M., Alminana, C., Calvete, J.J., Sanz, L., Roca, J., and Martinez, E.A. (2009). PSP-I/PSP-II spermadhesin exert a decapacitation effect on highly extended boar spermatozoa. International journal of andrology *32*, 505-513.

Calvete, J.J., Carrera, E., Sanz, L., and Topfer-Petersen, E. (1996). Boar spermadhesins AQN-1 and AQN-3: oligosaccharide and zona pellucida binding characteristics. Biological chemistry *377*, 521-527.

Calvete, J.J., Solis, D., Sanz, L., Diaz-Maurino, T., and Topfer-Petersen, E. (1994). Glycosylated boar spermadhesin AWN-1 isoforms. Biological origin, structural characterization by lectin mapping, localization of O-glycosylation sites, and effect of glycosylation on ligand binding. Biological chemistry Hoppe-Seyler *375*, 667-673.

Carmona, E., Weerachatyanukul, W., Soboloff, T., Fluharty, A.L., White, D., Promdee, L., Ekker, M., Berger, T., Buhr, M., and Tanphaichitr, N. (2002a). Arylsulfatase a is present on the pig sperm surface and is involved in sperm-zona pellucida binding. Developmental biology *247*, 182-196.

Carmona, E., Weerachatyanukul, W., Xu, H., Fluharty, A., Anupriwan, A., Shoushtarian, A., Chakrabandhu, K., and Tanphaichitr, N. (2002b). Binding of arylsulfatase A to mouse sperm inhibits gamete interaction and induces the acrosome reaction. Biology of reproduction *66*, 1820-1827.

Chang, M.C. (1951). Fertilizing capacity of spermatozoa deposited into the fallopian tubes. Nature *168*, 697-698.

Chang, M.C. (1959). Fertilization of rabbit ova in vitro. Nature *184(Suppl 7)*, 466-467.

Cheng, A., Le, T., Palacios, M., Bookbinder, L.H., Wassarman, P.M., Suzuki, F., and Bleil, J.D. (1994). Sperm-egg recognition in the mouse: characterization of sp56, a sperm protein having specific affinity for ZP3. The Journal of cell biology *125*, 867-878.

Cheng, C.Y., and Mruk, D.D. (2002). Cell junction dynamics in the testis: Sertoli-germ cell interactions and male contraceptive development. Physiological reviews *82*, 825-874.

Cheng, C.Y., and Mruk, D.D. (2010). A local autocrine axis in the testes that regulates spermatogenesis. Nature reviews Endocrinology *6*, 380-395.

Cheng, C.Y., and Mruk, D.D. (2012). The blood-testis barrier and its implications for male contraception. Pharmacological reviews *64*, 16-64.

Chruszcz, M., Laidler, P., Monkiewicz, M., Ortlund, E., Lebioda, L., and Lewinski, K. (2003). Crystal structure of a covalent intermediate of endogenous human arylsulfatase A. Journal of inorganic biochemistry *96*, 386-392.

Chung, S., Wang, S.P., Pan, L., Mitchell, G., Trasler, J., and Hermo, L. (2001). Infertility and testicular defects in hormone-sensitive lipase-deficient mice. Endocrinology *142*, 4272-4281.

Cismasiu, V.B., Denes, S.A., Reilander, H., Michel, H., and Szedlacsek, S.E. (2004). The MAM (meprin/A5-protein/PTPmu) domain is a homophilic binding site promoting the

lateral dimerization of receptor-like protein-tyrosine phosphatase mu. The Journal of biological chemistry *279*, 26922-26931.

Clermont, Y. (1972). Kinetics of spermatogenesis in mammals: seminiferous epithelium cycle and spermatogonial renewal. Physiological reviews *52*, 198-236.

Cooke, H.J., and Saunders, P.T. (2002). Mouse models of male infertility. Nature reviews Genetics *3*, 790-801.

Coonrod, S.A., Herr, J.C., and Westhusin, M.E. (1996). Inhibition of bovine fertilization in vitro by antibodies to SP-10. Journal of reproduction and fertility *107*, 287-297.

Cooper, T.G., and Orgebin-Crist, M.C. (1975). The effect of epididymal and testicular fluids on the fertilising capacity of testicular and epididymal spermatozoa. Andrologia *7*, 85-93.

Cooper, T.G., and Orgebin-Crist, M.C. (1977). Effect of aging on the fertilizing capacity of testicular spermatozoa from the rabbit. Biology of reproduction *16*, 258-266.

Cornwall, G.A. (2009). New insights into epididymal biology and function. Human reproduction update *15*, 213-227.

Cox, T.M., and Cachon-Gonzalez, M.B. (2012). The cellular pathology of lysosomal diseases. The Journal of pathology *226*, 241-254.

Crepieux, P., Marion, S., Martinat, N., Fafeur, V., Vern, Y.L., Kerboeuf, D., Guillou, F., and Reiter, E. (2001). The ERK-dependent signalling is stage-specifically modulated by FSH, during primary Sertoli cell maturation. Oncogene *20*, 4696-4709.

Cross, N.L., and Overstreet, J.W. (1987). Glycoconjugates of the human sperm surface: distribution and alterations that accompany capacitation in vitro. Gamete research *16*, 23-35.

Dacheux, J.L., Belghazi, M., Lanson, Y., and Dacheux, F. (2006). Human epididymal secretome and proteome. Molecular and cellular endocrinology *250*, 36-42.

Dacheux, J.L., Belleannee, C., Jones, R., Labas, V., Belghazi, M., Guyonnet, B., Druart, X., Gatti, J.L., and Dacheux, F. (2009). Mammalian epididymal proteome. Molecular and cellular endocrinology *306*, 45-50.

Dacheux, J.L., Castella, S., Gatti, J.L., and Dacheux, F. (2005). Epididymal cell secretory activities and the role of proteins in boar sperm maturation. Theriogenology *63*, 319-341.

Dacheux, J.L., Gatti, J.L., and Dacheux, F. (2003). Contribution of epididymal secretory proteins for spermatozoa maturation. Microscopy research and technique *61*, 7-17.

Danshina, P.V., Geyer, C.B., Dai, Q., Goulding, E.H., Willis, W.D., Kitto, G.B., McCarrey, J.R., Eddy, E.M., and O'Brien, D.A. (2010). Phosphoglycerate kinase 2 (PGK2) is essential for sperm function and male fertility in mice. Biology of reproduction *82*, 136-145.

Davidova, N., Jonakova, V., and Manaskova-Postlerova, P. (2009). Expression and localization of acrosin inhibitor in boar reproductive tract. Cell and tissue research *338*, 303-311.

Davis, B.K. (1981). Timing of fertilization in mammals: sperm cholesterol/phospholipid ratio as a determinant of the capacitation interval. Proceedings of the National Academy of Sciences of the United States of America *78*, 7560-7564.

Davis, B.K., Byrne, R., and Bedigian, K. (1980). Studies on the mechanism of capacitation: albumin-mediated changes in plasma membrane lipids during in vitro incubation of rat sperm cells. Proceedings of the National Academy of Sciences of the United States of America *77*, 1546-1550.

Davis, B.K., Byrne, R., and Hungund, B. (1979). Studies on the mechanism of capacitation. II. Evidence for lipid transfer between plasma membrane of rat sperm and serum albumin during capacitation in vitro. Biochimica et biophysica acta *558*, 257-266.

De Blas, G.A., Roggero, C.M., Tomes, C.N., and Mayorga, L.S. (2005). Dynamics of SNARE assembly and disassembly during sperm acrosomal exocytosis. PLoS biology *3*, e323.

de Kretser, D.M. (1997). Male infertility. Lancet *349*, 787-790.

De Kretser, D.M., and Baker, H.W. (1999). Infertility in men: recent advances and continuing controversies. The Journal of clinical endocrinology and metabolism *84*, 3443-3450.

de Lamirande, E., and Gagnon, C. (1993). A positive role for the superoxide anion in triggering hyperactivation and capacitation of human spermatozoa. International journal of andrology *16*, 21-25.

de Lamirande, E., and O'Flaherty, C. (2008). Sperm activation: role of reactive oxygen species and kinases. Biochimica et biophysica acta *1784*, 106-115.

De los Reyes, M., and Barros, C. (2000). Immunolocalization of proacrosin/acrosin in bovine sperm and sperm penetration through the zona pellucida. Animal reproduction science *58*, 215-228.

de Vries, K.J., Wiedmer, T., Sims, P.J., and Gadella, B.M. (2003). Caspase-independent exposure of aminophospholipids and tyrosine phosphorylation in bicarbonate responsive human sperm cells. Biology of reproduction *68*, 2122-2134.

Deconinck, N., Messaaoui, A., Ziereisen, F., Kadhim, H., Sznajer, Y., Pelc, K., Nassogne, M.C., Vanier, M.T., and Dan, B. (2008). Metachromatic leukodystrophy without arylsulfatase A deficiency: a new case of saposin-B deficiency. European journal of paediatric neurology : EJPN : official journal of the European Paediatric Neurology Society *12*, 46-50.

Deguchi, E., Tani, T., Watanabe, H., Yamada, S., and Kondoh, G. (2007). Dipeptidase-inactivated tACE action in vivo: selective inhibition of sperm-zona pellucida binding in the mouse. Biology of reproduction *77*, 794-802.

Dierks, T., Schmidt, B., Borissenko, L.V., Peng, J., Preusser, A., Mariappan, M., and von Figura, K. (2003). Multiple sulfatase deficiency is caused by mutations in the gene encoding the human C(alpha)-formylglycine generating enzyme. Cell *113*, 435-444.

Dohle, G.R., Halley, D.J., Van Hemel, J.O., van den Ouwel, A.M., Pieters, M.H., Weber, R.F., and Govaerts, L.C. (2002). Genetic risk factors in infertile men with severe oligozoospermia and azoospermia. Hum Reprod *17*, 13-16.

Dostalova, Z., Calvete, J.J., Sanz, L., and Topfer-Petersen, E. (1995). Boar spermadhesin AWN-1. Oligosaccharide and zona pellucida binding characteristics. European journal of biochemistry / FEBS *230*, 329-336.

Dube, C., Leclerc, P., Baba, T., Reyes-Moreno, C., and Bailey, J.L. (2005). The proacrosin binding protein, sp32, is tyrosine phosphorylated during capacitation of pig sperm. Journal of andrology *26*, 519-528.

Duchen, L.W., Eicher, E.M., Jacobs, J.M., Scaravilli, F., and Teixeira, F. (1980). Hereditary leucodystrophy in the mouse: the new mutant twitcher. Brain : a journal of neurology *103*, 695-710.

Dudkiewicz, A.B. (1984). Purification of boar acrosomal arylsulfatase A and possible role in the penetration of cumulus cells. Biology of reproduction *30*, 1005-1014.

Dudkiewicz, A.B., Srivastava, P.N., Yang, C.H., and Williams, W.L. (1979). Extraction of human and rabbit acrosomes: a comparison of sequential and sonication methods. Andrologia *11*, 355-366.

Dugail, I. (2014). Lysosome/lipid droplet interplay in metabolic diseases. Biochimie *96*, 102-105.

Dun, M.D., Smith, N.D., Baker, M.A., Lin, M., Aitken, R.J., and Nixon, B. (2011). The chaperonin containing TCP1 complex (CCT/TRiC) is involved in mediating sperm-oocyte interaction. The Journal of biological chemistry *286*, 36875-36887.

Dym, M. (1977). The male reproductive system. In Histology, L. Weiss, ed. (New York: McGraw-Hill Book Company), pp. 979-1038.

Dym, M. (1994). Spermatogonial stem cells of the testis. Proceedings of the National Academy of Sciences of the United States of America *91*, 11287-11289.

Eckhardt, M. (2008). The role and metabolism of sulfatide in the nervous system. Molecular neurobiology *37*, 93-103.

Eddy, E.M. (2002). Male germ cell gene expression. Recent progress in hormone research *57*, 103-128.

Eddy, E.M. (2006). The Spermatozoon. In The Physiology of Reproduction, E. Knobil, and J.D. Neill, eds. (San Diego: Elsevier Inc), pp. 3-54.

Edwards, R.G., Talbert, L., Israelstam, D., Nino, H.V., and Johnson, M.H. (1968). Diffusion chamber for exposing spermatozoa to human uterine secretions. American journal of obstetrics and gynecology *102*, 388-396.

Ensslin, M., Vogel, T., Calvete, J.J., Thole, H.H., Schmidtke, J., Matsuda, T., and Topfer-Petersen, E. (1998). Molecular cloning and characterization of P47, a novel boar sperm-associated zona pellucida-binding protein homologous to a family of mammalian secretory proteins. Biology of reproduction *58*, 1057-1064.

Ensslin, M.A., and Shur, B.D. (2003). Identification of mouse sperm SED1, a bimotif EGF repeat and discoidin-domain protein involved in sperm-egg binding. Cell *114*, 405-417.

Esposito, G., Jaiswal, B.S., Xie, F., Krajnc-Franken, M.A., Robben, T.J., Strik, A.M., Kuil, C., Philipsen, R.L., van Duin, M., Conti, M., *et al.* (2004). Mice deficient for soluble adenylyl cyclase are infertile because of a severe sperm-motility defect. Proceedings of the National Academy of Sciences of the United States of America *101*, 2993-2998.

Fayrer-Hosken, R.A., Brackett, B.G., and Brown, J. (1987). Reversible inhibition of rabbit sperm-fertilizing ability by cholesterol sulfate. Biology of reproduction *36*, 878-883.

Fazeli, A., Hage, W.J., Cheng, F.P., Voorhout, W.F., Marks, A., Bevers, M.M., and Colenbrander, B. (1997). Acrosome-intact boar spermatozoa initiate binding to the homologous zona pellucida in vitro. Biology of reproduction *56*, 430-438.

Ficarro, S., Chertihin, O., Westbrook, V.A., White, F., Jayes, F., Kalab, P., Marto, J.A., Shabanowitz, J., Herr, J.C., Hunt, D.F., *et al.* (2003). Phosphoproteome analysis of capacitated human sperm. Evidence of tyrosine phosphorylation of a kinase-anchoring protein 3 and valosin-containing protein/p97 during capacitation. The Journal of biological chemistry *278*, 11579-11589.

Flesch, F.M., Voorhout, W.F., Colenbrander, B., van Golde, L.M., and Gadella, B.M. (1998). Use of lectins to characterize plasma membrane preparations from boar spermatozoa: a novel technique for monitoring membrane purity and quantity. Biology of reproduction *59*, 1530-1539.

Florman, H.M., and Ducibella, T. (2006). Fertilization in mammals. In Knobil and Neil's Physiology of Reproduction, J.D. Neill, ed. (New York: Elsevier), pp. 55-112.

Fluharty, A.L., and Edmond, J. (1978). Arylsulfatases A and B from human liver. Methods in enzymology *50*, 537-547.

Fluharty, A.L., Stevens, R.L., Miller, R.T., Shapiro, S.S., and Kihara, H. (1976). Ascorbic acid-2-sulfate sulfhohydrolase activity of human arylsulfatase A. Biochimica et biophysica acta *429*, 508-516.

Foster, J.A., Friday, B.B., Maulit, M.T., Blobel, C., Winfrey, V.P., Olson, G.E., Kim, K.S., and Gerton, G.L. (1997). AM67, a secretory component of the guinea pig sperm acrosomal matrix, is related to mouse sperm protein sp56 and the complement component 4-binding proteins. The Journal of biological chemistry *272*, 12714-12722.

Foster, J.A., and Herr, J.C. (1992). Interactions of human sperm acrosomal protein SP-10 with the acrosomal membranes. Biology of reproduction *46*, 981-990.

Foster, L.J., De Hoog, C.L., and Mann, M. (2003). Unbiased quantitative proteomics of lipid rafts reveals high specificity for signaling factors. Proceedings of the National Academy of Sciences of the United States of America *100*, 5813-5818.

Fouchecourt, S., Metayer, S., Locatelli, A., Dacheux, F., and Dacheux, J.L. (2000). Stallion epididymal fluid proteome: qualitative and quantitative characterization; secretion and dynamic changes of major proteins. Biology of reproduction *62*, 1790-1803.

Franca, L.R., Ogawa, T., Avarbock, M.R., Brinster, R.L., and Russell, L.D. (1998). Germ cell genotype controls cell cycle during spermatogenesis in the rat. Biology of reproduction *59*, 1371-1377.

Franchini, L., Panza, L., Kongmanas, K., Tanphaichitr, N., Faull, K.F., and Ronchetti, F. (2008). An efficient and convenient synthesis of deuterium-labelled seminolipid isotopomers and their ESI-MS characterization. Chemistry and physics of lipids *152*, 78-85.

Frank, M. (2000). MAL, a proteolipid in glycosphingolipid enriched domains: functional implications in myelin and beyond. Progress in neurobiology *60*, 531-544.

Fraser, L.R. (1984). Mouse sperm capacitation in vitro involves loss of a surface-associated inhibitory component. Journal of reproduction and fertility *72*, 373-384.

Fraser, L.R. (1998). Interactions between a decapacitation factor and mouse spermatozoa appear to involve fucose residues and a GPI-anchored receptor. Molecular reproduction and development *51*, 193-202.

Fraser, L.R., Harrison, R.A., and Herod, J.E. (1990). Characterization of a decapacitation factor associated with epididymal mouse spermatozoa. Journal of reproduction and fertility *89*, 135-148.

Fredman, P., Mansson, J.E., Rynmark, B.M., Josefsen, K., Ekblond, A., Halldner, L., Osterbye, T., Horn, T., and Buschard, K. (2000). The glycosphingolipid sulfatide in the islets of Langerhans in rat pancreas is processed through recycling: possible involvement in insulin trafficking. Glycobiology *10*, 39-50.

Freysz, L., Farooqui, A.A., Adamczewska-Goncerzewicz, Z., and Mandel, P. (1979). Lysosomal hydrolases in neuronal, astroglial, and olidodendroglial enriched fractions of rabbit and beef brain. Journal of lipid research *20*, 503-508.

Friedrich, M.V., Gohring, W., Morgelin, M., Brancaccio, A., David, G., and Timpl, R. (1999). Structural basis of glycosaminoglycan modification and of heterotypic interactions of perlecan domain V. Journal of molecular biology *294*, 259-270.

Fujimoto, H., Tadano-Aritomi, K., Tokumasu, A., Ito, K., Hikita, T., Suzuki, K., and Ishizuka, I. (2000). Requirement of seminolipid in spermatogenesis revealed by UDP-galactose: Ceramide galactosyltransferase-deficient mice. The Journal of biological chemistry *275*, 22623-22626.

Furimsky, A., Vuong, N., Xu, H., Kumarathasan, P., Xu, M., Weerachatyanukul, W., Bou Khalil, M., Kates, M., and Tanphaichitr, N. (2005). Percoll gradient-centrifuged capacitated mouse sperm have increased fertilizing ability and higher contents of sulfogalactosylglycerolipid and docosahexaenoic acid-containing phosphatidylcholine compared to washed capacitated mouse sperm. Biology of reproduction *72*, 574-583.

Gadella, B.M. (2012). Dynamic regulation of sperm interactions with the zona pellucida prior to and after fertilisation. Reproduction, fertility, and development *25*, 26-37.

Gadella, B.M., Hammache, D., Pieroni, G., Colenbrander, B., van Golde, L.M., and Fantini, J. (1998). Glycolipids as potential binding sites for HIV: topology in the sperm plasma membrane in relation to the regulation of membrane fusion. Journal of reproductive immunology *41*, 233-253.

Gadella, B.M., and Harrison, R.A. (2000). The capacitating agent bicarbonate induces protein kinase A-dependent changes in phospholipid transbilayer behavior in the sperm plasma membrane. Development *127*, 2407-2420.

Gadella, B.M., and Harrison, R.A. (2002). Capacitation induces cyclic adenosine 3',5'-monophosphate-dependent, but apoptosis-unrelated, exposure of aminophospholipids at the apical head plasma membrane of boar sperm cells. Biology of reproduction *67*, 340-350.

Gahlay, G., Gauthier, L., Baibakov, B., Epifano, O., and Dean, J. (2010). Gamete recognition in mice depends on the cleavage status of an egg's zona pellucida protein. Science *329*, 216-219.

Gatti, J.L., Castella, S., Dacheux, F., Ecroyd, H., Metayer, S., Thimon, V., and Dacheux, J.L. (2004). Post-testicular sperm environment and fertility. Animal reproduction science *82-83*, 321-339.

Gatti, J.L., Druart, X., Syntin, P., Guerin, Y., Dacheux, J.L., and Dacheux, F. (2000). Biochemical characterization of two ram cauda epididymal maturation-dependent sperm glycoproteins. Biology of reproduction *62*, 950-958.

Gerland, P., Raftery, A.E., Sevcikova, H., Li, N., Gu, D., Spoorenberg, T., Alkema, L., Fosdick, B.K., Chunn, J., Lalic, N., *et al.* (2014). World population stabilization unlikely this century. Science *346*, 234-237.

Ghosh, D. (2007). Human sulfatases: a structural perspective to catalysis. Cellular and molecular life sciences : CMLS *64*, 2013-2022.

Gibbons, R., Adeoya-Osiguwa, S.A., and Fraser, L.R. (2005). A mouse sperm decapacitation factor receptor is phosphatidylethanolamine-binding protein 1. Reproduction *130*, 497-508.

Gieselmann, V., Matzner, U., Hess, B., Lullmann-Rauch, R., Coenen, R., Hartmann, D., D'Hooge, R., DeDeyn, P., and Nagels, G. (1998). Metachromatic leukodystrophy: molecular genetics and an animal model. Journal of inherited metabolic disease *21*, 564-574.

Gillis, G., Peterson, R., Russell, L., Hook, L., and Freund, M. (1978). Isolation and characterization of membrane vesicles from human and boar spermatozoa: methods using nitrogen cavitation and ionophore induced vesiculation. Preparative biochemistry *8*, 363-378.

Gillot, I., Jehl-Pietri, C., Gounon, P., Luquet, S., Rassoulzadegan, M., Grimaldi, P., and Vidal, F. (2005). Germ cells and fatty acids induce translocation of CD36 scavenger receptor to the plasma membrane of Sertoli cells. Journal of cell science *118*, 3027-3035.

Gonzalez-Fernandez, L., Macias-Garcia, B., Loux, S.C., Varner, D.D., and Hinrichs, K. (2013). Focal adhesion kinases and calcium/calmodulin-dependent protein kinases regulate protein tyrosine phosphorylation in stallion sperm. Biology of reproduction *88*, 138.

Gopalakrishnan, B., Aravinda, S., Pawshe, C.H., Totey, S.M., Nagpal, S., Salunke, D.M., and Shaha, C. (1998). Studies on glutathione S-transferases important for sperm function: evidence of catalytic activity-independent functions. The Biochemical journal *329 (Pt 2)*, 231-241.

Goto-Inoue, N., Hayasaka, T., Zaima, N., and Setou, M. (2009). The specific localization of seminolipid molecular species on mouse testis during testicular maturation revealed by imaging mass spectrometry. Glycobiology *19*, 950-957.

Greve, J.M., and Wassarman, P.M. (1985). Mouse egg extracellular coat is a matrix of interconnected filaments possessing a structural repeat. Journal of molecular biology *181*, 253-264.

Griffiths, G.S., Galileo, D.S., Aravindan, R.G., and Martin-DeLeon, P.A. (2009). Clusterin facilitates exchange of glycosyl phosphatidylinositol-linked SPAM1 between reproductive luminal fluids and mouse and human sperm membranes. Biology of reproduction *81*, 562-570.

Griffiths, W.J., and Wang, Y. (2009). Mass spectrometry: from proteomics to metabolomics and lipidomics. Chemical Society reviews *38*, 1882-1896.

Griswold, M.D. (1995). Interactions between germ cells and Sertoli cells in the testis. Biology of reproduction *52*, 211-216.

Griswold, M.D., and McLean, D. (2006). The Sertoli Cell. In Knobil and Neill's Physiology of Reproduction, J.D. Neill, T.M. Plant, D.W. Pfaff, J.R.G. Challis, D.M. de Kretser, J.S. Richards, and P.M. Wassarman, eds. (New York: Elsevier), pp. 949-975.

Guidobaldi, H.A., Teves, M.E., Unates, D.R., Anastasia, A., and Giojalas, L.C. (2008). Progesterone from the cumulus cells is the sperm chemoattractant secreted by the rabbit oocyte cumulus complex. PloS one *3*, e3040.

Hackstein, J.H., Hochstenbach, R., and Pearson, P.L. (2000). Towards an understanding of the genetics of human male infertility: lessons from flies. Trends in genetics : TIG *16*, 565-572.

Hagaman, J.R., Moyer, J.S., Bachman, E.S., Sibony, M., Magyar, P.L., Welch, J.E., Smithies, O., Krege, J.H., and O'Brien, D.A. (1998). Angiotensin-converting enzyme and male fertility. Proceedings of the National Academy of Sciences of the United States of America *95*, 2552-2557.

Han, C., Park, I., Lee, B., Jin, S., Choi, H., Kwon, J.T., Kwon, Y.I., Kim do, H., Park, Z.Y., and Cho, C. (2011). Identification of heat shock protein 5, calnexin and integral membrane protein 2B as Adam7-interacting membrane proteins in mouse sperm. Journal of cellular physiology *226*, 1186-1195.

Han, X., Cheng, H., Fryer, J.D., Fagan, A.M., and Holtzman, D.M. (2003). Novel role for apolipoprotein E in the central nervous system. Modulation of sulfatide content. The Journal of biological chemistry *278*, 8043-8051.

Han, X., and Gross, R.W. (1994). Electrospray ionization mass spectroscopic analysis of human erythrocyte plasma membrane phospholipids. Proceedings of the National Academy of Sciences of the United States of America *91*, 10635-10639.

Hanson, S.R., Best, M.D., and Wong, C.H. (2004). Sulfatases: structure, mechanism, biological activity, inhibition, and synthetic utility. Angew Chem Int Ed Engl *43*, 5736-5763.

Hardy, D.M., and Garbers, D.L. (1995). A sperm membrane protein that binds in a species-specific manner to the egg extracellular matrix is homologous to von Willebrand factor. The Journal of biological chemistry *270*, 26025-26028.

Harris, J.D., Hibler, D.W., Fontenot, G.K., Hsu, K.T., Yurewicz, E.C., and Sacco, A.G. (1994). Cloning and characterization of zona pellucida genes and cDNAs from a variety of mammalian species: the ZPA, ZPB and ZPC gene families. DNA sequence : the journal of DNA sequencing and mapping *4*, 361-393.

Harrison, R.A., and Gadella, B.M. (2005). Bicarbonate-induced membrane processing in sperm capacitation. Theriogenology *63*, 342-351.

Hedrick, J.L., and Wardrip, N.J. (1987). On the macromolecular composition of the zona pellucida from porcine oocytes. Developmental biology *121*, 478-488.

Hemachand, T., Gopalakrishnan, B., Salunke, D.M., Totey, S.M., and Shaha, C. (2002). Sperm plasma-membrane-associated glutathione S-transferases as gamete recognition molecules. Journal of cell science *115*, 2053-2065.

Herlyn, H., and Zischler, H. (2008). The molecular evolution of sperm zonadhesin. The International journal of developmental biology *52*, 781-790.

Hermo, L., Chung, S., Gregory, M., Smith, C.E., Wang, S.P., El-Alfy, M., Cyr, D.G., Mitchell, G.A., and Trasler, J. (2008). Alterations in the testis of hormone sensitive lipase-deficient mice is associated with decreased sperm counts, sperm motility, and fertility. Molecular reproduction and development *75*, 565-577.

Hermo, L., Wright, J., Oko, R., and Morales, C.R. (1991). Role of epithelial cells of the male excurrent duct system of the rat in the endocytosis or secretion of sulfated glycoprotein-2 (clusterin). Biology of reproduction *44*, 1113-1131.

Hernandez-Guzman, F.G., Higashiyama, T., Pangborn, W., Osawa, Y., and Ghosh, D. (2003). Structure of human estrone sulfatase suggests functional roles of membrane association. The Journal of biological chemistry *278*, 22989-22997.

Hess, B., Saftig, P., Hartmann, D., Coenen, R., Lullmann-Rauch, R., Goebel, H.H., Evers, M., von Figura, K., D'Hooge, R., Nagels, G., *et al.* (1996). Phenotype of arylsulfatase A-deficient mice: relationship to human metachromatic leukodystrophy. Proceedings of the National Academy of Sciences of the United States of America *93*, 14821-14826.

Hickox, J.R., Bi, M., and Hardy, D.M. (2001). Heterogeneous processing and zona pellucida binding activity of pig zonadhesin. The Journal of biological chemistry *276*, 41502-41509.

Hiraiwa, M., Martin, B.M., Kishimoto, Y., Conner, G.E., Tsuji, S., and O'Brien, J.S. (1997). Lysosomal proteolysis of prosaposin, the precursor of saposins (sphingolipid activator proteins): its mechanism and inhibition by ganglioside. Archives of biochemistry and biophysics *341*, 17-24.

Hogan, B., Costantini, F., and Lacy, E. (1994). Manipulating the mouse embryo: a laboratory manual (Cold Spring Harbor: Cold Spring Harbor Laboratory).

Holt, G.D., Krivan, H.C., Gasic, G.J., and Ginsburg, V. (1989). Antistasin, an inhibitor of coagulation and metastasis, binds to sulfatide (Gal(3-SO4) beta 1-1Cer) and has a sequence homology with other proteins that bind sulfated glycoconjugates. The Journal of biological chemistry *264*, 12138-12140.

Honke, K., Hirahara, Y., Dupree, J., Suzuki, K., Popko, B., Fukushima, K., Fukushima, J., Nagasawa, T., Yoshida, N., Wada, Y., *et al.* (2002). Paranodal junction formation and

spermatogenesis require sulfoglycolipids. Proceedings of the National Academy of Sciences of the United States of America *99*, 4227-4232.

Howes, E., Pascall, J.C., Engel, W., and Jones, R. (2001). Interactions between mouse ZP2 glycoprotein and proacrosin; a mechanism for secondary binding of sperm to the zona pellucida during fertilization. Journal of cell science *114*, 4127-4136.

Huckins, C. (1978). The morphology and kinetics of spermatogonial degeneration in normal adult rats: an analysis using a simplified classification of the germinal epithelium. The Anatomical record *190*, 905-926.

Hunnicutt, G.R., Primakoff, P., and Myles, D.G. (1996). Sperm surface protein PH-20 is bifunctional: one activity is a hyaluronidase and a second, distinct activity is required in secondary sperm-zona binding. Biology of reproduction *55*, 80-86.

Ida, M., Satoh, A., Matsumoto, I., and Kojima-Aikawa, K. (2004). Human annexin V binds to sulfatide: contribution to regulation of blood coagulation. Journal of biochemistry *135*, 583-588.

Ideo, H., Seko, A., Ishizuka, I., and Yamashita, K. (2003). The N-terminal carbohydrate recognition domain of galectin-8 recognizes specific glycosphingolipids with high affinity. Glycobiology *13*, 713-723.

Ideo, H., Seko, A., Ohkura, T., Matta, K.L., and Yamashita, K. (2002). High-affinity binding of recombinant human galectin-4 to SO(3)(-)-->3Galbeta1-->3GalNAc pyranoside. Glycobiology *12*, 199-208.

Igdoura, S.A., and Morales, C.R. (1995). Role of sulfated glycoprotein-1 (SGP-1) in the disposal of residual bodies by Sertoli cells of the rat. Molecular reproduction and development *40*, 91-102.

Igdoura, S.A., Rasky, A., and Morales, C.R. (1996). Trafficking of sulfated glycoprotein-1 (prosaposin) to lysosomes or to the extracellular space in rat Sertoli cells. Cell and tissue research *283*, 385-394.

Igisu, H., Shimomura, K., Kishimoto, Y., and Suzuki, K. (1983). Lipids of developing brain of twitcher mouse. An authentic murine model of human Krabbe disease. Brain : a journal of neurology *106 (Pt 2)*, 405-417.

Ikawa, M., Inoue, N., Benham, A.M., and Okabe, M. (2010). Fertilization: a sperm's journey to and interaction with the oocyte. The Journal of clinical investigation *120*, 984-994.

Ishizuka, I. (1997). Chemistry and functional distribution of sulfoglycolipids. Progress in lipid research *36*, 245-319.

Ishizuka, I., Suzuki, M., and Yamakawa, T. (1973). Isolation and characterization of a novel sulfoglycolipid, 'seminolipid,' from boar testis and spermatozoa. Journal of biochemistry *73*, 77-87.

Jannini, E.A., Ulisse, S., Cecconi, S., Cironi, L., Colonna, R., D'Armiento, M., Santoni, A., and Cifone, M.G. (1994). Follicle-stimulating hormone-induced phospholipase A2 activity and eicosanoid generation in rat Sertoli cells. Biology of reproduction *51*, 140-145.

Jaspard, B., Fournier, N., Vieitez, G., Atger, V., Barbaras, R., Vieu, C., Manent, J., Chap, H., Perret, B., and Collet, X. (1997). Structural and functional comparison of HDL from homologous human plasma and follicular fluid. A model for extravascular fluid. Arteriosclerosis, thrombosis, and vascular biology *17*, 1605-1613.

Jegou, B. (1993). The Sertoli-germ cell communication network in mammals. International review of cytology *147*, 25-96.

Jin, M., Fujiwara, E., Kakiuchi, Y., Okabe, M., Satouh, Y., Baba, S.A., Chiba, K., and Hirohashi, N. (2011). Most fertilizing mouse spermatozoa begin their acrosome reaction before contact with the zona pellucida during in vitro fertilization. Proceedings of the National Academy of Sciences of the United States of America *108*, 4892-4896.

Jonakova, V., Kraus, M., Veselsky, L., Cechova, D., Bezouska, K., and Ticha, M. (1998). Spermadhesins of the AQN and AWN families, DQH sperm surface protein and HNK protein in the heparin-binding fraction of boar seminal plasma. Journal of reproduction and fertility *114*, 25-34.

Jonakova, V., Manaskova, P., and Ticha, M. (2007). Separation, characterization and identification of boar seminal plasma proteins. Journal of chromatography B, Analytical technologies in the biomedical and life sciences *849*, 307-314.

Jones, R., Howes, E., Dunne, P.D., James, P., Bruckbauer, A., and Klenerman, D. (2010). Tracking diffusion of GM1 gangliosides and zona pellucida binding molecules in sperm plasma membranes following cholesterol efflux. Developmental biology *339*, 398-406.

Kates, M. (1986). Technique of lipidology: isolation, analysis and identification of lipids. In Laboratory Techniques in Biochemistry and Molecular Biology, R.H. Burdon, ed. (New York: Elsevier), pp. 100-278.

Keber, R., Rozman, D., and Horvat, S. (2013). Sterols in spermatogenesis and sperm maturation. Journal of lipid research *54*, 20-33.

Kerr, C.L., Hanna, W.F., Shaper, J.H., and Wright, W.W. (2002). Characterization of zona pellucida glycoprotein 3 (ZP3) and ZP2 binding sites on acrosome-intact mouse sperm. Biology of reproduction *66*, 1585-1595.

Kerr, J.B., and De Kretser, D.M. (1975). Cyclic variations in Sertoli cell lipid content throughout the spermatogenic cycle in the rat. Journal of reproduction and fertility *43*, 1-8.

Kerr, J.B., Loveland, K.L., O'Bryan, M.K., and de Kretser, D.M. (2006). Cytology of the Testis and Intrinsic Control Mechanisms. In Knobil and Neill's Physiology of Reproduction, J.D. Neill, T.M. Plant, D.W. Pfaff, J.R.G. Challis, and D.M. de Kretser, eds. (New York: Elsevier), pp. 827-947.

Kierszenbaum, A.L. (2002). Histology and cell biology: an introduction to pathology (St. Louis: Mosby, Inc.).

Kim, E., Yamashita, M., Nakanishi, T., Park, K.E., Kimura, M., Kashiwabara, S., and Baba, T. (2006). Mouse sperm lacking ADAM1b/ADAM2 fertilin can fuse with the egg plasma membrane and effect fertilization. The Journal of biological chemistry *281*, 5634-5639.

Kim, K.S., Cha, M.C., and Gerton, G.L. (2001). Mouse sperm protein sp56 is a component of the acrosomal matrix. Biology of reproduction *64*, 36-43.

Kim, K.S., and Gerton, G.L. (2003). Differential release of soluble and matrix components: evidence for intermediate states of secretion during spontaneous acrosomal exocytosis in mouse sperm. Developmental biology *264*, 141-152.

Knapp, A., Kornblatt, M.J., Schachter, H., and Murray, R.K. (1973). Studies on the biosynthesis of testicular sulfoglycerogalactolipid: demonstration of a Golgi-associated sulfotransferase activity. Biochemical and biophysical research communications *55*, 179-186.

Kofeler, H.C., Fauland, A., Rechberger, G.N., and Trotzmuller, M. (2012). Mass spectrometry based lipidomics: an overview of technological platforms. Metabolites *2*, 19-38.

Kohlschutter, A. (2013). Lysosomal leukodystrophies: Krabbe disease and metachromatic leukodystrophy. Handbook of clinical neurology *113*, 1611-1618.

Kohn, F.M., Dammshauser, I., Neukamm, C., Renneberg, H., Siems, W.E., Schill, W.B., and Aumuller, G. (1998). Ultrastructural localization of angiotensin-converting enzyme in ejaculated human spermatozoa. Hum Reprod *13*, 604-610.

Kolter, T., and Sandhoff, K. (2005). Principles of lysosomal membrane digestion: stimulation of sphingolipid degradation by sphingolipid activator proteins and anionic lysosomal lipids. Annual review of cell and developmental biology *21*, 81-103.

Komljenovic, D., Sandhoff, R., Teigler, A., Heid, H., Just, W.W., and Gorgas, K. (2009). Disruption of blood-testis barrier dynamics in ether-lipid-deficient mice. Cell and tissue research *337*, 281-299.

Kongmanas, K., Kruevaisayawan, H., Saewu, A., Sugeng, C., Fernandes, J., Souda, P., Angel, J.B., Faull, K.F., Aitken, R.J., Whitelegge, J., *et al.* (2014). Proteomic

Characterization of Pig Sperm Anterior Head Plasma Membrane Reveals Roles of Acrosomal Proteins in ZP3 Binding. Journal of cellular physiology.

Kongmanas, K., Xu, H., Yaghoubian, A., Franchini, L., Panza, L., Ronchetti, F., Faull, K., and Tanphaichitr, N. (2010). Quantification of seminolipid by LC-ESI-MS/MS-multiple reaction monitoring: compensatory levels in Cgt(+/(-)) mice. Journal of lipid research *51*, 3548-3558.

Korah, N., Smith, C.E., D'Azzo, A., El-Alfy, M., and Hermo, L. (2003). Increase in macrophages in the testis of cathepsin a deficient mice suggests an important role for these cells in the interstitial space of this tissue. Molecular reproduction and development *64*, 302-320.

Kornblatt, M.J. (1979). Synthesis and turnover of sulfogalactoglycerolipid, a membrane lipid, during spermatogenesis. Canadian journal of biochemistry *57*, 255-258.

Kornblatt, M.J., Knapp, A., Levine, M., Schachter, H., and Murray, R.K. (1974). Studies on the structure and formation during spermatogenesis of the sulfoglycerogalactolipid of rat testis. Canadian journal of biochemistry *52*, 689-697.

Kornblatt, M.J., Schachter, H., and Murray, R.K. (1972). Partial characterization of a novel glycerogalactolipid from rat testis. Biochemical and biophysical research communications *48*, 1489-1494.

Kreysing, J., Polten, A., Hess, B., von Figura, K., Menz, K., Steiner, F., and Gieselmann, V. (1994a). Structure of the mouse arylsulfatase A gene and cDNA. Genomics *19*, 249-256.

Kreysing, J., Polten, A., Lukatela, G., Matzner, U., von Figura, K., and Gieselmann, V. (1994b). Translational control of arylsulfatase A expression in mouse testis. The Journal of biological chemistry *269*, 23255-23261.

Kurosawa, N., Kadomatsu, K., Ikematsu, S., Sakuma, S., Kimura, T., and Muramatsu, T. (2000). Midkine binds specifically to sulfatide the role of sulfatide in cell attachment to midkine-coated surfaces. European journal of biochemistry / FEBS *267*, 344-351.

Lachance, C., Fortier, M., Thimon, V., Sullivan, R., Bailey, J.L., and Leclerc, P. (2010). Localization of Hsp60 and Grp78 in the human testis, epididymis and mature spermatozoa. International journal of andrology *33*, 33-44.

Laemmli, U.K. (1970). Cleavage of structural proteins during the assembly of the head of bacteriophage T4. Nature *227*, 680-685.

Langlais, J., Kan, F.W., Granger, L., Raymond, L., Bleau, G., and Roberts, K.D. (1988). Identification of sterol acceptors that stimulate cholesterol efflux from human spermatozoa during in vitro capacitation. Gamete research *20*, 185-201.

Langlais, J., Zollinger, M., Plante, L., Chapdelaine, A., Bleau, G., and Roberts, K.D. (1981). Localization of cholesteryl sulfate in human spermatozoa in support of a hypothesis for the mechanism of capacitation. Proceedings of the National Academy of Sciences of the United States of America *78*, 7266-7270.

Lasserre, A., Barrozo, R., Tezon, J.G., Miranda, P.V., and Vazquez-Levin, M.H. (2001). Human epididymal proteins and sperm function during fertilization: un update. Biological research *34*, 165-178.

Law, H., Itkonnen, O., and Lingwood, C.A. (1988). Sulfogalactolipid binding protein SLIP 1: a conserved function for a conserved protein. Journal of cellular physiology *137*, 462-468.

Legault, Y., Bouthillier, M., Bleau, G., Chapdelaine, A., and Roberts, K.D. (1979). The sterol and sterol sulfate content of the male hamster reproductive tract. Biology of reproduction *20*, 1213-1219.

Lenzi, A., Picardo, M., Gandini, L., and Dondero, F. (1996). Lipids of the sperm plasma membrane: from polyunsaturated fatty acids considered as markers of sperm function to possible scavenger therapy. Human reproduction update *2*, 246-256.

Letts, P.J., Hunt, R.C., Shirley, M.A., Pinteric, L., and Schachter, H. (1978). Late spermatocytes from immature rat testis: Isolation, electron microscopy, letin agglutinability and capacity for glycoprotein and sulfogalactoglycerolipid biosynthesis. Biochim Biophys Acta *541*, 59-75.

Levine, M., Bain, J., Narashimhan, R., Palmer, B., Yates, A.J., and Murray, R.K. (1976). A comparative study of the glycolipids of human, bird and fish testes and of human sperm. Biochimica et biophysica acta *441*, 134-145.

Li, J.C., Lee, T.W., Mruk, T.D., and Cheng, C.Y. (2001). Regulation of Sertoli cell myotubularin (rMTM) expression by germ cells in vitro. Journal of andrology *22*, 266-277.

Lin, Y., Mahan, K., Lathrop, W.F., Myles, D.G., and Primakoff, P. (1994). A hyaluronidase activity of the sperm plasma membrane protein PH-20 enables sperm to penetrate the cumulus cell layer surrounding the egg. The Journal of cell biology *125*, 1157-1163.

Lin, Y.N., Roy, A., Yan, W., Burns, K.H., and Matzuk, M.M. (2007). Loss of zona pellucida binding proteins in the acrosomal matrix disrupts acrosome biogenesis and sperm morphogenesis. Molecular and cellular biology *27*, 6794-6805.

Lingwood, C., and Nutikka, A. (1991). Studies on the spermatogenic sulfogalactolipid binding protein SLIP 1. Journal of cellular physiology *146*, 258-263.

Lingwood, C., Schramayr, S., and Quinn, P. (1990). Male germ cell specific sulfogalactoglycerolipid is recognized and degraded by mycoplasmas associated with male infertility. Journal of cellular physiology *142*, 170-176.

Lingwood, C.A. (1985). Protein-glycolipid interactions during spermatogenesis. Binding of specific germ cell proteins to sulfatoxygalactosylacylalkylglycerol, the major glycolipid of mammalian male germ cells. Canadian journal of biochemistry and cell biology = Revue canadienne de biochimie et biologie cellulaire *63*, 1077-1085.

Litscher, E.S., Williams, Z., and Wassarman, P.M. (2009). Zona pellucida glycoprotein ZP3 and fertilization in mammals. Molecular reproduction and development *76*, 933-941.

Lopez, L.C., Bayna, E.M., Litoff, D., Shaper, N.L., Shaper, J.H., and Shur, B.D. (1985). Receptor function of mouse sperm surface galactosyltransferase during fertilization. The Journal of cell biology *101*, 1501-1510.

Lu, Q., Hasty, P., and Shur, B.D. (1997). Targeted mutation in beta1,4-galactosyltransferase leads to pituitary insufficiency and neonatal lethality. Developmental biology *181*, 257-267.

Luddi, A., Strazza, M., Carbone, M., Moretti, E., and Costantino-Ceccarini, E. (2005). Galactosylceramidase deficiency causes sperm abnormalities in the mouse model of globoid cell leukodystrophy. Experimental cell research *304*, 59-68.

Lukatela, G., Krauss, N., Theis, K., Selmer, T., Gieselmann, V., von Figura, K., and Saenger, W. (1998). Crystal structure of human arylsulfatase A: the aldehyde function and the metal ion at the active site suggest a novel mechanism for sulfate ester hydrolysis. Biochemistry *37*, 3654-3664.

Lullmann-Rauch, R., Matzner, U., Franken, S., Hartmann, D., and Gieselmann, V. (2001). Lysosomal sulfoglycolipid storage in the kidneys of mice deficient for arylsulfatase A (ASA) and of double-knockout mice deficient for ASA and galactosylceramide synthase. Histochemistry and cell biology *116*, 161-169.

Mahony, M.C., and Gwathmey, T. (1999). Protein tyrosine phosphorylation during hyperactivated motility of cynomolgus monkey (Macaca fascicularis) spermatozoa. Biology of reproduction *60*, 1239-1243.

Mamelak, D., and Lingwood, C. (2001). The ATPase domain of hsp70 possesses a unique binding specificity for 3'-sulfogalactolipids. The Journal of biological chemistry *276*, 449-456.

Matsuda, J., and Suzuki, K. (2007). Krabbe Disease (Globoid Cell Leukodystrophy). In Lysosomal Storage Disorders, J.A. Barranger, and M.A. Cabrera-Salazar, eds. (New York: Springer), pp. 269-283.

Mehl, E., and Jatzkewitz, H. (1968). Cerebroside 3-sulfate as a physiological substrate of arylsulfatase A. Biochimica et biophysica acta *151*, 619-627.

Melendrez, C.S., Meizel, S., and Berger, T. (1994). Comparison of the ability of progesterone and heat solubilized porcine zona pellucida to initiate the porcine sperm acrosome reaction in vitro. Molecular reproduction and development *39*, 433-438.

Meroni, S.B., Riera, M.F., Pellizzari, E.H., Schteingart, H.F., and Cigorraga, S.B. (2003). Possible role of arachidonic acid in the regulation of lactate production in rat Sertoli cells. International journal of andrology *26*, 310-317.

Miki, K., Qu, W., Goulding, E.H., Willis, W.D., Bunch, D.O., Strader, L.F., Perreault, S.D., Eddy, E.M., and O'Brien, D.A. (2004). Glyceraldehyde 3-phosphate dehydrogenase-S, a sperm-specific glycolytic enzyme, is required for sperm motility and male fertility. Proceedings of the National Academy of Sciences of the United States of America *101*, 16501-16506.

Miki, T., Kaneda, M., Iida, K., Hasegawa, G., Murakami, M., Yamamoto, N., Asou, H., and Kasahara, K. (2013). An anti-sulfatide antibody O4 immunoprecipitates sulfatide rafts including Fyn, Lyn and the G protein alpha subunit in rat primary immature oligodendrocytes. Glycoconjugate journal *30*, 819-823.

Miller, D.J., Macek, M.B., and Shur, B.D. (1992). Complementarity between sperm surface beta-1,4-galactosyltransferase and egg-coat ZP3 mediates sperm-egg binding. Nature *357*, 589-593.

Mohan, P.S., Laitinen, J., Merenmies, J., Rauvala, H., and Jungalwala, F.B. (1992). Sulfoglycolipids bind to adhesive protein amphoterin (P30) in the nervous system. Biochemical and biophysical research communications *182*, 689-696.

Molander-Melin, M., Pernber, Z., Franken, S., Gieselmann, V., Mansson, J.E., and Fredman, P. (2004). Accumulation of sulfatide in neuronal and glial cells of arylsulfatase A deficient mice. Journal of neurocytology *33*, 417-427.

Morales, C.R., Hay, N., El-Alfy, M., and Zhao, Q. (1998). Distribution of mouse sulfated glycoprotein-1 (prosaposin) in the testis and other tissues. Journal of andrology *19*, 156-164.

Mori, E., Baba, T., Iwamatsu, A., and Mori, T. (1993). Purification and characterization of a 38-kDa protein, sp38, with zona pellucida-binding property from porcine epididymal sperm. Biochemical and biophysical research communications *196*, 196-202.

Mori, E., Kashiwabara, S., Baba, T., Inagaki, Y., and Mori, T. (1995). Amino acid sequences of porcine Sp38 and proacrosin required for binding to the zona pellucida. Developmental biology *168*, 575-583.

Moviglia, G.A., Cavicchia, J.C., and Bertini, F. (1982). Lysosomal enzymes in cells separated from rat testis. Journal of reproduction and fertility *66*, 123-127.

Mruk, D.D., and Cheng, C.Y. (2004). Sertoli-Sertoli and Sertoli-germ cell interactions and their significance in germ cell movement in the seminiferous epithelium during spermatogenesis. Endocrine reviews *25*, 747-806.

Muro, Y., Buffone, M.G., Okabe, M., and Gerton, G.L. (2012). Function of the acrosomal matrix: zona pellucida 3 receptor (ZP3R/sp56) is not essential for mouse fertilization. Biology of reproduction *86*, 1-6.

Nassar, A., Mahony, M., Morshedi, M., Lin, M.H., Srisombut, C., and Oehninger, S. (1999). Modulation of sperm tail protein tyrosine phosphorylation by pentoxifylline and its correlation with hyperactivated motility. Fertility and sterility *71*, 919-923.

Needham, L.K., and Schnaar, R.L. (1993). The HNK-1 reactive sulfoglucuronyl glycolipids are ligands for L-selectin and P-selectin but not E-selectin. Proceedings of the National Academy of Sciences of the United States of America *90*, 1359-1363.

Newton, S.C., Blaschuk, O.W., and Millette, C.F. (1993). N-cadherin mediates Sertoli cell-spermatogenic cell adhesion. Developmental dynamics : an official publication of the American Association of Anatomists *197*, 1-13.

Nichol, L.W., and Roy, A.B. (1965). The Sulfatase of Ox Liver. Ix. The Polymerization of Sulfatase A. Biochemistry *4*, 386-396.

Nixon, B., and Aitken, R.J. (2009). The biological significance of detergent-resistant membranes in spermatozoa. Journal of reproductive immunology *83*, 8-13.

Nixon, B., Aitken, R.J., and McLaughlin, E.A. (2007). New insights into the molecular mechanisms of sperm-egg interaction. Cellular and molecular life sciences : CMLS *64*, 1805-1823.

Nixon, B., Asquith, K.L., and John Aitken, R. (2005). The role of molecular chaperones in mouse sperm-egg interactions. Molecular and cellular endocrinology *240*, 1-10.

Nixon, B., Bielanowicz, A., McLaughlin, E.A., Tanphaichitr, N., Ensslin, M.A., and Aitken, R.J. (2009). Composition and significance of detergent resistant membranes in mouse spermatozoa. Journal of cellular physiology *218*, 122-134.

Nixon, B., Mitchell, L.A., Anderson, A.L., McLaughlin, E.A., O'Bryan M, K., and Aitken, R.J. (2011). Proteomic and functional analysis of human sperm detergent resistant membranes. Journal of cellular physiology *226*, 2651-2665.

Noland, T.D., Davis, L.S., and Olson, G.E. (1989). Regulation of proacrosin conversion in isolated guinea pig sperm acrosomal apical segments. The Journal of biological chemistry *264*, 13586-13590.

O'Brien, J.S., and Kishimoto, Y. (1991). Saposin proteins: structure, function, and role in human lysosomal storage disorders. FASEB journal : official publication of the Federation of American Societies for Experimental Biology *5*, 301-308.

O'Flaherty, C., de Lamirande, E., and Gagnon, C. (2006). Positive role of reactive oxygen species in mammalian sperm capacitation: triggering and modulation of phosphorylation events. Free radical biology & medicine *41*, 528-540.

Oliva, R., de Mateo, S., and Estanyol, J.M. (2009). Sperm cell proteomics. Proteomics *9*, 1004-1017.

Olson, G.E., Winfrey, V.P., Bi, M., Hardy, D.M., and NagDas, S.K. (2004). Zonadhesin assembly into the hamster sperm acrosomal matrix occurs by distinct targeting strategies during spermiogenesis and maturation in the epididymis. Biology of reproduction *71*, 1128-1134.

Olson, L.D., and Gilbert, A.A. (1993). Characteristics of Mycoplasma hominis adhesion. Journal of bacteriology *175*, 3224-3227.

Orth, J.M. (1984). The role of follicle-stimulating hormone in controlling Sertoli cell proliferation in testes of fetal rats. Endocrinology *115*, 1248-1255.

Overstreet, J.W., Lin, Y., Yudin, A.I., Meyers, S.A., Primakoff, P., Myles, D.G., Katz, D.F., and Vandevoort, C.A. (1995). Location of the PH-20 protein on acrosome-intact and acrosome-reacted spermatozoa of cynomolgus macaques. Biology of reproduction *52*, 105-114.

Pancake, S.J., Holt, G.D., Mellouk, S., and Hoffman, S.L. (1993). Malaria sporozoites and circumsporozoite protein bind sulfated glycans: carbohydrate binding properties predicted from sequence homologies with other lectins. Parassitologia *35 Suppl*, 77-80.

Peterson, R., Russell, L., Bundman, D., and Freund, M. (1980). Evaluation of the purity of boar sperm plasma membranes prepared by nitrogen cavitation. Biology of reproduction *23*, 637-645.

Petrunkina, A.M., Harrison, R.A., and Topfer-Petersen, E. (2000). Only low levels of spermadhesin AWN are detectable on the surface of live ejaculated boar spermatozoa. Reproduction, fertility, and development *12*, 361-371.

Pike, L.J. (2009). The challenge of lipid rafts. Journal of lipid research *50 Suppl*, S323-328.

Piomboni, P., Governini, L., Gori, M., Puggioni, E., Costantino-Ceccarini, E., and Luddi, A. (2014). New players in the infertility of a mouse model of lysosomal storage disease: the hypothalamus-pituitary-gonadal axis. Frontiers in endocrinology *4*, 204.

Platt, F.M., Boland, B., and van der Spoel, A.C. (2012). The cell biology of disease: lysosomal storage disorders: the cellular impact of lysosomal dysfunction. The Journal of cell biology *199*, 723-734.

Polakoski, K.L., and Parrish, R.F. (1977). Boar proacrosin. Purification and preliminary activation studies of proacrosin isolated from ejaculated boar sperm. The Journal of biological chemistry *252*, 1888-1894.

Primakoff, P., Hyatt, H., and Myles, D.G. (1985). A role for the migrating sperm surface antigen PH-20 in guinea pig sperm binding to the egg zona pellucida. The Journal of cell biology *101*, 2239-2244.

Puigmule, M., Fabrega, A., Yeste, M., Bonet, S., and Pinart, E. (2011). Study of the proacrosin-acrosin system in epididymal, ejaculated and in vitro capacitated boar spermatozoa. Reproduction, fertility, and development *23*, 837-845.

Qi, H., Moran, M.M., Navarro, B., Chong, J.A., Krapivinsky, G., Krapivinsky, L., Kirichok, Y., Ramsey, I.S., Quill, T.A., and Clapham, D.E. (2007). All four CatSper ion channel proteins are required for male fertility and sperm cell hyperactivated motility. Proceedings of the National Academy of Sciences of the United States of America *104*, 1219-1223.

Quaas, A., and Dokras, A. (2008). Diagnosis and treatment of unexplained infertility. Reviews in obstetrics & gynecology *1*, 69-76.

Quinta, H.R., Galigniana, N.M., Erlejman, A.G., Lagadari, M., Piwien-Pilipuk, G., and Galigniana, M.D. (2011). Management of cytoskeleton architecture by molecular chaperones and immunophilins. Cellular signalling *23*, 1907-1920.

Rankin, T., Familari, M., Lee, E., Ginsberg, A., Dwyer, N., Blanchette-Mackie, J., Drago, J., Westphal, H., and Dean, J. (1996). Mice homozygous for an insertional mutation in the Zp3 gene lack a zona pellucida and are infertile. Development *122*, 2903-2910.

Rankin, T., Talbot, P., Lee, E., and Dean, J. (1999). Abnormal zonae pellucidae in mice lacking ZP1 result in early embryonic loss. Development *126*, 3847-3855.

Rankin, T.L., O'Brien, M., Lee, E., Wigglesworth, K., Eppig, J., and Dean, J. (2001). Defective zonae pellucidae in Zp2-null mice disrupt folliculogenesis, fertility and development. Development *128*, 1119-1126.

Rato, L., Alves, M.G., Socorro, S., Duarte, A.I., Cavaco, J.E., and Oliveira, P.F. (2012). Metabolic regulation is important for spermatogenesis. Nature reviews Urology *9*, 330-338.

Rattanachaiyanont, M., Weerachatyanukul, W., Leveille, M.C., Taylor, T., D'Amours, D., Rivers, D., Leader, A., and Tanphaichitr, N. (2001). Anti-SLIP1-reactive proteins exist on human spermatozoa and are involved in zona pellucida binding. Molecular human reproduction *7*, 633-640.

Reddy, J.M., Audhya, T.K., Goodpasture, J.C., and Zaneveld, L.J. (1982). Properties of a highly purified antifertility factor from human seminal plasma. Biology of reproduction *27*, 1076-1083.

Reddy, J.M., Stark, R.A., and Zaneveld, L.J. (1979). A high molecular weight antifertility factor from human seminal plasma. Journal of reproduction and fertility *57*, 437-446.

Redgrove, K.A., Aitken, R.J., and Nixon, B. (2012). More Than a Simple Lock and Key Mechanism: Unraveling the Intricacies of Sperm-Zona Pellucida Binding, Binding Protein, PhD. Kotb Abdelmohsen (Ed.), ISBN: 978-953-51-0758-3, InTech, DOI: 10.5772/50499. Available from: http://www.intechopen.com/books/binding-protein/more-than-a-simple-lock-and-key-mechanism-unraveling-the-intricacies-of-sperm-zona-pellucida-bindingMore Than a Simple Lock and Key Mechanism: Unraveling the Intricacies of Sperm-Zona Pellucida Binding.

Redgrove, K.A., Anderson, A.L., Dun, M.D., McLaughlin, E.A., O'Bryan, M.K., Aitken, R.J., and Nixon, B. (2011). Involvement of multimeric protein complexes in mediating the capacitation-dependent binding of human spermatozoa to homologous zonae pellucidae. Developmental biology *356*, 460-474.

Rejraji, H., Sion, B., Prensier, G., Carreras, M., Motta, C., Frenoux, J.M., Vericel, E., Grizard, G., Vernet, P., and Drevet, J.R. (2006). Lipid remodeling of murine epididymosomes and spermatozoa during epididymal maturation. Biology of reproduction *74*, 1104-1113.

Rivlin, J., Mendel, J., Rubinstein, S., Etkovitz, N., and Breitbart, H. (2004). Role of hydrogen peroxide in sperm capacitation and acrosome reaction. Biology of reproduction *70*, 518-522.

Rizzoli, S.O., and Jahn, R. (2007). Kiss-and-run, collapse and 'readily retrievable' vesicles. Traffic *8*, 1137-1144.

Roberts, D.D. (1988). Interactions of thrombospondin with sulfated glycolipids and proteoglycans of human melanoma cells. Cancer research *48*, 6785-6793.

Roberts, D.D., Rao, C.N., Magnani, J.L., Spitalnik, S.L., Liotta, L.A., and Ginsburg, V. (1985). Laminin binds specifically to sulfated glycolipids. Proceedings of the National Academy of Sciences of the United States of America *82*, 1306-1310.

Roberts, D.D., Williams, S.B., Gralnick, H.R., and Ginsburg, V. (1986). von Willebrand factor binds specifically to sulfated glycolipids. The Journal of biological chemistry *261*, 3306-3309.

Roberts, K.D. (1987). Sterol sulfates in the epididymis; synthesis and possible function in the reproductive process. Journal of steroid biochemistry *27*, 337-341.

Rochwerger, L., and Cuasnicu, P.S. (1992). Redistribution of a rat sperm epididymal glycoprotein after in vitro and in vivo capacitation. Molecular reproduction and development *31*, 34-41.

Rodemer, C., Thai, T.P., Brugger, B., Gorgas, K., and Just, W. (2003). Targeted disruption of ether lipid synthesis in mice. Advances in experimental medicine and biology *544*, 355-368.

Rolim, A.E., Henrique-Araujo, R., Ferraz, E.G., de Araujo Alves Dultra, F.K., and Fernandez, L.G. (2014). Lipidomics in the study of lipid metabolism: Current perspectives in the omic sciences. Gene *554*, 131-139.

Rosenberg, J.B., Haberichter, S.L., Jozwiak, M.A., Vokac, E.A., Kroner, P.A., Fahs, S.A., Kawai, Y., and Montgomery, R.R. (2002). The role of the D1 domain of the von Willebrand factor propeptide in multimerization of VWF. Blood *100*, 1699-1706.

Rousset, E., Harel, J., and Dubreuil, J.D. (1998). Sulfatide from the pig jejunum brush border epithelial cell surface is involved in binding of Escherichia coli enterotoxin b. Infection and immunity *66*, 5650-5658.

Roy, S.C., and Atreja, S.K. (2008). Effect of reactive oxygen species on capacitation and associated protein tyrosine phosphorylation in buffalo (Bubalus bubalis) spermatozoa. Animal reproduction science *107*, 68-84.

Russell, L.D. (1993). Morphological and Functional Evidence for Sertoli-germ Cell Relationships. In The Sertoli Cell, L.D. Russell, and M.D. Griswold, eds. (Clearwater, FL: Cache River Press).

Sacco, A.G., Yurewicz, E.C., Subramanian, M.G., and Matzat, P.D. (1989). Porcine zona pellucida: association of sperm receptor activity with the alpha-glycoprotein component of the Mr = 55,000 family. Biology of reproduction *41*, 523-532.

Sakac, D., Zachos, M., and Lingwood, C.A. (1992). Purification of the testicular galactolipid: 3'-phosphoadenosine 5'-phosphosulfate sulfotransferase. The Journal of biological chemistry *267*, 1655-1659.

Sandra, K., and Sandra, P. (2013). Lipidomics from an analytical perspective. Current opinion in chemical biology *17*, 847-853.

Sato, H., Taketomi, Y., Isogai, Y., Miki, Y., Yamamoto, K., Masuda, S., Hosono, T., Arata, S., Ishikawa, Y., Ishii, T., *et al.* (2010). Group III secreted phospholipase A2 regulates epididymal sperm maturation and fertility in mice. The Journal of clinical investigation *120*, 1400-1414.

Schenk, M., Koppisetty, C.A., Santos, D.C., Carmona, E., Bhatia, S., Nyholm, P.G., and Tanphaichitr, N. (2009). Interaction of arylsulfatase-A (ASA) with its natural sulfoglycolipid substrates: a computational and site-directed mutagenesis study. Glycoconjugate journal *26*, 1029-1045.

Schott, I., Hartmann, D., Gieselmann, V., and Lullmann-Rauch, R. (2001). Sulfatide storage in visceral organs of arylsulfatase A-deficient mice. Virchows Archiv : an international journal of pathology *439*, 90-96.

Schroeder, R., London, E., and Brown, D. (1994). Interactions between saturated acyl chains confer detergent resistance on lipids and glycosylphosphatidylinositol (GPI)-anchored proteins: GPI-anchored proteins in liposomes and cells show similar behavior. Proceedings of the National Academy of Sciences of the United States of America *91*, 12130-12134.

Schuck, S., Honsho, M., Ekroos, K., Shevchenko, A., and Simons, K. (2003). Resistance of cell membranes to different detergents. Proceedings of the National Academy of Sciences of the United States of America *100*, 5795-5800.

Schulze, H., Kolter, T., and Sandhoff, K. (2009). Principles of lysosomal membrane degradation: Cellular topology and biochemistry of lysosomal lipid degradation. Biochimica et biophysica acta *1793*, 674-683.

Scully, N.F., Shaper, J.H., and Shur, B.D. (1987). Spatial and temporal expression of cell surface galactosyltransferase during mouse spermatogenesis and epididymal maturation. Developmental biology *124*, 111-124.

Shadan, S., James, P.S., Howes, E.A., and Jones, R. (2004). Cholesterol efflux alters lipid raft stability and distribution during capacitation of boar spermatozoa. Biology of reproduction *71*, 253-265.

Shalgi, R., Matityahu, A., Gaunt, S.J., and Jones, R. (1990). Antigens on rat spermatozoa with a potential role in fertilization. Molecular reproduction and development *25*, 286-296.

Simons, K., and Ehehalt, R. (2002). Cholesterol, lipid rafts, and disease. The Journal of clinical investigation *110*, 597-603.

Simons, K., and Ikonen, E. (1997). Functional rafts in cell membranes. Nature *387*, 569-572.

Simons, K., and Toomre, D. (2000). Lipid rafts and signal transduction. Nature reviews Molecular cell biology *1*, 31-39.

Singh, A.P., and Rajender, S. (2014). CatSper channel, sperm function and male fertility. Reproductive biomedicine online.

Singh, R., Kaushik, S., Wang, Y., Xiang, Y., Novak, I., Komatsu, M., Tanaka, K., Cuervo, A.M., and Czaja, M.J. (2009). Autophagy regulates lipid metabolism. Nature *458*, 1131-1135.

Sion, B., Grizard, G., and Boucher, D. (2001). Quantitative analysis of desmosterol, cholesterol and cholesterol sulfate in semen by high-performance liquid chromatography. Journal of chromatography A *935*, 259-265.

Sleight, S.B., Miranda, P.V., Plaskett, N.W., Maier, B., Lysiak, J., Scrable, H., Herr, J.C., and Visconti, P.E. (2005). Isolation and proteomic analysis of mouse sperm detergent-resistant membrane fractions: evidence for dissociation of lipid rafts during capacitation. Biology of reproduction *73*, 721-729.

Smart, E.J., Ying, Y.S., Mineo, C., and Anderson, R.G. (1995). A detergent-free method for purifying caveolae membrane from tissue culture cells. Proceedings of the National Academy of Sciences of the United States of America *92*, 10104-10108.

Smeeding, T.M. (2014). Economics. Adjusting to the fertility bust. Science *346*, 163-164.

Sommerlade, H.J., Selmer, T., Ingendoh, A., Gieselmann, V., von Figura, K., Neifer, K., and Schmidt, B. (1994). Glycosylation and phosphorylation of arylsulfatase A. The Journal of biological chemistry *269*, 20977-20981.

Sonnino, S., and Prinetti, A. (2013). Membrane domains and the "lipid raft" concept. Current medicinal chemistry *20*, 4-21.

Spiegel, R., Bach, G., Sury, V., Mengistu, G., Meidan, B., Shalev, S., Shneor, Y., Mandel, H., and Zeigler, M. (2005). A mutation in the saposin A coding region of the prosaposin gene in an infant presenting as Krabbe disease: first report of saposin A deficiency in humans. Molecular genetics and metabolism *84*, 160-166.

Sprenger, R.R., and Horrevoets, A.J. (2007). The ins and outs of lipid domain proteomics. Proteomics *7*, 2895-2903.

Sprong, H., Kruithof, B., Leijendekker, R., Slot, J.W., van Meer, G., and van der Sluijs, P. (1998). UDP-galactose:ceramide galactosyltransferase is a class I integral membrane protein of the endoplasmic reticulum. The Journal of biological chemistry *273*, 25880-25888.

Stein, C., Gieselmann, V., Kreysing, J., Schmidt, B., Pohlmann, R., Waheed, A., Meyer, H.E., O'Brien, J.S., and von Figura, K. (1989). Cloning and expression of human arylsulfatase A. The Journal of biological chemistry *264*, 1252-1259.

Stein, K.K., Go, J.C., Lane, W.S., Primakoff, P., and Myles, D.G. (2006). Proteomic analysis of sperm regions that mediate sperm-egg interactions. Proteomics *6*, 3533-3543.

Stein, K.K., Go, J.C., Primakoff, P., and Myles, D.G. (2005). Defects in secretory pathway trafficking during sperm development in Adam2 knockout mice. Biology of reproduction *73*, 1032-1038.

Suzuki, Y., Toda, Y., Tamatani, T., Watanabe, T., Suzuki, T., Nakao, T., Murase, K., Kiso, M., Hasegawa, A., Tadano-Aritomi, K., *et al.* (1993). Sulfated glycolipids are ligands for a lymphocyte homing receptor, L-selectin (LECAM-1), Binding epitope in sulfated sugar chain. Biochemical and biophysical research communications *190*, 426-434.

Tadano-Aritomi, K., Hikita, T., Fujimoto, H., Suzuki, K., Motegi, K., and Ishizuka, I. (2000). Kidney lipids in galactosylceramide synthase-deficient mice. Absence of galactosylsulfatide and compensatory increase in more polar sulfoglycolipids. Journal of lipid research *41*, 1237-1243.

Tahmasbpour, E., Balasubramanian, D., and Agarwal, A. (2014). A multi-faceted approach to understanding male infertility: gene mutations, molecular defects and assisted reproductive techniques (ART). Journal of assisted reproduction and genetics *31*, 1115-1137.

Takahashi, T., and Suzuki, T. (2012). Role of sulfatide in normal and pathological cells and tissues. Journal of lipid research *53*, 1437-1450.

Talbot, P. (1984). Hyaluronidase dissolves a component in the hamster zona pellucida. The Journal of experimental zoology *229*, 309-316.

Tanphaichitr, N., Bou Khalil, M., Weerachatyanukul, W., Kates, M., Xu, H., Carmona, E., Attar, M., and Carrier, D. (2003). Physiological and biophysical properties of male germ cell sulfogalactosylglycerolipid. In Lipid Metabolism and Male Fertility, S. De Vriese, ed. (Champaign, IL: AOCS Press), pp. 125-148.

Tanphaichitr, N., Carmona, E., Bou Khalil, M., Xu, H., Berger, T., and Gerton, G.L. (2007). New insights into sperm-zona pellucida interaction: involvement of sperm lipid rafts. Frontiers in bioscience : a journal and virtual library *12*, 1748-1766.

Tanphaichitr, N., Faull, K.F., Yaghoubian, A., and Xu, H. (2007b). Lipid Rafts and Sulfogalactosylglycerolipid (SGG) in Sperm Functions: Consensus and Controversy. Trends in Glycoscience and Glycotechnology *19*, 67-83.

Tanphaichitr, N., Moase, C., Taylor, T., Surewicz, K., Hansen, C., Namking, M., Berube, B., Kamolvarin, N., Lingwood, C.A., Sullivan, R., *et al.* (1998). Isolation of antiSLIP1-reactive boar sperm P68/62 and its binding to mammalian zona pellucida. Molecular reproduction and development *49*, 203-216.

Tanphaichitr, N., Smith, J., and Kates, M. (1990). Levels of sulfogalactosylglycerolipid in capacitated motile and immotile mouse spermatozoa. Biochemistry and cell biology = Biochimie et biologie cellulaire *68*, 528-535.

Tanphaichitr, N., Smith, J., Mongkolsirikieart, S., Gradil, C., and Lingwood, C.A. (1993). Role of a gamete-specific sulfoglycolipid immobilizing protein on mouse sperm-egg binding. Developmental biology *156*, 164-175.

Tanphaichitr, N., Tayabali, A., Gradil, C., Juneja, S., Leveille, M.C., and Lingwood, C.A. (1992). Role of a germ cell-specific sulfolipid-immobilizing protein (SLIP1) in mouse in vivo fertilization. Molecular reproduction and development *32*, 17-22.

Tanphaichitr, N., Taylor, T., White, D., Rattanachaiyanont, M., and Moase, C. (1998b). Arylsulfatase-A is a component of boar sperm SLIP1 (P68) and may be involved in sperm-zona pellucida binding. Biology of Reproduction *58 Suppl.*, 158a.

Tanphaichitr, N., White, D., Taylor, T., Attar, M., Rattanachaiyanont, M., and Kates, M. (1999). Role of male germ-cell specific sulfogalactosylglycerolipid (SGG) and its binding protein, SLIP1, in mammalian sperm-egg interaction. In The Male Gamete: From Basic Knowledge to Clinical Applications, C. Gagnon, ed. (Vienna,IL: Cache Press), pp. 227-235.

Tantibhedhyangkul, J., Weerachatyanukul, W., Carmona, E., Xu, H., Anupriwan, A., Michaud, D., and Tanphaichitr, N. (2002). Role of sperm surface arylsulfatase A in mouse sperm-zona pellucida binding. Biology of reproduction *67*, 212-219.

Tardif, S., and Cormier, N. (2011). Role of zonadhesin during sperm-egg interaction: a species-specific acrosomal molecule with multiple functions. Molecular human reproduction *17*, 661-668.

Tardif, S., Guyonnet, B., Cormier, N., and Cornwall, G.A. (2012). Alteration in the processing of the ACRBP/sp32 protein and sperm head/acrosome malformations in proprotein convertase 4 (PCSK4) null mice. Molecular human reproduction *18*, 298-307.

Tardif, S., Wilson, M.D., Wagner, R., Hunt, P., Gertsenstein, M., Nagy, A., Lobe, C., Koop, B.F., and Hardy, D.M. (2010). Zonadhesin is essential for species specificity of sperm adhesion to the egg zona pellucida. The Journal of biological chemistry *285*, 24863-24870.

Tarulli, G.A., Stanton, P.G., and Meachem, S.J. (2012). Is the adult Sertoli cell terminally differentiated? Biology of reproduction *87*, 13, 11-11.

Thaler, C.D., Thomas, M., and Ramalie, J.R. (2006). Reorganization of mouse sperm lipid rafts by capacitation. Molecular reproduction and development *73*, 1541-1549.

Therien, I., Soubeyrand, S., and Manjunath, P. (1997). Major proteins of bovine seminal plasma modulate sperm capacitation by high-density lipoprotein. Biology of reproduction *57*, 1080-1088.

Tohyama, J., Vanier, M.T., Suzuki, K., Ezoe, T., and Matsuda, J. (2000). Paradoxical influence of acid beta-galactosidase gene dosage on phenotype of the twitcher mouse (genetic galactosylceramidase deficiency). Human molecular genetics *9*, 1699-1707.

Tollner, T.L., Yudin, A.I., Tarantal, A.F., Treece, C.A., Overstreet, J.W., and Cherr, G.N. (2008). Beta-defensin 126 on the surface of macaque sperm mediates attachment of sperm to oviductal epithelia. Biology of reproduction *78*, 400-412.

Towbin, H., and Gordon, J. (1984). Immunoblotting and dot immunobinding--current status and outlook. Journal of immunological methods *72*, 313-340.

Trasler, J., Saberi, F., Somani, I.H., Adamali, H.I., Huang, J.Q., Fortunato, S.R., Ritter, G., Gu, M., Aebersold, R., Gravel, R.A., *et al.* (1998). Characterization of the testis and epididymis in mouse models of human Tay Sachs and Sandhoff diseases and partial determination of accumulated gangliosides. Endocrinology *139*, 3280-3288.

Tsai, P.S., Brewis, I.A., van Maaren, J., and Gadella, B.M. (2012). Involvement of complexin 2 in docking, locking and unlocking of different SNARE complexes during sperm capacitation and induced acrosomal exocytosis. PloS one *7*, e32603.

Tulsiani, D.R., and Abou-Haila, A. (2012). Biological Processes that Prepare Mammalian Spermatozoa to Interact with an Egg and Fertilize It. Scientifica *2012*, 607427.

Tulsiani, D.R., Skudlarek, M.D., Araki, Y., and Orgebin-Crist, M.C. (1995). Purification and characterization of two forms of beta-D-galactosidase from rat epididymal luminal fluid: evidence for their role in the modification of sperm plasma membrane glycoprotein(s). The Biochemical journal *305 (Pt 1)*, 41-50.

Tulsiani, D.R., Yoshida-Komiya, H., and Araki, Y. (1997). Mammalian fertilization: a carbohydrate-mediated event. Biology of reproduction *57*, 487-494.

Ueno, K., Ishizuka, I., and Yamakawa, T. (1977). Glycolipid composition of human testis at different ages and the stereochemical configuration of seminolipid. Biochimica et biophysica acta *487*, 61-73.

Vagedes, P., Saenger, W., and Knapp, E.W. (2002). Driving forces of protein association: the dimer-octamer equilibrium in arylsulfatase A. Biophysical journal *83*, 3066-3078.

van Gestel, R.A., Brewis, I.A., Ashton, P.R., Brouwers, J.F., and Gadella, B.M. (2007). Multiple proteins present in purified porcine sperm apical plasma membranes interact with the zona pellucida of the oocyte. Molecular human reproduction *13*, 445-454.

van Gestel, R.A., Brewis, I.A., Ashton, P.R., Helms, J.B., Brouwers, J.F., and Gadella, B.M. (2005). Capacitation-dependent concentration of lipid rafts in the apical ridge head area of porcine sperm cells. Molecular human reproduction *11*, 583-590.

Veselsky, L., Peknicova, J., Cechova, D., Kraus, M., Geussova, G., and Jonakova, V. (1999). Characterization of boar spermadhesins by monoclonal and polyclonal antibodies and their role in binding to oocytes. Am J Reprod Immunol *42*, 187-197.

Visconti, P.E., and Kopf, G.S. (1998). Regulation of protein phosphorylation during sperm capacitation. Biology of reproduction *59*, 1-6.

Visconti, P.E., Westbrook, V.A., Chertihin, O., Demarco, I., Sleight, S., and Diekman, A.B. (2002). Novel signaling pathways involved in sperm acquisition of fertilizing capacity. Journal of reproductive immunology *53*, 133-150.

Vitner, E.B., Platt, F.M., and Futerman, A.H. (2010). Common and uncommon pathogenic cascades in lysosomal storage diseases. The Journal of biological chemistry *285*, 20423-20427.

von Bulow, R., Schmidt, B., Dierks, T., von Figura, K., and Uson, I. (2001). Crystal structure of an enzyme-substrate complex provides insight into the interaction between human arylsulfatase A and its substrates during catalysis. Journal of molecular biology *305*, 269-277.

von Figura, K., Gieselmann, V., and Jaeken, J. (2001). Metachromatic Leukodystrophy. In The Online Metabolic & Molecular Bases of Inherited Disease (New York: The McGraw-Hill Companies), pp. 3695-3724.

Vos, J.P., Lopes-Cardozo, M., and Gadella, B.M. (1994). Metabolic and functional aspects of sulfogalactolipids. Biochimica et biophysica acta *1211*, 125-149.

Waheed, A., and van Etten, R.L. (1980). Chemical characterization and substrate specificity of rabbit liver aryl sulfatase A. Biochimica et biophysica acta *614*, 92-101.

Waldow, A., Schmidt, B., Dierks, T., von Bulow, R., and von Figura, K. (1999). Amino acid residues forming the active site of arylsulfatase A. Role in catalytic activity and substrate binding. The Journal of biological chemistry *274*, 12284-12288.

Walsh, A., Whelan, D., Bielanowicz, A., Skinner, B., Aitken, R.J., O'Bryan, M.K., and Nixon, B. (2008). Identification of the molecular chaperone, heat shock protein 1 (chaperonin 10), in the reproductive tract and in capacitating spermatozoa in the male mouse. Biology of reproduction *78*, 983-993.

Wang, H., Xiong, W., Chen, Y., Ma, Q., Ma, J., Ge, Y., and Han, D. (2006). Evaluation on the phagocytosis of apoptotic spermatogenic cells by Sertoli cells in vitro through detecting lipid droplet formation by Oil Red O staining. Reproduction *132*, 485-492.

Wassarman, P.M., and Litscher, E.S. (2008). Mammalian fertilization: the egg's multifunctional zona pellucida. The International journal of developmental biology *52*, 665-676.

Weber, J.E., Russell, L.D., Wong, V., and Peterson, R.N. (1983). Three-dimensional reconstruction of a rat stage V Sertoli cell: II. Morphometry of Sertoli--Sertoli and Sertoli--germ-cell relationships. The American journal of anatomy *167*, 163-179.

Weerachatyanukul, W., Probodh, I., Kongmanas, K., Tanphaichitr, N., and Johnston, L.J. (2007). Visualizing the localization of sulfoglycolipids in lipid raft domains in model membranes and sperm membrane extracts. Biochimica et biophysica acta *1768*, 299-310.

Weerachatyanukul, W., Rattanachaiyanont, M., Carmona, E., Furimsky, A., Mai, A., Shoushtarian, A., Sirichotiyakul, S., Ballakier, H., Leader, A., and Tanphaichitr, N. (2001).

Sulfogalactosylglycerolipid is involved in human gamete interaction. Molecular reproduction and development *60*, 569-578.

Weerachatyanukul, W., Xu, H., Anupriwan, A., Carmona, E., Wade, M., Hermo, L., da Silva, S.M., Rippstein, P., Sobhon, P., Sretarugsa, P., *et al.* (2003). Acquisition of arylsulfatase A onto the mouse sperm surface during epididymal transit. Biology of reproduction *69*, 1183-1192.

Wenk, M.R. (2005). The emerging field of lipidomics. Nature reviews Drug discovery *4*, 594-610.

Wertheimer, E., Krapf, D., de la Vega-Beltran, J.L., Sanchez-Cardenas, C., Navarrete, F., Haddad, D., Escoffier, J., Salicioni, A.M., Levin, L.R., Buck, J., *et al.* (2013). Compartmentalization of distinct cAMP signaling pathways in mammalian sperm. The Journal of biological chemistry *288*, 35307-35320.

White, D., Weerachatyanukul, W., Gadella, B., Kamolvarin, N., Attar, M., and Tanphaichitr, N. (2000). Role of sperm sulfogalactosylglycerolipid in mouse sperm-zona pellucida binding. Biology of reproduction *63*, 147-155.

Whitfield, P.D., Sharp, P.C., Taylor, R., and Meikle, P. (2001). Quantification of galactosylsphingosine in the twitcher mouse using electrospray ionization-tandem mass spectrometry. Journal of lipid research *42*, 2092-2095.

WHO (2010). WHO Laboratory Manual for the Examination and Processing of Human Semen, Vol Fifth (Geneva: World Health Organization).

Wittig, I., Braun, H.P., and Schagger, H. (2006). Blue native PAGE. Nature protocols *1*, 418-428.

Wolf, D.E., Hagopian, S.S., and Ishijima, S. (1986). Changes in sperm plasma membrane lipid diffusibility after hyperactivation during in vitro capacitation in the mouse. The Journal of cell biology *102*, 1372-1377.

Wu, A., Anupriwan, A., Iamsaard, S., Chakrabandhu, K., Santos, D.C., Rupar, T., Tsang, B.K., Carmona, E., and Tanphaichitr, N. (2007). Sperm surface arylsulfatase A can disperse the cumulus matrix of cumulus oocyte complexes. Journal of cellular physiology *213*, 201-211.

Xiong, W., Wang, H., Wu, H., Chen, Y., and Han, D. (2009). Apoptotic spermatogenic cells can be energy sources for Sertoli cells. Reproduction *137*, 469-479.

Xu, H., Kongmanas, K., Kadunganattil, S., Smith, C.E., Rupar, T., Goto-Inoue, N., Hermo, L., Faull, K.F., and Tanphaichitr, N. (2011). Arylsulfatase A deficiency causes seminolipid accumulation and a lysosomal storage disorder in Sertoli cells. Journal of lipid research *52*, 2187-2197.

Xu, H., Liu, F., Srakaew, N., Koppisetty, C., Nyholm, P.G., Carmona, E., and Tanphaichitr, N. (2012). Sperm arylsulfatase A binds to mZP2 and mZP3 glycoproteins in a nonenzymatic manner. Reproduction *144*, 209-219.

Yamagata, K., Murayama, K., Okabe, M., Toshimori, K., Nakanishi, T., Kashiwabara, S., and Baba, T. (1998). Acrosin accelerates the dispersal of sperm acrosomal proteins during acrosome reaction. The Journal of biological chemistry *273*, 10470-10474.

Yamashita, M., Honda, A., Ogura, A., Kashiwabara, S., Fukami, K., and Baba, T. (2008). Reduced fertility of mouse epididymal sperm lacking Prss21/Tesp5 is rescued by sperm exposure to uterine microenvironment. Genes to cells : devoted to molecular & cellular mechanisms *13*, 1001-1013.

Yamato, K., Handa, S., and Yamakawa, T. (1974). Purification of arylsulfatase A from boar testis and its activities toward seminolipid and sulfatide. Journal of biochemistry *75*, 1241-1247.

Yanagimachi, R. (1994). Mammalian fertilization. In The Physiology of Reproduction, E. Knobil, ed. (New York: Raven Press Ltd.), pp. 189-317.

Yanagimachi, R., and Chang, M.C. (1963). Sperm Ascent through the Oviduct of the Hamster and Rabbit in Relation to the Time of Ovulation. Journal of reproduction and fertility *6*, 413-420.

Yang, C.H., Srivastava, P.N., and Williams, W.L. (1974). Purification and properties of aryl sulfatases from rabbit sperm acrosomes. Proc Soc Exp Biol Med *145*, 721-725.
Yonezawa, N., Hatanaka, Y., Takeyama, H., and Nakano, M. (1995). Binding of pig sperm receptor in the zona pellucida to the boar sperm acrosome. Journal of reproduction and fertility *103*, 1-8.

Yu, Y., Xu, W., Yi, Y.J., Sutovsky, P., and Oko, R. (2006). The extracellular protein coat of the inner acrosomal membrane is involved in zona pellucida binding and penetration during fertilization: characterization of its most prominent polypeptide (IAM38). Developmental biology *290*, 32-43.

Yurewicz, E.C., Pack, B.A., Armant, D.R., and Sacco, A.G. (1993). Porcine zona pellucida ZP3 alpha glycoprotein mediates binding of the biotin-labeled M(r) 55,000 family (ZP3) to boar sperm membrane vesicles. Molecular reproduction and development *36*, 382-389.

Yurewicz, E.C., Sacco, A.G., Gupta, S.K., Xu, N., and Gage, D.A. (1998). Hetero-oligomerization-dependent binding of pig oocyte zona pellucida glycoproteins ZPB and ZPC to boar sperm membrane vesicles. The Journal of biological chemistry *273*, 7488-7494.

Zeng, Y., Oberdorf, J.A., and Florman, H.M. (1996). pH regulation in mouse sperm: identification of Na(+)-, Cl(-)-, and HCO3(-)-dependent and arylaminobenzoate-dependent regulatory mechanisms and characterization of their roles in sperm capacitation. Developmental biology *173*, 510-520.

Zhang, H., and Martin-Deleon, P.A. (2003). Mouse epididymal Spam1 (pH-20) is released in the luminal fluid with its lipid anchor. Journal of andrology *24*, 51-58.

Zhang, Y., Hayashi, Y., Cheng, X., Watanabe, T., Wang, X., Taniguchi, N., and Honke, K. (2005). Testis-specific sulfoglycolipid, seminolipid, is essential for germ cell function in spermatogenesis. Glycobiology *15*, 649-654.

Zhao, R., Wu, J.Q., Li, Y.Y., Zhou, Y., Ji, H.L., and Li, Y.R. (2014). Efficacy of a combined contraceptive regimen consisting of condoms and emergency contraception pills. BMC public health *14*, 354.

Appendix Figure 1

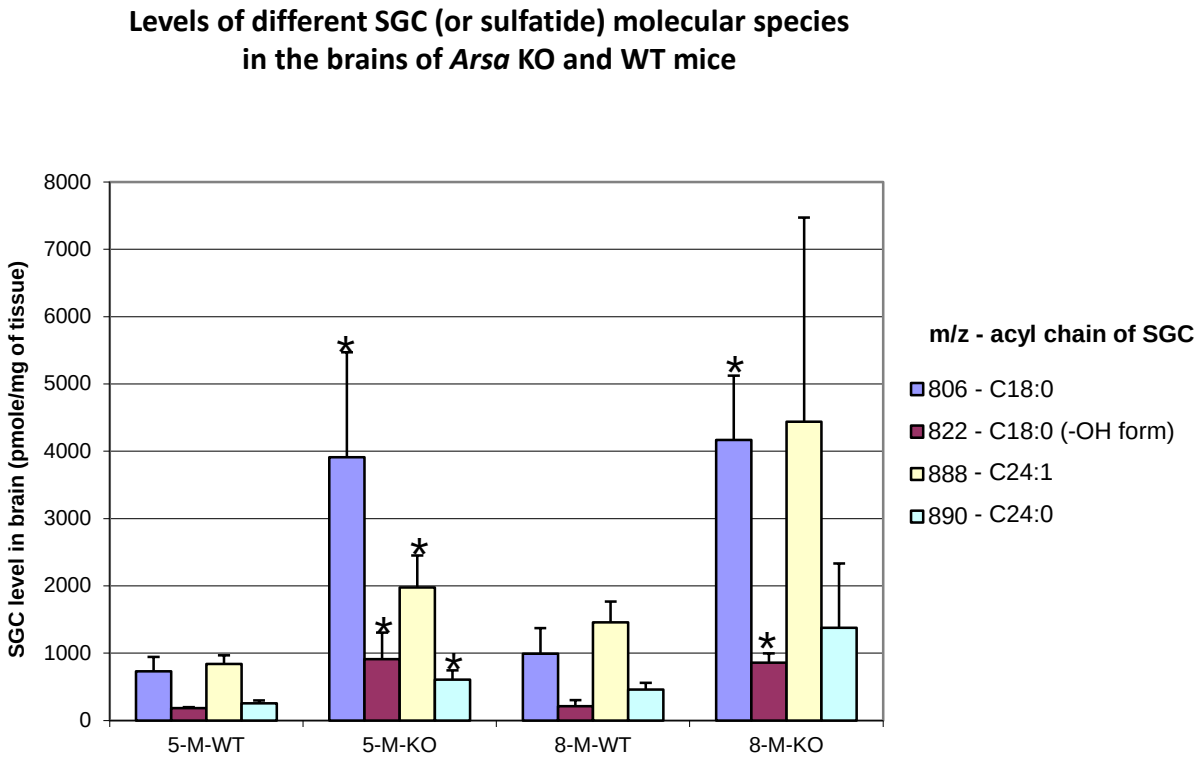

Appendix Figure 1: SGC accumulation in brains of *Arsa* knockout (KO) mice at both 5 and 8 months of age. Brains dissected from 5-month-old (5-M) and 8-month-old (8-M) *Arsa* KO mice and age-matched wild type (WT) mice were weighed, homogenized, and subjected to the lipid extraction. Levels of different SGC molecular species in brain lipid samples were determined by ESI-MS/MS-MRM quantification. Data are presented as mean ± S.D. of SGC levels in 3 different animals of each age/genotype. Asterisk indicates a significant difference ($P < 0.05$) of the SGC level between the KO mice and the age-matched WT animals.

Appendix Figure 2

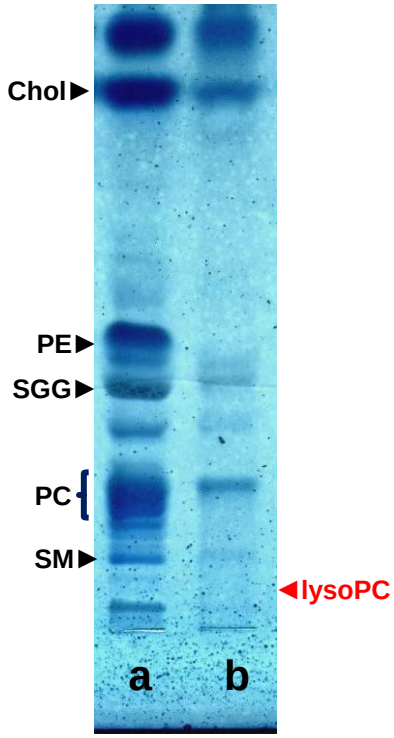

Appendix Figure 2: HPTLC profiles of 8-month-old *Arsa* KO mouse testis (a) and sperm (b) lipid extracts. Lipids extracted from testis tissue (5 mg) and sperm (5 million) of an 8-month-old *Arsa* KO mouse was subjected to separation on a HPTLC plate using chloroform:methanol:water-65:25:4 (v/v/v) as a running solvent system. The developed HPTLC plate was then stained with Coomassie blue G-250 solution, resulting in the blue staining of all lipids.
Lipid standards, including cholesterol (Chol), phosphatidylethanolamine (PE), phosphatidylcholine (PC), sulfogalactosylglycerlipid (SGG), sphingomylin (SM) and lysophosphatidylcholine (lysoPC), were co-chromatographed with the lipid samples as markers for lipid identification. ***Note that a lipid band with the same R_f as the lysoPC standard was absent in both testis and sperm lipid samples. This finding indicated that lysoPC was not present or present at a very low amount in these samples.***

Appendix Figure 3

A

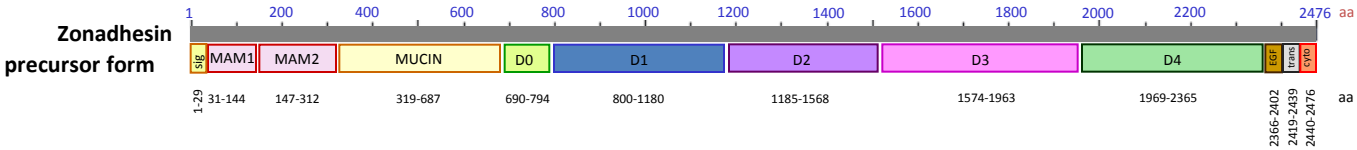

B

	Total spectral counts of zonadhesin domains in CAP APM vesicle extracts						
Sample/Domain	**MAM2**	**D1**	**D2**	**D3**	**D4**	**Other**	**Total**
CAP APM vesicles	1	5	8	3	3	2	22

	Total spectral counts of zonadhesin domains in APM HMW protein complexes of non-capacitated and capacitated sperm							
Sample/Domain	**MAM2**	**D0**	**D1**	**D2**	**D3**	**D4**	**Other**	**Total**
NON-CAP	2	2	15	28	14	6	5	72
CAP	4	5	28	61	28	13	8	147

Appendix Figure 3: A) Structural domains of zonadhesin. The precursor form of zonadhesin contains a signal peptide, 2 MAM domains (MAM = meprin/A5 antigen/mu receptor tyrosine phosphatase), von Willebrand factor (VWF) D domains (1 partial D0, 1 D1, 1 D2, 1 D3 and 1 D4 domain), an EGF-like domain, a transmembrane domain and a cytoplasmic domain. **B) Total spectral counts of peptides corresponding to different zonadhesin domains identified by MS.** *Top panel:* Numbers of different zonadhesin domains identified in total capacitated (CAP) sperm APM vesicle protein extracts. *Bottom panel:* Numbers of different zonadhesin domains identified in HMW protein complexes prepared from non-capacitated (NON-CAP) and capacitated sperm APM vesicles.

Appendix Figure 4

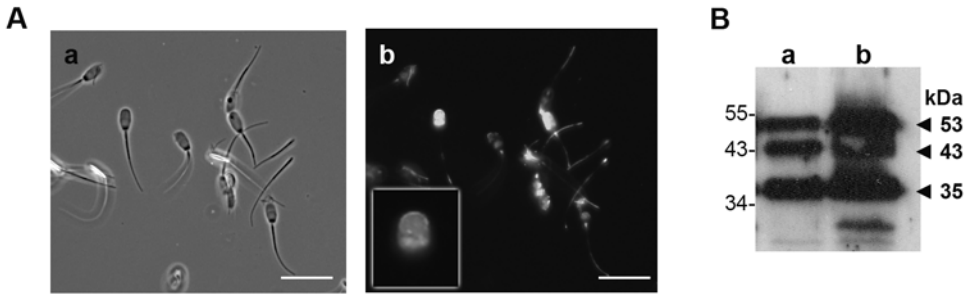

Appendix Figure 4: A) Localization of proacrosin/acrosin on the surface of nitrogen-cavitated sperm, which had lost the APM. Phase contrast image (a) and fluorescent image (b) of aldehyde-fixed nitrogen-cavitated Non-cap sperm stained with anti-proacrosin/acrosin antibody. Note that a similar staining pattern was obtained with nitrogen-cavitated Cap sperm (data not shown). Inset in panel b shows the close-up view of proacrosin/acrosin staining on the sperm head surface. Bar = 20 µm. **B) Immunodetection of proform (53 kDa) intermediate (43 kDa) and mature (35 kDa) forms of proacrosin/acrosin in whole cell lysates of intact (a) and nitrogen-cavitated (b) Non-cap sperm.**

Appendix Figure 5

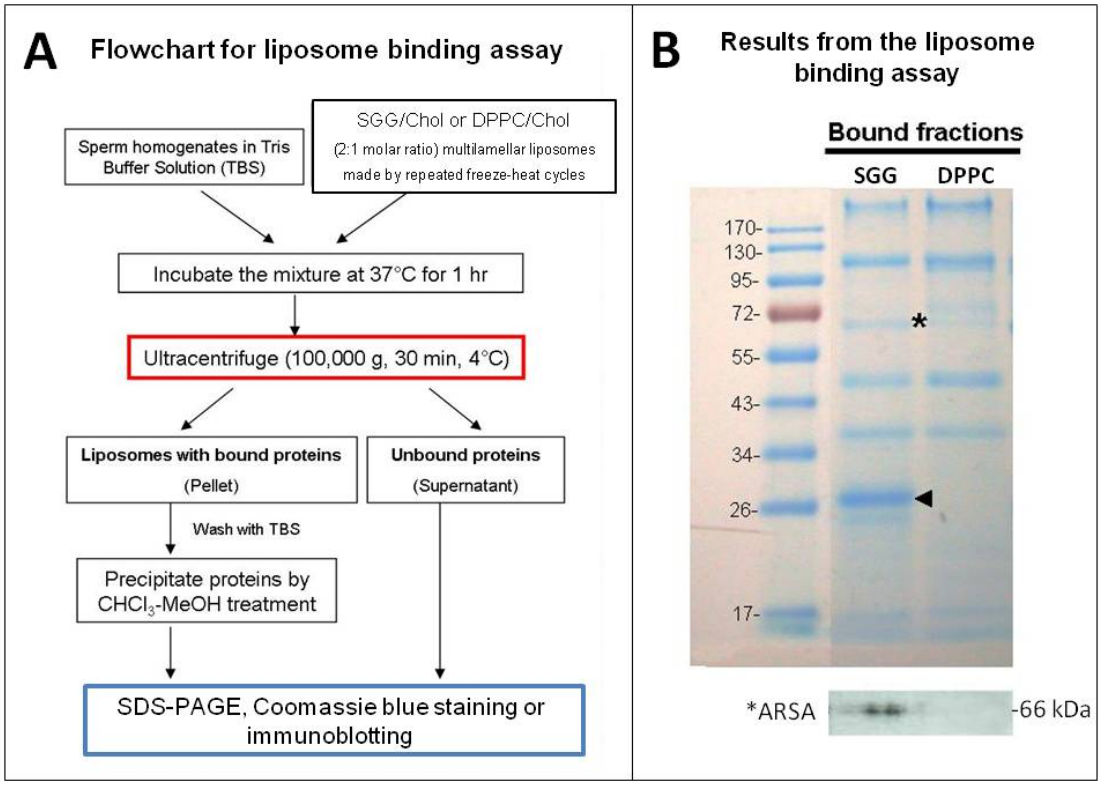

Appendix Figure 5: Identification of SGG-binding proteins in the soluble protein fraction of pig sperm homogenate. A) Flowchart showing a procedure for our liposome binding assay used for isolation of sperm proteins with specific SGG affinity. Multilamellar liposomes were made from mixture of SGG or dipalmityl-palmitoylphosphatidylcholine (DPPC) with cholesterol (Chol) at 2:1 molar ratio by repeated freezing and heating. Cholesterol was used as a stabilizer for liposome constructrion. DPPC, another major sperm lipid component, was used as a negative control. The soluble fraction of pig sperm homogenates partially purified by Q-sepharose anionic exchange chromatography was used as a protein source for the liposome binding assay. This soluble protein fraction is prepared routinely in our lab as part of the ARSA purification. Since ARSA is known to specifically bind to SGG, we used this protein fraction, containing ARSA and other anionic sperm soluble proteins, in preliminary experiments to validate our liposome binding assay. Following 1 hour incubation of protein samples with liposomes, the protein-liposome mixture was subjected to ultracentrifugation to pellet the liposomes with bound proteins. The pellet was washed twice with Tris buffered saline (TBS) to remove loosely bound proteins prior to treatement with chloroform methanol to separate proteins from the liposomes. The chloroform-methanol treated proteins were then resolved on SDS-PAGE, and stained with Coomassie blue solution or subjected to immunoblotting analysis. **B)** A representative gel and blot from three experiments of liposome binding assays. *Top panel*: the protein bands at ~66 kDa (asterisk) and ~28 kDa (arrowhead) were detected specifically and consistently in the SGG liposome-bound protein fractions. ***The 28 kDa band of unknown protein was further subjected to tryptic digestion and mass spectrometry, and this protein was then identified as acrosin-binding protein (ACRBP or sp32).*** *Bottom panel*: As expected, immunoblotting analysis using anti-ARSA antibody revealed that the 66 kDa band was ARSA.

Appendix Figure 6

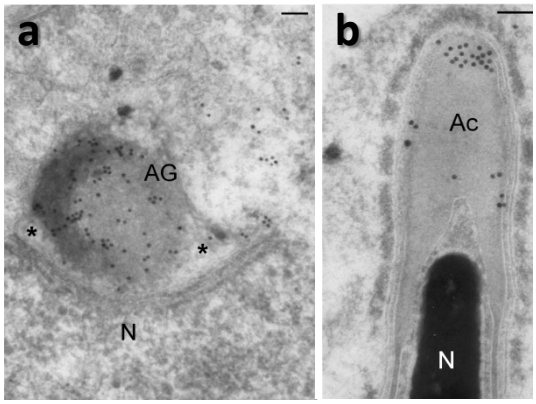

Appendix Figure 6: Immunogold transmission electron microscopy localization of ARSA in acrosomal regions of mouse spermatogenic cells. Mouse testis blocks (~1 mm) fixed in 4% paraformaldehyde and 0.5% glutaraldehyde in 0.1 M cacodylate buffer, pH 7.2, containing 0.2 M sucrose were processed and sectioned for transmission electron microscopy. The sections were then stained with 25 μg/ml antiAS-A IgG and subsequently with 15 nm gold coupled goat anti-rabbit IgG (EY lab). After a successive wash with PBS-0.05% tween 20, the sections were counterstained with saturated aqueous uranyl acetate and Reynold lead citrate and viewed under a Hitachi 7000 transmission electron microscope at 75 kV. Bar = 0.2 μm. ***Note the gold particles in the developing acrosomal granule (AG) of a round spermatid (a) and the acrosome (Ac) of an elongated spermatid (b).***

Appendix Figure 7

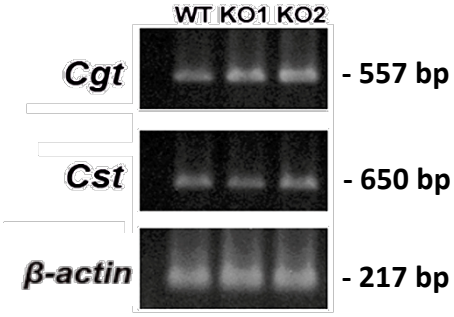

Appendix Figure 7: Unchanged *Cgt* and *Cst* expression in testicular germ cells (TGCs) of 8-month-old *Arsa* KO mice. RNA was extracted from TGCs prepared from 2 *Arsa* KO mice and an age-matched WT mouse as described in the Materials and methods section. The extracted RNA was reversed transcribed into first strand cDNA using a Retroscript Kit (Ambion, Burlington, ON, Canada), following the company's instruction. PCR conditions and primers for *Cgt* and *Cst* were as previously described (Kongmanas et al., 2010). PCR of *β*-actin was also performed in the same samples, following the method previously described (Griffith et al., 1999) for the semi-quantitative comparison of other PCR products between samples.

References:

Kongmanas, K., H.Xu, A.Yaghoubian, L.Franchini, L.Panza, F.Ronchetti, K.F.Faull, and N.Tanphaichitr. 2010. Quantification of seminolpid by LC-ESI-MS/MS-multiple reaction monitoring: compensatory levels in *Cgt*$^{+/-}$ mice. *J Lipid Res.* 51:3548-3558.

Griffith, T.S., S.R.Wiley, M.Z.Kubin, L.M.Sedger, C.R.Maliszewski, and N.A.Fanger. 1999. Monocyte-mediated tumoricidal activity via the tumor necrosis factor-related cytokine, TRAIL. *J Exp. Med* 189:1343-1354.

Appendix Table 1: All proteins identified in APM vesicle extracts of Non-cap and/or Cap sperm samples by quantitative (gel-free) proteomic approach.

	Protein name/Accession		Pig 1				Pig 2				Pig 3				
			NON-CAP		CAP		NON-CAP		CAP		NON-CAP		CAP		
	Full name	Swiss-Prot	Spectral count	%coverage	Spectral count	%coverage	Spectral count	%coverage	Spectral count	%coverage	Spectral count	%coverage	Spectral count	%coverage	Comments
#	**Proteins found in both NON-CAP and CAP**														
	Sperm proteins with relevence in gamete interaction														
1	Lactadherin (Milk fat globule-EGF factor 8)	MFGM_PIG	60	52.3	145	58.7	24	44	83	52.6	56	50.1	163	57	**Increase in all 3 CAP**
2	Carbohydrate-binding protein AQN-3	AQN3_PIG	11	30.2	10	37.1	6	21.6	5	34.5	6	21.6	6	27.6	
3	Carbohydrate-binding protein AWN	AWN_HORSE	7	36.1	10	55.6	4	29.3	6	48.9	5	32.3	7	49.6	**Increase in all 3 CAP**
4	Acrosin	ACRO_PIG	8	15.4	14	24.8	2	4.6	4	15.4	8	14.5	17	22.2	**Increase in all 3 CAP**
5	Acrosin-binding protein precursor (sp32)	ACRBP_PIG	3	5.8	9	14.5	1	2.6	11	10.8	1	1.3	7	14	**Increase in all 3 CAP**
6	Angiotensin-converting enzyme	ACE_RABIT	5	4.1	9	5.6	2	1.7	5	4	nd	nd	3	3.4	**Increase in all 3 CAP**
7	Zona pellucida-binding protein 1	ZPBP1_PIG	1	3.1	2	7.4	nd	nd	nd	nd	2	7.4	5	9.7	
	Epididymal fluid/seminal plasma proteins														
1	Major seminal plasma glycoprotein PSP-I	PSP1_PIG	1	11.3	1	11.3	1	11.3	5	32.3	nd	nd	nd	nd	
2	Major seminal plasma glycoprotein PSP-II	PSP2_PIG/BOVIN	1	10.2	1	12.4	2	11.7	nd	nd	nd	nd	3	24.1	
3	Clusterin	CLUS_PIG/SHEEP	nd	nd	1	4.3	nd	nd	1	19.7	2	4.9	nd	nd	
	Chaperones														
1	Heat shock protein HSP 90-alpha (HSP 86)	HS90A_HORSE/BOVIN	6	9.7	13	22.4	nd	nd	2	2.2	5	7.9	3	5.4	
2	Heat shock 70 kDa protein 1-like	HS71L_BOVIN/PIG	14	14.4	11	21.1	nd	nd	nd	nd	15	22	11	17.5	
3	Transitional endoplasmic reticulum ATPase	TERA_PIG	nd	nd	2	4	1	1.6	1	1.6	nd	nd	1	4.2	
4	T-complex protein 1 subunit zeta (TCP-1-zeta)	TCPZ_PIG/BOVIN	1	2.3	1	12.5	nd	nd	nd	nd	nd	nd	nd	nd	
	Cytoskeleton proteins														
1	Tubulin polymerization-promoting protein family member 2	TPPP2_BOVIN	10	37.4	8	36.3	7	35.1	8	36.3	5	46.2	8	47.7	**Increase in all 3 CAP**
2	Tubulin beta-4 chain	TBB4_BOVIN	1	6.1	1	5.9	nd	nd	nd	nd	nd	nd	nd	nd	
	Ubiquitin and proteasomes														
1	Ubiquitin	UBIQ_BOVIN/SHEEP	12	64.5	7	60.5	3	40.8	2	38.2	4	25	2	19.7	
2	Proteasome subunit alpha type 2	PSA2_BOVIN	1	4.3	2	10.7	nd	nd	nd	nd	1	4.3	1	4.3	
3	Ubiquitin domain-containing protein 2	UBTD2_BOVIN	1	3.8	2	6	nd	nd	1	5.6	nd	nd	nd	nd	
4	Proteasome subunit beta type 1 precursor	PSB1_BOVIN	nd	nd	2	14.1	nd	nd	nd	nd	1	5.8	nd	nd	
	Enzymes														
1	Adenylate kinase isoenzyme 1	KAD1_PIG	45	87.6	35	74.4	11	37.6	16	51	30	74.7	26	67.5	
2	14-3-3 protein zeta/delta	1433Z_BOVIN/SHEEP	15	42	11	46.1	5	11.8	3	9	3	13.9	7	31.4	
3	Phosphoglycerate mutase 2	PGAM2_BOVIN	13	28.5	14	41.5	4	12.3	8	28.5	7	19	8	19.4	**Increase in all 3 CAP**
4	Phosphoglycerate kinase, testis specific	PGK2_PIG	6	20.6	8	26.1	1	2.2	1	2.2	5	12.5	4	12	
5	Hexokinase-1	HXK1_BOVIN	6	7.4	12	11.2	1	1.4	nd	nd	5	6.6	8	8.8	
6	Calmodulin-dependent calcineurin A subunit alpha isoform	PP2BA_BOVIN	1	2.5	nd	nd	1	1.7	1	2.5	1	1.7	1	2.1	
7	Aldose reductase	ALDR_PIG	2	6.6	6	30.1	nd	nd	nd	nd	2	6.6	1	2.2	
8	Putative deoxyribonuclease TATDN3	TATD3_BOVIN	3	4	1	4	nd	nd	nd	nd	1	4	1	4	
9	Alpha-enolase	ENOA_BOVIN	1	3.7	3	7.8	nd	nd	nd	nd	2	7.4	1	2.3	
10	Hexokinase-2	HXK2_PIG	nd	nd	3	3.5	nd	nd	nd	nd	3	3.8	3	3.4	

11	cAMP-dependent protein kinase, alpha-catalytic subunit	KAPCA_CANFA	1	6.9	3	11.7	nd	nd	nd	nd	nd	nd	1	6.9	
12	Plasma membrane calcium-transporting ATPase 1	AT2B1_PIG	1	0.9	1	0.9	1	0.9	nd	nd	1	0.9	nd	nd	
13	Inositol monophosphatase	IMPA1_BOVIN	1	5.8	2	12.6	nd	nd	1	5.8	nd	nd	nd	nd	
14	Sodium/potassium-transporting ATPase subunit beta-3	AT1B3_BOVIN	1	3.9	1	3.9	nd	nd	nd	nd	nd	nd	1	3.9	
15	cAMP-dependent protein kinase type I-alpha regulatory subunit	KAP0_BOVIN	nd	nd	1	4.7	nd	nd	nd	nd	1	4.7	1	4.7	
16	Fructose-bisphosphate aldolase A	ALDOA_RABIT	1	4.1	1	3.8	nd	nd	1	3.8	nd	nd	nd	nd	
17	Glycylpeptide N-tetradecanoyltransferase 2	NMT2_BOVIN	1	1.2	1	1.2	nd	nd	1	1.2	nd	nd	nd	nd	
18	Protein-L-isoaspartate(D-aspartate) O-methyltransferase	PIMT_BOVIN/PIG	1	6.6	nd	nd	nd	nd	1	15	nd	nd	nd	nd	
19	Casein kinase II subunit alpha	CSK21_BOVIN	3	11.8	4	17.6	nd	nd	nd	nd	nd	nd	nd	nd	
20	Dipeptidyl peptidase 4	DPP4_PIG	nd	nd	nd	nd	nd	nd	nd	nd	1	2.2	3	5	
21	Casein kinase II subunit beta	CSK2B_BOVIN	1	4.2	1	6.5	nd	nd	nd	nd	nd	nd	nd	nd	
	Other proteins														
1	Vesicle-associated membrane protein 3	VAMP3_BOVIN	4	26.9	3	40.4	1	8.7	4	40.4	5	26.9	4	40.4	
2	Glucose transporter type 3	GTR3_BOVIN	3	3.6	5	15.2	2	8.9	2	8.9	3	3.6	4	15.2	
3	Calmodulin (CaM)	CALM_BOVIN	6	49	10	47.7	5	49	12	45	nd	nd	10	45	**Increase in all 3 CAP**
4	Phosphatidylethanolamine-binding protein 1	PEBP1_BOVIN	5	25.7	2	21.4	nd	nd	1	11.2	4	21.4	2	14.4	
5	Anoctamin-4	ANO4_BOVIN	3	2.1	1	2.1	nd	nd	nd	nd	4	2.1	1	2.1	
6	Leukocyte surface antigen CD47 precursor	CD47_PIG	1	7.9	4	12.5	nd	nd	1	7.3	2	12.5	nd	nd	
7	Uncharacterized protein C1orf49 homolog	CA049_BOVIN	1	3.3	1	3.3	1	3.3	1	3.3	nd	nd	nd	nd	
8	PDZ domain-containing protein C16orf65 homolog	CP065_BOVIN	1	3.8	1	3.8	nd	nd	nd	nd	1	3.8	nd	nd	
9	Peroxiredoxin-5, mitochondrial precursor	PRDX5_BOVIN	1	5	1	5	nd	nd	nd	nd	1	5	nd	nd	
10	Cancer susceptibility candidate protein 1 homolog	CASC1_BOVIN	1	1.4	2	1.4	nd	nd	nd	nd	nd	nd	1	1.4	
11	Fibronectin (FN) (Fragment)	FINC_HORSE	1	2.7	3	1.9	nd	nd	nd	nd	2	5	nd	nd	
12	Coiled-coil domain-containing protein 151	CC151_BOVIN	1	1.9	1	1.9	nd	nd	1	1.9	nd	nd	nd	nd	
13	Histidine triad nucleotide-binding protein 1	HINT1_RABIT	1	19	1	19	nd	nd	nd	nd	1	19	nd	nd	
14	Ras-related protein Rab-2A	RAB2A_RABIT/CANFA	1	9	1	6.1	nd	nd	nd	nd	nd	nd	3	15.6	
15	Ryanodine receptor 1	RYR1_RABIT	1	0.3	nd	nd	nd	nd	1	0.3	nd	nd	nd	nd	
16	Ferritin heavy chain	FRIH_PIG	1	12.7	1	12.7	nd	nd	nd	nd	nd	nd	nd	nd	
17	Flotillin-1	FLOT1_BOVIN	1	3.5	1	3.5	nd	nd	nd	nd	nd	nd	nd	nd	
18	Transcriptional regulator ATRY (Fragments)	ATRY_MACEU	1	9.4	1	9.4	nd	nd	nd	nd	nd	nd	nd	nd	
	Proteins found only in CAP														
	Sperm proteins with relevence in gamete interaction														
1	Zonadhesin precursor	ZAN_PIG	nd	nd	12	6.9	nd	nd	1	0.7	nd	nd	22	11	**(Only in CAP)**
	Epididymal fluid/seminal plasma proteins														
1	Epididymal sperm-binding protein 1	ESPB1_PIG	nd	nd	1	3.6	nd	nd	nd	nd	nd	nd	nd	nd	**Only in 1 CAP**
2	Seminal plasma protein pB1	PB1_PIG	nd	nd	1	5.4	nd	nd	nd	nd	nd	nd	nd	nd	**Only in 1 CAP**

	Chaperones														
1	T-complex protein 1 subunit beta (TCP-1-beta)	TCPB_BOVIN	nd	nd	1	3	nd	nd	nd	nd	nd	nd	3	9.2	**Only in 2 CAP**
2	T-complex protein 1 subunit theta (TCP-1-theta)	TCPQ_BOVIN	nd	nd	nd	nd	nd	nd	nd	nd	nd	nd	1	2.2	**Only in 1 CAP**
	Cytoskeleton proteins														
1	Tubulin beta-2C chain	TBB2C_BOVIN	nd	nd	nd	nd	nd	nd	nd	nd	nd	nd	3	9.7	**Only in 1 CAP**
2	Tubulin alpha-3 chain	TBA3_BOVIN	nd	nd	nd	nd	nd	nd	nd	nd	nd	nd	3	8	**Only in 1 CAP**
3	Tubulin alpha-1C chain	TBA1C_BOVIN	nd	nd	1	4	nd	nd	nd	nd	nd	nd	nd	nd	**Only in 1 CAP**
4	Tubulin beta-5 chain	TBB5_BOVIN	nd	nd	1	4.3	nd	nd	nd	nd	nd	nd	nd	nd	**Only in 1 CAP**
	Ubiquitin and proteasomes														
1	Proteasome subunit alpha type 5	PSA5_BOVIN	nd	nd	2	10.4	nd	nd	nd	nd	nd	nd	nd	nd	**Only in 1 CAP**
2	26S proteasome non-ATPase regulatory subunit 8	PSMD8_BOVIN	nd	nd	1	12.1	nd	nd	nd	nd	nd	nd	nd	nd	**Only in 1 CAP**
3	Proteasome subunit alpha type 7	PSA7_BOVIN	nd	nd	2	14.9	nd	nd	nd	nd	nd	nd	nd	nd	**Only in 1 CAP**
4	Proteasome subunit alpha type 6	PSA6_BOVIN	nd	nd	1	4.9	nd	nd	nd	nd	nd	nd	nd	nd	**Only in 1 CAP**
5	Proteasome subunit beta type 6 precursor	PSB6_BOVIN	nd	nd	1	4.6	nd	nd	nd	nd	nd	nd	nd	nd	**Only in 1 CAP**
6	Proteasome subunit beta type-5	PSB5_BOVIN	nd	nd	1	5.3	nd	nd	nd	nd	nd	nd	nd	nd	**Only in 1 CAP**
7	Proteasome subunit beta type 2	PSB2_BOVIN	nd	nd	1	3	nd	nd	nd	nd	nd	nd	nd	nd	**Only in 1 CAP**
8	E3 ubiquitin-protein ligase KCMF1	KCMF1_BOVIN	nd	nd	nd	nd	nd	nd	nd	nd	nd	nd	1	9.2	**Only in 1 CAP**
9	Proteasome subunit beta type 4 precursor	PSB4_BOVIN	nd	nd	1	9.1	nd	nd	nd	nd	nd	nd	nd	nd	**Only in 1 CAP**
10	Proteasome subunit alpha type 1	PSA1_BOVIN	nd	nd	1	4.6	nd	nd	nd	nd	nd	nd	nd	nd	**Only in 1 CAP**
	Enzymes														
1	Glucose transporter type 5	GTR5_HORSE	nd	nd	1	1.2	nd	nd	1	1.2	nd	nd	nd	nd	**Only in 2 CAP**
2	Glucose-6-phosphate isomerase	G6PI_PIG	nd	nd	2	5.9	nd	nd	nd	nd	nd	nd	nd	nd	**Only in 1 CAP**
3	cAMP-dependent protein kinase type II-alpha regulatory subunit	KAP2_PIG	nd	nd	1	11	nd	nd	nd	nd	nd	nd	nd	nd	**Only in 1 CAP**
4	Quinone oxidoreductase	QOR_PIG	nd	nd	1	9.4	nd	nd	nd	nd	nd	nd	nd	nd	**Only in 1 CAP**
5	Malate dehydrogenase, mitochondrial precursor	MDHM_PIG	nd	nd	1	6.5	nd	nd	nd	nd	nd	nd	nd	nd	**Only in 1 CAP**
6	Triosephosphate isomerase	TPIS_RABIT	nd	nd	1	5.2	nd	nd	nd	nd	nd	nd	nd	nd	**Only in 1 CAP**
7	Potassium-transporting ATPase alpha chain 2	AT12A_RABIT	nd	nd	1	1.4	nd	nd	nd	nd	nd	nd	nd	nd	**Only in 1 CAP**
8	Phosphoinositide 3-kinase regulatory subunit 5	PI3R5_PIG	nd	nd	1	0.8	nd	nd	nd	nd	nd	nd	nd	nd	**Only in 1 CAP**
9	Alpha-S1-casein precursor	CASA1_BUBBU	nd	nd	nd	nd	nd	nd	1	5.1	nd	nd	nd	nd	**Only in 1 CAP**
10	Ras GTPase-activating protein 3	RASA3_BOVIN	nd	nd	nd	nd	nd	nd	1	1.4	nd	nd	nd	nd	**Only in 1 CAP**
11	40 kDa peptidyl-prolyl cis-trans isomerase	PPID_BOVIN	nd	nd	nd	nd	nd	nd	nd	nd	nd	nd	1	1.9	**Only in 1 CAP**
12	Glycosyltransferase 8 domain-containing protein 2	GL8D2_BOVIN	nd	nd	nd	nd	nd	nd	nd	nd	nd	nd	1	2.6	**Only in 1 CAP**
13	DNA-directed RNA polymerase III subunit RPC4	RPC4_BOVIN	nd	nd	nd	nd	nd	nd	nd	nd	nd	nd	1	2.3	**Only in 1 CAP**
14	Nicotinamide mononucleotide adenylyltransferase 1	NMNA1_BOVIN	nd	nd	nd	nd	nd	nd	nd	nd	nd	nd	1	4.3	**Only in 1 CAP**
15	Sodium/potassium-transporting ATPase subunit beta-3	AT1B3_RABIT	nd	nd	1	3.9	nd	nd	nd	nd	nd	nd	nd	nd	**Only in 1 CAP**
16	Aspartate aminotransferase, cytoplasmic	AATC_PIG	nd	nd	1	4.8	nd	nd	nd	nd	nd	nd	nd	nd	**Only in 1 CAP**

17	cAMP-dependent protein kinase type II-alpha regulatory subunit	KAP2_BOVIN	nd	nd	1	2.7	nd	nd	nd	nd	nd	nd	nd	nd	Only in 1 CAP
18	1-phosphatidylinositol-4,5-bisphosphate phosphodiesterase delta-4	PLCD4_PIG	nd	nd	1	2.5	nd	nd	nd	nd	nd	nd	nd	nd	Only in 1 CAP
19	Probable glutathione peroxidase 8	GPX8_BOVIN	nd	nd	1	2.9	nd	nd	nd	nd	nd	nd	nd	nd	Only in 1 CAP
20	Phosphoglucomutase-1	PGM1_BOVIN	nd	nd	1	3.2	nd	nd	nd	nd	nd	nd	nd	nd	Only in 1 CAP
21	Inositol-3-phosphate synthase 1	INO1_BOVIN	nd	nd	1	2.9	nd	nd	nd	nd	nd	nd	nd	nd	Only in 1 CAP
22	Potassium-transporting ATPase alpha chain 1	ATP4A_CANFA	nd	nd	1	1.8	nd	nd	nd	nd	nd	nd	nd	nd	Only in 1 CAP
	Other proteins														
1	Protein DJ-1	PARK7_BOVIN	nd	nd	3	16.4	nd	nd	1	12.2	nd	nd	nd	nd	Only in 2 CAP
2	DnaJ homolog subfamily C member 5	DNJC5_BOVIN	nd	nd	2	16.2	nd	nd	1	7.1	nd	nd	nd	nd	Only in 2 CAP
3	Nucleoside diphosphate kinase B	NDKB_PIG	nd	nd	1	12.5	nd	nd	nd	nd	nd	nd	1	12.5	Only in 2 CAP
4	Signal recognition particle receptor subunit alpha	SRPR_BOVIN	nd	nd	1	2.8	nd	nd	nd	nd	nd	nd	1	2.8	Only in 2 CAP
5	Lysozyme-like protein 1 precursor	LYZL1_BOVIN	nd	nd	1	4.1	nd	nd	nd	nd	nd	nd	1	4.7	Only in 2 CAP
6	Filensin (Beaded filament structural protein 1)	BFSP1_BOVIN	nd	nd	1	1.1	nd	nd	nd	nd	nd	nd	1	1.1	Only in 2 CAP
7	Ropporin-1	ROP1_BOVIN	nd	nd	1	12.7	nd	nd	nd	nd	nd	nd	nd	nd	Only in 1 CAP
8	Syntaxin-binding protein 2	STXB2_CANFA	nd	nd	1	2.5	nd	nd	nd	nd	nd	nd	nd	nd	Only in 1 CAP
9	Serpin A3-1	SPA31_BOVIN	nd	nd	1	1.9	nd	nd	nd	nd	nd	nd	nd	nd	Only in 1 CAP
10	Peptide chain release factor 1-like,mitochondrial	RF1ML_BOVIN	nd	nd	1	1.8	nd	nd	nd	nd	nd	nd	nd	nd	Only in 1 CAP
11	Interferon gamma precursor	IFNG_DASNO	nd	nd	nd	nd	nd	nd	1	3.6	nd	nd	nd	nd	Only in 1 CAP
12	Hippocalcin-like protein 1	HPCL1_BOVIN	nd	nd	nd	nd	nd	nd	1	10.4	nd	nd	nd	nd	Only in 1 CAP
13	CDGSH iron sulfur domain-containing protein 1	CISD1_BOVIN	nd	nd	nd	nd	nd	nd	nd	nd	nd	nd	1	12.3	Only in 1 CAP
14	Tumor necrosis factor	TNFA_PIG	nd	nd	nd	nd	nd	nd	nd	nd	nd	nd	1	4.7	Only in 1 CAP
15	Regulator of G-protein signaling 7-binding protein	R7BP_BOVIN	nd	nd	nd	nd	nd	nd	nd	nd	nd	nd	1	2.7	Only in 1 CAP
16	Uncharacterized protein C13orf16 homolog	CM016_BOVIN	nd	nd	nd	nd	nd	nd	nd	nd	nd	nd	1	4.8	Only in 1 CAP
17	Alpha-actinin-2	ACTN2_BOVIN	nd	nd	1	0.9	nd	nd	nd	nd	nd	nd	nd	nd	Only in 1 CAP
18	Dynein light chain 2, cytoplasmic	DYL2_BOVIN	nd	nd	1	30.3	nd	nd	nd	nd	nd	nd	nd	nd	Only in 1 CAP
19	Testin	TES_RHIFE	nd	nd	1	2.4	nd	nd	nd	nd	nd	nd	nd	nd	Only in 1 CAP
20	Abnormal spindle-like microcephaly-associated protein homolog	ASPM_CANFA	nd	nd	1	0.3	nd	nd	nd	nd	nd	nd	nd	nd	Only in 1 CAP
21	Sodium- and chloride-dependent taurine transporter	SC6A6_CANFA	nd	nd	1	2.7	nd	nd	nd	nd	nd	nd	nd	nd	Only in 1 CAP
22	Peroxiredoxin-6	PRDX6_BOVIN	nd	nd	1	10.7	nd	nd	nd	nd	nd	nd	nd	nd	Only in 1 CAP
23	Uncharacterized protein C1orf156 homolog	CA156_BOVIN	nd	nd	1	4.3	nd	nd	nd	nd	nd	nd	nd	nd	Only in 1 CAP
24	Nuclear transport factor 2	NTF2_BOVIN	nd	nd	1	12.6	nd	nd	nd	nd	nd	nd	nd	nd	Only in 1 CAP
25	Moesin (Membrane-organizing extension spike protein)	MOES_PIG	nd	nd	1	2.1	nd	nd	nd	nd	nd	nd	nd	nd	Only in 1 CAP
26	Cylicin-2 (Cylicin II)	CYLC2_BOVIN	nd	nd	1	2.9	nd	nd	nd	nd	nd	nd	nd	nd	Only in 1 CAP
27	Cytoskeleton-associated protein 2-like	CKP2L_BOVIN	nd	nd	1	1.7	nd	nd	nd	nd	nd	nd	nd	nd	Only in 1 CAP
	Proteins found only in NON-CAP														
	Sperm proteins with relevence in gamete interaction														
1	Carbohydrate-binding protein AQN-1	AQN1_PIG	2	30.6	nd	nd	nd	nd	nd	nd	nd	nd	nd	nd	**Only in 1 NC**

	Chaperones														
2	T-complex protein 1 subunit delta (TCP-1-delta)	TCPD_BOVIN	nd	nd	nd	nd	nd	nd	nd	nd	1	1.5	nd	nd	**Only in 1 NC**
3	T-complex protein 1 subunit eta	TCPH_BOVIN	1	2.6	nd	nd	nd	nd	nd	nd	nd	nd	nd	nd	**Only in 1 NC**
	Ubiquitin and proteasomes														
1	Proteasome subunit alpha type 3	PSA3_BOVIN	1	5.5	nd	nd	nd	nd	nd	nd	nd	nd	nd	nd	**Only in 1 NC**
2	Ubiquitin-like protein Nedd8 precursor (Neddylin)	NEDD8_BOVIN	nd	nd	nd	nd	1	23.5	nd	nd	nd	nd	nd	nd	**Only in 1 NC**
3	E3 ubiquitin-protein ligase RNF8	RNF8_BOVIN	1	2.9	nd	nd	nd	nd	nd	nd	nd	nd	nd	nd	**Only in 1 NC**
4	26S proteasome non-ATPase regulatory subunit 7	PSD7_BOVIN	1	7.5	nd	nd	nd	nd	nd	nd	nd	nd	nd	nd	**Only in 1 NC**
	Enzymes														
1	Casein kinase II subunit alpha	CSK21_RABIT	2	7.2	nd	nd	2	7.2	nd	nd	4	12	nd	nd	**Only in 2 NC**
2	Bleomycin hydrolase (Fragment)	BLMH_RABIT	nd	nd	nd	nd	nd	nd	nd	nd	1	5.4	nd	nd	**Only in 1 NC**
3	14-3-3 protein beta/alpha	1433B_SHEEP	nd	nd	nd	nd	nd	nd	nd	nd	2	11.4	nd	nd	**Only in 1 NC**
	Other proteins														
1	Vitamin D3 receptor	VDR_PIG	1	2.3	nd	nd	nd	nd	nd	nd	1	2.3	nd	nd	**Only in 2 NC**
2	COP9 signalosome complex subunit 4	CSN4_PIG	1	3.9	nd	nd	nd	nd	nd	nd	nd	nd	nd	nd	**Only in 1 NC**
3	14-3-3 protein epsilon	1433E_BOVIN	1	6.7	nd	nd	nd	nd	nd	nd	nd	nd	nd	nd	**Only in 1 NC**
4	Leucine-rich repeat-containing protein 39	LRC39_BOVIN	nd	nd	nd	nd	nd	nd	nd	nd	1	3	nd	nd	**Only in 1 NC**
5	Ezrin (p81) (Cytovillin) (Villin-2)	EZRI_BOVIN	nd	nd	nd	nd	nd	nd	nd	nd	1	2.1	nd	nd	**Only in 1 NC**
6	ATP-binding cassette sub-family F member 1	ABCF1_PIG	nd	nd	nd	nd	1	1.6	nd	nd	nd	nd	nd	nd	**Only in 1 NC**
7	39S ribosomal protein L55, mitochondrial	RM55_BOVIN	nd	nd	nd	nd	nd	nd	nd	nd	1	5.6	nd	nd	**Only in 1 NC**
8	Lupus La protein homolog	LA_BOVIN	nd	nd	nd	nd	nd	nd	nd	nd	1	2	nd	nd	**Only in 1 NC**
9	Cytochrome c	CYC_MINSC	1	10.5	nd	nd	nd	nd	nd	nd	nd	nd	nd	nd	**Only in 1 NC**
10	Interleukin-5	IL5_SHEEP	1	4.5	nd	nd	nd	nd	nd	nd	nd	nd	nd	nd	**Only in 1 NC**
11	Rab GDP dissociation inhibitor beta	GDIB_PIG	1	2.9	nd	nd	nd	nd	nd	nd	nd	nd	nd	nd	**Only in 1 NC**
12	Tensin-1	TENS1_BOVIN	1	1.1	nd	nd	nd	nd	nd	nd	nd	nd	nd	nd	**Only in 1 NC**

Appendix Table 2: Non-cap and Cap APM vesicle proteins identified by gel-based analysis

Proteins found in common between gel-free and gel-based proteomic analyses are marked with the **bold** fonts.

#	Protein name	Swiss-Prot Accession	Total Spectral Counts	
			NON-CAP	CAP
	Sperm proteins with relevence in gamete interaction			
1	**Lactadherin (Milk fat globule-EGF factor 8) (MFG-E8) (MFGM) (Sperm surface protein SP47) (PP47) - Sus sc**	**MFGM_PIG/BOVIN**	**338**	**378**
2	**Acrosin OS=Sus scrofa GN=ACR PE=1 SV=5**	**ACRO_PIG**	**105**	**126**
3	**Angiotensin-converting enzyme, somatic isoform precursor (EC 3.4.15.1) (Dipeptidyl carboxypeptidase I) (**	**ACE_RABIT**	**17**	**31**
4	**Carbohydrate-binding protein AWN (Zona pellucida-binding protein AWN) (Spermadhesin AWN) (Seminal**	**AWN_HORSE/PIG**	**65**	**27**
5	**Acrosin-binding protein precursor (Proacrosin-binding protein sp32) (Fragment) - Sus scrofa (Pig)**	**ACRBP_PIG**	**27**	**27**
6	**Zonadhesin precursor - Sus scrofa (Pig)**	**ZAN_PIG**	**1**	**25**
7	**Carbohydrate-binding protein AQN-3 OS=Sus scrofa PE=1 SV=1**	**AQN3_PIG**	**24**	**9**
8	**Carbohydrate-binding protein AQN-1 (Zona pellucida-binding protein AQN-1) (Spermadhesin AQN-1) - Sus**	**AQN1_PIG**	**2**	**4**
9	**Zona pellucida-binding protein 1 OS=Sus scrofa GN=ZPBP PE=2 SV=1**	**ZPBP1_PIG**	**0**	**2**
10	Sperm acrosomal protein FSA-ACR.1 precursor (Fragment) - Vulpes vulpes (Red fox)	ASPX_VULVU	0	2
11	Sperm-associated acrosin inhibitor OS=Sus scrofa PE=1 SV=2	IACS_PIG	6	0
	Epididymal fluid/seminal plasma proteins			
1	**Epididymal sperm-binding protein 1 OS=Sus scrofa GN=ELSPBP1 PE=1 SV=1**	**ESPB1_PIG**	**60**	**46**
2	**Clusterin precursor (Complement cytolysis inhibitor) (CLI) (CP40) [Contains: Clusterin beta chain; Clusterin**	**CLUS_PIG/BOVIN**	**31**	**14**
3	**Seminal plasma protein pB1 OS=Sus scrofa PE=1 SV=2**	**PB1_PIG**	**10**	**11**
4	Seminal plasma sperm motility inhibitor precursor - Sus scrofa (Pig)	SPMI_PIG	20	10
5	Seminal plasma acrosin inhibitor A1 - Sus scrofa (Pig)	IACA_PIG	18	7
6	**Major seminal plasma glycoprotein PSP-II OS=Sus scrofa PE=1 SV=2**	**PSP2_PIG**	**1**	**1**
7	Epididymal secretory protein E1 precursor (Niemann Pick type C2 protein homolog) (cE1) - Canis familiaris (D	NPC2_CANFA	1	0
8	**Major seminal plasma glycoprotein PSP-I OS=Sus scrofa PE=1 SV=2**	**PSP1_PIG**	**1**	**0**
	Chaperones			
1	**Heat shock 70 kDa protein 1-like OS=Sus scrofa GN=HSPA1L PE=2 SV=1**	**HS71L_PIG/BOVIN**	**12**	**24**
2	**Heat shock protein HSP 90-alpha - Bos taurus (Bovine)**	**HS90A_BOVIN/HORSE**	**47**	**23**
3	**T-complex protein 1 subunit delta (TCP-1-delta) (CCT-delta) - Bos taurus (Bovine)**	**TCPD_BOVIN**	**7**	**2**
4	**T-complex protein 1 subunit theta (TCP-1-theta) (CCT-theta) - Bos taurus (Bovine)**	**TCPQ_BOVIN**	**5**	**2**
5	**Transitional endoplasmic reticulum ATPase (TER ATPase) (15S Mg(2+)-ATPase p97 subunit) (Valosin-contai**	**TERA_PIG**	**8**	**2**
6	Heat shock protein 75 kDa, mitochondrial precursor (HSP 75) (Tumor necrosis factor type 1 receptor-associa	TRAP1_BOVIN	0	1
7	**T-complex protein 1 subunit beta (TCP-1-beta) (CCT-beta) - Bos taurus (Bovine)**	**TCPB_BOVIN**	**5**	**1**
8	**T-complex protein 1 subunit eta (TCP-1-eta) (CCT-eta) - Bos taurus (Bovine)**	**TCPH_BOVIN**	**1**	**1**
9	Heat shock-related 70 kDa protein 2 OS=Bos taurus GN=HSPA2 PE=2 SV=2	HSP72_BOVIN	5	0
10	**T-complex protein 1 subunit zeta (TCP-1-zeta) (CCT-zeta) (CCT-zeta-1) - Bos taurus (Bovine)**	**TCPZ_BOVIN**	**4**	**0**
	Cytoskeleton proteins			
1	**Tubulin beta-4 chain - Bos taurus (Bovine)**	**TBB4_BOVIN**	**2**	**12**
2	**Tubulin beta-2C chain - Bos taurus (Bovine)**	**TBB2C_BOVIN**	**14**	**11**
3	**Tubulin alpha-3 chain OS=Bos taurus GN=TUBA3 PE=2 SV=1**	**TBA3_BOVIN**	**15**	**8**

4	**Tubulin alpha-1C chain OS=Bos taurus GN=TUBA1C PE=1 SV=1**	**TBA1C_BOVIN**	**0**	**2**
5	**Tubulin polymerization-promoting protein family member 2 OS=Bos taurus GN=TPPP2 PE=2 SV=1**	**TPPP2_BOVIN**	**2**	**2**
6	Actin, cytoplasmic 1 - Bos taurus (Bovine)	ACTB_BOVIN	8	1
	Ubiquitin and proteasomes			
1	**Ubiquitin - Bos taurus (Bovine)**	**UBIQ_BOVIN**	**18**	**12**
2	**Proteasome subunit alpha type 3 (EC 3.4.25.1) - Bos taurus (Bovine)**	**PSA3_BOVIN**	**3**	**3**
3	**Proteasome subunit alpha type 6 (EC 3.4.25.1) - Bos taurus (Bovine)**	**PSA6_BOVIN**	**4**	**3**
4	Proteasome subunit alpha type 4 (EC 3.4.25.1) - Bos taurus (Bovine)	PSA4_BOVIN	2	3
5	**Proteasome subunit beta type 1 precursor (EC 3.4.25.1) - Bos taurus (Bovine)**	**PSB1_BOVIN**	**4**	**3**
6	**Proteasome subunit beta type 6 precursor (EC 3.4.25.1) - Bos taurus (Bovine)**	**PSB6_BOVIN**	**2**	**2**
7	**Proteasome subunit alpha type 7 (EC 3.4.25.1) - Bos taurus (Bovine)**	**PSA7_BOVIN**	**2**	**2**
8	**Proteasome subunit alpha type 5 (EC 3.4.25.1) - Bos taurus (Bovine)**	**PSA5_BOVIN**	**1**	**2**
9	**26S proteasome non-ATPase regulatory subunit 7 OS=Bos taurus GN=PSMD7 PE=2 SV=1**	**PSD7_BOVIN**	**0**	**2**
10	**Proteasome subunit beta type 2 (EC 3.4.25.1) - Bos taurus (Bovine)**	**PSB2_BOVIN**	**0**	**2**
11	Ubiquitin domain-containing protein 1 OS=Bos taurus GN=UBTD1 PE=2 SV=1	UBTD1_BOVIN	1	2
12	**Ubiquitin domain-containing protein 2 - Bos taurus (Bovine)**	**UBTD2_BOVIN**	**0**	**2**
13	**Proteasome subunit alpha type 1 (EC 3.4.25.1) - Bos taurus (Bovine)**	**PSA1_BOVIN**	**2**	**1**
14	**Proteasome subunit beta type 4 precursor (EC 3.4.25.1) (Proteasome beta chain) (Macropain beta chain) (**	**PSB4_PIG**	**1**	**1**
15	**Proteasome subunit beta type-5 OS=Bos taurus GN=PSMB5 PE=1 SV=1**	**PSB5_BOVIN**	**1**	**1**
16	Proteasome subunit beta type-7 OS=Sus scrofa GN=PSMB7 PE=2 SV=2	PSB7_PIG	1	0
17	Proteasome subunit beta type 4 precursor (EC 3.4.25.1) - Bos taurus (Bovine)	PSB4_BOVIN	1	0
18	**Proteasome subunit alpha type 2 (EC 3.4.25.1) - Bos taurus (Bovine)**	**PSA2_BOVIN**	**3**	**0**
19	Ubiquitin-like modifier-activating enzyme 1 - Oryctolagus cuniculus (Rabbit)	UBA1_RABIT	2	0
	Enzymes			
1	**Hexokinase-1 (EC 2.7.1.1) (Hexokinase type I) (HK I) (Brain form hexokinase) - Bos taurus (Bovine)**	**HXK1_BOVIN**	**21**	**23**
2	**Adenylate kinase isoenzyme 1 (EC 2.7.4.3) (ATP-AMP transphosphorylase) (AK1) (Myokinase) - Sus scrofa (**	**KAD1_PIG/RABIT**	**22**	**22**
3	**14-3-3 protein zeta/delta (Protein kinase C inhibitor protein 1) (KCIP-1) (Factor activating exoenzyme S) (FA**	**1433Z_BOVIN**	**14**	**13**
4	**Phosphoglycerate mutase 2 OS=Bos taurus GN=PGAM2 PE=2 SV=1**	**PGAM2_BOVIN**	**13**	**12**
5	**Dipeptidyl peptidase 4 (EC 3.4.14.5) (Dipeptidyl peptidase IV) (DPP IV) (T-cell activation antigen CD26) [Co**	**DPP4_PIG**	**11**	**11**
6	Gamma-glutamyltranspeptidase 1 precursor (EC 2.3.2.2) (Gamma-glutamyltransferase 1) (GGT 1) (CD224 ant	GGT1_PIG	38	9
7	**Alpha-enolase - Bos taurus (Bovine)**	**ENOA_BOVIN**	**12**	**7**
8	**Potassium-transporting ATPase alpha chain 2 (EC 3.6.3.10) (Proton pump) (Non-gastric H(+)/K(+) ATPase su**	**AT12A_RABIT**	**4**	**6**
9	**cAMP-dependent protein kinase, alpha-catalytic subunit (EC 2.7.11.11) (PKA C-alpha) - Canis familiaris (Do**	**KAPCA_CANFA**	**4**	**6**
10	**Aldose reductase OS=Sus scrofa GN=AKR1B1 PE=1 SV=2**	**ALDR_PIG**	**20**	**6**
11	**Aspartate aminotransferase, cytoplasmic (EC 2.6.1.1) (Transaminase A) (Glutamate oxaloacetate transami**	**AATC_PIG**	**14**	**6**
12	**Hexokinase-2 OS=Sus scrofa GN=HK2 PE=2 SV=1**	**HXK2_PIG**	**8**	**5**
13	Beta-hexosaminidase beta chain precursor (EC 3.2.1.52) (N-acetyl-beta-glucosaminidase) (Beta-N-acetylhexo	HEXB_PIG	8	5
14	Sodium/potassium-transporting ATPase subunit alpha-2 OS=Bos taurus GN=ATP1A2 PE=2 SV=1	AT1A2_BOVIN	6	4
15	**Inositol monophosphatase (EC 3.1.3.25) (IMPase) (IMP) (Inositol-1(or 4)-monophosphatase) (Lithium-sens**	**IMPA1_PIG**	**7**	**4**
16	**Potassium-transporting ATPase alpha chain 1 (EC 3.6.3.10) (Proton pump) (Gastric H(+)/K(+) ATPase subun**	**ATP4A_CANFA**	**4**	**3**

17	**Casein kinase II subunit alpha (EC 2.7.11.1) (CK II) - Bos taurus (Bovine)**	**CSK21_BOVIN**	**4**	**3**
18	**Serine/threonine-protein phosphatase 2B catalytic subunit alpha isoform (EC 3.1.3.16) (Calmodulin-depen**	**PP2BA_BOVIN**	**9**	**3**
19	Glycerol-3-phosphate dehydrogenase [NAD+], cytoplasmic (EC 1.1.1.8) (GPD-C) (GPDH-C) - Bos taurus (Bovin	GPDA_BOVIN/RABIT	4	4
20	**Phosphoglucomutase-1 OS=Bos taurus GN=PGM1 PE=2 SV=1**	**PGM1_BOVIN**	**7**	**3**
21	**Alpha-S1-casein precursor - Bubalus bubalis (Domestic water buffalo)**	**CASA1_BUBBU**	**0**	**3**
22	**Phosphoglycerate kinase, testis specific (EC 2.7.2.3) - Sus scrofa (Pig)**	**PGK2_PIG**	**7**	**2**
23	Integrin-linked kinase-associated serine/threonine phosphatase 2C (EC 3.1.3.16) (ILKAP) - Bos taurus (Bovine	ILKAP_BOVIN	2	2
24	Alkaline phosphatase, tissue-nonspecific isozyme OS=Bos taurus GN=ALPL PE=1 SV=2	PPBT_BOVIN	15	2
25	4-trimethylaminobutyraldehyde dehydrogenase (EC 1.2.1.47) (TMABADH) (Aldehyde dehydrogenase 9A1) (E	AL9A1_BOVIN	5	2
26	Thioredoxin reductase 1, cytoplasmic OS=Bos taurus GN=TXNRD1 PE=2 SV=3	TRXR1_BOVIN	1	2
27	Aconitate hydratase, mitochondrial precursor (EC 4.2.1.3) (Citrate hydro-lyase) (Aconitase) - Sus scrofa (Pig)	ACON_PIG	3	2
28	Gamma-glutamyl hydrolase OS=Bos taurus GN=GGH PE=2 SV=1	GGH_BOVIN	0	2
29	**Glycylpeptide N-tetradecanoyltransferase 2 (EC 2.3.1.97) (Peptide N-myristoyltransferase 2) (Myristoyl-Co**	**NMT2_BOVIN**	**0**	**2**
30	GTPase-activating protein and VPS9 domain-containing protein 1 OS=Bos taurus GN=GAPVD1 PE=2 SV=1	GAPD1_BOVIN	0	2
31	**Plasma membrane calcium-transporting ATPase 1 (EC 3.6.3.8) (PMCA1) (Plasma membrane calcium pump**	**AT2B1_PIG**	**1**	**1**
32	ATP synthase subunit beta, mitochondrial precursor (EC 3.6.3.14) - Bos taurus (Bovine)	ATPB_BOVIN	1	1
33	**Phosphatidylethanolamine-binding protein 1 (PEBP-1) (HCNPpp) (Raf kinase inhibitor protein) (RKIP) [Cont**	**PEBP1_CANFA**	**2**	**1**
34	RAC-alpha serine/threonine-protein kinase (EC 2.7.11.1) (RAC-PK-alpha) (Protein kinase B) (PKB) - Bos taurus	AKT1_BOVIN	0	1
35	Casein kinase II subunit beta OS=Bos taurus GN=CSNK2B PE=1 SV=1	CSK2B_BOVIN	1	1
36	**cAMP-dependent protein kinase type I-alpha regulatory subunit OS=Bos taurus GN=PRKAR1A PE=1 SV=2**	**KAP0_BOVIN**	**2**	**1**
37	Serine/threonine-protein phosphatase PP1-gamma catalytic subunit OS=Bos taurus GN=PPP1CC PE=2 SV=1	PP1G_BOVIN	0	1
38	Cytosol aminopeptidase (EC 3.4.11.1) (Leucine aminopeptidase) (LAP) (Leucyl aminopeptidase) (Leucine amir	AMPL_BOVIN	1	1
39	Aminopeptidase N (EC 3.4.11.2) (pAPN) (Alanyl aminopeptidase) (Microsomal aminopeptidase) (Aminopepti	AMPN_PIG	14	1
40	Aspartyl aminopeptidase OS=Bos taurus GN=DNPEP PE=2 SV=1	DNPEP_BOVIN	2	1
41	L-lactate dehydrogenase C chain (EC 1.1.1.27) (LDH-C) (LDH testis subunit) (LDH-X) - Sus scrofa (Pig)	LDHC_PIG	1	1
42	**Quinone oxidoreductase (EC 1.6.5.5) (NADPH:quinone reductase) (Zeta-crystallin) - Sus scrofa (Pig)**	**QOR_PIG**	**4**	**1**
43	NADH-cytochrome b5 reductase 3 (Fragment) OS=Sus scrofa GN=CYB5R3 PE=1 SV=1	NB5R3_PIG	0	1
44	Arylsulfatase A precursor (EC 3.1.6.8) (ASA) (Cerebroside-sulfatase) - Bos taurus (Bovine)	ARSA_BOVIN	0	1
45	Leukocyte elastase inhibitor (LEI) (Serpin B1) - Equus caballus (Horse)	ILEU_HORSE	0	1
46	**Triosephosphate isomerase (EC 5.3.1.1) (TIM) (Triose-phosphate isomerase) - Oryctolagus cuniculus (Rabb**	**TPIS_RABIT**	**1**	**1**
47	**1-phosphatidylinositol-4,5-bisphosphate phosphodiesterase delta-4 OS=Sus scrofa GN=PLCD4 PE=2 SV=1**	**PLCD4_PIG**	**3**	**1**
48	Histone deacetylase 1 OS=Bos taurus GN=HDAC1 PE=2 SV=1	HDAC1_BOVIN	0	1
49	tRNA guanosine-2'-O-methyltransferase TRM11 homolog OS=Bos taurus GN=TRMT11 PE=2 SV=1	TRM11_BOVIN	0	1
50	**Fructose-bisphosphate aldolase A (EC 4.1.2.13) (Muscle-type aldolase) - Oryctolagus cuniculus (Rabbit)**	**ALDOA_RABIT**	**9**	**1**
51	Betaine--homocysteine S-methyltransferase 1 (EC 2.1.1.5) (Fragment) - Sus scrofa (Pig)	BHMT1_PIG	0	1
52	Palmitoyl-protein thioesterase 1 precursor (EC 3.1.2.22) (PPT-1) (Palmitoyl-protein hydrolase 1) - Bos taurus	PPT1_BOVIN	0	1
53	Acetylcholinesterase OS=Felis catus GN=ACHE PE=3 SV=1	ACES_FELCA	0	1
54	**Glucose-6-phosphate isomerase (EC 5.3.1.9) (GPI) (Phosphoglucose isomerase) (PGI) (Phosphohexose isom**	**G6PI_BOVIN/PIG**	**9**	**1**
55	Uricase (EC 1.7.3.3) (Urate oxidase) - Sus scrofa (Pig)	URIC_PIG	1	1
56	Vacuolar ATP synthase subunit H (EC 3.6.3.14) (V-ATPase H subunit) (Vacuolar proton pump subunit H) (V-AT	VATH_PIG	1	0

57	**Sodium/potassium-transporting ATPase subunit beta-3 OS=Bos taurus GN=ATP1B3 PE=2 SV=1**	**AT1B3_BOVIN**	**3**	**0**
58	**cAMP-dependent protein kinase type II-alpha regulatory subunit OS=Bos taurus GN=PRKAR2A PE=1 SV=2**	**KAP2_BOVIN**	**2**	**0**
59	Phosphoglycerate kinase 1 (EC 2.7.2.3) - Bos taurus (Bovine)	PGK1_BOVIN	3	0
60	**14-3-3 protein beta/alpha (Protein kinase C inhibitor protein 1) (KCIP-1) (Fragments) - Ovis aries (Sheep)**	**1433B_SHEEP**	**5**	**0**
61	Adenylate kinase isoenzyme 1 (EC 2.7.4.3) (ATP-AMP transphosphorylase) (AK1) (Myokinase) - Bos taurus (Bo	KAD1_BOVIN	10	0
62	Casein kinase II subunit alpha' (EC 2.7.11.1) (CK II) - Bos taurus (Bovine)	CSK22_BOVIN	1	0
63	Alkaline phosphatase, tissue-nonspecific isozyme precursor (EC 3.1.3.1) (AP-TNAP) (Liver/bone/kidney isozyr	PPBT_FELCA	7	0
64	Protein phosphatase 1A OS=Oryctolagus cuniculus GN=PPM1A PE=2 SV=1	PPM1A_RABIT	3	0
65	Xaa-Pro aminopeptidase 1 OS=Bos taurus GN=XPNPEP1 PE=2 SV=1	XPP1_BOVIN	1	0
66	Neprilysin (EC 3.4.24.11) (Neutral endopeptidase) (NEP) (Enkephalinase) (Neutral endopeptidase 24.11) (Atri	NEP_RABIT	7	0
67	Cytosolic non-specific dipeptidase OS=Bos taurus GN=CNDP2 PE=2 SV=1	CNDP2_BOVIN	1	0
68	Dihydrolipoyl dehydrogenase, mitochondrial precursor (EC 1.8.1.4) (Dihydrolipoamide dehydrogenase) - Sus	DLDH_PIG	1	0
69	Malate dehydrogenase, cytoplasmic (EC 1.1.1.37) (Cytosolic malate dehydrogenase) - Sus scrofa (Pig)	MDHC_PIG/BOVIN/FEL	17	0
70	17-beta-hydroxysteroid dehydrogenase 14 OS=Bos taurus GN=HSD17B14 PE=2 SV=1	DHB14_BOVIN	1	0
71	Alpha-aminoadipic semialdehyde dehydrogenase - Bos taurus (Bovine)	AL7A1_BOVIN	1	0
72	**Malate dehydrogenase, mitochondrial precursor (EC 1.1.1.37) - Sus scrofa (Pig)**	**MDHM_PIG**	**4**	**0**
73	GMP reductase 2 (EC 1.7.1.7) (Guanosine 5'-monophosphate oxidoreductase 2) (Guanosine monophosphate	GMPR2_BOVIN	1	0
74	Thioredoxin reductase 1, cytoplasmic OS=Sus scrofa GN=TXNRD1 PE=2 SV=3	TRXR1_PIG	5	0
75	Prostaglandin reductase 1 OS=Oryctolagus cuniculus GN=PTGR1 PE=2 SV=1	PTGR1_RABIT	1	0
76	Cystathionine gamma-lyase OS=Bos taurus GN=CTH PE=2 SV=1	CGL_BOVIN	1	0
77	Glutathione synthetase - Bos taurus (Bovine)	GSHB_BOVIN	1	0
78	N-acetylgalactosamine-6-sulfatase precursor (EC 3.1.6.4) (N-acetylgalactosamine-6-sulfate sulfatase) (Galact	GALNS_PIG	1	0
79	Superoxide dismutase [Cu-Zn] - Capra hircus (Goat)	SODC_CAPHI	1	0
80	DNA polymerase subunit gamma-2, mitochondrial OS=Bos taurus GN=POLG2 PE=2 SV=1	DPOG2_BOVIN	1	0
81	S-formylglutathione hydrolase (EC 3.1.2.12) (FGH) (Esterase D) - Sus scrofa (Pig)	ESTD_PIG	1	0
82	Glycosyltransferase-like domain-containing protein 1 OS=Bos taurus GN=GTDC1 PE=2 SV=1	GTDC1_BOVIN	1	0
83	DNA (cytosine-5)-methyltransferase 1 (EC 2.1.1.37) (Dnmt1) - Bos taurus (Bovine)	DNMT1_BOVIN	1	0
84	Citrate synthase, mitochondrial precursor (EC 2.3.3.1) - Sus scrofa (Pig)	CISY_PIG	1	0
85	Uroporphyrinogen decarboxylase OS=Ovis aries GN=UROD PE=1 SV=1	DCUP_SHEEP	1	0
86	**Inositol-3-phosphate synthase 1 OS=Bos taurus GN=ISYNA1 PE=2 SV=1**	**INO1_BOVIN**	**5**	**0**
87	**Bleomycin hydrolase (Fragment) OS=Oryctolagus cuniculus GN=BLMH PE=1 SV=1**	**BLMH_RABIT**	**2**	**0**
88	Adenosine deaminase OS=Bos taurus GN=ADA PE=1 SV=3	ADA_BOVIN	1	0
89	UTP--glucose-1-phosphate uridylyltransferase OS=Bos taurus GN=UGP2 PE=1 SV=2	UGPA_BOVIN	1	0
90	Beta-enolase - Bos taurus (Bovine)	ENOB_BOVIN	4	0
91	Adenosylhomocysteinase (EC 3.3.1.1) (S-adenosyl-L-homocysteine hydrolase) (AdoHcyase) - Bos taurus (Bovi	SAHH_BOVIN	1	0
92	FK506-binding protein 4 (EC 5.2.1.8) (Peptidyl-prolyl cis-trans isomerase) (PPIase) (Rotamase) (p59 protein) (	FKBP4_RABIT	1	0
	Other proteins			
1	**Leukocyte surface antigen CD47 precursor (Integrin-associated protein) (IAP) - Sus scrofa (Pig)**	**CD47_PIG**	**20**	**12**
2	Uncharacterized protein C19orf12 homolog OS=Bos taurus PE=2 SV=1	CS012_BOVIN	2	7
3	**Ras-related protein Rab-2A - Canis familiaris (Dog)**	**RAB2A_CANFA/RABIT**	**4**	**7**

4	**Solute carrier family 2, facilitated glucose transporter member 3 (Glucose transporter type 3, brain) (Fragn**	**GTR3_RABIT**	**4**	**6**
5	**Uncharacterized protein C1orf49 homolog - Bos taurus (Bovine)**	**CA049_BOVIN**	**3**	**4**
6	**Protein DJ-1 - Bos taurus (Bovine)**	**PARK7_BOVIN**	**8**	**4**
7	**PDZ domain-containing protein C16orf65 homolog - Bos taurus (Bovine)**	**CP065_BOVIN**	**4**	**4**
8	Lactotransferrin precursor - Sus scrofa (Pig)	TRFL_PIG	2	3
9	Phosphatidylethanolamine-binding protein 1 - Bos taurus (Bovine)	PEBP1_BOVIN	3	3
10	Brain acid soluble protein 1 OS=Bos taurus GN=BASP1 PE=1 SV=3	BASP1_BOVIN	12	3
11	**Rab GDP dissociation inhibitor beta (Rab GDI beta) (Guanosine diphosphate dissociation inhibitor 2) (GDI-2**	**GDIB_PIG/CANFA**	**7**	**3**
12	**Cancer susceptibility candidate protein 1 homolog OS=Bos taurus GN=CASC1 PE=2 SV=1**	**CASC1_BOVIN**	**0**	**2**
13	**Vesicle-associated membrane protein 3 (VAMP-3) (Synaptobrevin-3) - Bos taurus (Bovine)**	**VAMP3_BOVIN**	**2**	**1**
14	Syntaxin-7 OS=Bos taurus GN=STX7 PE=2 SV=1	STX7_BOVIN	1	1
15	Ras-related protein Rab-11A (Rab-11) - Canis familiaris (Dog)	RB11A_CANFA	0	1
16	**Abnormal spindle-like microcephaly-associated protein homolog - Bos taurus (Bovine)**	**ASPM_BOVIN**	**0**	**1**
17	Apolipoprotein C-III precursor (Apo-CIII) (ApoC-III) - Sus scrofa (Pig)	APOC3_PIG	1	1
18	Serum amyloid P-component OS=Bos taurus GN=APCS PE=2 SV=1	SAMP_BOVIN	2	1
19	Platelet factor 4 OS=Bos taurus GN=PF4 PE=1 SV=1	PLF4_BOVIN	0	1
20	CD59 glycoprotein precursor (Membrane attack complex inhibition factor) (MACIF) (MAC-inhibitory protein)	CD59_PIG	5	1
21	Coagulation factor V precursor (Activated protein C cofactor) [Contains: Coagulation factor V heavy chain; Cc	FA5_BOVIN	0	1
22	Alpha-fetoprotein precursor - Sus scrofa (Pig)	FETA_PIG	0	1
23	Lysosome-associated membrane glycoprotein 1 precursor (LAMP-1) (Chromaffin granule-associated membra	LAMP1_BOVIN	0	1
24	Sodium channel subunit beta-4 OS=Bos taurus GN=SCN4B PE=2 SV=1	SCN4B_BOVIN	0	1
25	Breast cancer metastasis-suppressor 1-like protein OS=Bos taurus GN=BRMS1L PE=2 SV=1	BRM1L_BOVIN	0	1
26	Calcium-binding protein 39 - Bos taurus (Bovine)	CAB39_BOVIN	0	1
27	Interleukin-1 alpha precursor (IL-1 alpha) - Bubalus carabanensis (Swamp type water buffalo)	IL1A_BUBCA	0	1
28	**Solute carrier family 2, facilitated glucose transporter member 3 (Glucose transporter type 3, brain) - Bos t**	**GTR3_BOVIN**	**1**	**1**
29	UPF0468 protein C16orf80 homolog OS=Bos taurus PE=2 SV=1	CP080_BOVIN	0	1
30	**Peroxiredoxin-5, mitochondrial precursor - Bos taurus (Bovine)**	**PRDX5_BOVIN**	**2**	**1**
31	IQ domain-containing protein G OS=Bos taurus GN=IQCG PE=2 SV=1	IQCG_BOVIN	0	1
32	Protein FAM190A OS=Bos taurus GN=FAM190A PE=2 SV=1	F190A_BOVIN	0	1
33	**Transcriptional regulator ATRY (Fragments) OS=Macropus eugenii GN=ATRY PE=2 SV=1**	**ATRY_MACEU**	**0**	**1**
34	PHD finger protein 11 OS=Bos taurus GN=PHF11 PE=2 SV=1	PHF11_BOVIN	0	1
35	Cytoplasmic tRNA 2-thiolation protein 2 OS=Bos taurus GN=CTU2 PE=2 SV=1	CTU2_BOVIN	0	1
36	Rho GDP-dissociation inhibitor 1 OS=Bos taurus GN=ARHGDIA PE=1 SV=3	GDIR1_BOVIN	2	0
37	Rab GDP dissociation inhibitor alpha (Rab GDI alpha) (Guanosine diphosphate dissociation inhibitor 1) (GDI-1	GDIA_CANFA	1	0
38	**Ezrin (p81) (Cytovillin) (Villin-2) - Bos taurus (Bovine)**	**EZRI_BOVIN**	**14**	**0**
39	Endophilin-B1 OS=Bos taurus GN=SH3GLB1 PE=2 SV=1	SHLB1_BOVIN	1	0
40	**Syntaxin-binding protein 2 (Unc-18 homolog 2) (Unc-18B) (Unc18-2) - Canis familiaris (Dog)**	**STXB2_CANFA**	**4**	**0**
41	Apolipoprotein A-I-binding protein OS=Sus scrofa GN=APOA1BP PE=2 SV=1	AIBP_PIG	1	0
42	**Fibronectin (FN) (Fragment) - Equus caballus (Horse)**	**FINC_HORSE**	**1**	**0**
43	Uncharacterized protein C3orf14 homolog - Bos taurus (Bovine)	CC014_BOVIN	1	0

44	Small glutamine-rich tetratricopeptide repeat-containing protein alpha OS=Bos taurus GN=SGTA PE=2 SV=1	SGTA_BOVIN	1	0
45	Protein FAM107B OS=Bos taurus GN=FAM107B PE=2 SV=1	F107B_BOVIN	1	0
46	TBC1 domain family member 20 OS=Bos taurus GN=TBC1D20 PE=2 SV=1	TBC20_BOVIN	1	0
47	Anion exchange protein 4 OS=Oryctolagus cuniculus GN=SLC4A9 PE=1 SV=2	B3A4_RABIT	1	0
48	Peroxiredoxin-1 OS=Bos taurus GN=PRDX1 PE=2 SV=1	PRDX1_BOVIN	2	0
49	Plastin-3 OS=Bos taurus GN=PLS3 PE=2 SV=1	PLST_BOVIN	3	0
50	Annexin A2 OS=Sus scrofa GN=ANXA2 PE=1 SV=4	ANXA2_PIG	4	0
51	Phosphatidylethanolamine-binding protein 1 - Oryctolagus cuniculus (Rabbit)	PEBP1_RABIT	1	0
52	CREB-regulated transcription coactivator 2 OS=Bos taurus GN=CRTC2 PE=2 SV=1	CRTC2_BOVIN	1	0
53	Guanine nucleotide-binding protein G(I)/G(S)/G(T) subunit beta 1 (Transducin beta chain 1) - Bos taurus (Bov	GBB1_BOVIN	3	0
54	Histone H1t - Sus scrofa (Pig)	H1T_PIG	1	0
55	Small nuclear ribonucleoprotein Sm D2 (snRNP core protein D2) (Sm-D2) (Fragment) - Sus scrofa (Pig)	SMD2_PIG	1	0